Flood Regime of Rivers in the Danube River Basin

This Follow-up volume (Volume IX) of the Hydrological Monograph of the Danube River Basin was prepared by an international group of authors under the steering committee's leadership of the Project No. 9 "*Flood regime of rivers in the Danube River basin"*.

Committee Chairperson: **Pavla Pekárová**
Members of the Steering Committee
Dipl.Geogr. Jörg Uwe Belz
Dr. Eva Soukalová
Dr. Petr Janál
Dr. Pavol Miklánek
Dr. Gábor Bálint †
Prof. Stevan Prohaska

Input data used in this Follow-up volume (Volume IX) of the Hydrological Monograph of the Danube River Basin were prepared by the individual National Committees of IHP UNESCO of the Danube Basin countries for their respective stations and opened up for preparation of the follow-up volume. Any use of the data for other purpose than Regional collaboration of the Danube countries is subject to approval of the respective National Committee of IHP UNESCO.

The final version was prepared by the Slovak National Committee for IHP UNESCO
at the Institute of Hydrology, Slovak Academy of Sciences.

Reviewed by: Ing. Milan Onderka, PhD.
MSc. Viorel Chendes, PhD.

ISBN: 978-80-89139-45-3, print version
EAN: 9788089139453

ISBN: 978-80-89139-46-0, pdf
EAN: 9788089139460
DOI: 10.31577/2019.9788089139460

Pavla Pekárová, Pavol Miklánek
Editors

FLOOD REGIME OF RIVERS IN THE DANUBE RIVER BASIN

The Danube and its Basin – Hydrological Monograph Follow-up Volume IX

United Nations
Educational, Scientific and
Cultural Organization

Regional Co-operation of the Danube Countries within the Frame of the International Hydrological Programme of UNESCO

and

Slovak Academy of Sciences, Institute of Hydrology

Bratislava 2019

How to cite this monograph
Pekárová, P., Miklánek, P. (eds.), 2019. *Flood regime of rivers in the Danube River basin*. Follow-up volume IX of the Regional Co-operation of the Danube Countries in IHP UNESCO. IH SAS, Bratislava, 215 p. + 527 p. app., DOI: 10.31577/2019.9788089139460.
How to cite the chapter in this monograph
Authors, Title of the chapter. In: Pekárová, P., Miklánek, P. (eds.), 2019. *Flood regime of rivers in the Danube River basin*. Follow-up volume IX of the Regional Co-operation of the Danube Countries in IHP UNESCO. IH SAS, Bratislava, 215 p. + 527 p. app., DOI: 10.31577/2019.9788089139460.

Title: FLOOD REGIME OF RIVERS IN THE DANUBE RIVER BASIN
Editors: Pavla Pekárová and Pavol Miklánek

Authors: Pavla Pekárová, Pavol Miklánek, Stevan Prohaska, Petr Janál, Jörg Uwe Belz, Radu Drobot, Mitja Brilly, Ján Pekár, Dana Halmová, Veronika Bačová Mitková, Jakub Mészáros, Marcel Garaj, Nejc Bezak, Aurelian Florentin Draghia, Ole Rössler, Martin Morlot, Liudmyla Gorbachova, Aleksandra Ilić, Maria Larina-Pooth, Danko Biondić, Mira Kobold, Esena Kupusović, Michael Mürlebach, Eva Soukalová, Gábor Bálint, Peter Škoda, Philipp Stanzel, Mojca Šraj, Sorin Teodor

Publisher: Institute of Hydrology of the Slovak Academy of Sciences in Bratislava
Printing office: VEDA Publishing House of the SAS
Year of publication: December 2019
Publication: 1st edition
Printing: 150 pcs.

Dedicated to
Hydrologists and Water Scientists

Authors

Veronika Bačová Mitková,
Slovak Academy of Sciences, Institute of Hydrology, Dúbravská cesta 9, 814 04 Bratislava, Slovakia, mitkova@uh.savba.sk

Gábor Bálint,
Died, formerly VITUKI Environmental Protection and Water Resources Research Institute, Budapest, Hungary

Jörg Uwe Belz,
Federal Institute of Hydrology, Am Mainzer Tor 1, 56068 Koblenz, Germany, belz@bafg.de

Nejc Bezak,
University of Ljubljana, Faculty of Civil and Geodetic Engineering, Jamova 2, Ljubljana, Slovenia, nejc.bezak@fgg.uni-lj.si

Danko Biondić,
Hrvatske vode, Ul. grada Vukovara 220, 10000 Zagreb l, Croatia, dbiondic@voda.hr

Mitja Brilly,
University of Ljubljana, Faculty of Civil and Geodetic Engineering, Jamova 2, Ljubljana, Slovenia, mitja.brilly@fgg.uni-lj.si

Aurelian Florentin Draghia,
Technical University of Civil Engineering Bucharest, Bd. Lacul Tei nr. 122 - 124, Sector 2, Bucuresti 020396, Romania, draghia aurelian@yahoo.com

Radu Drobot,
Technical University of Civil Engineering Bucharest, Bd. Lacul Tei nr. 122 - 124, Sector 2, Bucuresti 020396, Romania, drobot@utcb.ro

Marcel Garaj,
Slovak Academy of Sciences, Institute of Hydrology, Dúbravská cesta 9, 814 04 Bratislava, Slovakia, garaj@uh.savba.sk

Liudmyla Gorbachova,
Ukrainian Hydrometeorological Institute, Nauki Prospekt. 37, Kyiv 03028, Ukraine, gorbachova@uhmi.org.ua

Dana Halmová,
Slovak Academy of Sciences, Institute of Hydrology, Dúbravská cesta 9, 814 04 Bratislava, Slovakia, halmova@uh.savba.sk

Aleksandra Ilić,
University of Niš, Faculty of Civil Engineering and Architecture, Aleksandra Medvedeva 14, 18000 Niš, Serbia, aleksandra.ilic@gaf.ni.ac.rs

Petr Janál,
Regional Office Brno, Czech Hydrometeorological Institute, Kroftova 43, 616 67 Brno, Czechia, petr.janal@chmi.cz

Maria Larina-Pooth,
Federal Institute of Hydrology, Am Mainzer Tor 1, 56068 Koblenz, Germany, larina@bafg.de

Mira Kobold,
Ministry of the Environment and Spatial Planning, Slovenian Environment Agency, Vojkova 1b, 1000 Ljubljana, Slovenia, mira.kobold@gov.si

Esena Kupusović,
Federal Hydrometeorologica Institute, Bardakčije 12; 71 000 Sarajevo, Bosnia and Herzegovina, esena.kupusovic@fhmzbih.gov.ba

Jakub Mészáros,
Slovak Academy of Sciences, Institute of Hydrology, Dúbravská cesta 9, 814 04 Bratislava, Slovakia, jakubmeszaros@uh.savba.sk

Pavol Miklánek,
Slovak Academy of Sciences, Institute of Hydrology, Dúbravská cesta 9, 814 04 Bratislava, Slovakia, miklanek@uh.savba.sk

Martin Morlot,
University of Ljubljana, Faculty of Civil and Geodetic Engineering, Jamova 2, Ljubljana, Slovenia, matin.morlot@fgg.uni-lj.si

Michael Mürlebach,
Federal Institute of Hydrology, Am Mainzer Tor 1, 56068 Koblenz, Germany, muerlebach@bafg.de

Ján Pekár,
Comenius University in Bratislava, Faculty of Mathematics, Physics, and Informatics, Mlynská dolina F1, 842 48 Bratislava, Slovakia, pekar@fmph.uniba.sk

Pavla Pekárová,
Slovak Academy of Sciences, Institute of Hydrology, Dúbravská cesta 9, 814 04 Bratislava, Slovakia, pekarova@uh.savba.sk

Stevan Prohaska,
Jaroslav Černi Water Institute, Jaroslava Černog 80, 11 000 Belgrade, Serbia, stevan.prohaska@jcerni.rs

Ole Rössler,
Federal Institute of Hydrology, Am Mainzer Tor 1, 56068 Koblenz, Germany, roessler@bafg.de

Eva Soukalová,
Retired, formerly Regional Office Brno, Czech Hydrometeorological Institute, Kroftova 43, 616 67 Brno, Czechia

Peter Škoda,
Slovak Hydrometeorological Institute, Bratislava, Jeséniova 17, 833 15 Bratislava

Philipp Stanzel,
BOKU - University of Natural Resources and Life Sciences, Vienna, Institute for Hydrology and Water Management, Muthgasse 18, A-1190 Wien, Austria, philipp.stanzel@boku.ac.at

Mojca Šraj,
University of Ljubljana, Faculty of Civil and Geodetic Engineering, Jamova 2, Ljubljana, Slovenia, mojca.sraj@fgg.uni-lj.si

Sorin Teodor,
National Institute of Hydrology and Water Management, Sos. Bucharest-Ploiesti 97, sector 1, Bucharest, 013686, Romania, sorin.teodor@hidro.ro

Project 9: Flood regime of rivers in the Danube River basin
http://www.ih.savba.sk/danubeflood

Members of the Steering Committee

Dipl.Geogr. Jörg Uwe Belz
Dr. Eva Soukalová
Dr. Petr Janál
Dr. Pavla Pekárová, chair person
Dr. Pavol Miklánek
Dr. Gábor Bálint ■
Prof. Stevan Prohaska

LIST OF NOMINATED EXPERTS (NE), AND COOPERATING SPECIALISTS (CS)

G e r m a n y, NE
Dipl.Geogr. Jörg Uwe Belz
Federal Institute of Hydrology, Department M1 - Hydrometry and Hydrological Survey, Am Mainzer Tor 1, 56068 Koblenz
E-mail belz@bafg.de

A u s t r i a
DI Philipp Stanzel
BOKU - Universität für Bodenkultur, Department für Wasser-Atmosphäre-Umwelt, Institut für Wasserwirtschaft, Hydrologie und konstruktiven Wasserbau, Muthgasse 18, A-1190 Wien
E-mail: philipp.stanzel@boku.ac.at

C z e c h R e p u b l i c, NE
Ing. Petr Janál, PhD., Dr. Eva Soukalová, Regional Office Brno, Czech Hydrometeorological Institute Kroftova 43, CZ-616 67 Brno
E-mail: petr.janal@chmi.cz

S l o v a k i a, NE, coordinator
RNDr. Pavla Pekárová, DrSc., RNDr. Pavol Miklánek, CSc., Institute of Hydrology, SAS, Dúbravská cesta 9, 841 04 Bratislava
E-mail: pekarova@uh.savba.sk
CS
RNDr. Peter Škoda, Mgr. Katarína Melová, PhD., Slovak Hydrometeorological Institute, Bratislava, Jeséniova 17, 833 15 Bratislava

H u n g a r y, NE
Dr. Gábor Bálint▪,
Died, formerly VITUKI Environmental Protection and Water Resources Research Institute, Budapest, Hungary

S l o v e n i a,
Dr. Mira Kobold, Dipl. Physicist NE
Ministry of the Environment and Spatial Planning, Slovenian Environment Agency, Vojkova 1b, 1000 Ljubljana
E-mail: mira.kobold@gov.si

Mitja Brilly NE
Mojca Šraj CS
University of Ljubljana, Faculty of Civil and Geodetic Engineering, Jamova 2, Ljubljana, Slovenia
E-mail: mitja.brilly@fgg.uni-lj.si

C r o a t i a, NE
Danko Biondić
Hrvatske vode, Ul. grada Vukovara 220, 10000 Zagreb l, Croatia.
E-mail: dbiondic@voda.hr

S e r b i a, NE
Prof. Stevan Prohaska
Institute for Development of Water Resources "Jaroslav Cerni", Jaroslava Černog street 80, P.O. Box 3354, 11226 Belgrade
E-mail: stevan.prohaska@jcerni.rs

B o s n i a a n d H e r z e g o v i n a, NE
Mrs. Esena Kupusovic, M.S.C.E.
Head Department of Hydrology, Federal Hydrometeorologica Institute, Bardakčije 12; 71 000 Sarajevo
E-mail: esena.kupusovic@fhmzbih.gov.ba

R o m a n i a, NE
Prof. Radu Drobot
UTCB, Bucharest, Romania
drobot@utcb.ro

Sorin Teodor, Ioan Jelev
National Institute of Hydrology and Water Management, Sos. Bucharest-Ploiesti 97, sector 1, Bucharest, 013686
E-mail: sorin.teodor@hidro.ro

U k r a i n e, NE, CS
Dr. Liudmyla Gorbachova, Dr. Borys Khrystiuk, Ph.D., Ukrainian Hydrometeorological Institute, Nauki Prospekt. 37, Kyiv 03028,
E-mail: gorbachova@uhmi.org.ua, khryst@uhmi.org.ua

Contents

Foreword

Thanks to years of effort, extremely important scientific research work has been completed “FLOOD REGIME OF RIVERS IN THE DANUBE RIVER BASIN, the Danube and its Basin – Hydrological Monograph Follow-up Volume IX“.

We receive with this volume basis for understanding the occurrence of floods in the basin with: a historical overview of individual floods, analysis of homogeneity, cyclicality and long-term trends, seasonality, extreme discharges of selected water stations, coincidence of flood waves in the main river basin and major side tributaries, least and not last theoretical design hydrographs and regionalization of river basin flood regimes. The study has extraordinary practical importance for Flood risk management in the Danube river basin and is an example of a scientific approach of hydrological flood risk analysis. The work is the basis for further work and trans-border co-operation between the national services responsible for flood protection and the implementation of the Flood Directive. It is a long time waited and urgent report for understanding the nature of floods in the Danube river basin.

Thirty scientists from eleven countries of the Danube River Basin participated in the work with modest financial support. The work was developed under the auspices of the National Committees of IHP UNESCO of the Regional cooperation of the countries in the Danube River Basin. The largest part of the work was performed and carried out by the Institute of Hydrology of the Slovak Academy of Sciences, which also successfully conducted the research.

Ljubljana, 25.10.2019 Mitja Brilly

Co-ordinator of Regional Hydrological co-operation
of the Danube Countries in the frame of IHP UNESCO

1 Average daily discharge and annual peak discharge series collection

Pavla Pekárová, Pavol Miklánek, Gábor Bálint, Jörg Uwe Belz, Danko Biondić, Liudmyla Gorbachova, Mira Kobold, Esena Kupusović, Eva Soukalová, Stevan Prohaska, Peter Škoda, Philipp Stanzel, and Sorin Teodor

1.1 Introduction

The territory of the Danube River Basin is one of the most flood-endangered regions in Europe. It is therefore essential to have decent knowledge of its flood regime in order to generalize long-term observations made throughout the whole Danube territory.

Expanding population – and the development of civilization in general – makes the society more vulnerable to floods. This concerns both, the aftermaths of floods and incidents of long lasting periods of droughts. Economic prosperity of each country is reliant on the availability of sufficient water resources. In general, the economic growth and high living standards are responsible for higher water demand (although, e.g. water consumption in Slovakia decreased after 1989 mainly due to economic slow-down and higher costs of water). Because the amount of water resources is limited, the social and economic growth will be expressively limited in the future in many parts of the world.

The quantity of water contained in rivers, which are the largest utilizable source of water, fluctuates during the year considerably. In the Danube River, the highest flows are observed as a consequence of spring snowmelt-induced runoff in March and during summer when rainfall is at its maximum. In general, deficit of water in the Danube Basin is observed at the end of summer. Seasonal variability in the runoff can create serious problems both during periods of elevated runoff and limited water supply during dry periods.

One of the basic objectives of hydrology in the first half of the 20th century was to propose technical measures to control flows in rivers throughout the whole year. Today, requirements for water resources are often controversial, depending on the needs of various users and industry sectors such as water transport, energy production, irrigation, land drainage, flood protection, industrial and municipal water supply, fish breeding, recreation, water pollution control, and biodiversity preservation. These manifold requirements for water inevitably call for an integrated water management.

Analyses of long observations river flow revealed that the use of water resources is limited by their **multi-annual variability**. The theory natural multi-annual variability is not entirely new (Williams, 1961; Balek, 1968). Some more than 50 years ago – when the Nasser (Aswan) dam was being designed on the Nile river – Hurst (1951) expressed his opinion that **the whole Earth climatic system is subject to long-term oscillations**. By studying more than 900 time series of data on Nile water levels over more than 790 years, dendro-chronological series, sediments in seas and lakes, etc., he observed a spectacular behaviour of the geophysical time series, which has become known as the „Hurst phenomenon“. This term describes the tendency of dry and wet years to cluster together into longer dry and wet periods.

The existence of regular long-term cycles breaks the axiom of independence of hydrological time series. This axiom is a pre-condition for the calculation of all hydrological and meteorological characteristics based on observation data. For instance, to determine the frequency distribution of mean annual discharge *Qa* it is assumed that the *Qa* value does not depend on the preceding value, e.g. discharge that occurred 7-, 14-, 21-, or 28-years ago.

Correct identification of long-term cycles in a particular region makes it possible to predict runoff for 20–30 years in advance. Reliable estimates and predictions are of immense economic importance for decision-makers when managing water resources (construction of water storage reservoirs, energy production in hydroelectric plants, needs of the water for irrigation, etc.)

For instance, in Slovakia, a wet period started in 1996 followed by severe floods each year after a series of 14 dry years between 1980 and 1993 (Fig.1.1). Floods in recent years caused substantial damage to both private and communal property, including fatalities. For

example, 47 people died in the severe flood on the Malá Svinka River (eastern Slovakia) in 1998, and two persons lost their life in the 2002 summer floods.
From the analysed long precipitation series observed at the nearby meteorological stations (Mosonmagyarovar, Vienna, and Brno) we can conclude that precipitation depths before the year 1871 were lower compared to the 1981–1990 decade (Fig. 1.2). The best example of long-term trend in precipitation is discernible in the data records from the meteorological station at Brno. The period between 1803 and 1830 was most likely exceptional in terms of precipitation in the Danubian lowland region. We approximated the long-term trend by a 4th degree polynomial. Markedly drier periods occurred every 120–140 years.

The pronounced differences in air temperature are also determined by the area of the Danube basin and its elongated shape stretching from the west to the east. The average annual air temperature within the basin ranges from –2°C to +12°C. The lowest annual mean temperature was measured at Sonnblick, whilst the highest mean annual temperature was observed in the northern part of the Hungarian Lowland (Fig. 1.3) and at the Black Sea coast. In the entire Danube Basin, July is the warmest month, and January is the coldest month (Stančík and Jovanovic, 1988).

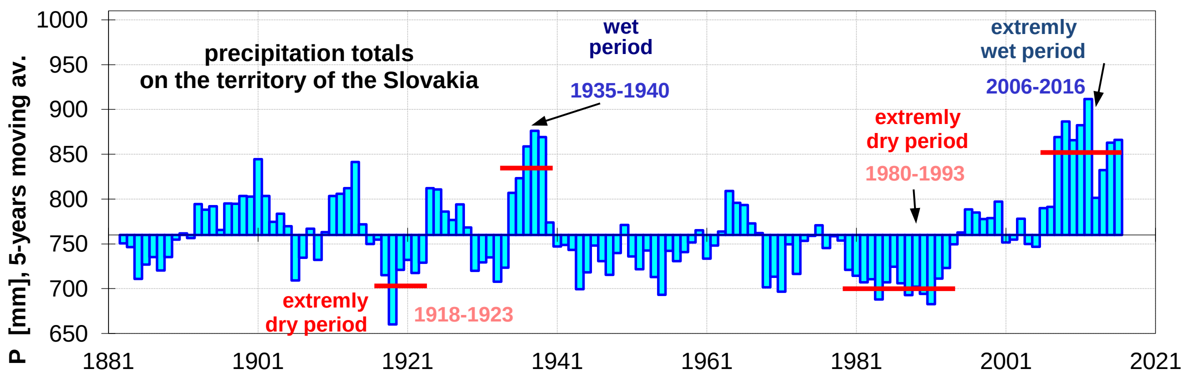

a)

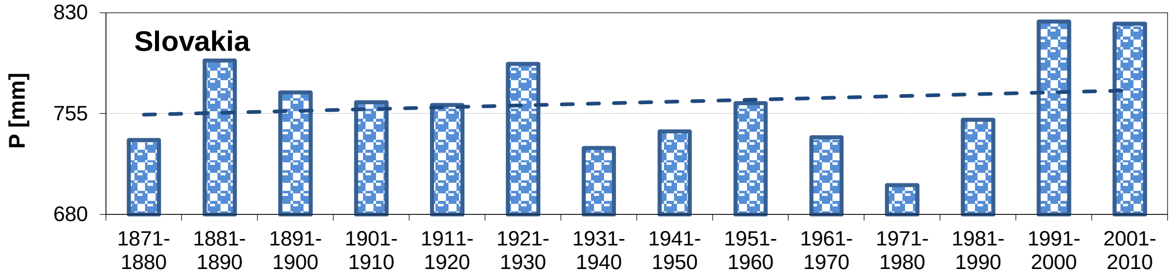

b)

Fig. 1.1 *a) Moving averages of the mean annual areal precipitation amounts from 203 stations, Slovakia, period: 1881–2016. Extremely dry periods in the 1918–1923 period and 1980–1993 period, and the extremely wet periods of 1938–1940 and 2006–2016. b) 10-year averages of precipitation totals in Slovakia.*

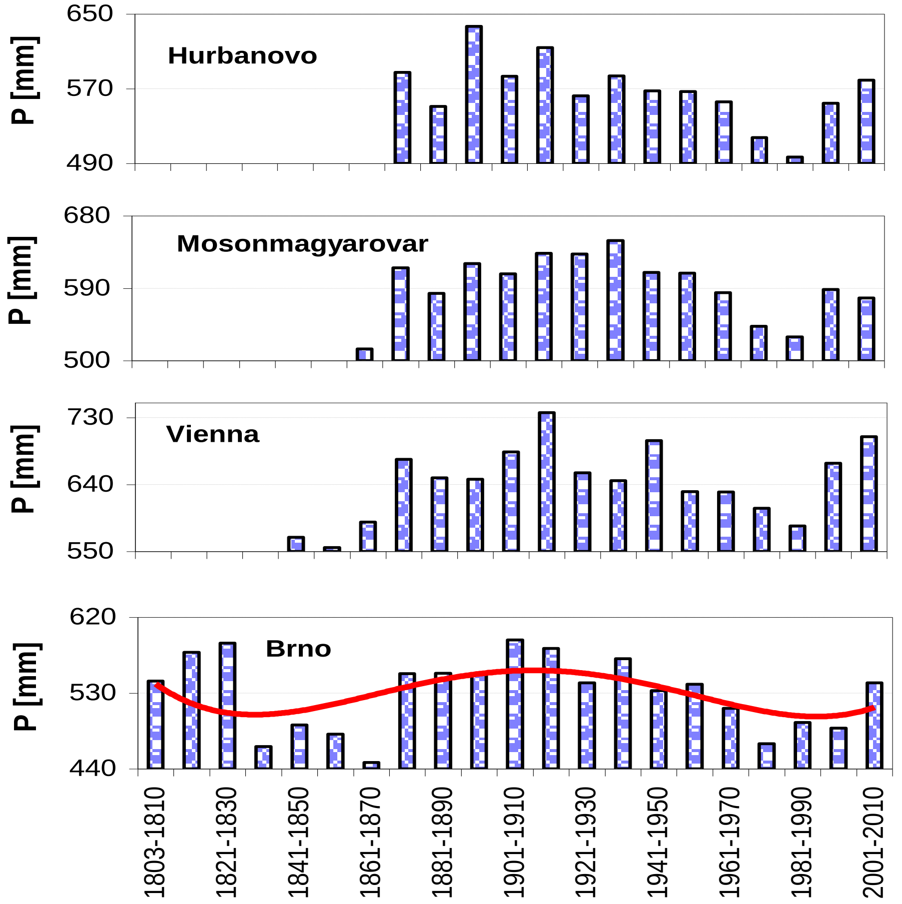

Fig. 1.2 *10-year average of precipitation at Hurbanovo (1871–2010), Mosonmagyarovar (1861–2009), Vienna (1841–2009), and Brno (1803–2010).*

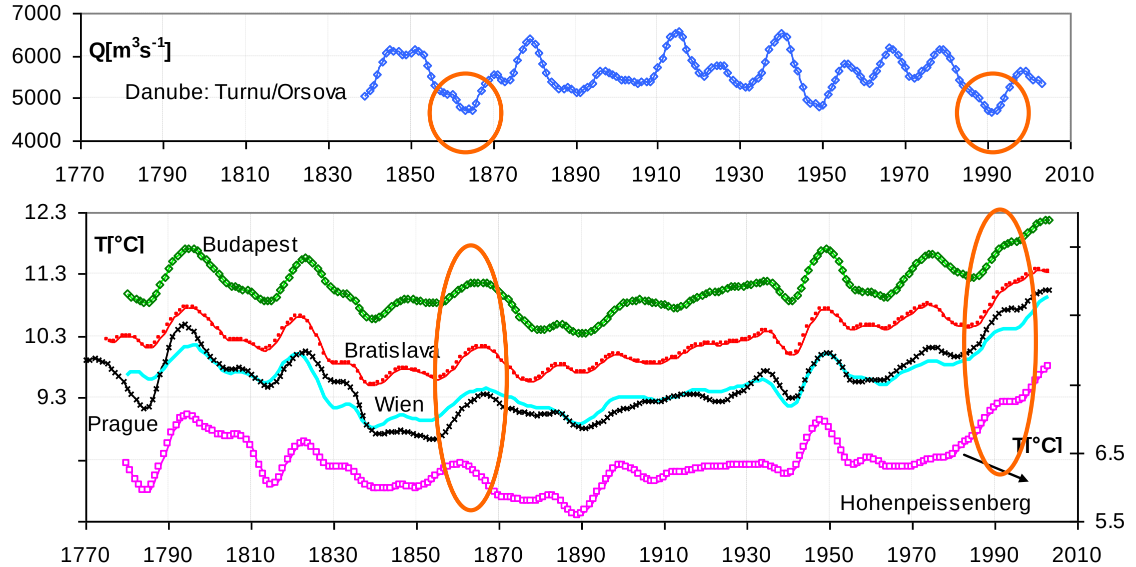

Fig. 1.3 *Filtered mean annual discharge of the Danube at Orsova and annual air temperature, HP-filter lambda=50. Budapest, Bratislava, Prague: Klementinum, Wien, and Hohenpeissenberg stations, 1780–2004 period.*

In this monograph we attempted to find answers to the following questions:

- *Are the hydrological extremes rising in the long run?*
- *Will the hydrologic characteristics change?*
- *Are there any regular multi-annual natural cycles in discharge time series?*
- *Is it possible to identify the length of these cycles?*
- *What will be the probable runoff in the Danube basin in the near future?*

Finding answers to these questions is not an easy task. To provide reliable answers it is necessary:

- to begin with a detailed statistical analysis of the longest possible hydrological time series, to minimize subjective researcher's assumptions;
- to extend the existing databases with archived historical material, to identify possible changes in the data series applying multiple mathematical tools, to use the most recent methods of mathematical statistics and stochastic mathematical modelling as a response to the regional specificity of the Danube basin's hydrological characteristics;
- to compare runoff changes in catchments affected by anthropogenic activities with the unaffected ones;
- to consider linkages between several related phenomena:
- to shed light on the impact of anthropogenic activities on runoff changes in catchments – reservoir constructions, river embankments, areal drainage, etc.,
- to study the impacts of phenomena like ENSO (El Niño Southern Oscillation), NAO (North Atlantic Oscillation), QBO (Quasi biennial Oscillation), and AO (Arctic Oscillation).

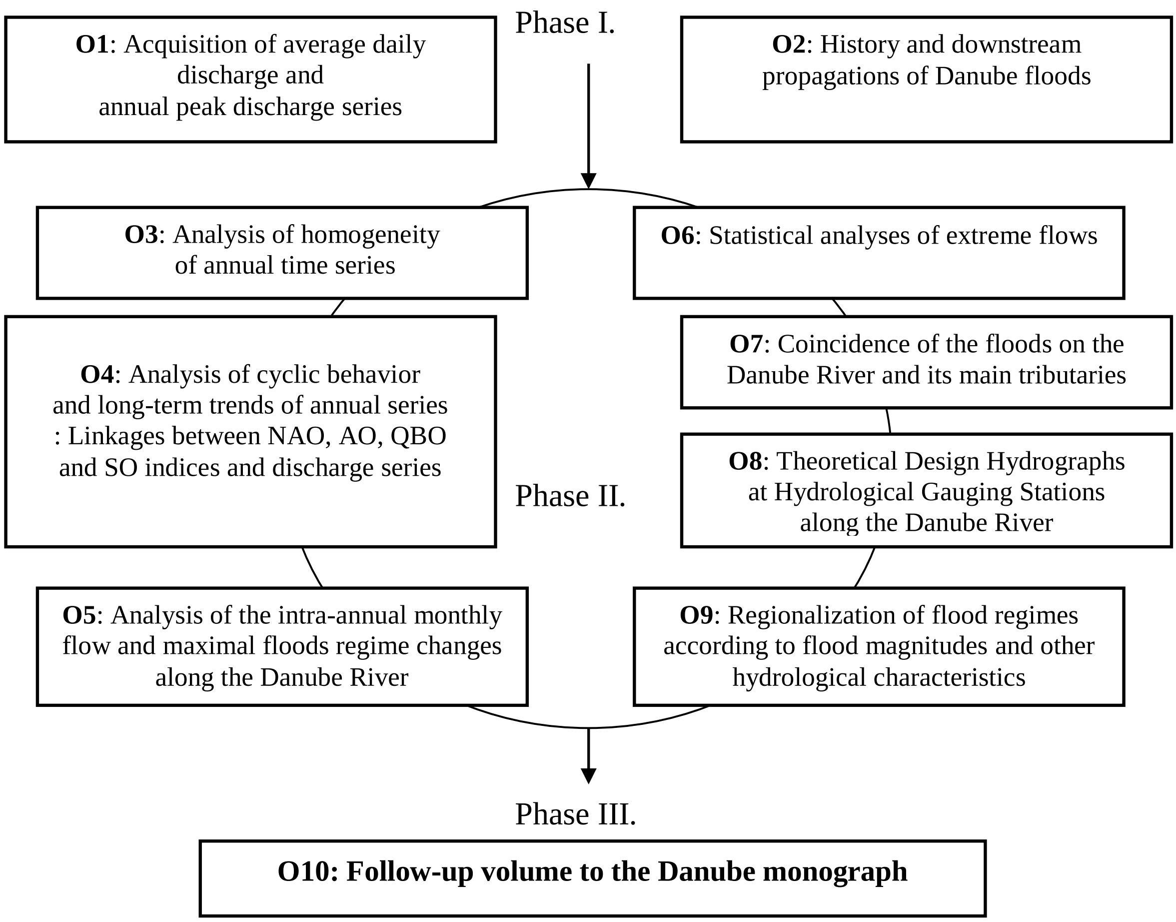

Fig. 1.4 Flood regime of rivers within the Danube River basin project objectives.

1.2 Brief description of the Danube basin

The Danube River with its total length of 2857 km and the long-term daily mean discharge of approximately 6500 m^3s^{-1} is the second largest river in Europe. With its total length it ranks as the twenty-first biggest river in the world, in terms of drainage area it ranks twenty-fifth with its drainage area of 817,000 km^2. The Danube basin extends from the central Europe to the Black Sea. The extreme points of the basin are 8º 09′ and 29º 45′ of the Eastern longitude, and 42º 05′ and 50º 15′ of the Northern latitude (Stancik & Jovanovic, 1988). Out of the whole Danube basin area, 36% are covered with mountains: very tall (over 4,000 m in the Alps), and tall (1,000–2,000 m in the Carpathians, the Balkans and the Dinaric Alps); 64% represent medium-high and low areas (tablelands, hills and plains) (Bondar and Iordache, 2017) (Fig. 1.5). Its landscape geomorphology is characterised by a diversity of morphological patterns and the river channel itself can be divided into 6 sections (Fig. 1.6a) based on the river slope (Lászlóffy, 1965). The shape of the Danube basin is asymmetrical, with about 56% of the area located on the right side and 44% on the left side of the river (Fig. 1.6b).

In terms of physical-geographical conditions (position, relief and vegetation), a specific continental-temperate climate has developed in the course of time, its characteristic parametric values according Bondar and Iordache (2017) are given below:

– The annual mean air temperature is between 8°C in the upper part of the basin and 12°C in its lower part; absolute air extremes reach +37°C in summer and –36°C in winter. Temperature highs of +43° and temperature lows of –33 °C have been recorded in the plain-area of the Lower Danube sector.

– Precipitation, as the major climatic factor of the Danube basin, is involved in the formation of water runoff affecting the river's flow regime. With regard to the diversity of atmospheric circulation patterns and of the landform-types forming the basin, precipitation is distributed unevenly. In the lowland areas the annual mean ranges from 400 to 600 mm, while 800–1,200 mm has been recorded in the Carpathians and 1,800–2,500 in the Alps (Fig. 1.7a).

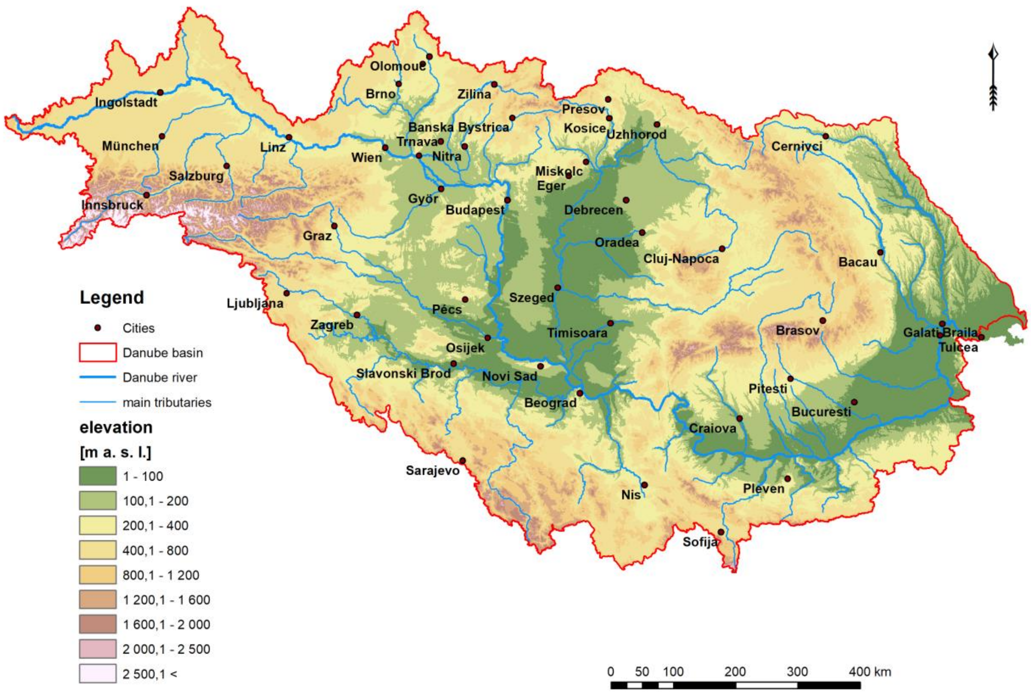

Fig. 1.5 Danube River basin orography.

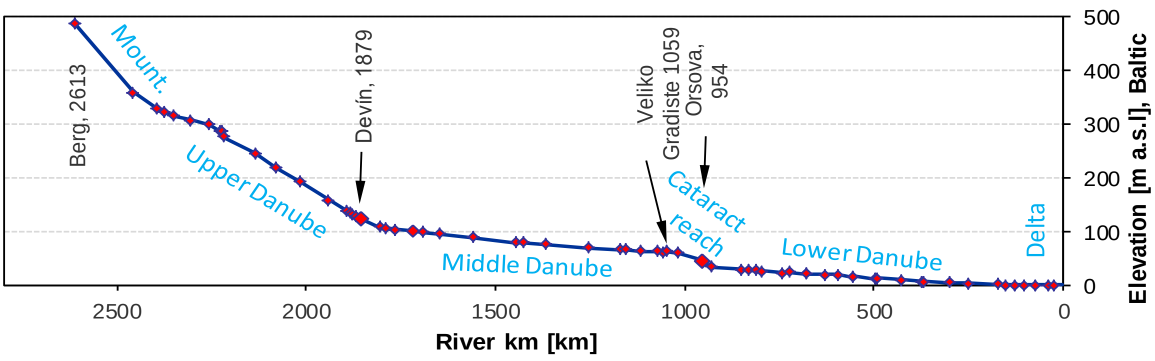

Fig. 1.6a *The major Danube River sections.*

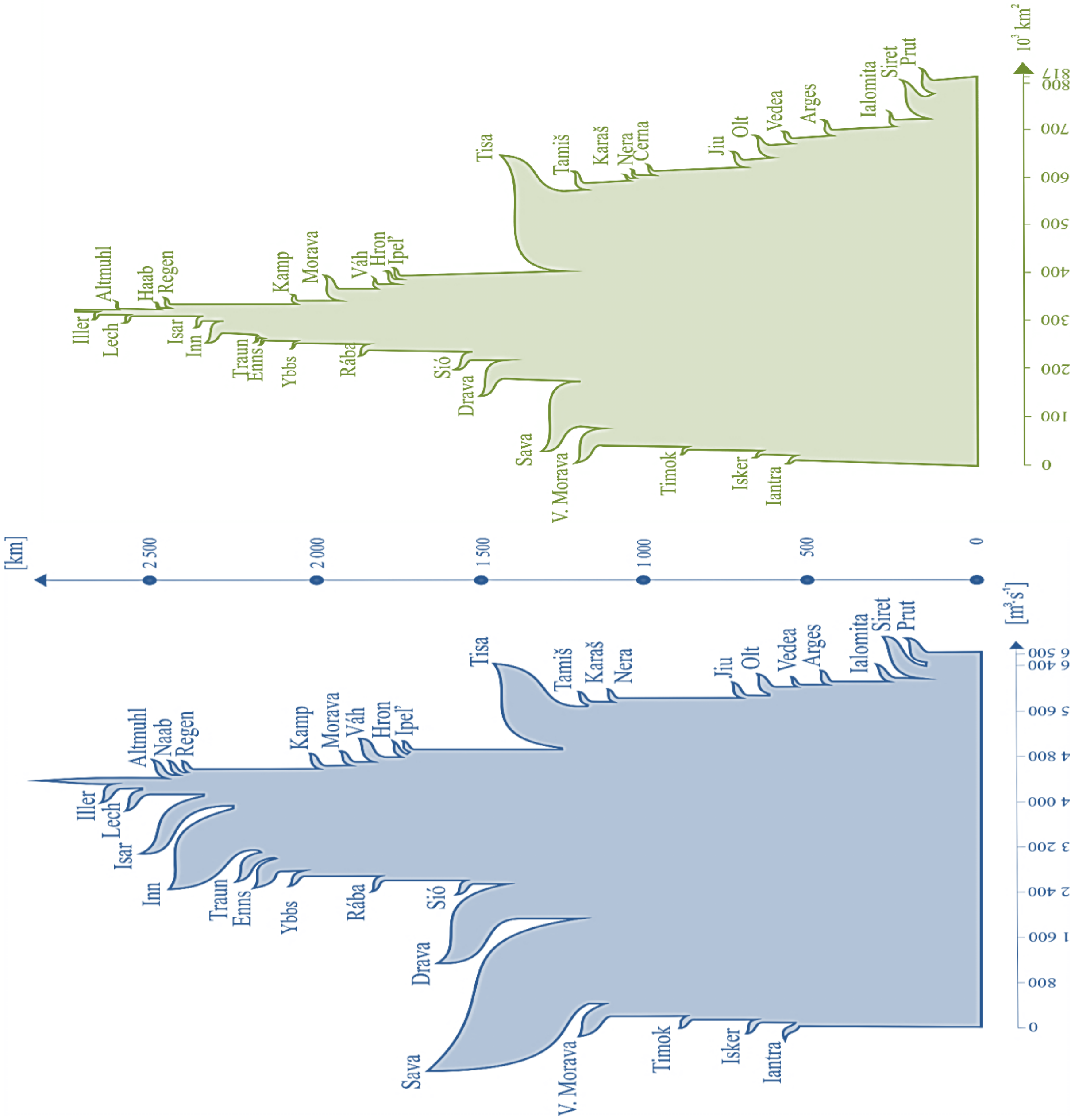

Fig. 1.6b *The Danube and its tributaries, areas of sub-basins and long term discharge.*

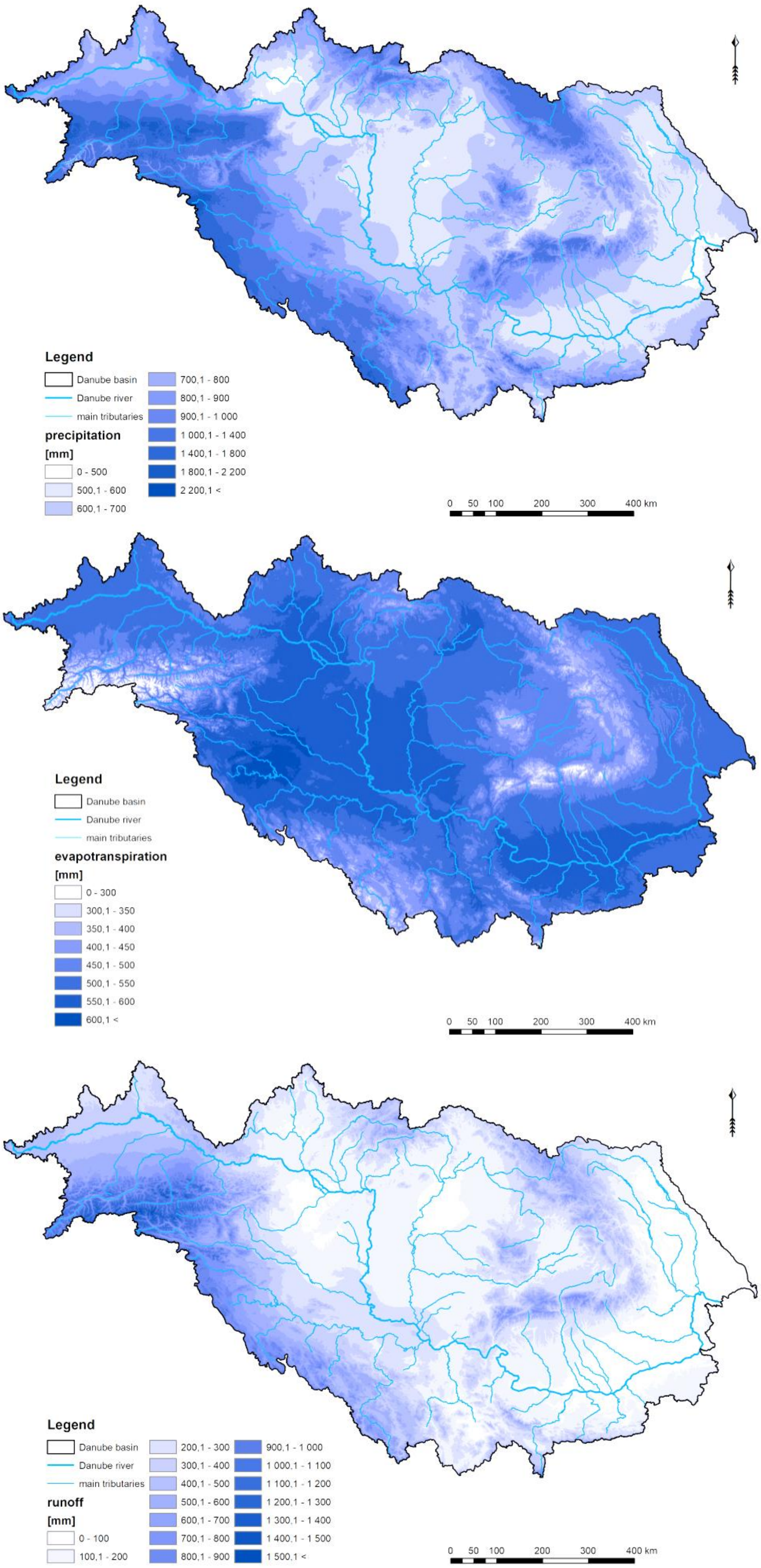

Fig. 1.7 Precipitation, evapotranspiration and runoff in the Danube basin, 1960–1990 adapted from Petrovič et al., (2006).

– According to Petrovič et al. (2006), the mean annual actual evapotranspiration estimated on data from 1961 to 1990 varied between 179 mm and 618 mm (Fig. 1.7b).
– Figure 1.7c presents the map of mean annual runoff during the period 1960–1990 (Petrovič et al., 2006). The minimum and maximum values in the map are 14 mm and 1584 mm, respectively.

1.2.1 The Danube discharge data

An effective investigation of the natural runoff variability at any of the river gauging stations inevitably requires reliable and long records of river flow observations. An example of long-term runoff variability is depicted in Figs. 1.8. The catchment area should be large enough to eliminate the effect of local runoff fluctuation. As mentioned earlier, such catchments with anthropogenic impacts on runoff such as water transfers to neighboring catchments, and reservoirs for multiannual runoff control, should be disqualified from analysis.

In accordance with the objective O1 (see Fig. 1.4) of the Project proposal, we created a database of mean daily discharges and annual maximum discharges from 20 selected stations on the Danube River (Fig. 1.9, Table 1.1) with high quality and long-term data series, and additional 60 time series of relatively anthropogenically unaffected rivers within the Danube basin (Table 1.2). Discharge from five gauges were affected significantly. This represents data from 65 river gauging stations located on Danube tributaries and 20 stations on the river Danube itself. All available data have been acquired as mean daily series, and maximum annual discharge series (see the data on the enclosed CD).

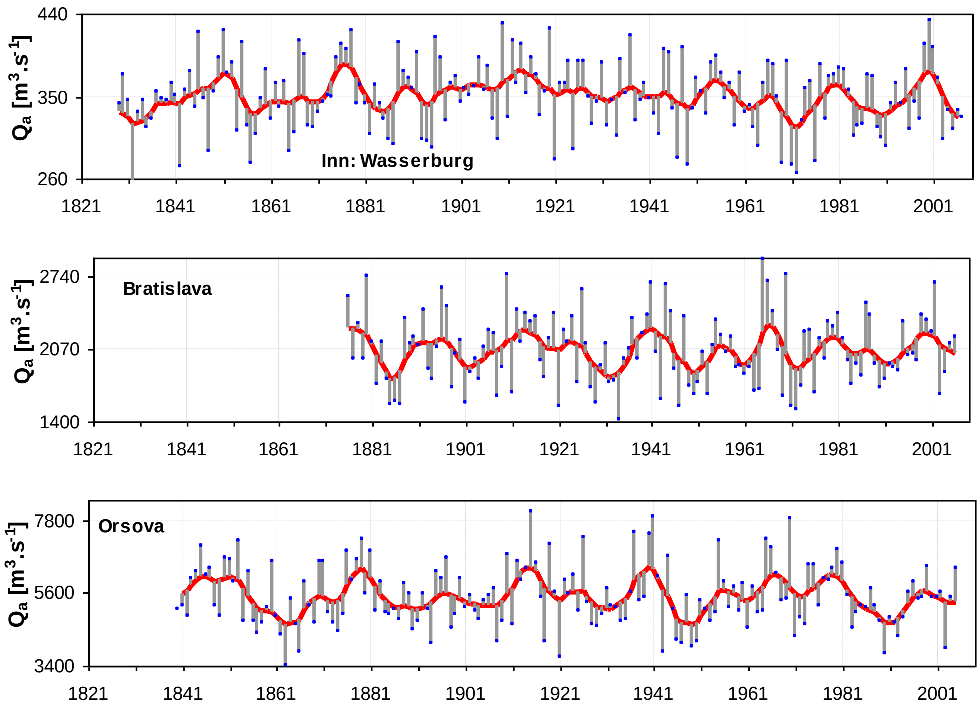

Fig. 1.8 *Average annual discharge in selected stations (blue points), deviations from double 5-years moving averages (bold red line).*

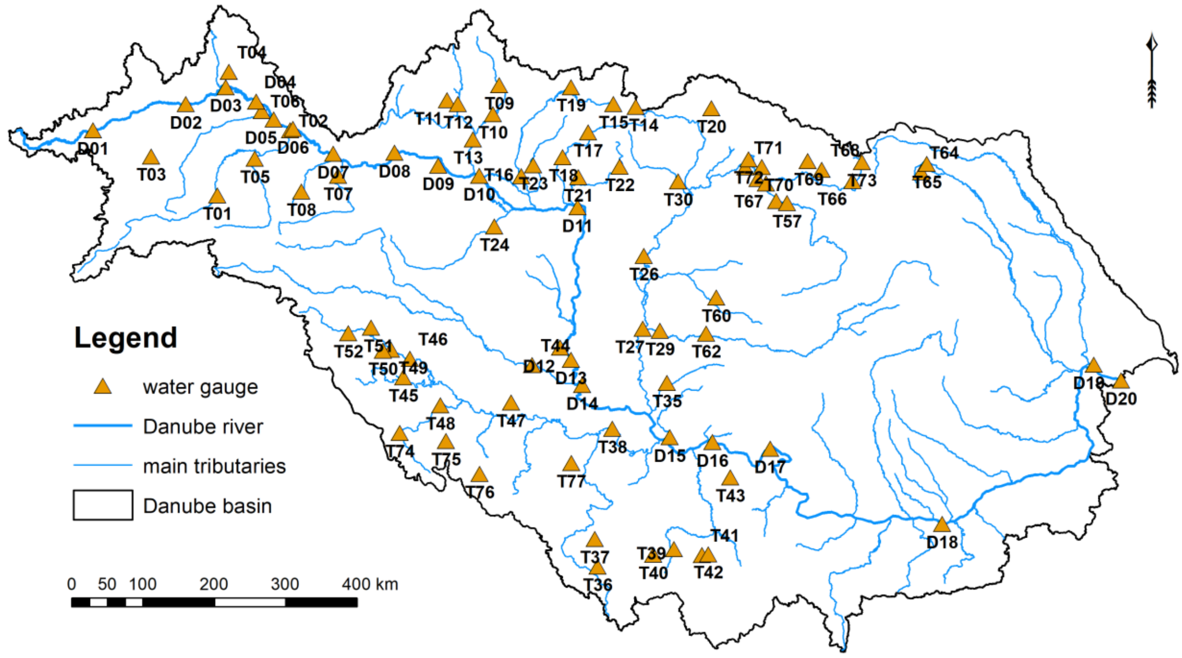

Fig.1.9 Water gauges on the Danube River and on the Danube tributaries.

Table 1.1. List of selected stations on the Danube River, *Qa* – mean annual discharge, *V* – annual runoff volume, *R* – runoff depth, period 1931–2005

	RIVER	GAUGE	COUNTRY	AREA [km²]	LAT	LONG	ALTITUDE [m a.s.l.]	Q_a [m³/s]	*V* 10⁹ [m³/y]	*R* [mm/y]
D01	Danube	Berg	GE	4047	48.27	9.73	489.9	38.0	1.20	296
D02	Danube	Ingolstadt	GE	20001	48.75	11.42	360.4	313.0	9.87	494
D03	Danube	Regensburg-Schwabelweis	GE	35399	49.02	12.14	324.5	444.0	14.00	396
D04	Danube	Pfelling	GE	37687	48.88	12.75	308.2	468.8	14.78	392
D05	Danube	Hofkirchen	GE	47496	48.68	13.12	299.6	640.0	20.18	425
D06	Danube	Achleiten	GE	76653	48.58	13.50	288.0	1428.0	45.03	587
D07	Danube	Linz	AT	79490	48.31	14.30	248.2	1464.0	46.17	581
D08	Danube	Stein-Krems / Kienstock	AT	96045	48.38	15.46	189.5	1892.0	59.67	621
D09	Danube	Wien-Nussdorf	AT	101700	48.25	16.30	157.0	1920.4	60.56	596
D10	Danube	Bratislava / Devín	SK	131338	48.14	17.11	129.3	2050.0	64.65	492
D11	Danube	Nagymaros	HU	183534	47.78	18.95	99.8	2336.0	73.67	401
D12	Danube	Mohács	HU	209064	46.00	18.67	79.4	2354.0	74.24	355
D13	Danube	Bezdan	SR	210250	45.85	18.87	81.1	2357.0	74.33	354
D14	Danube	Bogojevo	SR	251593	45.53	19.08	78.0	2893.0	91.23	363
D15	Danube	Pancevo	SR	525009	44.87	20.64	67.8	5320.0	167.77	320
D16	Danube	Veliko Gradiste	SR	570375	44.80	21.40	62.7	5560.0	175.34	307
D17	Danube	Orsova / Turnu Severin	RO	576232	44.70	22.42	44.4	5602.0	176.66	307
D18	Danube	Zimnicea	RO	658400	43.63	25.36	16.2	6007.0	189.44	288
D19	Danube	Reni	UKR	805700	45.45	28.27	4.0	6702.0	211.35	262
D20	Danube	Ceatal Izmail	RO	807000	45.22	28.73	0.6	6415.0	202.30	251

Table 1.2. List of selected stations on the Danube tributaries

		RIVER	GAUGE	COUNTRY	AREA [km²]	LAT	LONG	ALTITUDE [m a.s.l.]	Q_a [m³/s]	V 10^9 [m³/y]	R [mm/y]
1	T01	Inn	Oberaudorf	GE	9712	47.65	12.20	464.0	354.0	11.16	1150
2	T02	Inn	Passau-Ingling	GE	26084	48.56	13.45	289.2	740.0	23.34	895
3	T03	Lech	Landsberg	GE	2295	48.04	10.88	582.3	83.0	2.62	1141
4	T04	Regen	Regenstauf	GE	2658	49.22	12.17	337.0	38.0	1.20	451
5	T05	Salzach	Burghausen	GE	6649	48.16	12.83	352.0	259.5	8.18	1231
6	T06	Issar	Plattling	GE	8839	48.77	12.88	316.0	175.0	5.52	624
7	T07	Enns	Steyr	AT	5915	48.04	14.43	284.0	200.2	6.31	1067
8	T08	Traun	Ebensee	AT	1258	47.80	13.76	422.2	64.0	2.02	1604
9	T09	Morava	Kromeriz	CZ	7014	49.3	17.4	184.2	51.3	1.62	231
10	T10	Morava	Straznice	CZ	9147	48.93	17.3	163.3	59.6	1.88	205
11	T11	Jihlava	Ivancice	CZ	2681	49.08	16.41	194.0	11.5	0.36	135
12	T12	Svratka	Zidlochovice	CZ	3939	49.04	16.62	178.0	15.4	0.49	123
13	T13	Morava	Mor.Sv.Jan	SK	24129	48.60	16.94	146.0	107.6	3.39	141
14	T14	Bela	Podbanske	SK	93	49.14	19.90	922.7	3.0	0.09	1017
15	T15	Vah	L. Mikulas	SK	1107	49.09	19.61	568.0	20.6	0.65	586
16	T16	Vah	Sala	SK	11218	48.16	17.88	109.0	145.7	4.60	410
17	T17	Hron	B. Bystrica	SK	1766	48.73	19.13	334.0	24.5	0.77	437
18	T18	Hron	Brehy	SK	3821	48.41	18.65	195.0	47.2	1.49	390
19	T19	Kysuca	Kysucke N. Mesto	SK	955	49.30	18.79	346.0	16.4	0.52	542
20	T20	Topla	Hanusovce	SK	1050	49.03	21.50	160.4	8.0	0.25	239
21	T21	Krupinica	Plastovce	SK	303	48.16	18.96	139.5	2.0	0.06	208
22	T22	Ipel	Holisa	SK	686	48.30	19.74	172.0	3.1	0.10	144
23	T23	Nitra	Nitrianska Streda	SK	2094	48.30	18.10	158.3	14.7	0.46	221
24	T24	Raba	Arpas	HU	6610	47.51	17.40	113.13	34.0	1.07	162
25	T25	Tisza	Vasarosnameny	HU	25100	48.12	22.34	102,0	361.0	11.38	454
26	T26	Tisza	Szolnok	HU	73113	47.17	20.19	78.78	539.0	17.00	232
27	T27	Tisza	Szeged	HU	138408	46.25	20.17	74.0	828.3	26.12	189
28	T28	Szamos	Csenger	HU	15283	47.83	22.68	113.0	127.3	4.01	263
29	T29	Maros	Mako	HU	30149	46.22	20.48	80.0	173.1	5.46	181
30	T30	Sajo	Felsoezsolca	HU	6440	48.11	20.84	107.0	30.6	0.96	150
31	T35	Tisza	Senta	SR	141715	45.56	20.06	73	798.0	25.17	178
32	T36	Lim	Prijepolje	SR	3160	43.23	19.38	442	78.0	2.46	778
33	T37	Drina	Bajina Basta	SR	14797	43.58	19.33	211	340.0	10.72	725
34	T38	Sava	Sremska Mitrovica	SR	87966	44.98	19.62	72	1560.0	49.20	559
35	T39	Moravica	Arilje	SR	832	43.45	20.07	322	11.0	0.35	417
36	T40	Ibar	Lopatnica Lakat	SR	7818	43.38	20.34	225	57.0	1.80	230
37	T41	Zapadna Morava	Jasika	SR	14721	43.37	21.18	139	104.0	3.28	223
38	T42	Juzna Morava	Mojsinje	SR	15390	43.38	21.29	136	93.0	2.93	191
39	T43	Velika Morava	Ljubicevski most	SR	37320	44.35	21.07	73	230.0	7.25	194
40	T44	Drava	Donji Miholjac	HR	37142	45.77	18.17	88.5	538.0	16.97	457
41	T45	Kupa	Jamnicka Kiselica	HR	6877	45.55	15.86	100.8	175.0	5.52	803
42	T46	Sava	Zagreb (incl. Catez)	HR	12450	45.79	15.96	112,3	311.0	9.81	788
43	T47	Orljava	Pleternica Most	HR	745	45.29	17.81	113.8	5.2	0.16	221
44	T48	Una	Kostajnica	HR	8876	45.22	16.55	103.2	232.0	7.32	824
45	T49	Sava	Čatež	SI	10186	45.89	15.61	137,3	282.0	8.89	873
46	T50	Krka	Podbočje	SI	2238	45.87	15.47	146	55.0	1.73	775
47	T51	Savinja	Laško	SI	1663	46.15	15.23	215	41.8	1.32	792
48	T52	Sava	Litija	SI	4821	46.06	14.82	230	168.0	5.30	1099
49	T57	Szamos	Satu Mare	RO	15388	47.80	22.88	127.0	126.1	3.98	259
50	T60	Crisul Negru	Zerind	RO	3702	46.63	21.52	1872.0	29.4	0.93	250
51	T62	Maros	Arad	RO	27280	46.18	21.32	618.0	169.5	5.34	196
52	T64	Siret	Storozhinec	UKR	672	48.09	25.43	356	6.0	0.19	282
53	T65	Prut	Chernivcy	UKR	6890	48.19	25.55	165	74.0	2.33	339
54	T66	Tisza	Rakhiv	UKR	1070	48.04	24.13	435	25.0	0.79	737
55	T67	Tisza	Vylok	UKR	9140	48.06	22.50	118	210.0	6.62	725
56	T68	Teresva	Ust-Chorna	UKR	572	48.20	23.56	524	19.0	0.60	1048
57	T69	Rika	Mizhhirya	UKR	550	48.32	23.30	439	14.0	0.44	803
58	T70	Latorycya	Mucacheve	UKR	1360	48.27	22.43	123	26.0	0.82	603
59	T71	Latorycya	Chop	UKR	2870	48.27	22.12	105	36.0	1.14	396
60	T72	Uzh	Uzhhorod	UKR	1970	48.37	22.18	114	29.0	0.91	464
61	T73	Prut	Jaremcha	UKR	597	48.27	24.33	507	12.0	0.38	634
62	T74	Una	Kralje	BA	3536	44.84	15.85	209	98.0	3.09	874
63	T75	Sana	Sanski Most	BA	2008	44.77	16.68	156	68.0	2.14	1068
64	T76	Vrbas	Kozluk Jajce	BA	3161	44.37	17.29	342	29.0	0.91	289
65	T77	Bosna	Maglaj	BA	6619	44.54	18.09	150	130.0	4.10	619

1.2.1.1 Example of the gap-filling in daily flow records of the Danube at Bratislava for 1876–1890

According to Horváthová (2003), the first observations of water stages on the river Danube started at Komárno in 1805, then at Vienna in 1821 (Lauda et al, 1809). The first water level gauge (stage recorder) on the Romanian section of the Danube was installed during the Austro-Hungarian Empire at Orsova in 1838 (Bondar and Iordache, 2017).

To evaluate the hydrological regime of the upper part of the Danube River, the average values of daily discharge taken at the Bratislava/Devín gauge were used. The Slovakia's part of the Danube River spans from the mouth of the Ipeľ River at the 1708.2 river km to the mouth of the Morava River 1880.2 rkm with a total length of 172 km. Upstream of the Bratislava gauge (1868.8 r km), the Danube drains an area of 131,338 km^2.
First water level measurements on the Danube River at Bratislava were made in 1823. The gauge datum was located at 131.08 m J (Adria system) (Fig. 1.10). After 1876 the average daily river stages were recorded in Hungarian yearbooks Vízállások (1890) (Fig. 1.11a). In 1942, the Bratislava gauge datum was lowered by two meters down to 129.08 m J (Adria system). After 1964, the gauge datum was determined at 128.46 m B.p.v (Baltic system).

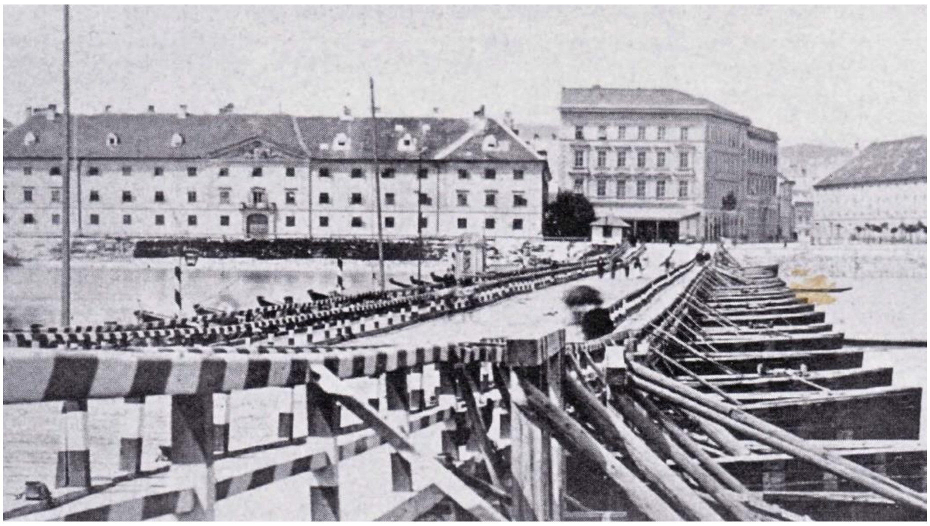

a) 1870

b) 2007

Fig. 1.10 a) Water gauge in Bratislava in 1870. (Photo Korper, 1870)
b) Water gauge in Bratislava in July 2007. (Photo Pekárová, 2007).

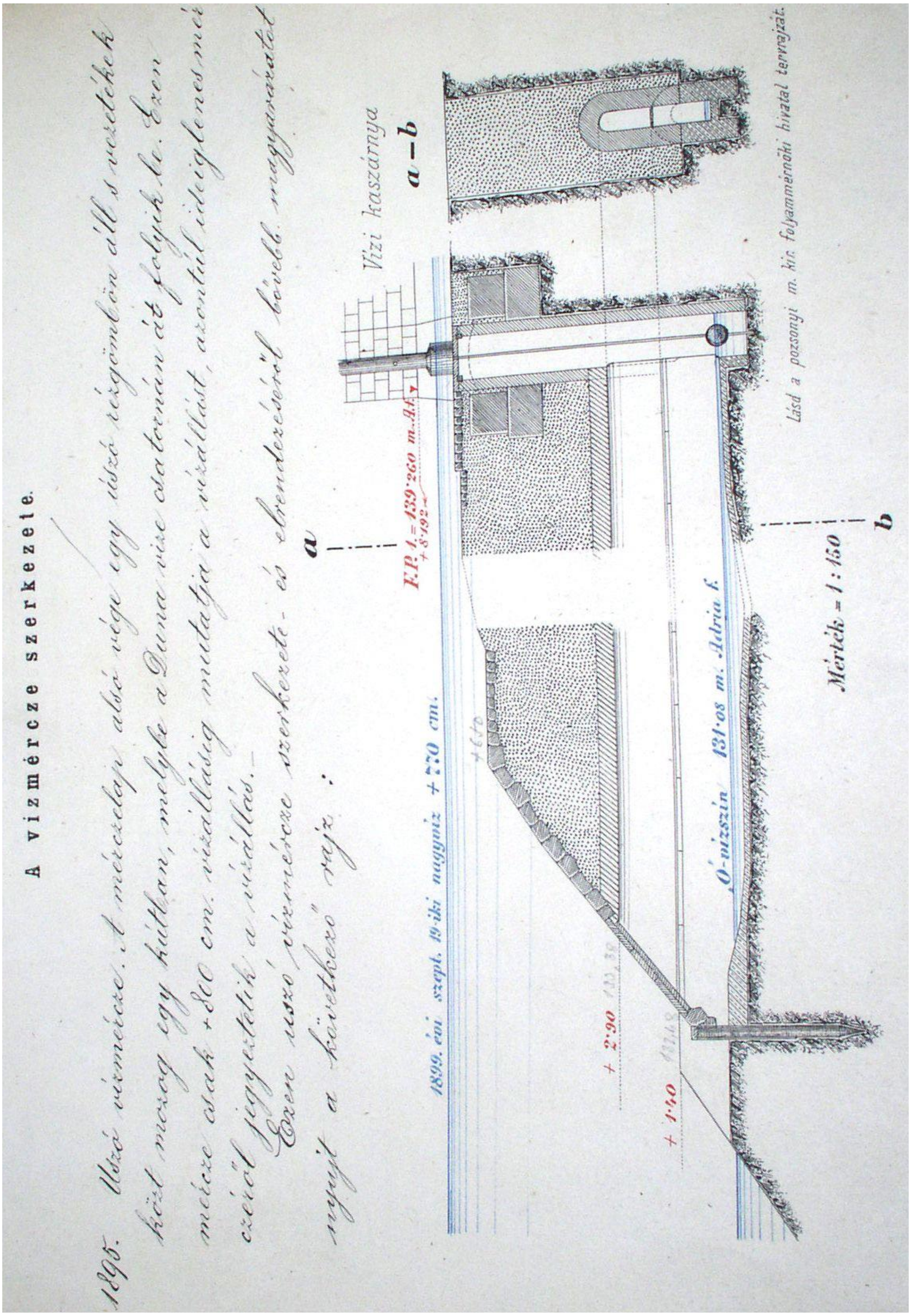

Fig. 1.11a Schematics of the river stage gauge at Bratislava, 1895 (from VITUKI's archives, photo: Miklánek, 2005).

First discharge observations at Bratislava, based on measurements of flow velocities, were made in 1882 (Škoda and Turbek, 1995; Svoboda et al., 2000). The observations revealed that the river channel at Bratislava was subject to scouring long time before the river was dammed at the town of Čuňovo (due to construction of the Gabčíkovo Hydro Project) in 1992. Deepening of the river's channel bottom can be assessed from the changes in the rating curve, as shown in Fig. 1.12 (Mitková, 2002; Miklánek et al., 2002).

Water level measurements on the Danube River at Bratislava have been routinely processed since 1901. In 2003, the staff of the SHMI (Slovak Hydrometeorological Institute) extended the average daily discharge series by adding data from 1891–1900.

In 2007, the average daily flow records were extended by adding another series of 15-years capturing discharge between 1876 and 1890 (Pekárová et al., 2007a). The historical rating curve (Fig. 1.12), valid before 1903 (according to Zatkalík (1965) and Pacl (1955)), was approximated by two third-order polynomials. The average daily water stages for this period were obtained from data sets recorded in archive yearbooks (Vízállások, 1890). Using discharges (Q) and water stages (WS) for gauge heights below 480 cm, and above 480 cm, the following equations were derived:

$$Q = -0.0000077\, WS^3 + 0.02018\, WS^2 - 3.86\, WS + 597.366, \quad \text{for } WS \leq 480 \tag{1.1}$$

$$Q = 0.0000016\, WS^3 + 0.0098\, WS^2 + 0.0978\, WS + 52.69, \quad \text{for } WS > 480. \tag{1.2}$$

The average daily water stages were converted into average daily discharges for the period of fifteen years (1876–1890) for a detailed statistical analysis of changes in the runoff regime.

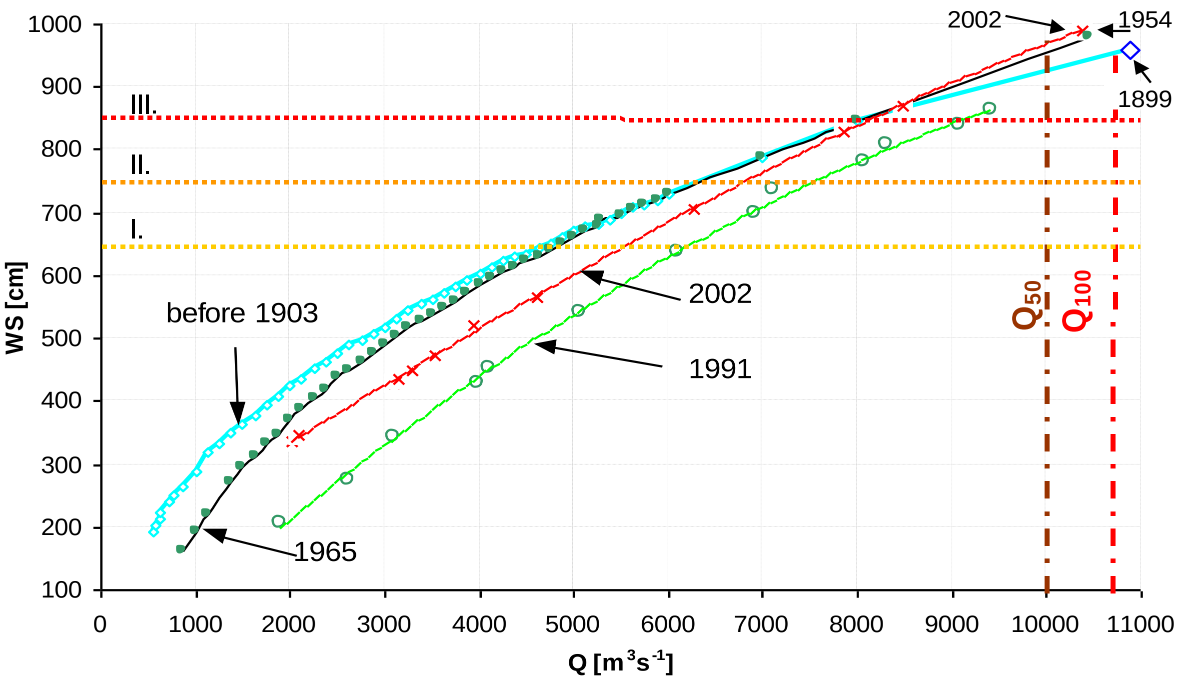

Fig.1.12 Changes of the Danube rating curve at Bratislava gauge (related to the present gauge zero datum).

1.3 Data structure

Input data used in this Follow-up volume (Volume IX) of the Hydrological Monograph of the Danube River Basin were prepared by the individual National Committees of IHP UNESCO of the Danube Basin countries for their respective stations and opened up for preparation of the follow-up volume. Any use of the data for other purpose than Regional collaboration of the Danube countries is subject to approval of the respective National Committee of IHP UNESCO.

The data were use within the frame of the Danube countries cooperation (International Hydrological Programme UNESCO, project No. 9, Flood regime of rivers in the Danube River basin). The data were burned on separate CD ROM which was supplied to all participating NC IHP UNESCO committees and it is not part of this follow-up volume.

Appendices

The outcomes of basic data processing and analysis are presented in the form of various tables and graphs in PDF format:

- Daily data, APPENDIX I.1,
- Annual data, APPENDIX I.2,
- Annual maximum data, APPENDIX I.3,
- Analysis of homogeneity, APPENDIX III,
- Monthly data, APPENDIX V,
- LP3 distribution functions – Design values APPENDIX VI,
- Coincidence of maximum annual discharges APPENDIX VII,
- Theoretical flood hydrographs APPENDIX VIII.

They contain primary statistical processing of the collected data and their numerical and graphical interpretation, for all of the analysed gauging stations.

In the following lines we present several examples of statistical analysis (Tables and graphs) for four Danube stations: Hofkirchen, Bratislava, Orsova, and Reni with daily discharge (Figs. 1.13a-d), annual discharge (Figs. 1.14a-d), and annual maximum discharge (Figs. 1.15a-d).

Explanation of the daily data analysis (Figs. 1.13a-d)

The symbols used in the upper tables embedded within Figs. 1.13a-d are as follows: Q stands for long-term annual discharge, q is long-term specific discharge, R is long-term annual runoff depth, c_s is coefficient of asymmetry, and c_v is coefficient of variability of the daily discharges.

The upper-most figure shows daily discharge and 4-years moving averages of the daily discharge for the whole observation period. The second figure depicts the long-term percentiles of daily discharge. Percentile P50 denotes the median of daily discharge. The third figure shows M-days discharges. The rest of the analysed stations are presented in the APPENDIX I.1.

Explanation of the annual data analysis (Figs. 1.14a-d)

The basic characteristics of annual data are indicated in tables embedded within Figs. 1.14a-d and a subsequent graphs generated for the average annual discharge. Symbols are the same as in the case of the daily data. The rest of the analysed stations are presented in the APPENDIX I.2.

Explanation of the Q_{max} *data analysis* (Figs. 1.15a-d)

The basic characteristics in tables and graphs are presented for annual maxima of discharge series. The rest of the analysed stations are presented in the APPENDIX I.3.

Daily discharge Danube - Hofkirchen

Area	47496	km^2
First Year	1901	
Last Year	2013	

Basic statistical characteristics

	mean	min	max	330-day	30-day	cs	cv
Q $[m^3s^{-1}]$	638	165	3450	338	1070	1.9	0.5
q $[l.s^{-1}km^{-2}]$	13.4	3.5	72.6	7.1	22.5		
R [mm]	423.7						

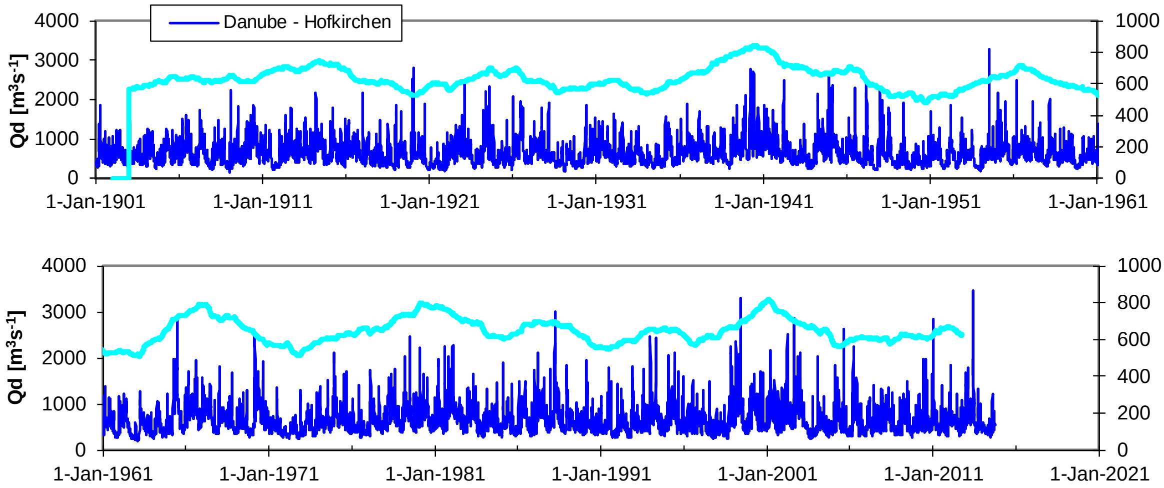

Fig. 1. Daily discharge and 4-years moving averages.

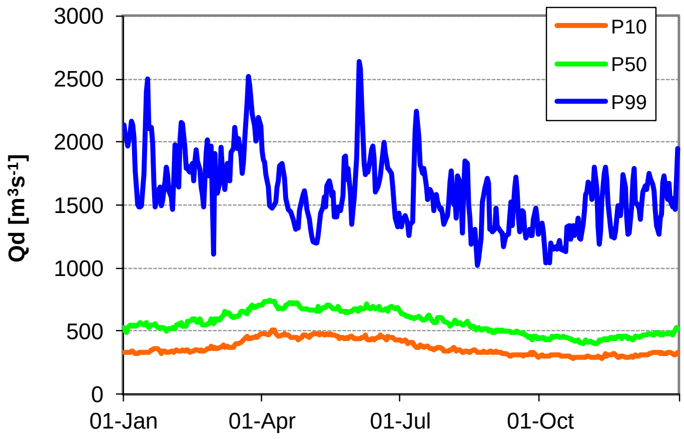

Fig. 2. Long-term percentiles of daily discharge.

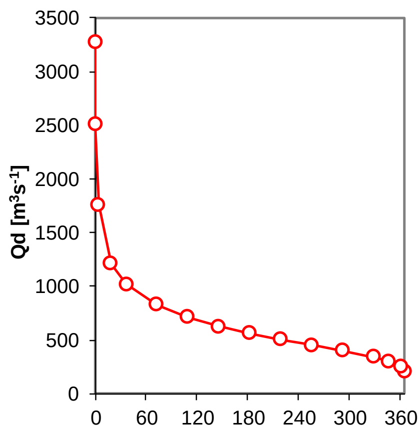

Fig. 3. M-days water.

Fig. 1.13a Basic data analysis of daily discharge at station Hofkirchen. Table: Q - long-term annual discharge, q - long-term specific discharge, R - long-term annual runoff depth, cs - coefficient of asymmetry, cv - coefficient of variability of the daily discharges. Figures 1-3: 1) Daily discharge and 4-years moving averages of the daily discharge for the whole period; 2) The long-term percentiles of daily discharge; 3) M-days discharges.

Daily discharge — Danube - Bratislava

Area	131338 km^2
First Year	1876
Last Year	2016

Basic statistical characteristics

	mean	min	max	330-day	30-day	cs	cv
Q [m^{3}s^{-1}]	2054	580	10810	1043	3428	1.7	0.48
q [l.s^{-1}km^{-2}]	15.6	4.4	82.3	7.9	26.1		
R [mm]	493.1						

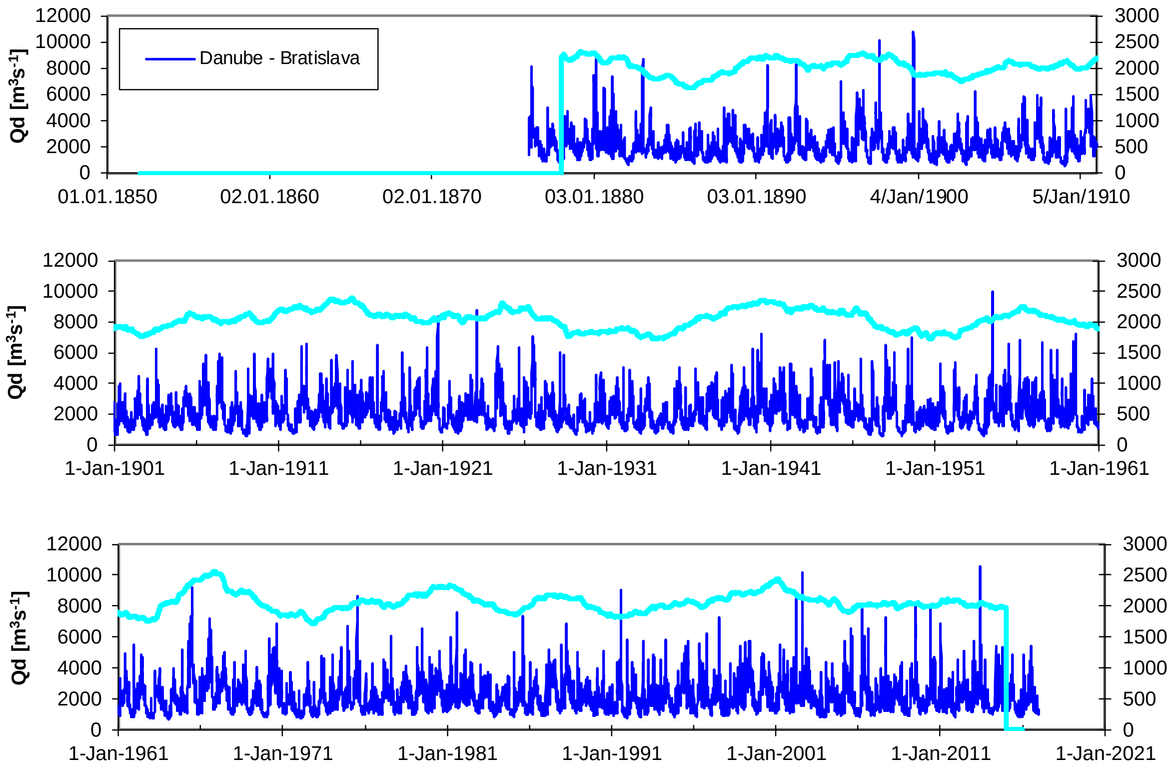

Fig. 1. Daily discharge and 4-years moving averages.

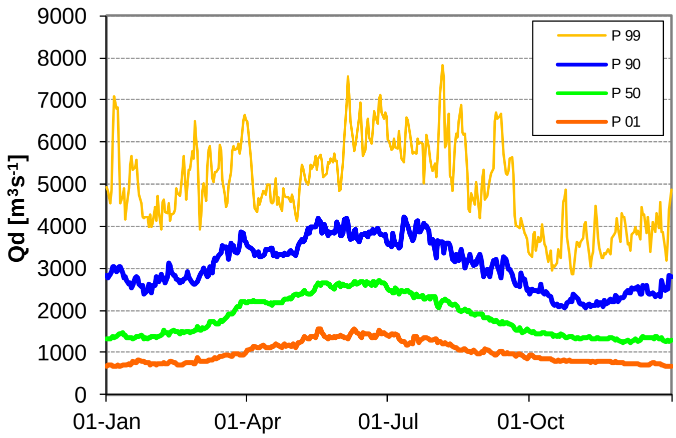

Fig. 2. Long-term percentiles of daily discharge.

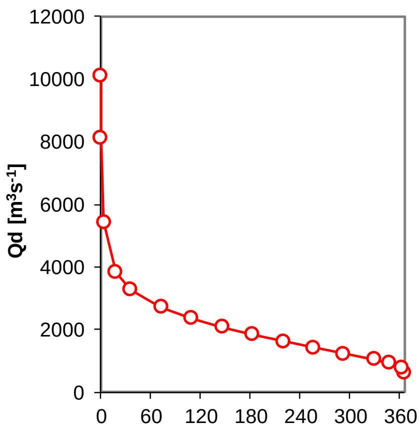

Fig. 3. M-days water.

Fig. 1.13b Basic data analysis of the daily discharge at station Bratislava. Table: Q - long-term annual discharge, q - long-term specific discharge, R - long-term annual runoff depth, cs - coefficient of asymmetry, cv - coefficient of variability of the daily discharges. Figures 1-3: 1) Daily discharge and 4-years moving averages of the daily discharge for the whole period; 2) The long-term percentiles of daily discharge; 3) M-days discharges.

Daily discharge Danube - Orsova

Area	576232 km^2
First Year	1850
Last Year	2005

Basic statistical characteristics

	mean	min	max	330-day	30-day	cs	cv
Q [m^{3}s^{-1}]	5565	1060	15092	2760	9020	0.7	0.4
q [l.s^{-1}km^{-2}]	9.7	1.8	26.2	4.8	15.7		
R [mm]	304.6						

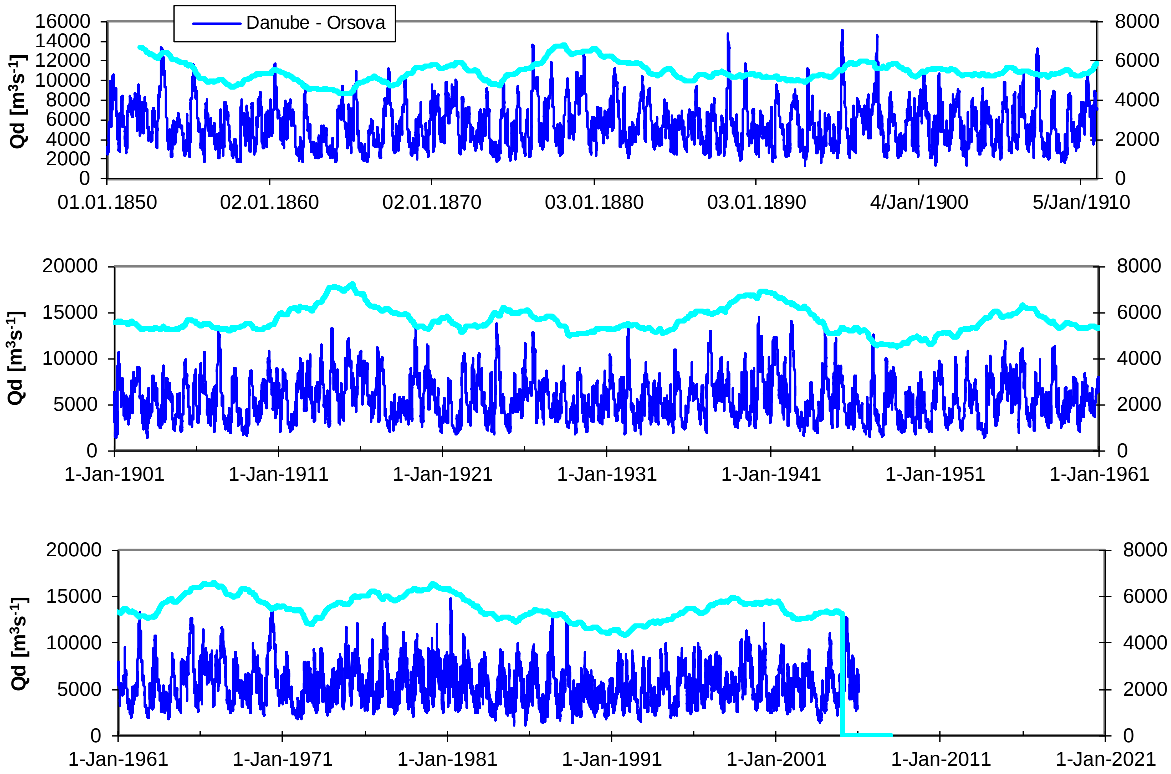

Fig. 1. Daily discharge and 4-years moving averages.

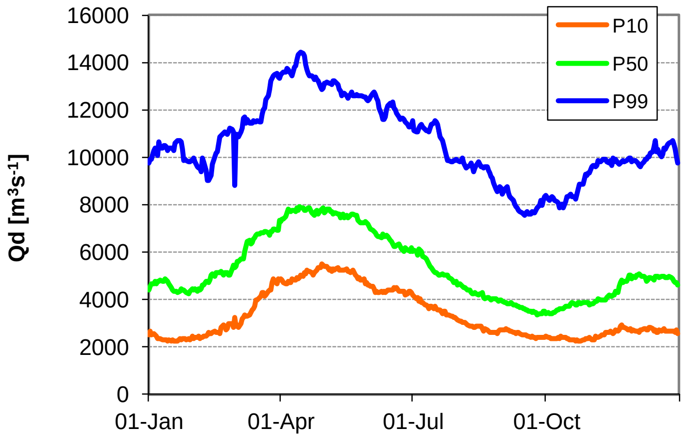

Fig. 2. Long-term percentiles of daily discharge.

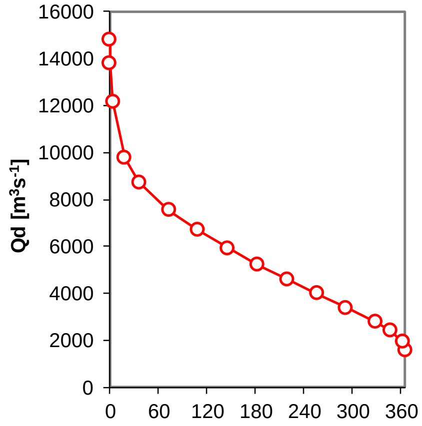

Fig. 3. M-days water.

Fig. 1.13c Basic data analysis of the daily discharge at station Orsova. Table: Q - long-term annual discharge, q - long-term specific discharge, R - long-term annual runoff depth, cs - coefficient of asymmetry, cv - coefficient of variability of the daily discharges. Figures 1-3: 1) Daily discharge and 4-years moving averages of the daily discharge for the whole period; 2) The long-term percentiles of daily discharge; 3) M-days discharges.

Daily discharge Danube-Reni

Area	805700	km^2
First Year	1921	
Last Year	2015	

Basic statistical characteristics

	mean	min	max	330-day	30-day	cs	cv
Q $[m^3s^{-1}]$	6539	1280	15900	3260	10800	0.6	0.4
q $[l.s^{-1}km^{-2}]$	8.1	1.6	19.7	4.0	13.4		
R [mm]	255.9						

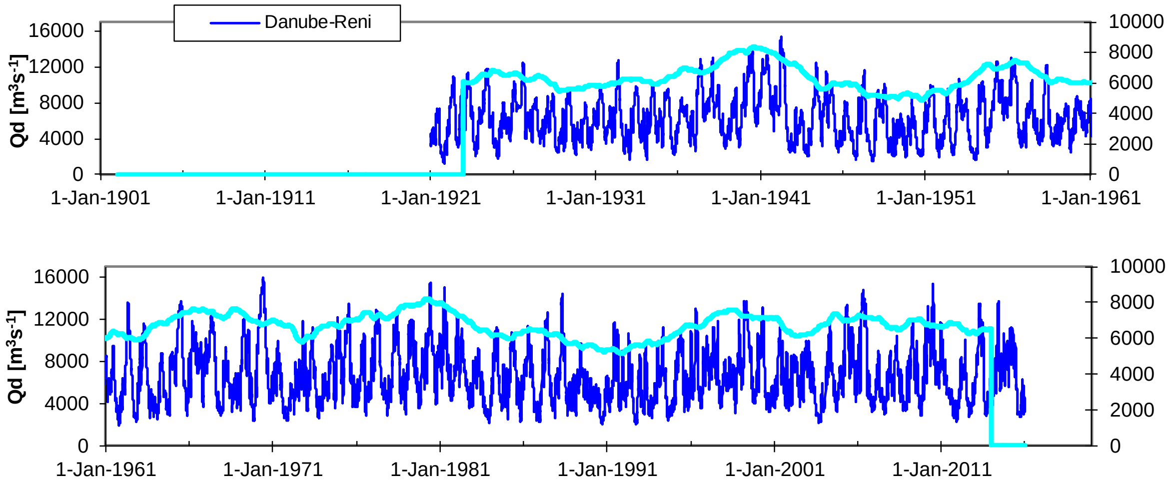

Fig. 1. Daily discharge and 4-years moving averages.

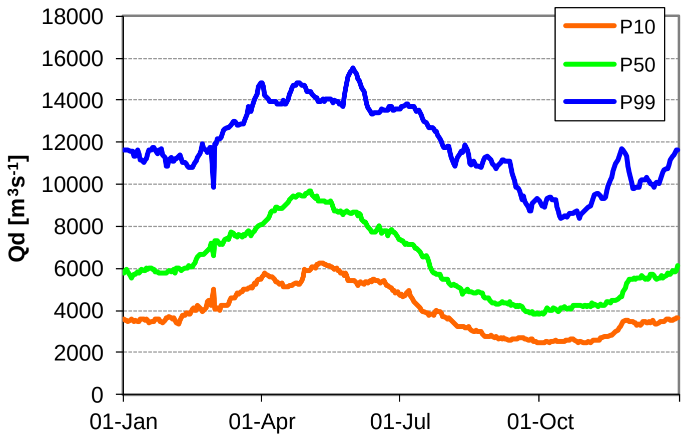

Fig. 2. Long-term percentiles of daily discharge.

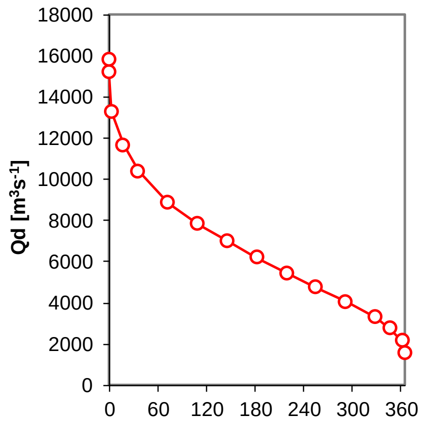

Fig. 3. M-days water.

Fig. 1.13d Basic data analysis of the daily discharge at station Reni. Table: Q - long-term annual discharge, q - long-term specific discharge, R - long-term annual runoff depth, cs - coefficient of asymmetry, cv - coefficient of variability of the daily discharges. Figures 1-3: 1) Daily discharge and 4-years moving averages of the daily discharge for the whole period; 2) The long-term percentiles of daily discharge; 3) M-days discharges.

River: Danube **Station: Hofkirchen** **Area: 47.496** 10^3 km^2 **GE**

Basic statistical characteristics

	Qa	qa	Qmin	Qmax	cs	cv	Med.	trend	Hurst
	m3/s	l/s/km2	m3/s	m3/s			m3/s		
1900-2010	**639**	**13.5**	**343**	**924**	**0.21**	**0.19**	**628**	**0.2514**	**0.548**

Period	Qa	qa	Qmin	Qmax	cs	cv
1871-1880						
1881-1890						
1891-1900						
1901-1910	622	13.1	540	851	1.70	0.16
1911-1920	647	13.6	488	757	-0.72	0.15
1921-1930	600	12.6	**343**	786	-0.33	0.26
1931-1940	673	14.2	415	908	-0.03	0.22
1941-1950	633	13.3	427	**924**	0.41	0.27
1951-1960	610	12.8	495	734	0.06	0.14
1961-1970	664	14.0	479	871	0.30	0.24
1971-1980	623	13.1	417	787	-0.36	0.21
1981-1990	671	14.1	558	819	0.35	0.15
1991-2000	635	13.4	508	803	0.52	0.17
2001-2010	646	13.6	535	916	1.70	0.18

Period	Qa	St.dev	qa	cs	cv
1886-1915	641	101	13.5	0.45	0.16
1901-1930	623	117	13.1	-0.26	0.19
1916-1945	646	148	13.6	-0.03	0.23
1931-1960	639	138	13.4	0.36	0.22
1946-1975	610	128	12.8	0.51	0.21
1961-1990	652	131	13.7	0.07	0.20
1976-2005	661	114	13.9	0.34	0.17

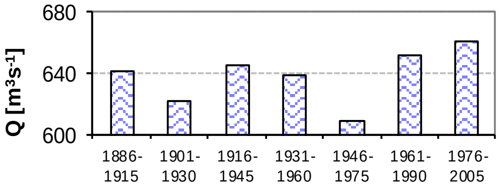

Long term 30-year discharge.

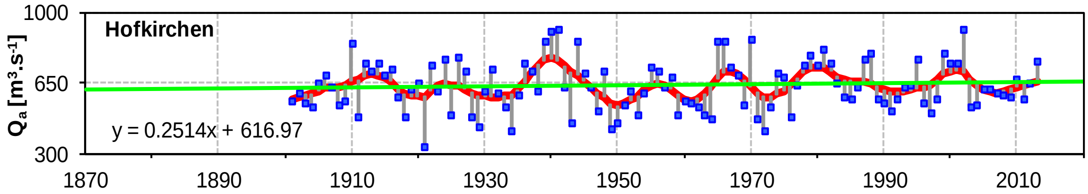

Maximum annual discharge, differences from 7-year moving averages.

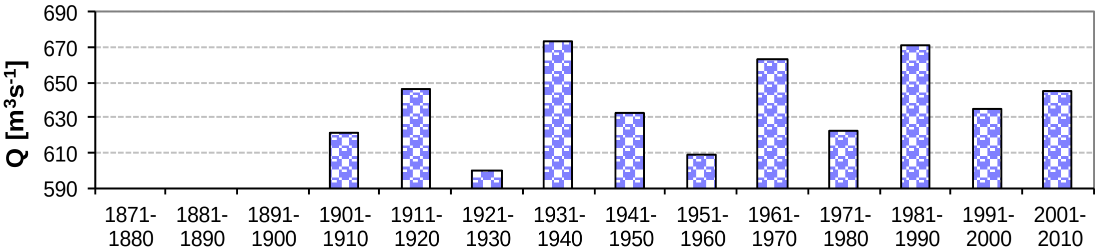

Long term 10-year discharge.

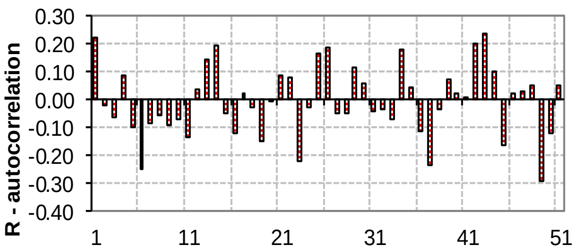

Autocorrelogram of yearly discharge.

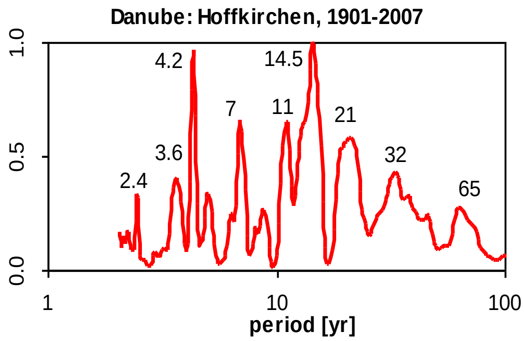

Fig. 1.14a Basic data analysis of the average yearly discharge at station Hofkirchen. Figures: Long-term 30-year discharge, Average annual discharge – differences from 7-year moving averages, Long-term 10-year discharges, Autocorrelogram and combined periodogram of annual discharge.

River: Danube **Station: Bratislava** **Area: 131.338** 10^3 km^2 **SK**

Basic statistical characteristics

	Qa	qa	Qmin	Qmax	cs	cv	Med.	trend	Hurst
	m3/s	l/s/km2	m3/s	m3/s			m3/s		
1876-2016	**2054**	**15.6**	**1420**	**2910**	**0.34**	**0.16**	**2035**	**-0.2428**	**0.515**

Period	Qa	qa	Qmin	Qmax	cs	cv
1871-1880						
1881-1890	1917	14.6	1556	2360	-0.01	0.16
1891-1900	2131	16.2	1716	2635	0.34	0.14
1901-1910	2003	15.3	1575	2768	1.08	0.17
1911-1920	2169	16.5	1666	2438	-0.86	0.13
1921-1930	2001	15.2	1543	2621	0.28	0.18
1931-1940	2007	15.3	**1420**	2393	-0.61	0.15
1941-1950	2061	15.7	1543	2688	0.33	0.22
1951-1960	2015	15.3	1657	2342	-0.27	0.10
1961-1970	2161	16.5	1634	**2910**	0.48	0.23
1971-1980	1968	15.0	1511	2331	-0.36	0.17
1981-1990	2059	15.7	1719	2499	0.47	0.14
1991-2000	2057	15.7	1789	2387	0.65	0.10
2001-2010	2083	15.9	1647	2689	0.72	0.14

Period	Qa	St.dev	qa	cs	cv
1886-1915	2071	326	15.8	0.15	0.16
1901-1930	2057	327	15.7	0.16	0.16
1916-1945	2074	344	15.8	-0.02	0.17
1931-1960	2028	321	15.4	0.21	0.16
1946-1975	2007	372	15.3	0.78	0.19
1961-1990	2063	374	15.7	0.53	0.18
1976-2005	2071	268	15.8	0.38	0.13

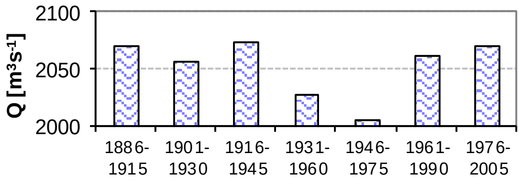

Long term 30-year discharge.

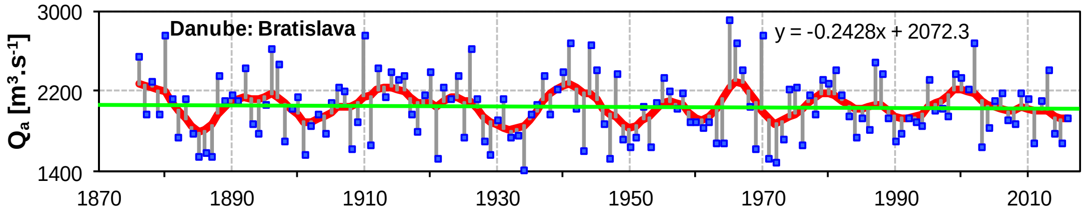

Maximum annual discharge, differences from 7-year moving averages.

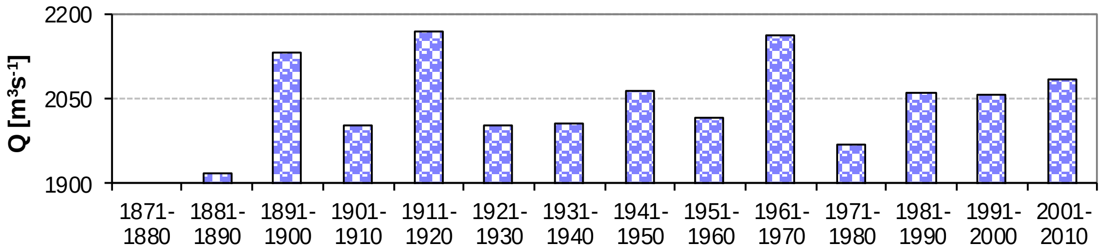

Long term 10-year discharge.

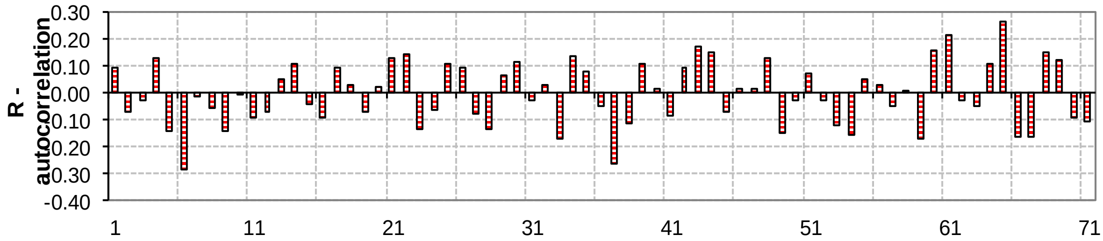

Autocorrelogram of yearly discharge.

Fig. 1.14b *Basic data analysis of the average yearly discharge at station Bratislava. Figures: Long-term 30-year discharge, Average annual discharge – differences from 7-year moving averages, Long-term 10-year discharges, Autocorrelogram of annual discharge.*

River: Danube **Station: Orsova** **Area: 576.232** 10^3 km^2 **RO**

Basic statistical characteristics

	Qa	qa	min	max	cs	cv	Med.	trend
	m3/s	l/s/km2	m3/s	m3/s			m3/s	
1876-2005	**5564**	**9.7**	**3472**	**8291**	**0.45**	**0.17**	**5427**	**-1.0677**

Period	Qmax	qmax	min	max	cs	cv
1821-1830						
1831-1840						
1841-1850	5923	10.3	4940	7083	-0.04	0.13
1851-1860	5675	9.8	4434	7243	0.23	0.18
1861-1870	4944	8.6	3472	6623	0.23	0.19
1871-1880	5856	10.2	4495	7272	0.03	0.17
1881-1890	5422	9.4	4536	6926	1.05	0.13
1891-1900	5476	9.5	4112	6738	-0.07	0.16
1901-1910	5456	9.5	4297	7029	0.79	0.13
1911-1920	6225	10.8	4292	8291	-0.01	0.19
1921-1930	5457	9.5	3832	7395	0.44	0.18
1931-1940	5875	10.2	4882	7648	1.27	0.16
1941-1950	5311	9.2	3956	8080	0.97	0.26
1951-1960	5659	9.8	4908	7405	1.70	0.13
1961-1970	5946	10.3	4533	7840	0.61	0.19
1971-1980	5706	9.9	4245	6910	-0.42	0.16
1981-1990	5156	8.9	3780	6516	-0.03	0.14
1991-2000	5298	9.2	4313	6411	0.18	0.12
2001-2009	5317	9.2	3914	6498	-0.16	0.16

Period	Qmax	St.dev	qmax	cs	cv
1811-1840					
1826-1855					
1841-1870	5514	979	9.6	-0.05	0.18
1856-1885	5394	979	9.4	0.29	0.18
1871-1900	5585	861	9.7	0.33	0.15
1886-1915	5601	917	9.7	0.82	0.16
1901-1930	5713	1007	9.9	0.54	0.18
1916-1945	5777	1072	10.0	0.40	0.19
1931-1960	5615	1048	9.7	0.72	0.19
1946-1975	5514	993	9.6	0.70	0.18
1961-1990	5603	953	9.7	0.45	0.17
1976-2005	5394	746	9.4	-0.16	0.14

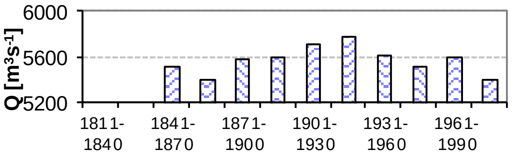

Long term 30-year discharge.

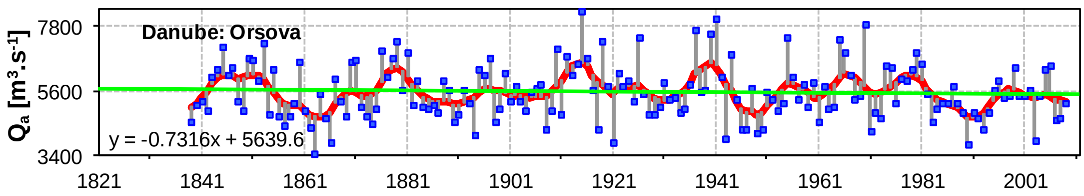

Average annual discharge, differences from 7-year moving averages.

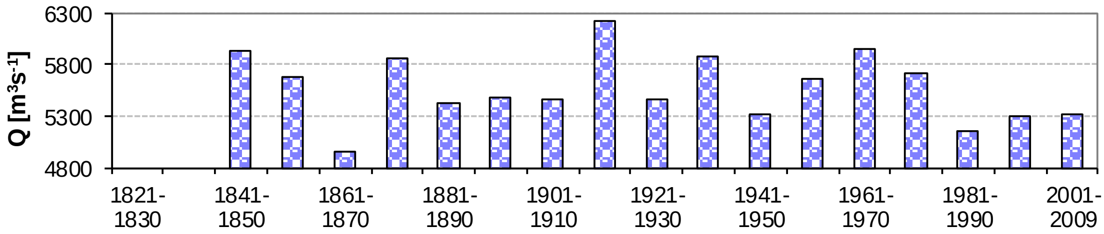

Long term 10-year discharge.

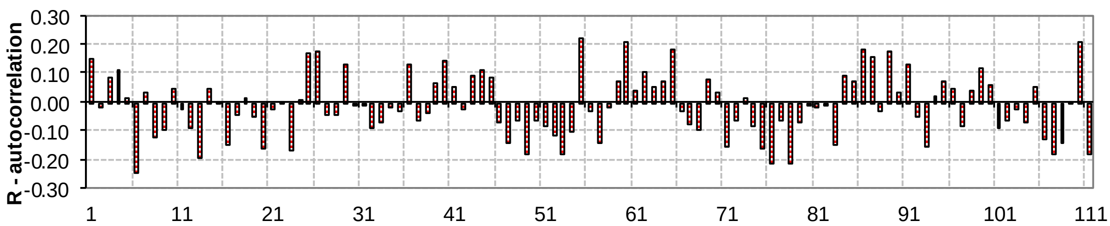

Autocorrelogram of yearly discharge.

Fig. 1.14c Basic data analysis of the average yearly discharge at station Orsova. Figures: Long-term 30-year discharge, Average annual discharge – differences from 7-year moving averages, Long-term 10-year discharges, Autocorrelogram of annual discharge.

River: Danube **Station: Reni** **Area: 805.700** 10^3 km^2 **UKR**

1875-1920 according to Bondar

Basic statistical characteristics

	Qa	qa	Qmin	Qmax	cs	cv	Med.	trend	Hurst
	m3/s	l/s/km2	m3/s	m3/s			m3/s		
1876-2005	**6416**	**8.0**	**3906**	**9916**	**0.44**	**0.19**	**6304**	**2.4441**	**0.684**

Period	Qa	qa	Qmin	Qmax	cs	cv
1871-1880	6520					
1881-1890	6070	7.5	4650	7200	-0.12	0.15
1891-1900	5790	7.2	4500	7700	0.59	0.18
1901-1910	5815	7.2	4400	7450	0.33	0.14
1911-1920	6696	8.3	4300	8800	-0.32	0.18
1921-1930	5975	7.4	**3906**	8144	0.19	0.20
1931-1940	6802	8.4	5644	9533	1.71	0.18
1941-1950	6044	7.5	4301	**9916**	1.05	0.30
1951-1960	6492	8.1	5375	8834	1.38	0.17
1961-1970	7062	8.8	5259	9602	0.51	0.20
1971-1980	6950	8.6	5272	8767	-0.02	0.16
1981-1990	6247	7.8	4194	8172	-0.21	0.17
1991-2000	6570	8.2	4873	8328	-0.07	0.16
2001-2010	6935	8.6	5015	9498	0.63	0.20

Period	Qa	St.dev	qa	cs	cv
1886-1915	5960	981	7.4	0.79	0.16
1901-1930	6162	1124	7.6	0.24	0.18
1916-1945	6542	1384	8.1	0.42	0.21
1931-1960	6446	1395	8.0	0.80	0.22
1946-1975	6421	1295	8.0	0.64	0.20
1961-1990	6753	1205	8.4	0.29	0.18
1976-2005	6644	1095	8.2	-0.07	0.16

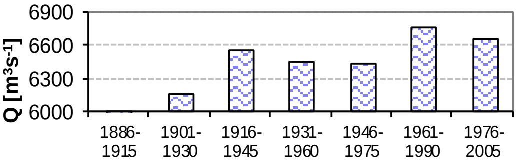

Long term 30-year discharge.

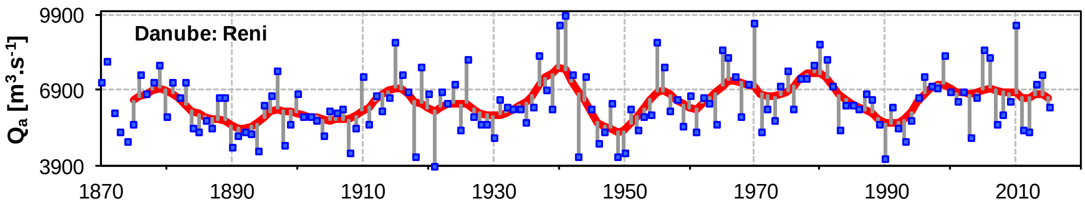

Average annual discharge, differences from 5-year moving averages.

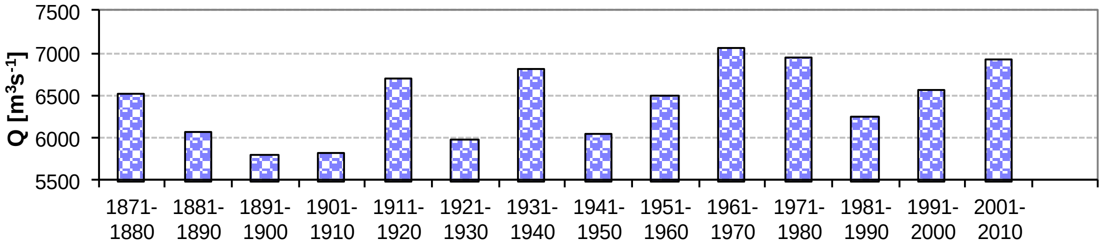

Long term 10-year discharge.

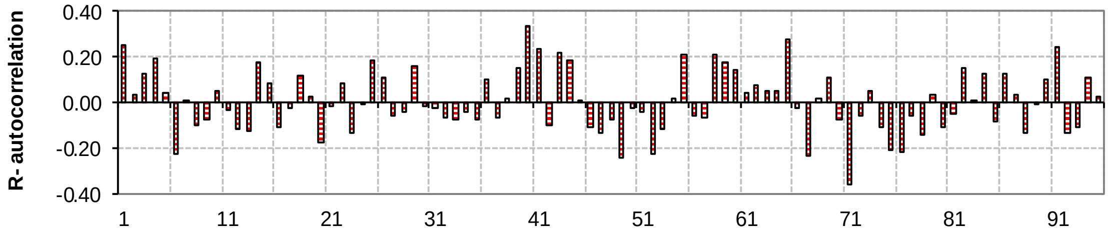

Autocorrelogram of yearly discharge.

Fig. 1.14d Basic data analysis of the average yearly discharge at station Reni. Figures: Long-term 30-year discharge, Average annual discharge – differences from 7-year moving averages, Long-term 10-year discharges, Autocorrelogram of annual discharge.

River: Danube **Station: Hofkirchen** **Area: 47.496** 10^3 km^2 **GE**

Qmax

Basic statistical characteristics

	Qmax	qmax	min	max	cs	cv	Med.	trend
	m3/s	l/s/km2	m3/s	m3/s			m3/s	
1876-2005	**1901**	**40.0**	**900**	**3700**	**0.66**	**0.29**	**1850**	**3.5483**

Period	Qmax	qmax	min	max	cs	cv
1871-1880						
1881-1890	1846	38.9	1250	**3700**	1.74	0.47
1891-1900	1900	40.0	**900**	2450	-0.82	0.28
1901-1910	1714	36.1	1250	2330	0.17	0.19
1911-1920	1935	40.7	1350	2830	0.69	0.24
1921-1930	1821	38.3	947	2490	-0.69	0.27
1931-1940	1683	35.4	956	2780	0.99	0.30
1941-1950	2109	44.4	1100	2600	-1.14	0.24
1951-1960	1932	40.7	1090	3320	0.87	0.34
1961-1970	1734	36.5	1220	2926	1.22	0.34
1971-1980	1758	37.0	1279	2503	0.54	0.25
1981-1990	1943	40.9	1081	3020	0.47	0.28
1991-2000	2131	44.9	1528	3300	1.08	0.25
2001-2010	2067	43.5	1400	2899	0.23	0.24

Period	Qmax	St.dev	qmax	cs	cv
1886-1915	1802	474	37.9	0.75	0.26
1901-1930	1823	430	38.4	0.14	0.24
1916-1945	1881	521	39.6	0.03	0.28
1931-1960	1908	572	40.2	0.34	0.30
1946-1975	1826	579	38.4	0.73	0.32
1961-1990	1812	518	38.1	0.73	0.29
1976-2005	2083	505	43.9	0.45	0.24

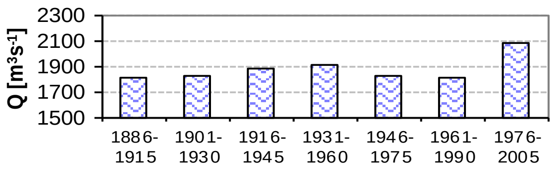

Long term 30-year discharge.

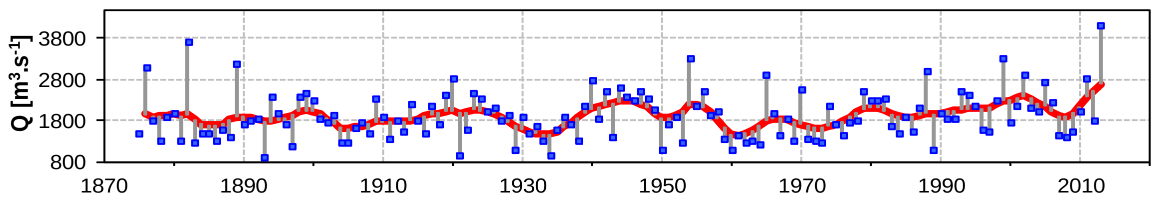

Maximum annual discharge, differences from 7-year moving averages.

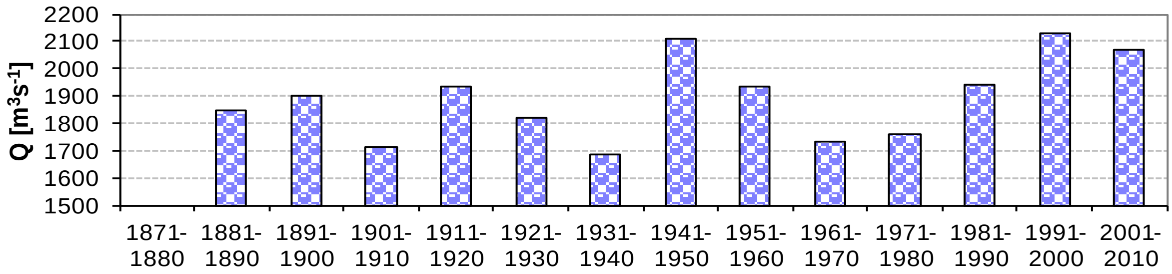

Long term 10-year discharge.

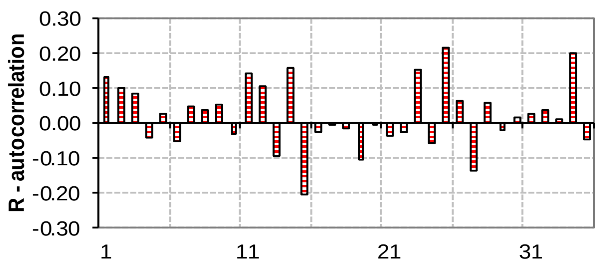

Autocorrelogram of yearly discharge.

Fig. 1.15a Basic data analysis of the maximum annual discharge at station Hofkirchen. Figures: Long-term 30-year discharge, Average annual discharge – differences from 7-year moving averages, Long-term 10-year discharge and Autocorrelogram of annual discharge.

River: Danube **Station: Bratislava** **Area: 131.338** 10^3 km^2 **SK**

Qmax

Basic statistical characteristics

	Qmax	qmax	min	max	cs	cv	Med.	trend
	m3/s	l/s/km2	m3/s	m3/s			m3/s	
1876-2005	**5960**	**45.4**	**3000**	**10870**	**0.81**	**0.28**	**5611**	**4.5663**

Period	Qmax	qmax	min	max	cs	cv
1871-1880						
1881-1890	5560	42.3	3570	9062	0.68	0.39
1891-1900	6433	49.0	3619	**10870**	0.61	0.41
1901-1910	5253	40.0	3653	6485	-0.36	0.20
1911-1920	5958	45.4	4510	8616	1.09	0.20
1921-1930	5793	44.1	3430	8998	0.48	0.31
1931-1940	5118	39.0	**3000**	7260	0.17	0.22
1941-1950	5714	43.5	3153	7160	-1.09	0.20
1951-1960	6472	49.3	4431	10400	1.21	0.27
1961-1970	5855	44.6	4042	9224	1.08	0.27
1971-1980	5649	43.0	4124	8715	1.03	0.26
1981-1990	5661	43.1	3693	7686	0.39	0.24
1991-2000	6397	48.7	5268	9430	2.08	0.19
2001-2010	6868	52.3	4435	10370	0.30	0.28
2011-2017	6422	48.9	4861	10640	1.99	0.31

Period	Qmax	St.dev	qmax	cs	cv
1886-1915	5679	1880	43.2	1.21	0.33
1901-1930	5668	1376	43.2	0.58	0.24
1916-1945	5633	1410	42.9	0.60	0.25
1931-1960	5768	1424	43.9	0.85	0.25
1946-1975	6029	1620	45.9	0.74	0.27
1961-1990	5722	1417	43.6	0.80	0.25
1976-2005	5996	1456	45.7	1.25	0.24

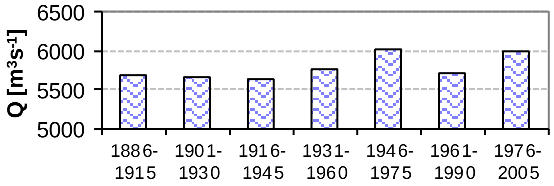

Long term 30-year discharge.

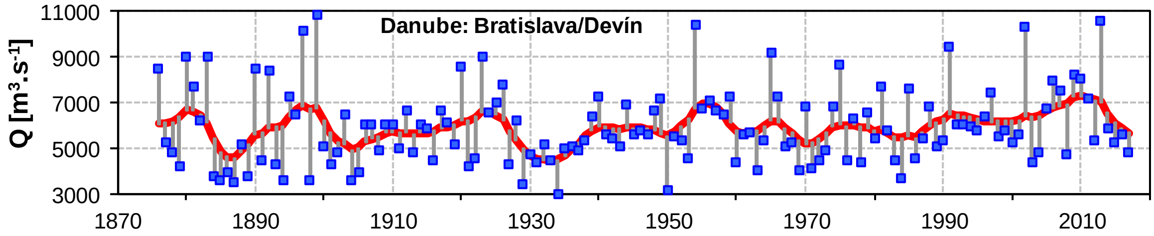

Maximum annual discharge, differences from 7-year moving averages.

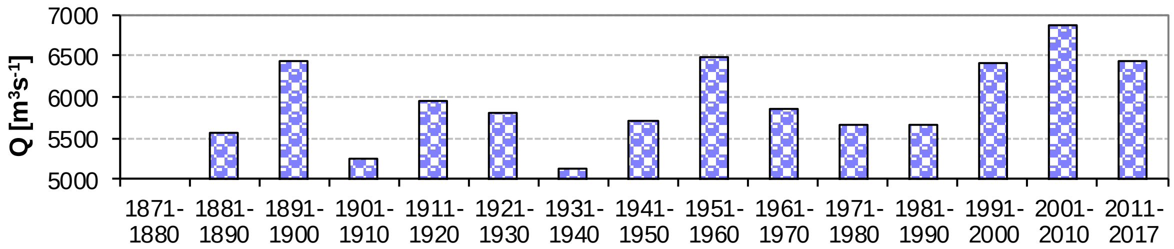

Long term 10-year discharge.

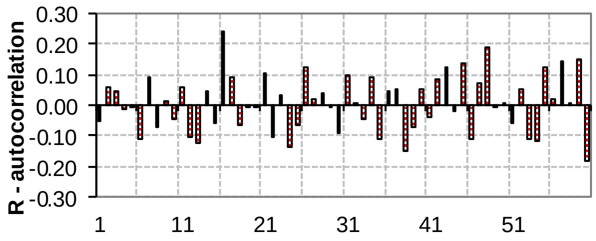

Autocorrelogram of yearly discharge.

Fig. 1.15b *Basic data analysis of the maximum annual discharge at station Bratislava. Figures: Long-term 30-year discharge, Average annual discharge – differences from 7-year moving averages, Long-term 10-year discharge and Autocorrelogram of annual discharge.*

River: Danube **Station: Orsova** **Area: 576.232** 10^3 km^2 **RO**

Qmax

Basic statistical characteristics

	Qmax	qmax	min	max	cs	cv	Med.	trend
	m3/s	l/s/km2	m3/s	m3/s			m3/s	
1876-2005	**10231**	**17.8**	**5376**	**15900**	**0.46**	**0.21**	**9886**	**10.5827**

Period	Qmax	qmax	min	max	cs	cv
1821-1830						
1831-1840						
1841-1850	9855	17.1	7853	13597	1.09	0.17
1851-1860	9403	16.3	6717	13341	0.78	0.23
1861-1870	8933	15.5	**5376**	11176	-0.86	0.22
1871-1880	10248	17.8	7341	13662	0.17	0.21
1881-1890	9852	17.1	7070	14719	0.86	0.24
1891-1900	10405	18.1	6800	15200	0.93	0.26
1901-1910	10584	18.4	8709	13600	0.74	0.15
1911-1920	11203	19.4	6681	14000	-0.91	0.18
1921-1930	10125	17.6	7806	14200	1.18	0.20
1931-1940	11138	19.3	8340	15100	0.79	0.20
1941-1950	10592	18.4	7320	**15900**	0.61	0.28
1951-1960	10181	17.7	7970	12000	-0.53	0.12
1961-1970	11130	19.3	8940	13710	0.19	0.16
1971-1980	10802	18.7	9001	12141	-0.39	0.11
1981-1990	10470	18.2	6253	14813	0.27	0.23
1991-2000	10105	17.5	9190	12145	1.26	0.10
2001-2010	10595	18.4	7700	15800	0.89	0.25

Period	Qmax	St.dev	qmax	cs	cv
1811-1840					
1826-1855	9731	1945	16.9	0.59	0.20
1841-1870	9397	1892	16.3	0.16	0.20
1856-1885	9442	1929	16.4	0.04	0.20
1871-1900	10168	2319	17.6	0.68	0.23
1886-1915	10638	2186	18.5	0.55	0.21
1901-1930	10637	1916	18.5	0.22	0.18
1916-1945	10855	2383	18.8	0.41	0.22
1931-1960	10637	2182	18.5	0.70	0.21
1946-1975	10399	1658	18.0	0.26	0.16
1961-1990	10801	1846	18.7	0.03	0.17
1976-2005	10453	1691	18.1	0.29	0.16

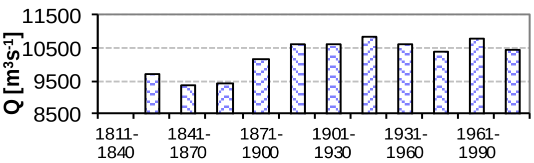

Long term 30-year discharge.

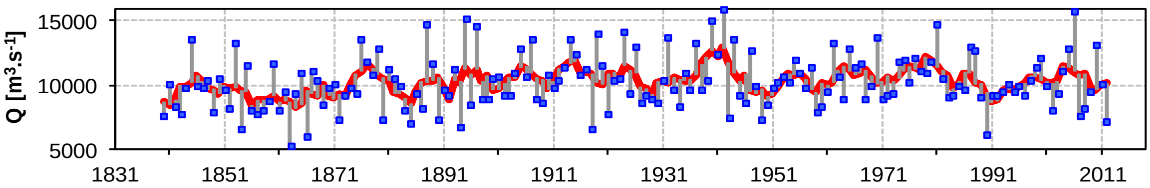

Maximum annual discharge, differences from 7-year moving averages.

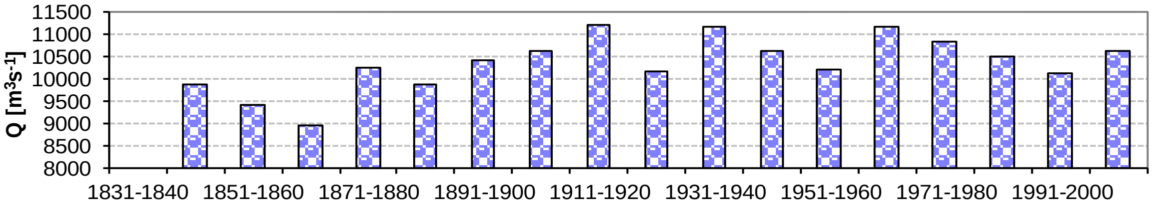

Long term 10-year discharge.

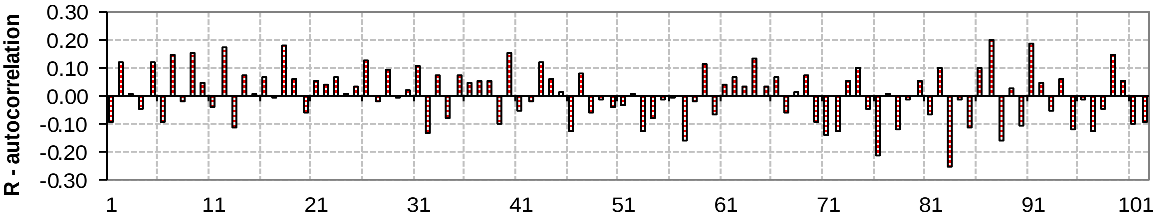

Autocorrelogram of yearly discharge.

Fig. 1.15c Basic data analysis of the maximum annual discharge at station Orsova. Figures: Long-term 30-year discharge, Average annual discharge – differences from 7-year moving averages, Long-term 10-year discharge and Autocorrelogram of annual discharge.

River: Danube **Station: Reni** **Area: 805.700** 10^3 km^2 **UKR**

Qmax 1931-1961 according to Ceatal

Basic statistical characteristics

	Qmax	qmax	min	max	cs	cv	Med.	trend
	m3/s	l/s/km2	m3/s	m3/s			m3/s	
1876-2005	**11154**	**13.8**	**6670**	**16000**	**0.00**	**0.18**	**11300**	**-2.1559**

Period	Qmax	qmax	min	max	cs	cv
1871-1880						
1881-1890						
1891-1900						
1901-1910						
1911-1920						
1921-1930	9880	12.3	7350	12500	0.14	0.17
1931-1940	10953	13.6	8600	13700	0.40	0.17
1941-1950	10553	13.1	6710	15300	0.23	0.26
1951-1960	10539	13.1	7870	13000	0.04	0.16
1961-1970	11945	14.8	8960	**16000**	0.24	0.19
1971-1980	12150	15.1	10000	15500	0.93	0.12
1981-1990	11384	14.1	**6670**	15000	-0.37	0.22
1991-2000	11734	14.6	9440	13700	-0.14	0.11
2001-2010	11815	14.7	9050	15400	0.59	0.18

Period	Qmax	St.dev	qmax	cs	cv
1886-1915					
1901-1930	9880	1715	12.3	0.14	0.17
1916-1945	10733	2120	13.3	0.26	0.20
1931-1960	10682	2088	13.3	0.18	0.20
1946-1975	10946	2019	13.6	0.16	0.18
1961-1990	11826	2065	14.7	-0.15	0.17
1976-2005	11713	1848	14.5	-0.28	0.16

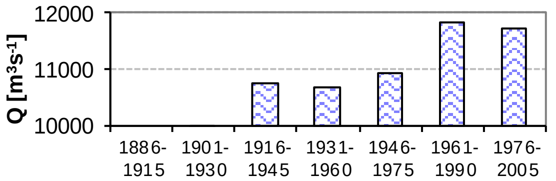

Long term 30-year discharge.

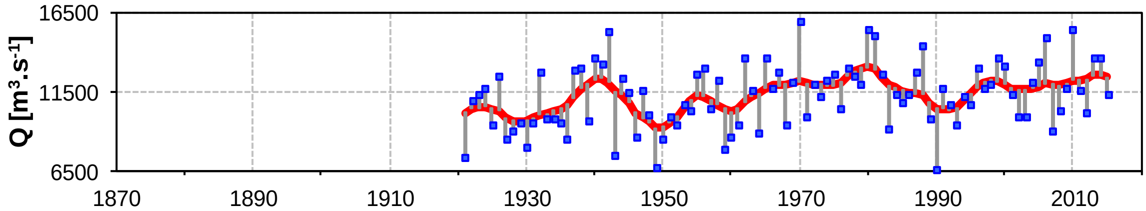

Maximum annual discharge, differences from 7-year moving averages.

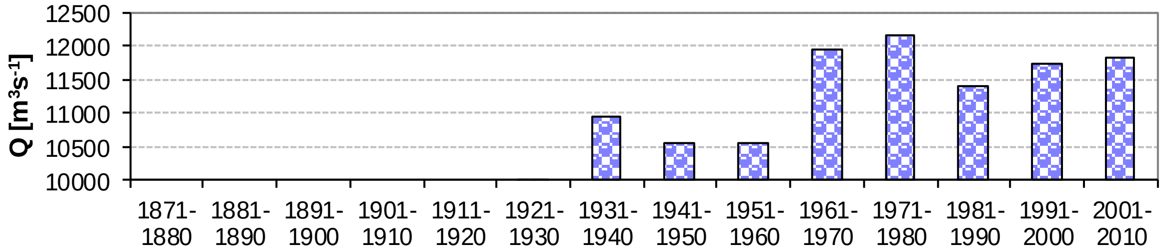

Long term 10-year discharge.

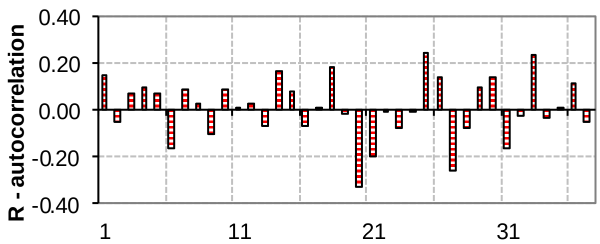

Autocorrelogram of yearly discharge.

Fig. 1.15d Basic data analysis of the maximum annual discharge at station Reni. Figures: Long-term 30-year discharge, Average annual discharge – differences from 7-year moving averages, Long-term 10-year discharge and Autocorrelogram of annual discharge.

References

Balek J. 1968. Linear Extrapolation of the Average Annual Runoff of Selected Rivers of Four Continents. (In Czech.) J. Hydrol. Hydromech., 16, 3, 402–428.

Bondar C, Iordache C. 2017. Sediment transport on the Danube River in the Romanian border area – characteristics. Rev. Roum. Géogr./Rom. Journ. Geogr., Bucureşti, 61, 1, 3–17.

Horváthová B. 2003. Flood is not only high water. (In Slovak.) VEDA, Bratislava, 232 pp.

Hurst HE. 1951. Long term storage capacity of reservoirs. Trans. Am. Soc. Civ. Eng., 116, 770–808.

Lászloffy W. 1965. Die Hydrographie der Donau. Der Fluss als Lebensraum. In: Liepolt, R. (ed.): Limnologie der Donau – Eine monographische Darstellung. II. Kapitel, Schweizerbart, Stuttgart. P. 16-57.

Miklánek P, Mikuličková M, Mitková V, Pekárová P. 2002. Changes of floods travel times on upper Danube. CD ROM Proceedings, XXI. Conference of the Danube countries, Bucharest, Romania, 12 pp.

Mitková V. 2002. Changes in travel times of flood waves on the Danube (In Slovak). Acta Hydrologica Slovaca, 3, 1, 20–27.

Pacl J. 1955. Danube floods in July 1954. (In Slovak). Hydrological study HMI, Praha, 26 pp.

Pekárová P, Pacl J, Škoda P, Miklánek P. 2007. Supplementation of average daily discharge data of the Danube River in Bratislava with the historical period 1876–1890. Acta Hydrologica Slovaca, ISSN 1335-6291, 8, 1, 3–12.

Petrovič P, Nachtnebel H, Kostka Z, Holko L, Miklánek P. 2006. Basin-wide water balance in the Danube River basin. The Danube and its basin-Hydrological monograph Part VIII-3, ISBN 80-89062-49-0, IHP UNESCO & VÚVH, Bratislava, 161 pp.+4 maps.

Škoda P, Turbek J. 1995. Monitoring of the Danube River hydrologic regime (In Slovak). Proc. Int. Conf. “Danube – the artery of Europe”. ZSVTS, Bratislava, 194–206.

Stančík A, Jovanović S. 1988. Hydrology of the River Danube. Publishing House Príroda, Bratislava, 272 pp + 4 maps.

Svoboda A, Pekárová P, Miklánek P. 2000. Flood hydrology of Danube between Devín and Nagymaros. SVH – ÚH SAV, 96 pp.

Vízállások, 1890. River stages of the Danube River (In Hungarian). Hornyanszky Viktor Könyvnyomdaja, Budapest.

Williams GR. 1961. Cyclical variations in the world-wide hydrological data. J. of Hydraulic division, 6: 71–88.

Zatkalík G. 1970. Calculation of the basic parameters of the discharge hydrographs (in Slovak). PhD Theses, 71 pp.

2 History and downstream propagation of the Danube floods

Pavla Pekárová, Pavol Miklánek, and Ján Pekár

2.1 Introduction

Studying floods requires periodically estimating peak discharge for a specified return period that is substantially longer than the available gauged record. Historical data can be used to augment a flood frequency analysis by providing information on floods that predate the period of systematic gauging (Bayliss and Reed, 2001). Floods are the extreme expression of natural phenomena. Floods have a firm place in the Danube Basin. The first records of floods can be traced back to the year 1012 A.D. The aim of this chapter is to analyse the occurrence of floods in the Upper/Central part of the Danube River based on historical archive evidence (period 1000–1875), historical flood marks, and measured discharge series (period 1876–2013). This chapter is based on the research outcomes of Pekárová et al. (2014).

Long hydrological observations on the Danube River are limited. Instrumental data can be completed with documentary data from historical sources such as various archive documents (Bel, 1735; Lauda et al., 1908; Neweklowsky, 1955; Kresser, 1957, 1970; Szlávik, 2002; Horváthová, 2003; Rohr, 2005, 2007; Brázdil and Kundzewicz, 2006; Kiss, 2009; Kiss and Laszlovszky, 2013; Munzar et al., 2006; Przybylak et al., 2010; Pišút, 2011; Stankoviansky and Pišút, 2011; Elleder et al., 2013; Melo and Bernáthová, 2013; Pekárová et al., 2013). Most of the presented information on historical floods in the Upper Danube region has been preserved in the form of flood marks, in newspaper articles, chronicles, official letters, books, maps and photos. Flood marks contain a brief description of a flooding event with indication of peak flood water level. In cities located alongside the Upper Danube (e.g. Passau, Linz, Mauthausen, Grain, Ybbs, Melk, Krems, or Hainburg an der Donau), there are still numerous flood marks witnessing historical floods, with the oldest one tracing back to the year 1501.

According to Lauda et al (1908) and Kresser (1957), the oldest evidence of floods on the Danube goes back to 1012 A.D. Other floods with severe consequences, as documented in historical annals, occurred in 1210, 1344, 1402, 1466, 1490, 1499, 1501, 1526, 1572, 1594, 1598, 1670, 1682, 1721, 1787, 1809, 1876, 1897, 1899, 1954, 1965, 2002, and 2013.

2.2 The Danube floods in the middle age

The analysis of occurrence of floods on the upper Danube is based on the historical flood marks in Passau, Linz, Mauthausen, Ybbs, Melk, Spitz, Krems, Hainburg, Bratislava, Štúrovo, and Budapest. The occurrence of the Danube floods in the medieval ages on its Austrian–Slovak–Hungarian portion was studied by Kiss (2011) in her dissertation. Here, floods of 1235, 1316, 1402, 1414, 1432, and 1490 (Fig. 2.1) are described as severe summer floods. In general, the 15th century is known by an occurrence of severe floods. Horváthová (2003) focused on the the Danube floods history at Bratislava. In her publication, she described the occurrence of floods based on analyses of archive materials. From the 15th century on, written evidence revealed that in Bratislava ice floods, or ice jams and ice barriers, damaging the bridge across the river were frequent. These floods damaged several buildings in the city. For example, in 1426, Sigismund of Luxemburg, the Hungarian, Bohemian, and Roman king, issued an order to repair flood levees damaged during preceding floods. In 1430, Sigismund ordered to construct a new bridge across the Danube. A part of the bridge was supported by piers, another part was floating boat-like structures known as pontoons. Written records on the damaged bridge can be considered as evidence of severe floods that occurred in the first half of the 15th century. For example, one pontoon was swept away on 20 March 1439, three bridge sections were swept away on 30 July 1440. The whole bridge was completely washed away on the Good Friday (Easter) of 1443.

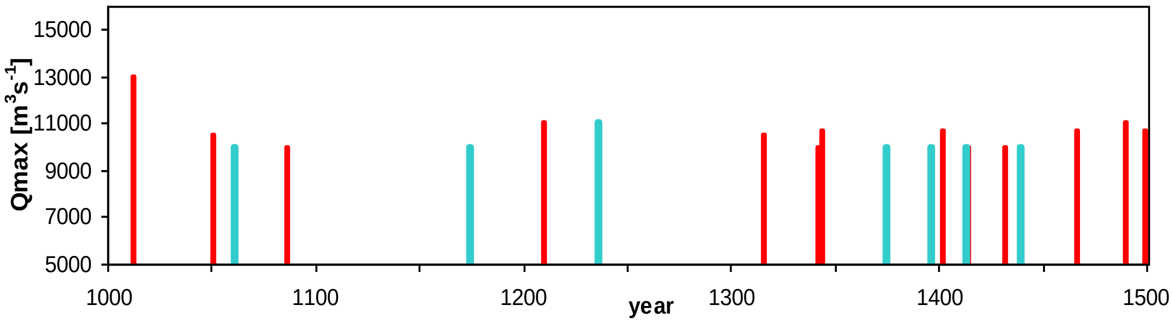

Fig. 2.1 *The Upper Danube (upstream Budapest) flood incidence since the year 1000 up to 1500 according to Kiss (2011) (red columns - summer floods, blue columns – ice floods).*

In 1472, Mathias Corvinus, the Hungarian king, ordered to build another bridge over the Danube at Bratislava. Its construction was similar to the previous one. In September 1478, a flood damaged three of the bridge segments. On the New Year of 1482 and in the spring of 1485, the bridge was damaged by ice floes. At the end of July 1485, the bridge was damaged again by another flood, and the subsequent flood wave of 1st September 1485 demolished it completely. According to chronicles, many people perished in Bavaria during the August 1485 flood. In 1486, the bridge at Bratislava was damaged again by ice floes, and the king Mathias Corvinus forced the city of Pressburg (now Bratislava) to repair it. High floods occurred also in 1490 and 1499.

2.3 The Danube flood marks within the 1501–1820 period

After 1500, the magnitude of Danube floods was recorded in the form flood marks placed on historical buildings in Germany and Austria. Such examples are shown on the photographs in Figs 2.2a-n taken in cities located along the river (Vilshofen, Passau, Linz, Mauthausen, Ybbs, Melk, Emmersdorf an der Donau, Dürnstein, Spitz, Schönbühel, Stein–Krems, Hainburg, Bratislava, and Budapest). These marks make it possible to imagine the real stage of water, and to compare them against each the others. It should be emphasized here that the channel morphology of the Danube changed several times throughout the centuries, and some of the flood marks were displaced after reconstructing the buildings. In addition, not every significant flood was marked. It is therefore necessary to rely on other archive sources in analysing the historical floods.

As shown in the photos, so far the largest flood, reliably and authentically marked on the Danube River stretch between Passau and Bratislava, occurred in August 1501 (Lauda et al., 1908; Kresser, 1957; Rohr, 2005). The peak discharge at Linz was estimated up to 12 000 m^3s^{-1}, and at Vienna it was 14 000 m^3s^{-1}. Discharge of 11 000 m^3s^{-1} at Ybbs was exceeded probably by the summer floods on 25 June 1682, 31 October 1787 and by a flood triggered by heavy rains on 3 February 1862 (Fig. 2.2e).

The economic impact of the “Millennium Flood” of 1501 can be reconstructed to a great detail: carpenters and other craftsmen worked from August to December in 1501, and again several months later in 1502, with the aim to repair the bridge (Rohr, 2005). Numerous meadows and orchards along the riverside were destroyed and their owners had to be relocated. The former land owners probably perished during the flood or just moved away.

Fig. 2.2a *The Danube flood marks, Vilshofen. Photo, Creative Commons 2010 (left).*
Flood mark 1595, Lauda et al, 1908 (right).

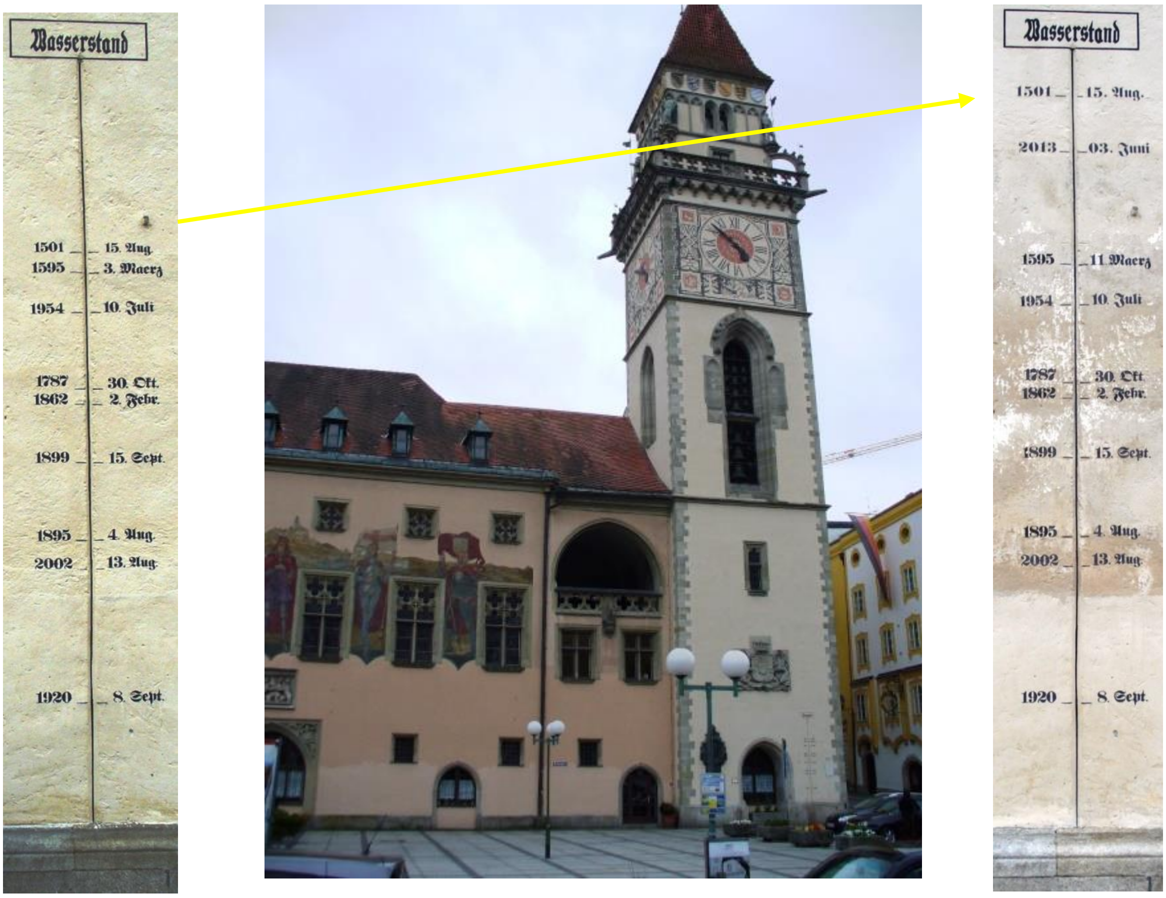

Fig. 2.2b *The Danube flood marks, Passau. (Photo Miklánek left 2010; right 2014).*
After the June 2013 flood the flood mark of 1501 was increased.

Fig. 2.2b' The Danube flood marks, Passau.
(Photo, left - Daneček, 2010; right - Lešková 2014; down - Robert Lesti, http://www.flickr.com/photos/45224155@N06/7793930312).

Fig. 2.2c The Danube flood marks, Linz 1501, 1954 and 1787. (Photo: right - Christian Wirth http://www.linzwiki.at/wiki/Datei:Linz_Urfahr_Hochwasserstand_1501.jpg/; down - http://commons.wikimedia.org/wiki/File:Linz_PA_Hochwasser1501_Gedenkstein_Glei%C3%9Fnerhaus.jpg).

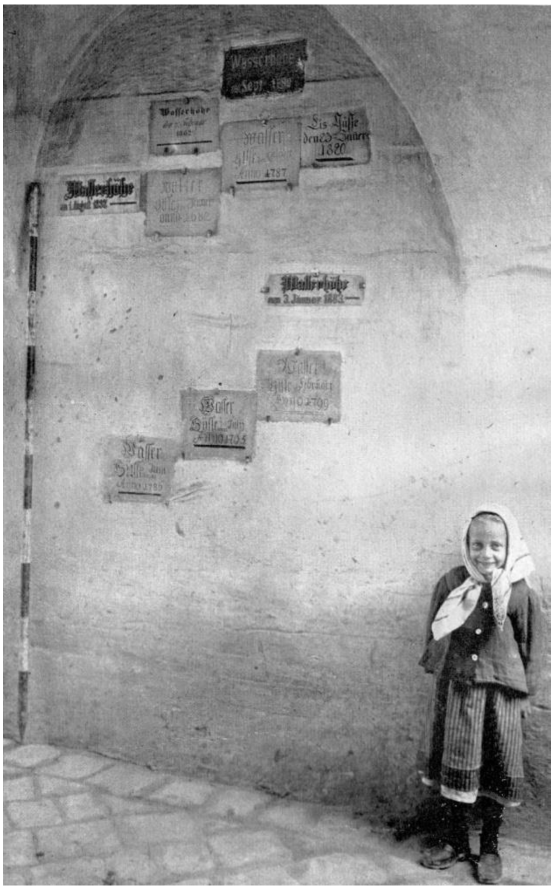

Photo from: Lauda et al. (1908)

Photo from: Kresser (1957)

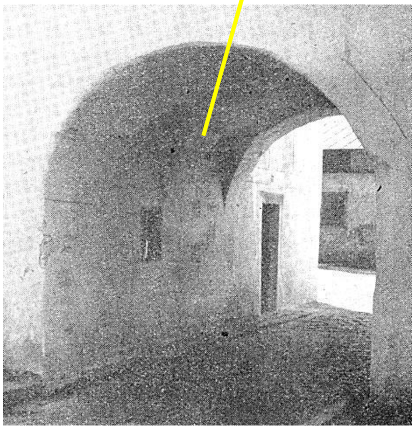

Photo: Pekárová, 2010, (after 1957 the flood marks were relocated)

Fig. 2.2d The Danube flood marks, Mauthausen.

Photo Lauda et al. (1908)

Photo Kresser (1957)

https://www.ybbs.gv.at/fotogalerie/

Photo: Miklánek 2010

https://mapio.net/s/58955250/

Fig. 2.2e The Danube flood marks, Ybbs.

Fig. 2.2f *The Danube flood marks, Melk, detail. (Photo: Miklánek, Pekárová, 2014).*

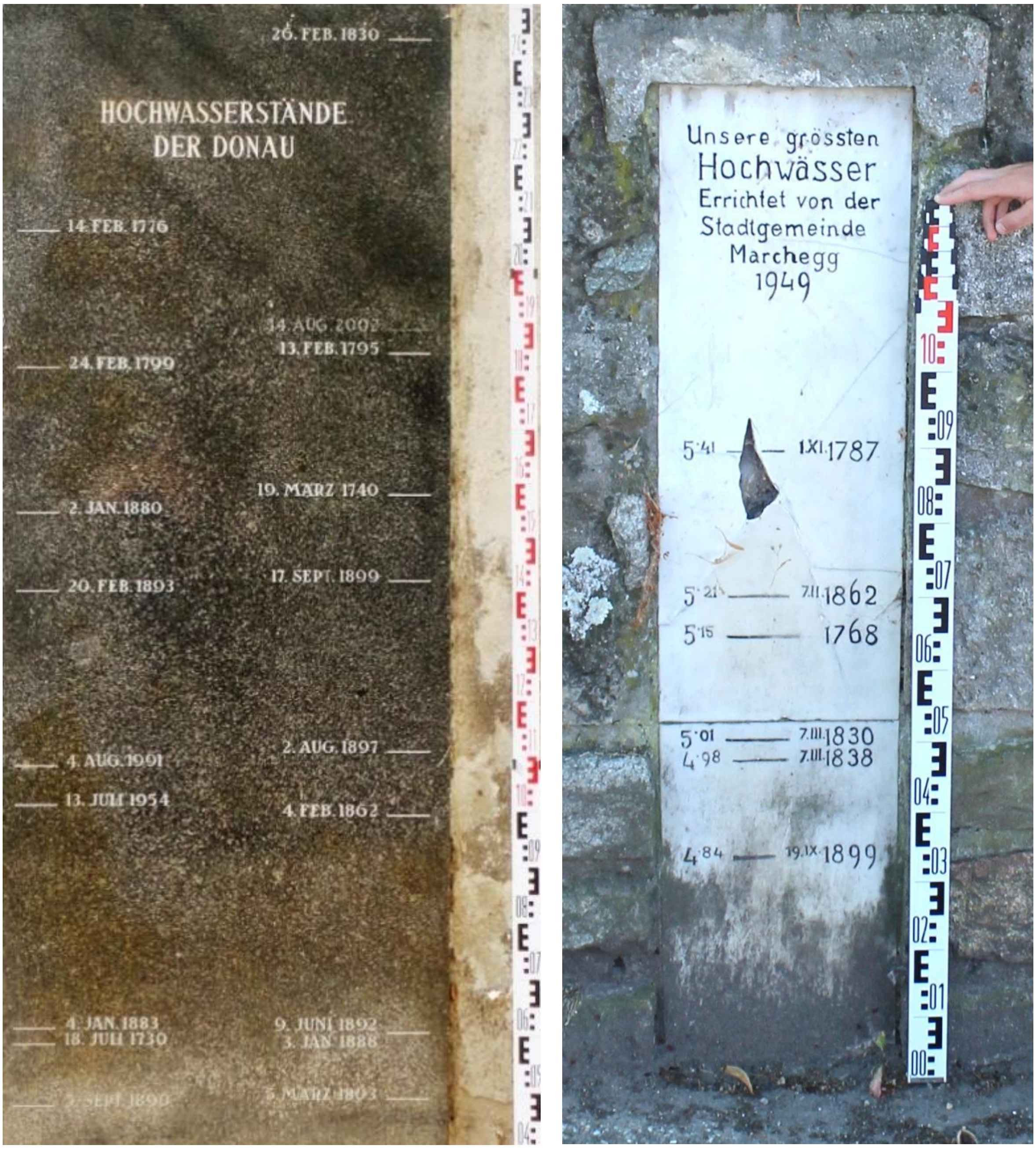

Fig. 2.2g Left - the Danube flood marks, Stein, detail. (Photo: Pekárová, 2014).
Right – Danube and Morava River floods, Marchegg (Photo: Miklánek, 2019).

Fig. 2.2h *The Danube flood marks, Hainburg. (cutout photo from Lauda et al. (1908) (big photo: Pekárová, 2011; Miklánek, 2019).*

Fig. 2.2i The Danube flood marks, Budapest. (Photo: Pekárová, 2011, 2014).

2.3.1 Flood marks in Bratislava before the instrumental period

At Bratislava, the Danube River formed many meandering arms in the past. The river bed regularly changed after every major flood. In the 13th century, one of the meandering arms led along the city walls, now the Hviezdoslav square. During catastrophic floods, the water stage in the Danube rose so much that water flooded the centre of the city.

The oldest flood marks within city limits of Bratislava are from the beginning of the 16th century (Pekárová at al., 2014). One flood mark was situated on the third pier of the Vydrická brána (Vydrická Gate), and the other one was placed on the border pole between Zuckermandel and Vydrica. A description of flood marks was first made by Matthias Bel in his fundamental work (Bel, 1735) as shown in Fig. 2.3. Unfortunately, finding the exact date of this flood is not an easy task. Unfortunately, Matthias Bel did not write down the year when the flood occurred, although he lived before the Vydrická Gate was demolished in 1778. The flood mark (a cross ingraved in the wall of the gate) on the Vydrická Gate was described by Bel's followers - Korabinský (1786) and Windisch (1780). Similar marks of the 1501 flood are still preserved in Passau (Fig. 2.3 down).

Fig. 2.3 *The Vydrická Gate from the year 1563, upper left - part of the king Maximilian coronation drawing, Dvořák, 2007; upper right - drawing according to K. H. Frech (Benyovszky, 2001). Middle - rest of the former Vydrická Gate (Photo Pekárová, 2011). Down - flood marks with a cross sign from the 1501 flood in Passau.*

The most severe flood in the 18th century – which became to be known as the All Saint's Flood – occurred between October and November in 1787. A detailed description of this flood on the Bratislava territory was presented by Pišút (2011). The stage of water in the Danube had been rising since 28 October 1787. On November 1, 1787, the water breached the right protective levee along the Vienna road – which was built by command of Maria Teresia only few years prior to the flood between 1773–1774. Water flooded the whole village of Engerau (now Petržalka) up to manucipality of Karlburg (now Rusovce). A large lake was formed here which served as a large polder. Consequently, thanks to the breach of the levee under the Vienna road with a total length of 406 meters, the inner city of Pressburg was flooded only partially. Nevertheless, water did flood the streets adjacent to the river and got into courtyards and cellars in the inner city. The water stage remained high from 26 October to 6 November 1787 (Preßburger Zeitung, No. 88, 89). The flood peaked on 3 November 1787 in Bratislava with an estimated discharge of 11 800 m^3s^{-1}. If the levee under the Vienna Road did not breach, the flood would probably peak higher at 12 200 m^3s^{-1}, a flood magnitude similar to the ice floods of 1809 and 1850 (Pišút, 2011). A flood mark describing this event has been preserved in Hainburg, Austria (Horváthová, 2003) and on the wall of the military barracks in Pressburg (Pišút, 2011). According to Preßburger Zeitung No. 88, the 1787 flood exceeded that of the large ice flood in 1775. This flood caused intense bank erosion and sediment transport.

2.3.1.1 Ice floods in Bratislava

The ice floods on the Danube were quite common during the small ice age (17th through 19th centuries). Ice jams on the Danube occurred often in winter, endangering the neighbouring land. Today, ice jams do not represent such a threat as they did in the past. The Danube does not freeze frequently anymore due to the modifications in the river channel morphology, rising air temperature, and water management. The large ice flood of 1526 is the first food documented in the municipal archives of the Bratislava city (Horváthová, 2003). The 1526 flood occurred unexpectedly overnight, with an aftermath of 53 fatalities. Other ice floods in Bratislava followed in the years 1721, 1775, 1784, 1809, 1813, 1847, 1850, 1895.

Pišút (2002, 2008, 2009) made a concise and detailed description of the 1809 Bratislava flood (2002, 2008, 2009). In 1809, the Danube River breached the right-hand embankments and water flooded Engerau (now the city suburb Petržalka). A memorial flood mark on this flood is still preserved on a stone cross located close to the horse racecourse (Fig. 2.4). The inscription on it goes: "*Zur Errinerung an 1809 von den Burgern Pressburgs 1869*" ("*In memory of 1809, from citizens of Pressburg, 1869*"). According to oral tradition, the large flood of 1809 brought a wooden cross to this place. Because nobody appealed to the cross, it was erected in front of the gamekeeper's lodge. As time passed, the wooden cross started to rot, and, in 1869, a stone cross was erected on its place (Fig. 2.4).

The most damaged parts on the left bank in the Bratislava city were: Zuckermadel, Vydrica, Gorkého St., Jesenského St., and Laurinská St., as well as Grösslingová St. A mark of this flood was located on building in the Lodná St. (Photo 2.5).

The 1809 ice flood belongs to the most extreme floods among the recorded ice floods because it affected not only the Danube–Komárno river reach with the local communities, but it also affected communities inhabiting the lower section of the Morava River. This flood damaged 35 houses in the municipality Vysoká pri Morave, and 30 houses near village of Zohor. In Komárno alone, on February, 2, 1809, due to backwater effect induced by ice jams, water breached the protective embankment and damaged 400 houses.

Fig. 2.4 *Overall view on the little chapel with cross dating from the year 1909, built on occasion of the 1809 flood centennial anniversary, and the gamekeeper's lodge with memorial plates (Photo Pekárová, 2011). The detail of the 1809 flood memorial plate, and the 1850 flood mark on the gamekeeper's lodge in Petržalka (Photo Pekárová, 2011).*

Fig. 2.5 *Flood mark from the 1809 flood at Lodná St. in Bratislava, (Photo from 1947- Bratislava municipality archive, AMB).*

2.4 The Danube floods within the 1821–2013 period

Catastrophic floods in the Upper sections of the Danube upstream the Bratislava gauge, in the Central/Middle and the Lower Danube from the Orsova gauge to the river delta, usually do not occur simultaneously (Pekárová et al., 2009). At Hofkirchen, the largest floods were observed in 1845, 1862, 1882, 1954, 1999 and 2013 (Fig. 2.6). Between Passau and Bratislava, the largest floods during the observation period occurred in 1830, 1862, 1897, 1899, 1954, 1965, 2002 and 2013. In the central section of the Danube major floods occurred in 1838, 1893, 1897, 1938, 1940, 1941, 1954, 1956, and 2006.

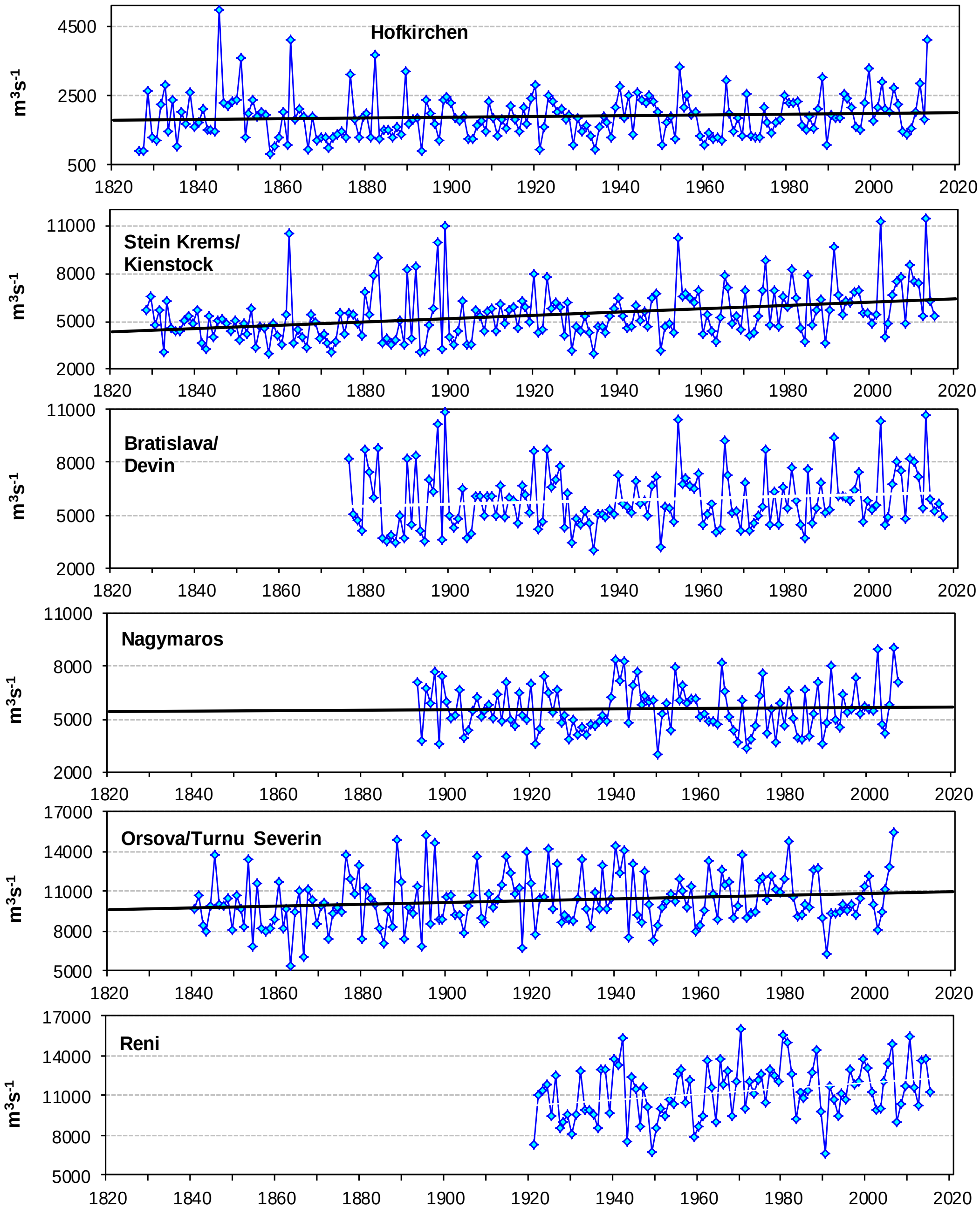

Fig. 2.6 Maximum annual discharge in selected stations downstream the Danube.

The highest discharge on the Upper Danube during the instrumental period occurred at Krems/Kienstock, 11 900 m^3s^{-1} in 2013, the second highest was 11 306 m^3s^{-1} in 2002 and the third one 11 200 m^3s^{-1} in 1899. At Bratislava the highest culmination discharge was in the year 1899 (Fig. 2.6). Observed and estimated water stages of significant floods at the Bratislava gauge are presented in Fig. 2.7. Significant floods on Danube River in three gauges are presented in Fig. 2.8a,b.

According to Bondar (2003), the largest floods in the lower part of the basin were in 1845, 1853, 1888, 1895, 1897, 1907, 1914, 1919, 1924, 1932, 1940, 1941, 1944, 1947, 1954, 1955, 1956, 1958, 1962, 1965, 1970, 1975, 1980, 1981, and 1988. A part of these floods occurred also as a result of ice jams along the Danube in the winter-spring season. Bondar and Panin (2001) estimated that during the flood in July 1897 at the Danube delta the discharge was 20 940 m^3s^{-1}.

In the years 1897, 1965, and in 2006, floods occurred in the whole Danube Basin (Fig. 2.9). The large floods at Bratislava last 5–10 days, the duration of large floods on the Lower Danube section exceed 40 days, but exceptionally they can last up to 200 days (e.g. in the year 1965).

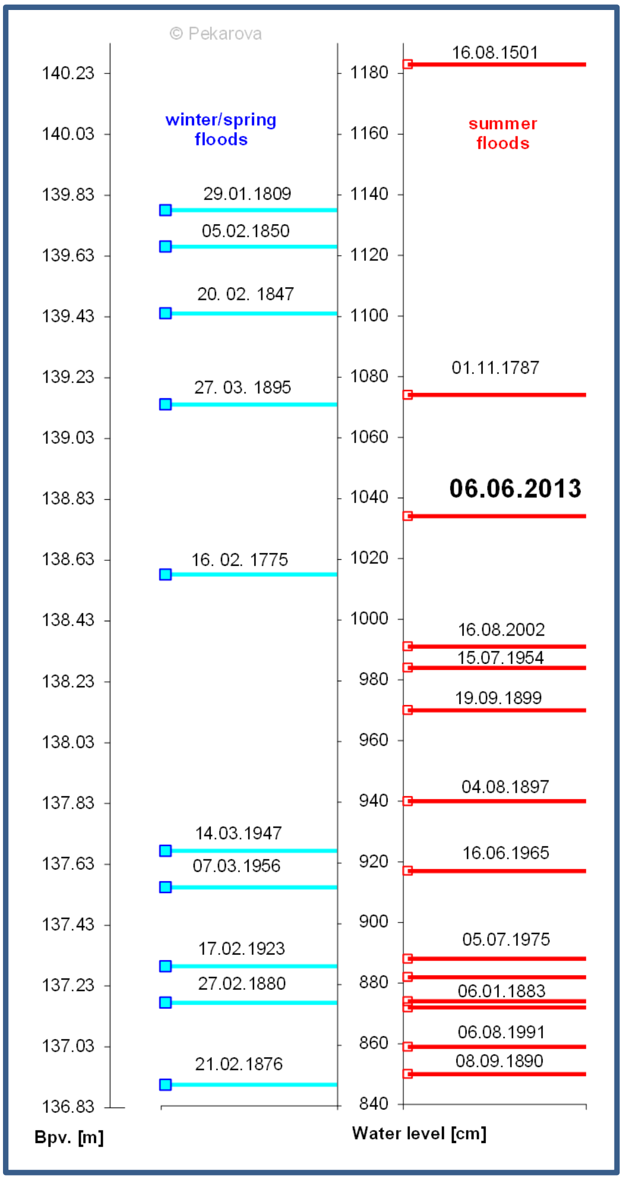

Fig. 2.7 Measured and estimated water stages of significant floods at the Bratislava gauge. Left column (blue points) – ice floods, right column (red points) – summer floods.

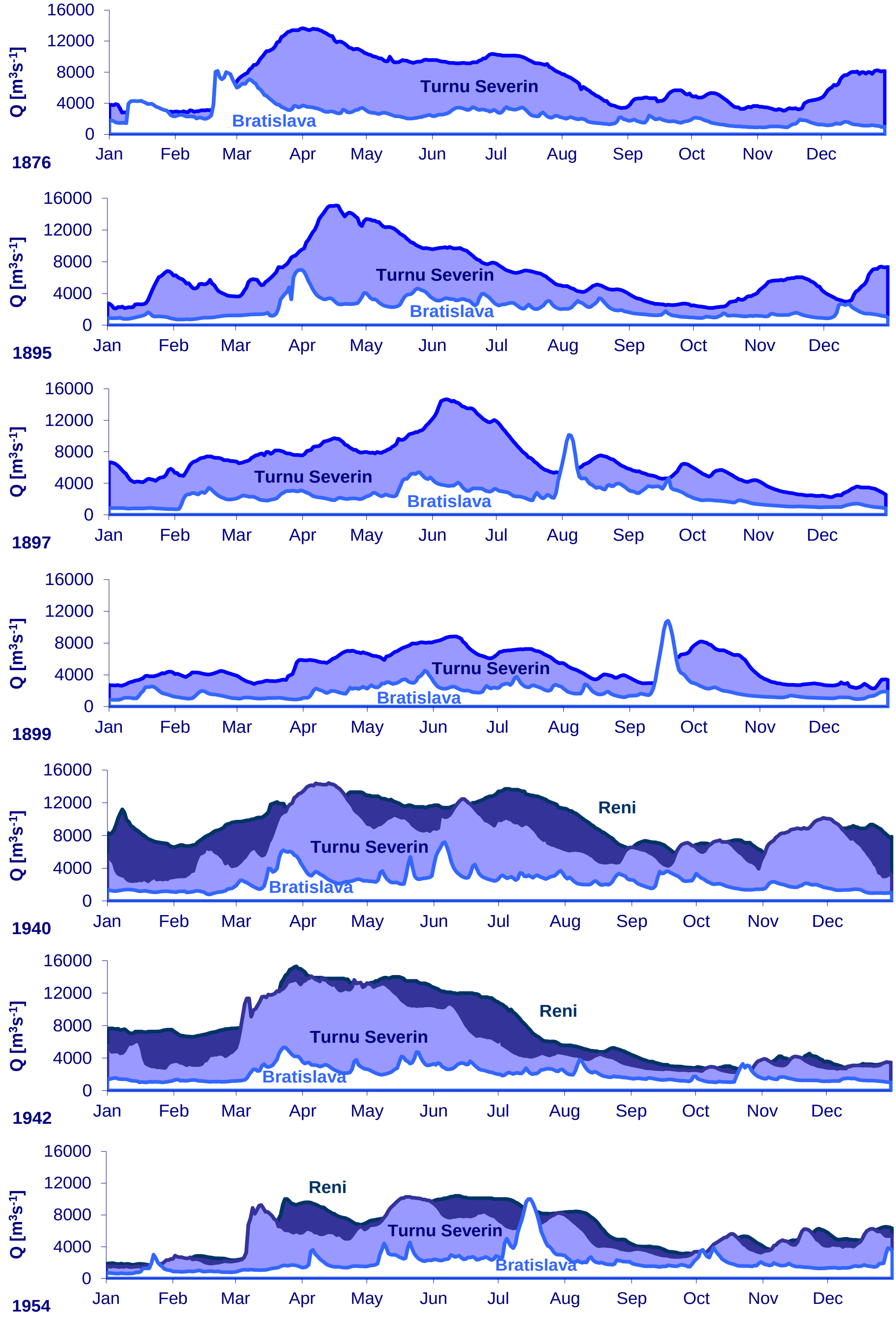

Fig. 2.8a *Daily discharge of the Danube River at water gauges: Bratislava, Turnu Severin/Orsova, and Reni.*

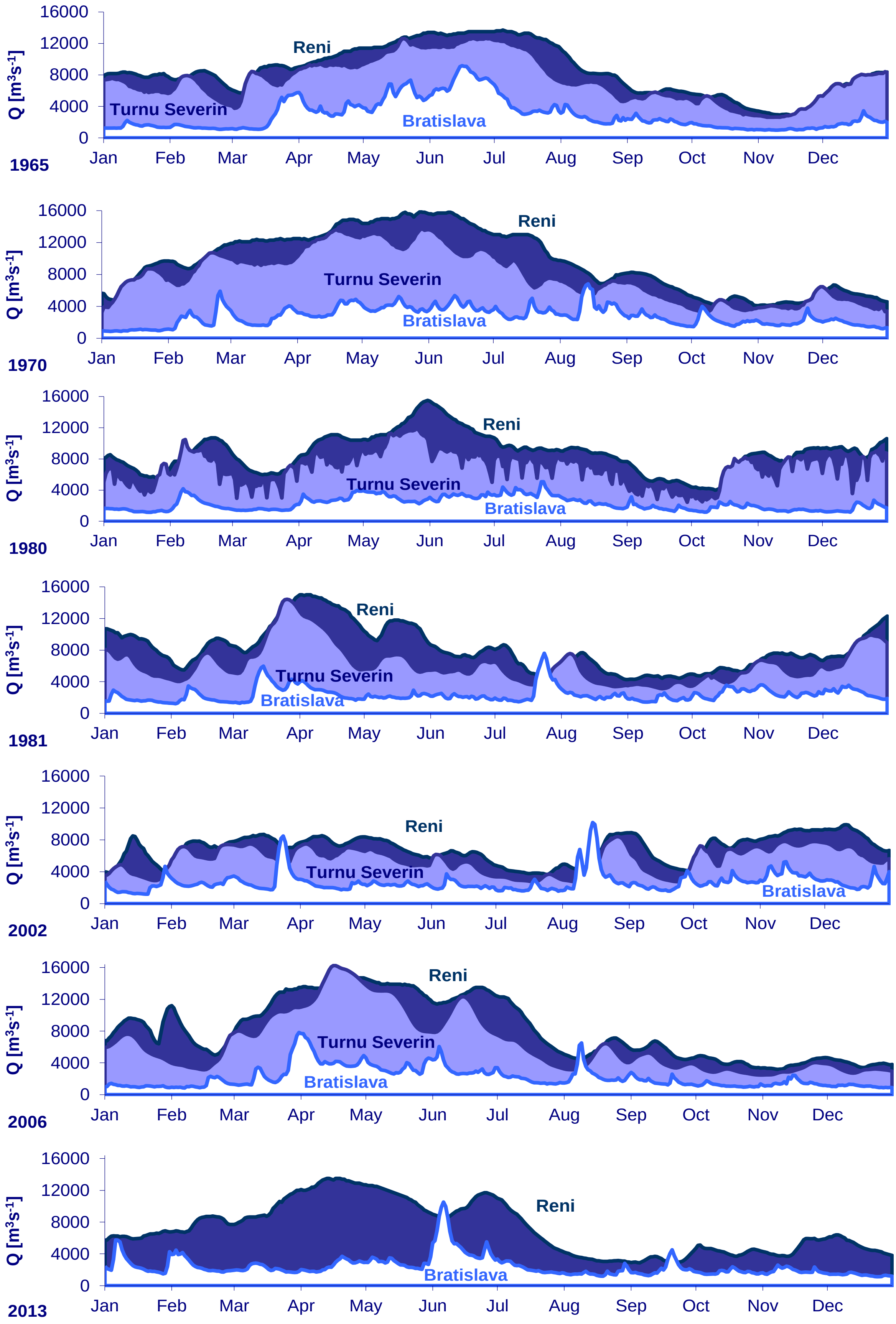

Fig. 2.8b Daily discharge of the Danube River at water gauges: Bratislava, Turnu Severin/Orsova, and Reni.

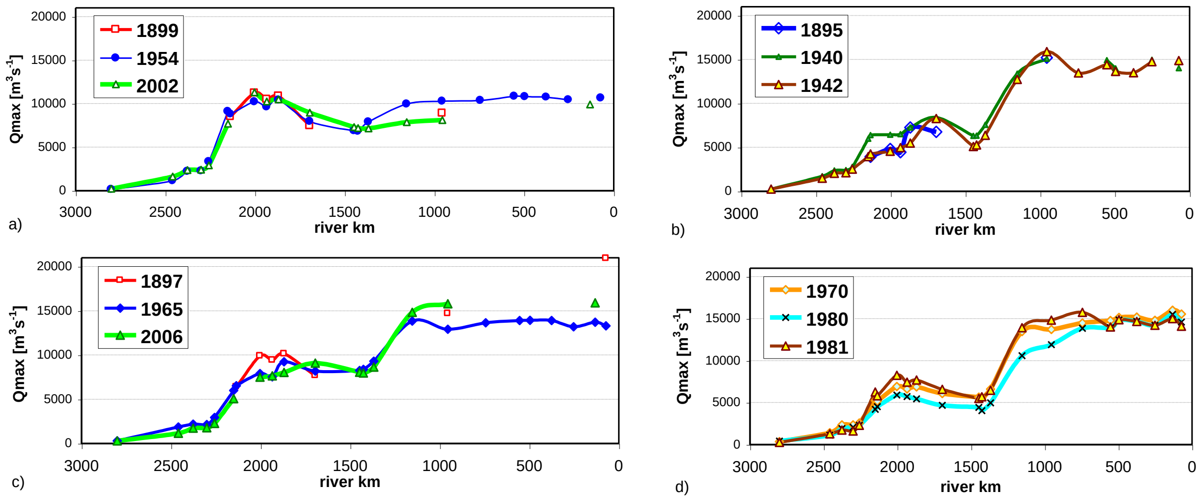

Fig. 2.9 *Extreme floods of the Danube along the channel.*

2.4.1 Travel time of floods

The travel time of the big flood waves between Hofkirchen (2 257 rkm) and Passau (2 226.7 rkm) is 25 hrs, with an average celerity of 30 km/day. The travel time of the wave between Passau (2 226 rkm) and Bratislava (1 869 rkm) was 96 hours in 2002 (wave celerity of 89 km/day), in 1954 it was 130 hours (wave celerity of 66 km/day). Examples of the travel times of the important floods in the reach Passau–Nagymaros are presented in Fig. 2.10.

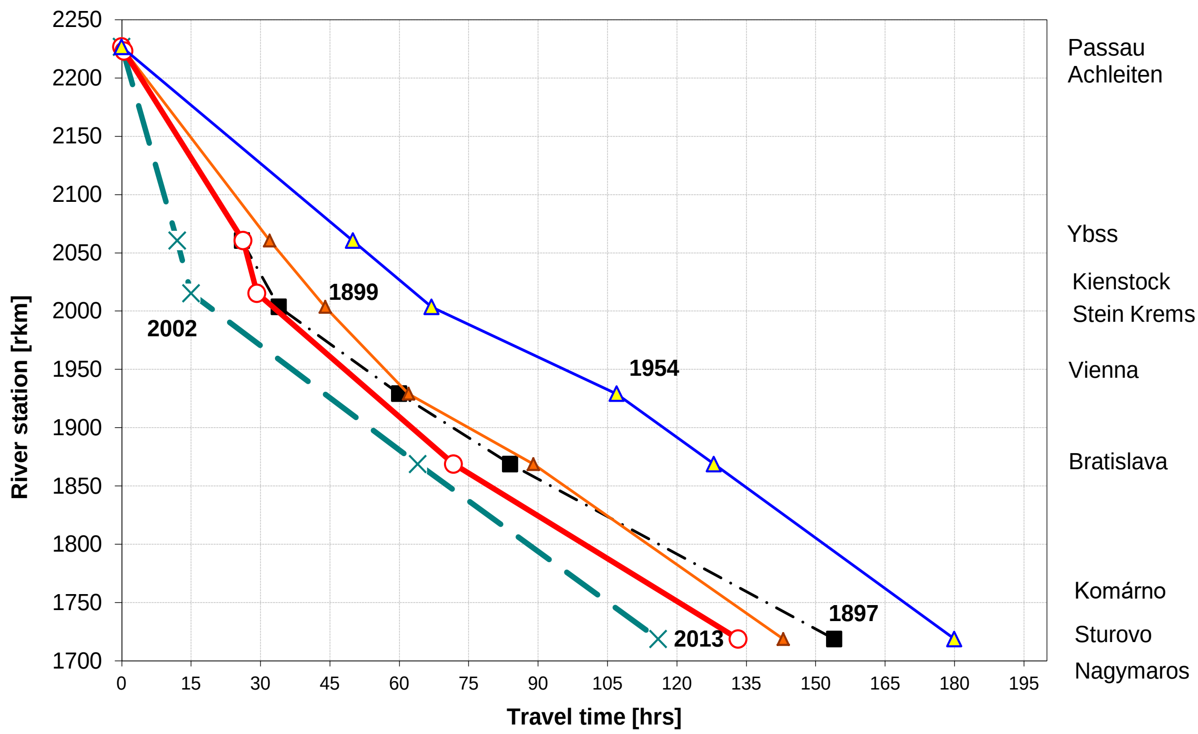

Fig. 2.10 *Travel times of the largest floods between Passau and Nagymaros.*

The travel time of the largest floods between Bratislava (1 869 rkm) and Orsova (955 rkm) is around 16 days, with an average celerity of 57 km/day. According to Bondar (2003) the time difference between the large floods at Orsova and Black Sea mouth is of 15–20 days, when the flood wave travels along the Danube River with an average celerity of about 53 km/day (Fig. 2.8).

2.5 Conclusions

Based on historical sources, we constructed series of significant historical floods on the Danube River that were observed upstream of Bratislava after 1501. In this river section, there about ten summer floods are known to occur before the year 1876 (Fig. 2.11). Out of these, the floods of 1501, 1682, and 1787 peaked probably with a higher discharge than that of the 1899 flood. However, these data do not show the frequency of large flood would change over the course of the last 500 years. The highest flood frequency in this river section during the instrumental observation period occurred in the last quarter of the 19th century (1876–1900) (Pekárová et al., 2014).

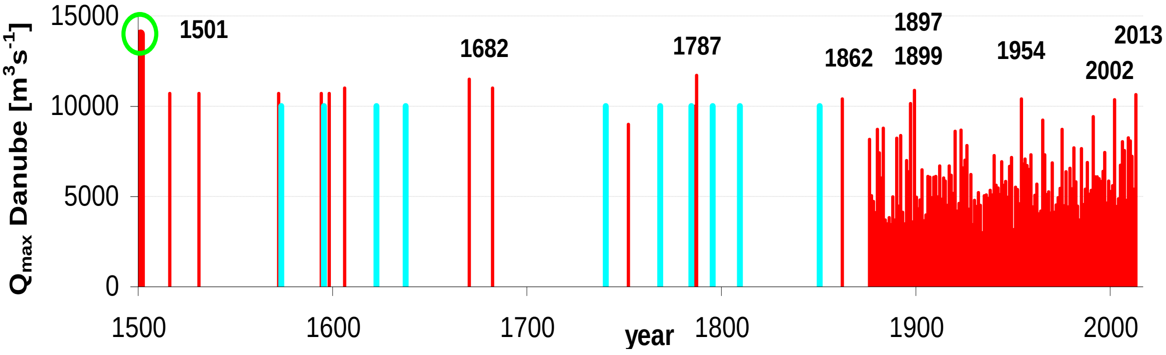

Fig. 2.11 Historical Danube River floods in river section Kienstock–Bratislava between 1500 and 1876 (red columns - summer floods, blue columns - winter floods); and after 1876 the observed annual peaks Q_{max} at the Bratislava water gauge are shown.

References

Bayliss, A. C., Reed, D., W. 2001. The use of historical data in flood frequency estimation. http://nora.nerc.ac.uk/id/eprint/8060/1/BaylissRepN008060CR.pdf Centre for Ecology and Hydrology UK, 92 pp.

Bel M. 1735. Notitia Hvngariae Novae Historico-Geographica: Divisa In Partes Qvatvor, Qvarvm Prima, Hvngariam Cis-Danvbianam; Altera, Trans-Danubianam; Tertia, Cis-Tibiscanam; Qvarta, Trans-Tibiscanam: Vniuersim XLVIII. Tomus Primus. http://oldbooks.savba.sk/digi/Lyc_B_VIII_33_I/start.htm

Bondar C, Panin N. 2001. The Danube delta hydrologic DataBase modeling. In:Proc. Intern. Workshop on „Modern and Ancient Environments and Processes“ in Jugur, Romania.

Brázdil R, Kundzewicz ZW. 2006. Historical hydrology – Editorial. *Hydrological Sciences Journal*, 51, 5, 733–738.

Elleder L, Herget J, Roggenkamp T, Nießen A. 2013. Historic floods in the city of Prague – a reconstruction of peak discharges for 1481–1825 based on documentary sources. *Hydrology Research*, 44, 2, 202–214.

Horváthová B. 2003. Flood is not only the high water. (Povodeň to nie je iba veľká voda.) VEDA, Bratislava, 232 pp. (in Slovak).

Kiss A. 2009. Historical climatology in Hungary: role of documentary evidence in the study of past climates and hydrometeorological extremes. *Időjárás*, 113 (4), 315–339.

Kiss A. 2011. Floods and long-term water-level changes in medieval Hungary. Doctoral dissertation. Central European University Budapest, Hungary, 323 pp.

Kiss A, Laszlovszky J. 2013. 14th–16th-century Danube floods and long-term water level changes in archaeological and sedimentary evidence in the western and central Carpathian Basin: an overview with documentary comparison, *J. Environ. Geogr*., 6, 1–11.

Kresser W. 1957. Floods of the Danube. (Die Hochwässer der Donau.) Springer Verlag, Wien, 95 pp. (in German).

Kresser W. 1970. The change in the flood discharge in the Danube at Vienna resulting from hydraulic structures along the river and its drainage area. In: Conference of the Danube Countries on Hydrological Forecasting, Beograd, 183–189.

Lauda E, Siedek R, Grengg R, Kovářík K, Goldbach J, Herbst A, Bozděch G, Halter R. 1908. Der Schutz der Reichshaupt- und Residenzstadt Wien gegen die Hochfluten des Donaustromes. Beiträge zur Hydrographie Österreichs. IX. Heft, Hydrographiser Dienst in Österreich.144 p.

Melo M, Bernáthová D. 2013. Historical floods in Slaná river basin since the end of the 18th century till the beginning of the 20th century (Historické povodne v povodí Slanej od konca 18. do začiatku 20. storočia). *Acta Hydrologica Slovaca*, 14, 2, 291–298 (in Slovak).

Miklánek P, Mikuličková M, Mitková V, Pekárová P. 2002. Changes of floods travel times on upper Danube. In: CD Proc. XXIst Conf. of the Danube Countries on Hydrological Forecasting (Bucharest, Romania), National Institute of Meteorology and Hydrology, Bucharest. ISBN 973-0-02759-5.

Mitková V, Pekárová P, Miklánek P, Pekár J. 2005. Analysis of flood propagation changes in the Kienstock–Bratislava reach of the Danube River. *Hydrolog. Sci. J.*, 50(4), 655–668.

NC, 2007. Indicators of Hydrologic Alteration. Version 7 User's Manual. The Nature Conservancy, Arlington.

Neweklowsky E. 1955. The Danube near Linz and its channel training (Die Donau bei Linz und ihre Regelung). In: Naturkundliches Jahrbuch der Stadt Linz 1; http://www.landesmuseum.at/pdf_frei_remote/NKJB_1_0171-0226.pdf, 171–226 (in German).

Pekárová P. 2009. Multiannual runoff variability in the upper Danube region. Doctor of Science Thesis, Bratislava, IH SAS, 151 p. <Http://147.213.145.2/pekarova>

Pekárová P, Halmová D, Bačová Mitková V, Miklánek P, Pekár J, Škoda P. 2013. Historic flood marks and flood frequency analysis of the Danube River at Bratislava, Slovakia. *J. Hydrol. Hydromech.*, 61, 4, 326–333.

Pekárová P, Onderka M, Pekár J, Miklánek P, Halmová D, Škoda P, Bačová Mitková V. 2008. Hydrologic Scenarios for the Danube River at Bratislava. Ostrava: KEY Publishing, 159 p. ISBN 978-80-87071-51-9.

Pekárová P, Miklánek P, Melo M, Halmová D, Pekár J, Bačová Mitková V. 2014. Flood marks along the Danube River between Passau and Bratislava. Bratislava. Veda, 102 pp. ISBN 978-80-224-1408-1.

Pišút P. 2011. The 1787 flood of the River Danube in Bratislava (Dunajská povodeň v roku 1787 a Bratislava). *Geographical Journal*, 63, 87–109 (in Slovak).

Rohr C. 2005. The Danube Floods and Their Human Response and Perception (14th to 17th C). *History of Meteorology*. 2, 71–86.

Rohr C. 2007. Extreme nature events in the Eastern Alps (Extreme Naturereignisse im Ostalpenraum). Naturerfahrung im Spätmittelalter und am Beginn der Neuzeit, Böhlau-Verlag GmbH, 640 pp (in German).

Stankoviansky M, Pišút P. 2011. Geomorphic response to the little ice age in Slovakia. *Geographia Polonica*, 84, Special Issue Part 1, 127–146.

Svoboda A, Pekárová P, Miklánek P. 2000. Flood Hydrology of Danube between Devín and Nagymaros. Bratislava: ÚH SAV; SVH, 96 p. ISBN 80-967808-9-1.

Szlávik L. 2002. Flood control. In: Somlyódy, L. (ed.): Strategic issues of the Hungarian water management, 205–243. Hungarian Academy of Sciences, Budapest (in Hungarian).

3 Analysis of homogeneity of annual time series

Petr Janál

3.1 Introduction

The accuracy and reliability of climate change, flood and drought modelling, water resources planning, determination of rainfall-runoff relationship, and river flow estimation models vary according to the quality of the data used. Factors such as method of gauging and data collection, the conditions around the station, station relocation, and the reliability of the measurement tool affect the homogeneity of the records. For this reason, the data recorded at gauging stations should be tested and checked for homogeneity prior to their use in research studies.

3.2 Methods

Available data consisted of daily average discharge series and annual maximum discharge series. Data from seventy seven water-gauging stations were processed. The included stations are listed in Table 1, which also shows the lengths of the series. In some stations, the series were not complete. Missing data is summarized in Table 2. The stations with gaps in data were also used in the analysis, but the particular series were shortened. The daily average discharges served as source data for the calculation of monthly and annual average discharges. Annual data refer to the hydrological years. Fourteen data series were tested for each station, the annual average and maximum discharges and the monthly average discharges for each month separately.

In order to perform the homogeneity analyses of data, two different tests of homogeneity were applied on each series, the standard normal homogeneity test (Alexandersson, 1986) and the Mann-Whitney-Pettit test (Pettit, 1979). Software Anclim (Štěpánek, 2007) was used to perform both tests. If inhomogeneity was found, that particular series was split at the point of inhomogeneity. Such newly created parts of series were tested again separately. The inhomogeneity was considered significant if T_o value exceeded 95% in the case of standard normal inhomogeneity test or if *p*-value was under 0.05 in the case of Mann-Whitney-Pettit test.

3.3 Results

All the results from the Danube stations are presented in the Tables at the end of the chapter (including insignificant inhomogeneities). The results from the Danube tributaries are included in APPENDIX III – Analysis of homogeneity. Both tests were compared and the obtained results were colour-distinguished. The inhomogeneities that were in this way identified as significant in both tests are summarized in Table 3. At least one significant inhomogeneity confirmed by both tests was found in 39 stations (see Table 3).

The legend is the same for all the tables below.
Standard Normal Homogeneity Test - Mark "<" is used where T_o value exceeds 95%.
Mann-Whitney-Pettit Test - Mark "<" is used where p-value is below 0.05.

(yellow)	Match in both tests.
(blue)	Significant inhomogeneity in one of the tests.
(purple)	Significant inhomogeneity in both tests.

Table 3.1 Gauging stations and data availability

RIVER	STATION	COUNTRY	DAILY DATA (Q_d)		EXTREME DATA (Q_{max})	
			from	to	from	to
Danube	Berg	GE	01.01.1930	31.12.2007	1930	2007
Danube	Ingolstadt	GE	01.01.1924	31.12.2007	1947	2007
Danube	Regensburg	GE	01.01.1924	31.12.2007	1924	2007
Danube	Pfelling	GE	01.01.1926	31.12.2007	1926	2007
Danube	Hofkirchen	GE	01.01.1901	31.12.2007	1901	2007
Danube	Achleiten	GE	01.01.1901	31.12.2007	1901	2007
Inn	Oberaudorf	GE	01.01.1901	31.12.2007	1901	2007
Inn	Passau-Ingling	GE	01.01.1921	31.12.2007	1921	2007
Lech	Landsberg	GE	01.01.1901	31.12.2007	1901	2007
Regen	Regenstauf	GE	01.01.1901	31.12.2007	1901	2007
Salzach	Burghausen	GE	01.01.1901	31.12.2007	1901	2007
Issar	Plattling	GE	01.01.1926	31.12.2007	1926	2007
Danube	Linz/Aschach	AT	01.01.1931	31.12.1990	1821	2002
Danube	Stein-Krems/Kienst	AT	01.01.1900	31.12.2003	1828	2006
Danube	Wien-Nussdorf	AT	01.01.1900	31.12.2006	1928	2006
Danube	Devin/Bratislava	SK	01.01.1876	31.12.2006	1876	2007
Danube	Nagymaros	HU	01.01.1893	31.12.2007	1893	2007
Danube	Mohács	HU	01.01.1930	31.12.2007	1930	2007
Danube	Bezdan	SR	01.01.1931	31.12.2007	1950	2006
Danube	Bogojevo	SR	01.01.1931	31.12.2007	1950	2006
Danube	Pancevo	SR	01.01.1931	31.12.2007	1946	2006
Danube	Veliko Gradiste	SR	01.01.1931	31.12.2007		
Danube	Orsova/Turnu Severi	RO	01.01.1900	31.12.2005		
Danube	Ceatal Izmail	RO	01.01.1931	31.12.2008		
Enns	Steyr	AT	01.01.1951	31.12.2005	1895	2007
Traun	Ebensee	AT	01.01.1951	31.12.2005	1951	2005
Morava	Kromeriz	CZ	01.01.1915	31.12.2007	1915	2007
Morava	Straznice	CZ	01.01.1920	31.12.2007	1921	2007
Jihlava	Ivancice	CZ	01.11.1923	31.12.2007	1924	2007
Svratka	Zidlochovice	CZ	01.11.1915	31.12.2007	1921	2007
Morava	Mor.Sv.Jan	SK	01.01.1922	31.10.2006	1895	2007
Bela	Podbanske	SK	01.01.1928	30.10.2006	1928	2008
Vah	L. Mikulas	SK	01.01.1921	31.10.2006	1921	2007
Vah	Sala	SK	01.01.1921	30.10.2006	1901	2007
Hron	B. Bystrica	SK	01.01.1931	31.10.2006	1931	2006
Hron	Brehy	SK	01.01.1931	31.10.2006	1924	2007
Kysuca	Kysucke N. Mesto	SK	01.01.1931	31.10.2006	1931	2007
Topla	Hanusovce	SK	01.01.1931	31.10.2006	1931	2007
Krupinica	Plastovce	SK	01.01.1931	31.10.2006	1931	2007
Ipel	Holisa	SK	01.01.1931	31.10.2006	1931	2006
Nitra	Nitrianska Streda	SK	01.11.1930	31.10.2007	1924	2006

RIVER	STATION	COUNTRY	DAILY DATA (Q_d)		EXTREME DATA (Q_{max})	
			from	to	from	to
Raba	Arpas	HU	01.12.1954	31.12.2007	1954	2007
Tisza	Vasarosnameny	HU	01.01.1882	31.12.2007	1882	2007
Tisza	Szolnok	HU	01.01.1920	31.12.2007		
Tisza	Szeged	HU	01.01.1921	31.12.2007	1921	2007
Szamos	Csenger	HU	01.01.1930	31.12.2007	1930	2007
Maros	Mako	HU	01.01.1930	31.12.2007	1930	2007
Sajo	Felsoezsolca	HU	01.01.1891	31.12.2007	1891	2007
Tisza	Senta	SR	01.01.1931	31.12.2007	1946	2006
Lim	Prijepolje	SR	01.01.1926	31.12.2007	1946	2006
Drina	Bajina Basta	SR	01.01.1926	31.12.2007	1946	2006
Sava	Sremska Mitrovic	SR	01.01.1926	31.12.2007	1946	2006
Moravica	Arilje	SR	01.01.1963	31.12.2007	1950	2006
Ibar	Lopatnica Lakat	SR	01.01.1948	31.12.2007	1948	2006
Zapadna Morava	Jasika	SR	01.01.1959	31.12.2007		
Juzna Morava	Mojsinje	SR	01.01.1948	31.12.2007	1950	2006
Velika Morava	Ljubicevski most	SR	01.01.1931	31.12.2007	1948	2006
Drava	Donji Miholjac	HR	01.01.1926	31.12.2007	1926	2007
Kupa	Jamnicka Kiselica	HR	01.01.1948	31.12.2007	1948	2007
Sava	Zagreb (incl. Cate	HR	01.01.1926	31.12.2008	1926	2008
Orljava	Pleternica Most	HR	01.01.1946	31.12.2008	1946	2008
Una	Kostajnica	HR	01.01.1926	31.12.2008	1926	2008
Sava	Čatež	SI	01.01.1956	31.12.2005		
Krka	Podbočje	SI	01.01.1933	31.12.2005		
Savinja	Laško	SI	17.03.1907	31.12.2005		
Sava	Litija	SI	01.01.1927	31.12.2005		
Siret	Storozhinec	UKR	01.01.1953	31.12.2005	1953	2005
Prut	Chernivcy	UKR	01.01.1895	31.12.2005	1895	2005
Tisza	Rakhiv	UKR	01.01.1947	31.12.2005	1947	2005
Tisza	Vylok	UKR	01.01.1954	31.12.2005	1954	2005
Rika	Mizhhirya	UKR	01.01.1947	31.12.2005	1946	2005
Latorycya	Mucacheve	UKR	01.01.1947	31.12.2005	1946	2005
Latorycya	Chop	UKR	01.01.1957	31.12.2005	1956	2005
Uzh	Uzhhorod	UKR	01.01.1947	31.12.2005	1946	2005
Prut	Jaremcha	UKR	01.01.1950	31.12.2005	1950	2005
Una	Kralje	BA	01.01.1969	31.12.2005	1969	2005
Vrbas	Kozluk Jajce	BA	01.01.1971	31.12.2005	1971	2005

Qd - Daily discharge
Qmax - yearly peak
Missing data in some years

Table 3.2 Summary of missing data in the series of average daily discharges

RIVER	STATION	COUNTRY	MISSING DATA	
			from	to
Danube	Berg	GE	01.03.1945	31.07.1945
Tisza	Vasarosnameny	HU	01.01.1882	31.10.1882
			01.11.1887	31.10.1888
			01.04.1895	10.04.1895
			31.08.1904	31.08.1904
			30.07.1914	31.07.1914
			01.05.1919	31.05.1919
			21.08.1919	22.08.1919
			01.09.1919	29.02.1920
			01.05.1920	30.06.1920
Tisza	Szolnok	HU	01.01.1920	31.10.1920
			01.10.1944	31.10.1944
			01.01.1945	09.02.1945
Szamos	Csenger	HU	14.08.1940	31.08.1940
			28.02.1950	28.02.1950
			07.07.1960	07.07.1960
			24.09.2004	30.09.2004
Maros	Mako	HU	01.11.1944	16.12.1944
			31.12.1959	31.12.1959
			31.10.1967	31.10.1967
			15.09.1981	15.09.1981
			01.08.1985	31.08.1958
Sajo	Felsoezsolca	HU	09.11.1944	09.11.1944
			12.11.1944	31.12.1944
			31.08.1968	31.08.1968
			14.07.2002	14.07.2002
Velika Morava	Ljubicevski most	SR	01.10.1944	16.01.1945
			01.01.1963	28.02.1963
			31.12.2007	31.12.2007
Una	Kostajnica	HR	01.06.1991	31.12.1991
Savinja	Laško	SI	24.07.1911	21.09.1911
			17.10.1911	23.10.1911
			01.12.1912	31.03.1913
			01.06.1918	30.06.1918
			01.10.1918	31.10.1918
			01.05.1919	21.10.1919
			01.02.1920	22.06.1920
			29.08.1920	12.01.1921
			06.04.1922	30.06.1922
			01.07.1925	29.09.1925
			27.02.1929	08.03.1929
			01.01.1940	31.12.1945
Siret	Storozhinec	UKR	11.09.1953	11.09.1953
			01.01.1961	31.12.1961
Prut	Chernivcy	UKR	01.01.1912	31.08.1919
			01.01.1925	31.12.1925
			01.01.1936	31.12.1944
			01.01.1969	31.12.1969

Table 3.3 Significant inhomogeneities confirmed by both tests

Station	Country	Series	Change	Station	Country	Series	Change
Danube Linz	AT	X	1942	Inn - Obersaudorf	GE	I	1974
		max	1890			III	1974
Danube St.Krems	AT	III	1937	Inn - Passau Ingling	GE	I	1974
		max	1954			XII	1973
Danube Wien	AT	IX	1942	Lech Landsberg	GE	II	1955
Enns Steyr	AT	I	1974			III	1940
Danube Nagymaros	HU	IX	1942			IV	1954
Raba Arpas	HU	II	1989	Regen Regenstauf	GE	I	1915
Tisza Vasarosnameny	HU	annual	1983	Salzach Burghausen	GE	I	1974
Tisza Szolnok	HU	VIII	1997	Issar Plattling	GE	IX	1937
Szamos Csenger	HU	IX	1964	Belá Podbánské	SK	II	1945
		X	1942			XII	1953
		max	1962	Hron Bánská Bystrica	SK	annual	1982
Tisza Senta	HU	X	1942	Krupnica Plastovce	SK	max	1968
Danube Bezdan	SR	VI	1935	Drava Donji Mihonjac	HR	XII	1958
		X	1946	Una Kostajnica	HR	XI	1967
Danube Pancevo	SR	VII	1981	Sava Catez	HR	II	1981
Lim Prijepolje	SR	II	1999			V	1992
		annual	1982			annual	1981
Drina Bajina Basta	SR	V	1982	Sava Litija	SI	VI	1992
		annual	1982	Siret Storozhinece	UKR	annual	1996
Sava Sremska Mitrovica	SR	XI	1945	Prut Chernivci	UKR	III	1983
Zapadna Morava Jasika	SR	XII	1982			X	1991
Juzna Morava Mojsinje	SR	max	1967			annual	1983
Danube Orsova/Turnu Severin	RO	III	1936			annual	1978
		IX	1955	Tisza Rakhiv	UKR	X	1991
Jihlava Ivančice	CZ	annual	1996	Lator Mucacheve	UKR	annual	1974
Svratka Židlochovice	CZ	max	1949	Prut Jaremcha	UKR	X	1991
Velička - Strážnice	CZ	III	1971			annual	1969

3.4 Conclusion

At least one significant inhomogeneity confirmed by both tests was found in 39 stations (see Table 3). Given that the total number of tested series is 1078, such results should be considered satisfactory. Most of the series ended in the years 2005 or 2007. Prolongation of the series probably should not change these results significantly. Subsequent revision and homogenization of the series requires additional information about gauging stations and should be done by local experts.

Following tables show all the results from the stations on the Danube channel (including insignificant inhomogeneities). The results from the Danube tributaries are in APPENDIX III – Analysis of homogeneity.

Danube Berg

Standard Normal Homogeneity Test

Month	Change		Period	n
I	1982		1930-2007	78
II	1983	<	1982-2007	26
II	1935		1930-2007	78
III	1999		1946-2007	62
IV	1962			
V	1964	<		
VI	1960			
VII	1947			
VIII	1941		1930-2007	78
IX	1941	<		
IX	1939	<	1930-1940	11
X	1941		1930-2007	78
X	1939	<	1930-1940	11
XI	1945		1930-2007	78
XII	1965			
XII	1966	<	1965-2007	43
annual	1965		1946-2007	62
max	1936		1930-2007	78

Mann-Whitney-Pettit Test

Month	Change		Period	n
I	1974		1930-2007	78
II	1955			
III	1999		1946-2007	62
IV	1962	<		
V	1961	<		
VI	1960			
VII	1953			
VIII	1942		1930-2007	78
IX	1941			
X	1973			
XI	1972			
XII	1972	<		
annual	1965		1946-2007	62
max	1977		1930-2007	78

Danube Ingolstadt

Standard Normal Homogeneity Test

Month	Change		Period	n
I	1974		1924-2007	84
II	1935			
III	1999			
IV	2007			
V	1925			
VI	1927			
VII	2001			
VIII	1925	<		
IX	1942			
X	1942			
X	1939	<	1924-1941	18
XI	1945		1924-2007	84
XI	1944	<	1924-1944	21
XII	1973	<	1924-2007	84
annual	1965		1925-2007	83
max	1999		1947-2007	61

Mann-Whitney-Pettit Test

Month	Change		Period	n
I	1974	<	1924-2007	84
II	1974			
III	1977			
IV	1962			
V	1943			
VI	1989			
VII	2001			
VIII	1942			
IX	1942			
X	1942			
X	1935	<	1924-1941	18
X	1973	<	1942-2007	66
XI	1972		1924-2007	84
XII	1972	<		
annual	1965		1925-2007	83
max	1978	<	1947-2007	61

Danube Regensburg

Standard Normal Homogeneity Test

Month	Change		Period	n
I	1974		1924-2007	84
II	1935			
III	1937			
IV	1962			
V	1925	<		
VI	1927			
VII	2001			
VIII	1925	<		
IX	1942			
X	1942			
X	1939	<	1924-1941	18
XI	1945		1924-2007	84
XII	1965			
annual	1965		1925-2007	83
max	1993		1924-2007	84

Mann-Whitney-Pettit Test

Month	Change		Period	n
I	1974	<	1924-2007	84
II	1966			
III	1977			
IV	1962			
V	1962			
V	1946	<	1924-1961	38
VI	1989		1924-2007	84
VII	2001			
VIII	1942			
IX	1942			
IX	1965	<	1942-2007	66
X	1946		1924-2007	94
XI	1942			
XII	1965	<		
annual	1965		1925-2007	83
max	1978		1924-2007	84

Danube Pfelling

Standard Normal Homogeneity Test

Month	Change		Period	n
I	1974		1926-2007	82
II	1935			
III	1937			
IV	1935			
V	1962			
VI	1927	<		
VII	1927			
VIII	1942			
IX	1942			
X	1942			
X	1939	<	1926-1941	16
XI	1945		1926-2007	82
XII	1965			
annual	1965		1927-2007	81
max	1993		1926-2007	82

Mann-Whitney-Pettit Test

Month	Change		Period	n
I	1974	<	1926-2007	82
II	1966			
III	1977			
IV	1962			
V	1961			
V	1946	<	1926-1960	35
VI	1945		1926-2007	82
VII	1959			
VIII	1942			
IX	1942			
X	1946			
XI	1942			
XII	1965	<		
annual	1965		1927-2007	81
max	1978		1926-2007	82

Danube Hofkirchen

Standard Normal Homogeneity Test

Month	Change		Period	n
I	1910		1901-2007	107
II	1935			
III	1999			
IV	1902			
V	1946			
VI	1996			
VII	2001			
VIII	1988			
IX	1942			
X	1998			
XI	1998			
XII	1973			
annual	1965			
max	1998			

Mann-Whitney-Pettit Test

Month	Change		Period	n
I	1974		1901-2007	107
II	1935			
III	1937			
III	1917	<	1901-1936	36
IV	1962		1901-2007	107
V	1946			
VI	1989			
VII	1982			
VIII	1989			
IX	1942			
X	1946			
XI	1922			
XII	1973			
annual	1965			
max	1979			

Danube Achleiten

Standard Normal Homogeneity Test

Month	Change		Period	n
I	1974		1901-2007	107
II	1935			
III	1999	<		
IV	2007			
V	1925			
VI	1988			
VII	1982			
VIII	1971			
IX	1942			
X	1946			
XI	1992			
XII	1973			
annual	2004		1902-2007	106
max	1939		1901-2007	107

Mann-Whitney-Pettit Test

Month	Change		Period	n
I	1974	<	1901-2007	107
II	1966	<		
III	1937	<		
IV	1935			
V	1925			
VI	1946			
VII	1982			
VIII	1971			
IX	1942			
X	1946			
XI	1972			
XII	1973			
annual	1946		1902-2007	106
max	1939		1901-2007	107

Danube Linz

Standard Normal Homogeneity Test

Month	Change		Period	n
I	1974		1931-1990	60
II	1935			
III	1937			
III	1943	<	1937-1990	54
IV	1935		1931-1990	60
V	1989			
VI	1971			
VII	1968			
VIII	1971			
IX	1942	<		
X	1946	<		
XI	1945			
XII	1973			
annual	1946		1932-1990	59
max	1890	<	1821-2002	182

Mann-Whitney-Pettit Test

Month	Change		Period	n
I	1974		1931-1990	60
II	1974			
III	1937			
IV	1971			
V	1971			
VI	1946	<		
VII	1960			
VIII	1971			
IX	1942			
X	1946	<		
XI	1946			
XII	1973			
annual	1946		1932-1990	59
max	1890	<	1821-2002	182

Danube St Krems

Standard Normal Homogeneity Test

Month	Change		Period	n
I	2003		1900-2003	104
II	1935			
III	1999	<		
III	1937	<	1900-1998	99
IV	1935		1900-2003	104
V	1905			
VI	1996			
VII	2002			
VIII	2003			
IX	1942			
X	1996			
XI	1992			
XII	1973	<		
annual	1910		1901-2003	103
max	1954	<	1828-2006	179

Mann-Whitney-Pettit Test

Month	Change		Period	n
I	1974		1900-2003	104
II	1966	<		
III	1937	<		
IV	1935			
V	1961			
VI	1988			
VII	1982			
VIII	1971			
IX	1942			
X	1946			
XI	1922			
XII	1964	<		
annual	1965		1901-2003	103
max	1906	<	1828-2006	179
max	1954	<	1906-2006	101

Danube Wien

Standard Normal Homogeneity Test

Month	Change		Period	n
I	1974		1900-2006	107
II	1935			
III	1999	<		
IV	2006			
V	1925			
VI	1988			
VII	1982			
VIII	1971			
IX	1942	<		
X	1946			
XI	1992			
XII	1973			
annual	1905		1901-2006	106
max	1890	<	1828-2006	179

Mann-Whitney-Pettit Test

Month	Change		Period	n
I	1974		1900-2006	107
II	1966			
III	1937	<		
IV	1935			
V	1925			
VI	1968			
VII	1982			
VIII	1971			
IX	1942	<		
X	1946			
XI	1912			
XII	1973			
annual	1910		1901-2006	106
max	1906	<	1828-2006	179

Danube Bratislava

Month	Change		Period	n
I	2006			
II	1877		1876-2006	131
III	1965			
III	1968	<	1965-2006	42
IV	1877			
V	1881			
VI	1881			
VII	1881			
VIII	1928		1876-2006	131
IX	1928			
X	1882			
XI	1882			
XII	1882			
annual	1928		1877-2006	130
max	1991		1876-2007	132

Month	Change		Period	n
I	1965			
II	1965			
III	1965			
IV	1965			
V	1965			
VI	1928		1876-2006	131
VII	1928			
VIII	1928			
IX	1928			
X	1928			
XI	1928			
XII	1928			
annual	1928		1877-2006	130
max	1939		1876-2007	132

Danube Nagymaros

Standard Normal Homogeneity Test

Month	Change		Period	n
I	1928			
II	1894			
III	1999		1893-2007	115
IV	2005			
V	1925			
VI	1968			
VI	1965	<	1893-1967	75
VII	1976			
VIII	1898		1893-2007	115
IX	1942	<		
IX	2007	<	1942-2007	66
X	1946			
XI	1910		1893-2007	115
XII	1900			
annual	1946		1894-2007	114
max	2006		1893-2008	115

Mann-Whitney-Pettit Test

Month	Change		Period	n
I	1933		1893-2007	115
I	1974	<	1933-2007	75
II	1949			
III	1977			
IV	1910			
V	1928			
VI	1968	<	1893-2007	115
VII	1968			
VIII	1961			
IX	1942	<		
X	1946			
XI	1946			
XI	1922	<	1893-1945	53
XII	1973		1893-2007	115
annual	1946		1894-2007	114
max	1994		1893-2008	115

Danube Mohács

Standard Normal Homogeneity Test

Month	Change		Period	n
I	1974			
II	1935			
III	1935			
IV	1937			
V	1935			
VI	1935		1930-2007	78
VII	2000			
VIII	1971			
IX	2007			
X	1946			
X	1954	<	1946-2007	62
XI	1942		1930-2007	78
XII	1974			
XII	1975		1974-2007	34
annual	1936		1931-2007	77
max	1935	<	1930-2007	78

Mann-Whitney-Pettit Test

Month	Change		Period	n
I	1974	<		
II	1974			
III	1999			
IV	1937			
V	1937			
VI	1968		1930-2007	78
VII	1968			
VIII	1971			
IX	1975			
X	1946			
XI	1942			
XII	1974			
annual	1936		1931-2007	77
max	1991	<	1930-2007	78

Danube Bezdan

Standard Normal Homogeneity Test

Month	Change		Period	n
I	1974		1931-1990	60
II	1949			
III	1949			
IV	1971			
V	1971			
VI	1946			
VI	1935	<	1931-1945	15
VII	1976		1931-1990	60
VIII	1971			
IX	1942	<		
X	1946	<		
XI	1942	<		
XI	1939	<	1931-1941	11
XII	1945		1931-1990	60
annual	1946		1932-1990	59
max	2006		1950-2006	57

Mann-Whitney-Pettit Test

Month	Change		Period	n
I	1974		1931-1990	60
II	1949			
III	1971			
III	1977	<	1971-1990	20
IV	1971		1931-1990	60
V	1968			
VI	1946	<		
VI	1935	<	1931-1945	15
VII	1968		1931-1990	60
VIII	1971			
IX	1942			
X	1946	<		
XI	1946	<		
XII	1942			
annual	1968		1932-1990	59
max	1994		1950-2006	57

Danube Bogojevo

Standard Normal Homogeneity Test

Month	Change		Period	n
I	1974		1931-2007	77
II	1984			
III	1949	<		
IV	1948			
V	1971			
VI	1945	<		
VI	1935	<	1931-1944	14
VII	1981	<	1931-2007	77
VIII	1983	<		
IX	1942	<		
X	1942	<		
XI	1942	<		
XI	1939	<	1931-1941	11
XII	1945		1931-2007	77
annual	1946	<	1932-2007	76
max	2006		1950-2006	57

Mann-Whitney-Pettit Test

Month	Change		Period	n
I	1974		1931-2007	77
I	1984	<	1974-2007	34
II	1984		1931-2007	77
III	1971	<		
IV	1971			
V	1971			
VI	1968	<		
VI	1989	<	1968-2007	40
VII	1981	<	1931-2007	77
VIII	1982	<		
IX	1942			
X	1946			
XI	1946	<		
XII	1942			
annual	1983	<	1932-2007	76
max	1994		1950-2006	57

Danube Pancevo

Standard Normal Homogeneity Test

Month	Change		Period	n
I	1948		1931-2007	77
II	1936			
III	1971			
IV	2004			
V	1943			
VI	1988			
VII	1981	<		
VIII	1983			
IX	1942			
X	1942			
XI	1942	<		
XII	1982			
annual	1943		1932-2007	76
max	2005		1946-2006	61

Mann-Whitney-Pettit Test

Month	Change		Period	n
I	1955		1931-2007	77
II	1965			
II	1984	<	1965-2007	43
III	1971	<	1931-2007	77
IV	1971			
V	1946			
VI	1988	<		
VII	1981	<		
VIII	1983	<		
IX	1942			
IX	1955	<	1942-2007	66
X	1942		1931-2007	77
XI	1942			
XII	1967			
annual	1983		1932-2007	76
max	1983		1946-2006	61

Danube Veliko Gradiste

Standard Normal Homogeneity Test

Month	Change		Period	n
I	1948		1931-2007	77
II	1936			
III	1971			
IV	2004			
V	1943			
VI	1988			
VII	1981			
VIII	1982			
IX	1942			
X	1942			
XI	1942	<		
XII	1982			
annual	1982			
max	-	-	-	-

Mann-Whitney-Pettit Test

Month	Change		Period	n
I	1955		1931-2007	77
II	1988			
II	1994	<	1988-2007	20
III	1971	<	1931-2007	77
IV	1989			
V	1981			
VI	1981	<		
VII	1981	<		
VIII	1982	<		
IX	1942			
X	1942			
XI	1942			
XII	1982			
annual	1982			
annual	1995	<	1982-2007	26
max	-	-	-	-

Danube Orsova/Turnu Severin

Standard Normal Homogeneity Test

Month	Change		Period	n
I	1910		1840-2005	166
II	1936	<		
III	1841			
IV	2004			
V	1943			
VI	1988	<		
VII	1981			
VIII	1983			
IX	1942			
IX	1955	<	1942-2005	64
X	1853		1840-2005	166
X	1851	<	1840-1852	13
XI	1853		1840-2005	166
XII	1869			
XII	1861	<	1840-1868	29
annual	1983		1840-2005	166
max	-	-	-	-

Mann-Whitney-Pettit Test

Month	Change		Period	n
I	1910	<	1840-2005	166
II	1936	<		
III	1900			
IV	1875			
V	1943	<		
VI	1945	<		
VII	1927			
VIII	1921			
IX	1942			
IX	1955	<	1942-2005	64
X	1942		1840-2005	166
XI	1942			
XII	1909			
annual	1983			
annual	1995	<	1983-2005	23
max	-	-	-	-

Danube Ceatal Izmail

Standard Normal Homogeneity Test

Month	Change		Period	n
I	1953		1931-1995	65
II	1965			
II	1987	<	1965-1995	31
III	1989		1931-1995	65
IV	1989			
V	1989			
VI	1943			
VII	1981			
VIII	1983			
IX	1990			
X	1942			
XI	1942			
XII	1982			
annual	1983		1932-1995	64
max	-	-	-	-

Mann-Whitney-Pettit Test

Month	Change		Period	n
I	1955		1931-1995	65
II	1965	<		
II	1984	<	1965-1995	31
III	1971		1931-1995	65
IV	1962			
V	1962			
V	1982	<	1962-1995	34
VI	1943		1931-1995	65
VII	1981			
VIII	1983			
IX	1955			
IX	1942	<	1931-1954	24
X	1964		1931-1995	65
X	1946	<	1931-1963	33
X	1985	<	1964-1995	32
XI	1942		1931-1995	65
XII	1982			
annual	1983		1932-1995	64
max	-	-	-	-

References

Alexandersson H. 1986. A homogeneity test applied to precipitation data. J. Climatol., 6, 661-675.

Pettit AN. 1979. A non-parametric approach to the changepoint problem. Appl. Stat., 28, 126-135.

Štěpánek P. 2007. AnClim - software for time series analysis (for Windows). Dept. of Geography, Fac. of Natural Sciences, Masaryk University, Brno. 1.47 MB

.

4 Analysis of cyclicity and long-term trends of annual series, and Q_{max} series

Pavla Pekárová, Ján Pekár, and Pavol Miklánek

4.1 Introduction

The development of mankind depends on availability of water resources. Even the first agricultural civilizations noticed the temporal variability of water resources and oscillation of the dry and wet periods.

Almost 60 years ago, Williams (1961) investigated the nature and causes of cyclical changes in hydrological data of the world. He tested a correlation between hydrological data and sunspot activity with varying success. The most frequently studied cycles in connection with precipitation, temperature and runoff variability are the 10.5-year (21-year) Hale cycles and the 88-year Gleissberg cycle of solar activity. Another cycle studied in connection with hydrological and climatic data is the 18.6-year cycle lunar–solar tidal period. This period, together with solar cycles, is analysed in detail by Currie (1996). Interesting results were obtained by Charvátová and Střeštík (1995, 2004), who employed the inertial motion of the Sun around the barycentre of the Solar System as the base in searching for the possible influence of the Solar System on climatic processes, especially on changes in the surface air temperature. Charvátová (2000) explained a solar activity cycle of about 2400 years by solar inertial motion. She described the 178.7-year basic cycle of solar motion. Similarly, Esper et al. (2002), Vasiliev and Dergachev (2002), and Liritzis and Fairbridge (2003) showed that multiannual cycles probably have their origin in motion of the Earth in space. Solanki et al. (2004) report a reconstruction of the sunspot number covering the past 11,400 years. According to their reconstruction, the level of solar activity during the past 70 years is exceptional, and the previous period of equally high activity occurred more than 8,000 years ago. These studies underline the theory of the dependence of climate variability of the Earth on solar activity.

As the series of measured hydrological and meteorological data become longer and easier to access worldwide it is possible to deal with a large amount of complex historical data. For example, Probst and Tardy (1987) and Labat et al. (2004) studied mean annual discharge fluctuations of major rivers distributed around the world. Probst and Tardy (1987) showed that North American and European runoffs fluctuate in opposition, whereas South American and African runoffs present synchronous fluctuations. Kane (1997) predicted the occurrence of droughts in northeast Brazil. He found that the forecast of droughts based on the appearance of El Niño alone would be wrong half the time. Instead, predictions based on significant periodicities (13 and 26 years) give reasonably good results. Brázdil and Tam (1990), Walanus and Soja (1995), Sosedko (1997), Pekárová et al. (2003) and Rao and Hamed (2003) found several different dry and wet periods (2.6, 3.5, 5, 20–21, 29–30 years) in the precipitation, temperature and discharge time series in the whole world.

It is clear that predicting discharge for several years ahead based only on deterministic models does not result in meaningful data. This is why the use of stochastic models proceeding from the stochastic characteristics of the measured discharge time series are required. During the 1990s, rapid progress in long-term time-series modelling was achieved. This progress was possible due to the development of several stochastic models of hydrological time series using the random sampling method (the Monte Carlo method), classical time series analysis, spectral analysis, or the Box–Jenkins methodology (van Gelder et al., 2000; Popa and Bosce, 2002; Brockwell and Davis, 2003; Lohre et al., 2003; Rao and Hamed, 2003).

The aim of this chapter is the analysis of the long-term trends of yearly discharge time series and runoff variability of the River Danube at different stations in the basin.

4.2 Identification of the long-term variability

It is possible to identify the cyclicity or randomness in the time series by auto-correlation and spectral analysis. Both methods were used to look for the long-term cycles of runoff decrease and increase in the analysed runoff time series.

4.2.1 Brief overview of the spectral analysis of random processes

Estimation of both, the *auto-covariance* and the *auto-correlation functions* of given empirical series $\{x_i\}_{i=1}^{n}$, is the base tool of time series analysis.
The auto-covariance function $R(\tau)$ can be estimated by the formula

$$R(\tau) = \frac{\sum_{i=1}^{n-\tau} (x_i - \bar{x}).(x_{i+\tau} - \bar{x}_{i+\tau})}{n-\tau}, \qquad (4.1)$$

where: $\bar{x}$ – mean of $\{x_i\}$.

The normalized auto-covariance function (with respect to the standard deviation s_x) provides an estimation of the auto-correlation function $\mathrm{r}(\tau)$ of the form

$$\mathrm{r}(\tau) = \frac{R(\tau)}{s_x^2}, \qquad (4.2)$$

where: $\tau = 0,1,2,\ldots m$; $m = n/2$.

Function $r(\tau)$ reaches its values within the interval <-1, 1>.

The spectral analysis is used to examine the periodical properties of random processes $\{x_i\}_{i=1}^{n}$. The spectral analysis generalizes a classical harmonic analysis by introducing the mean value in time, of the periodogram obtained from the individual realizations. The fundamental statistical characteristic of a spectral analysis is its *spectral density*.
The basic tool in estimating the spectral density is the *periodogram*. A periodogram (a line spectrum) is a plot of frequency and ordinate pairs for a specific time period. This graph breaks a time series into a set of sine waves of various frequencies. It is used to construct a frequency spectrum. A periodogram can be helpful in identifying randomness and seasonality in time series data, and in recognizing the predominance of negative or positive autocorrelation – a help you often need to identify an appropriate model for forecasting a given time series. If the periodogram contains one spike, the data may not be random. The spectral density is defined as a mean value of the set of periodogram for n→∞.
The periodogram is calculated according to:

$$I(\lambda_j) = \frac{1}{2\pi n}\left|\sum_{\tau=1}^{n} x_\tau e^{-i\tau\lambda_j}\right|^2 = \frac{1}{2\pi n}\left\{\left(\sum_{\tau=1}^{n} x_\tau.\sin(\tau.\lambda_j)\right)^2 + \left(\sum_{\tau=1}^{n} x_\tau.\cos(\tau.\lambda_j)\right)^2\right\}. \qquad (4.3)$$

We compute the squared correlation between the series and the sine/cosine waves of frequency λ_j. By the symmetry $I(\lambda_j) = I(-\lambda_j)$ we need only to consider $I(\lambda_j)$ on $0 \le \lambda_j \le \pi$.

For real centred series the periodogram $I(\lambda_j)$ can be estimated by auto-covariance function as

$$I\left(\lambda_j\right) = \frac{1}{2\pi}.\left(R_0 + 2\sum_{\tau=1}^{n-1} R_\tau.\cos(\tau.\lambda_j) \right), \qquad (4.4)$$

for Fourier frequencies:

$$\lambda_{j'} = \frac{2\pi.j}{n}, \quad \text{where} \quad j = \left\langle 1, \frac{n}{2} \right\rangle \qquad (4.5)$$

4.2.2 Combined periodogram method

It is clear that from the relationship (4.4) that for low frequencies, i.e. for long periods, we compute the periodogram with a sparse step. For example, if a time series is 100 years long, the periodogram is only computed for periods of 100/2 = 50 years, 100/3 = 33.3 years, 100/4 = 25 years, etc. If the real period is of 29 years, then we do not get the correct period. This is why it is necessary to pay the maximum attention to the analysis and not to rely only on results provided by mathematical tests without the appropriate analysis. One way how to reveal the real period is decreasing the length of the measured series, i.e. computing the periodogram for different "random" selections of the series followed by computing the average value of the periodogram. The result of this process we will name as combined periodogram. In order to obtain such a combined periodogram the code PERIOD has been written. This code computes periodograms for series successively shortened by two years (Pekárová, 2003).

For analysis of long-term multi-annual variability of the mean annual discharges, we used the four longest available discharge time series. The first one is from the Russian station on Neva at Sankt Petersburg (1859–2010). The second is from the Slovak station Bratislava (1876–2006). The third one originates from Romanian station Turnu Severin (1840–2006), since 1970 for Orsova. The fourth one is from Ukrainian station Reni (1840–2006). Fig 4.1 shows the deviation time series of the individual mean annual discharges from the double 5-years moving averages of the mean discharge values.

4.2.3 Autocorrelation and spectral analysis

Multiannual variability of discharges was studied by means of the autocorrelation and spectral analysis. Fig. 4.2a-b. (left column) shows the autocorrelogram of the mean annual discharges of the selected stations. It is evident (at Neva River from autocorrelogram and periodogram very clearly), that these time series are marked by the multi- annual cycles of the dry and wet periods, meaning that the data is not independent. Linear trend of the cyclic series is highly affected by its values at the beginning and at the end of the series. The effect of multi-annual cyclic components has to be eliminated from the time series before determining a linear trend.

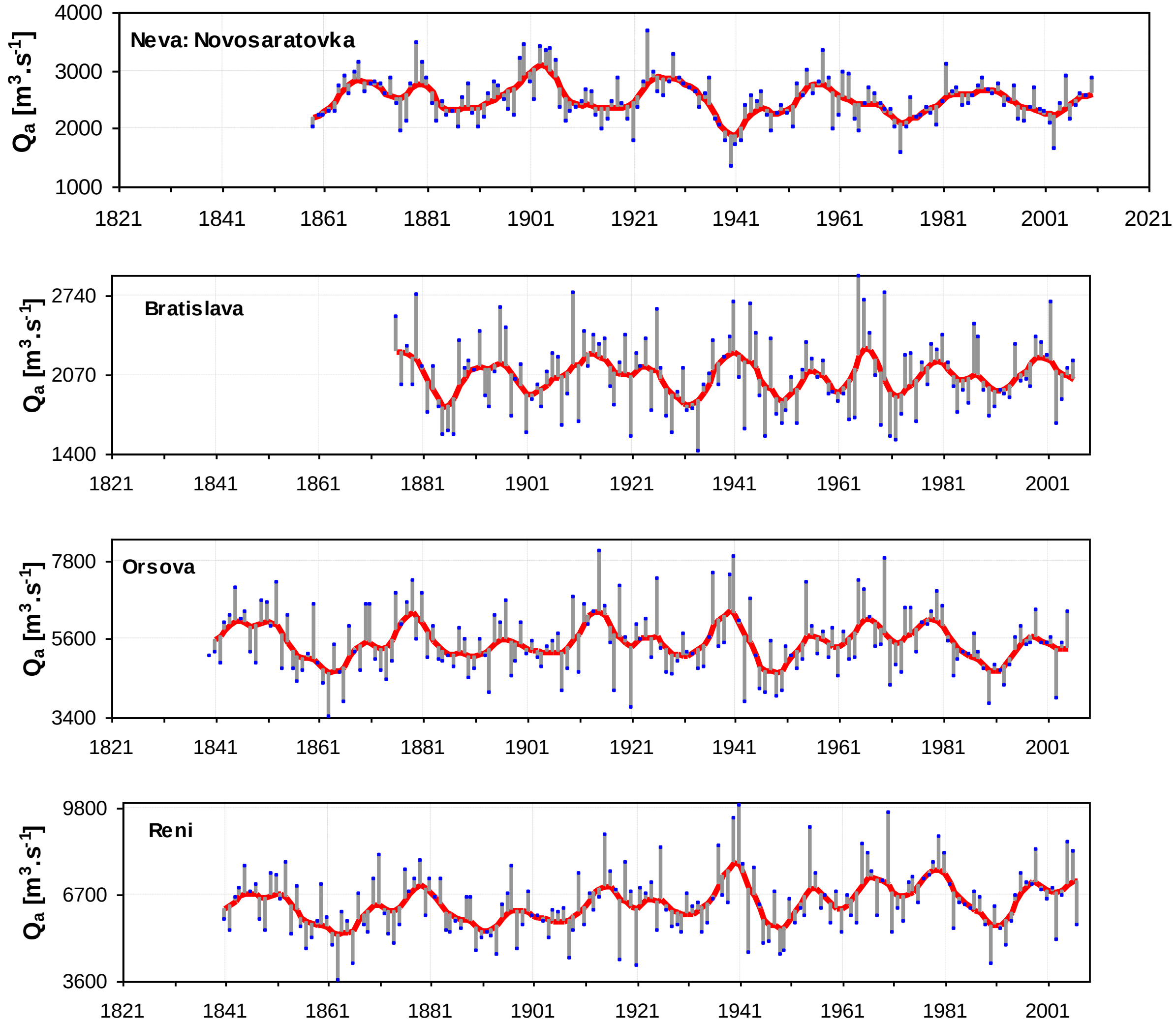

Fig. 4.1 *Average annual Neva and selected Danube stations discharge (points), deviations from the double 5-years moving averages (red bold line).*

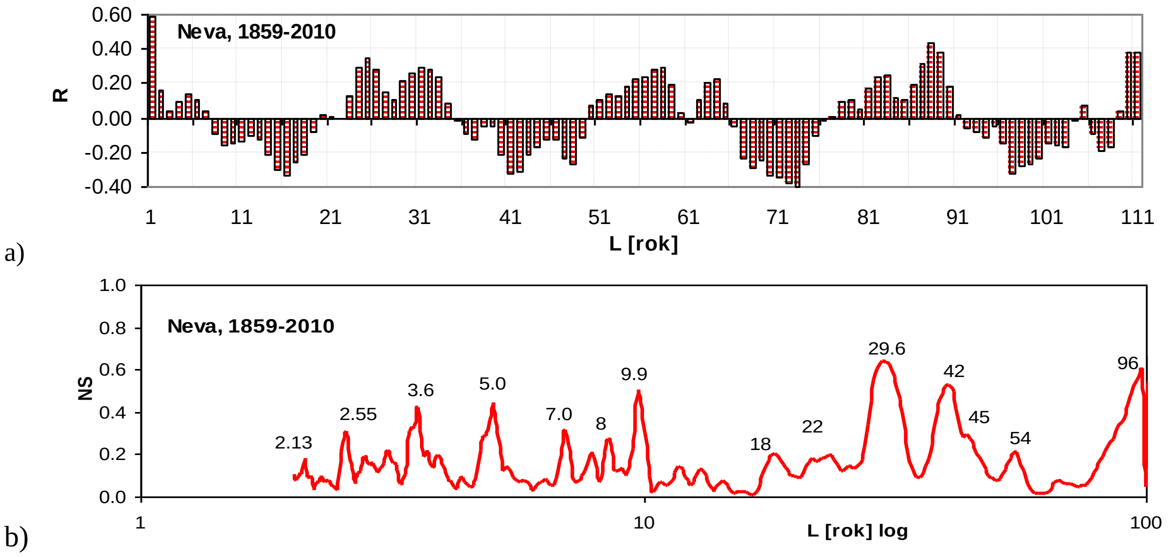

Fig. 4.2a. *a) Autocorrelogram (R – coefficient of correlation) and*
b) combined periodogram (NS- normalized spectrum, L – lag in years, logarithmic scale) of the Neva River discharge time series (1859-2010).

Autocorrelograms indicate a significant autocorrelation among the data of the time series. Negative autocorrelations were found for 6, and 9 year lags, positive autocorrelation were found for 13-14, 21-22, and 40-44 year lags. As the longer period lengths are not integers, it is not possible to identify them by means of the autocorrelograms of the annual values series. Therefore, the most significant period of 3.6 years does not noticeably show up on the autocorrelogram. It only slightly increases the autocorrelation coefficients for 3 and 4 years.

Therefore, the other significant periods were identified by **combined periodogram** method (Pekárová et al., 2003). This method revealed periods of 2.4, 3.6, 4.2, and 7 years, as well as long periods of 14, 22, 30 and 44 years (Fig. 4, right column).

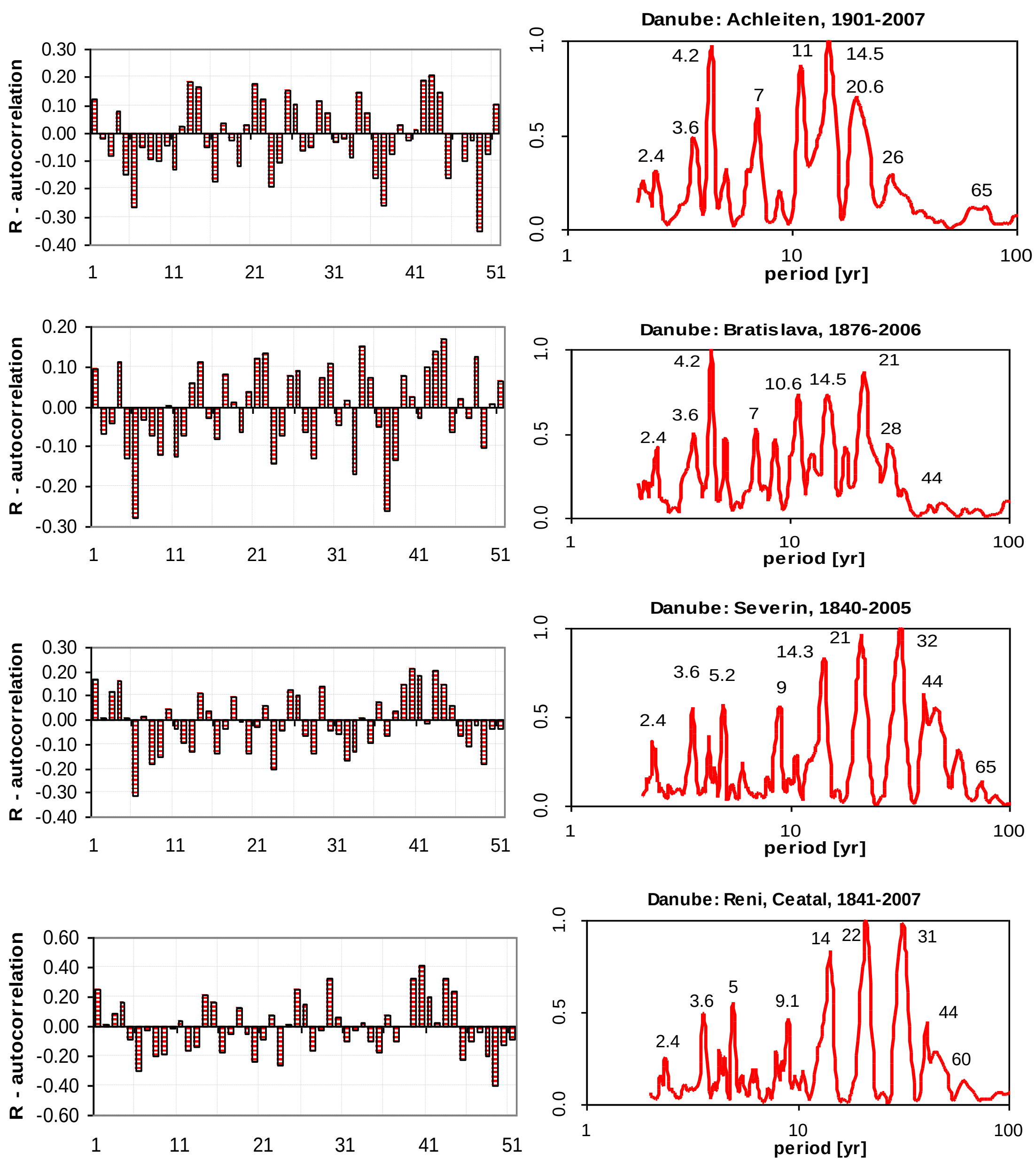

Fig. 4.2b Auto-correlograms (left column), and normalized combined periodograms (right column) of the mean annual discharges of the selected Danube River stations, significant periods.

As indicated in other studies (Pekárová, 2009), the cycle of 2.4 years is probably connected to QBO phenomena. The cycle of about 3.6 years probably depends on the Southern Oscillation (SO) represented by the SO index. The 44, 22, and 11 years cycles are connected to solar activity. The cycle length of approx. 28–31 years is related to the Arctic oscillation (AO), expressed by the AO index. Finally, the cycle of about 13 years is connected to the North Atlantic Oscillation (NAO), represented by the NAO index. Cross-correlograms and coherency coefficients have to be used to verify the teleconnections of the annual discharges in the Danube basin with the QBO, NAO, AO and SO phenomena and solar activity and thermohaline circulation.

4.3 Identification of the long-term trends

Generally, the zero hypothesis **H_0 - there is no trend** has to be tested against the alternative hypothesis **H_1 - there is a trend**. The parametric and non-parametric tests can be used for this purpose.

4.3.1 Parametric tests

The parametric test considers the linear regression of a random variable ***Y*** on time ***X***. The parameters of the trend line are calculated by using standard method for estimation of the parameters of a simple linear regression model, i.e. by using least square method. For the parametric trend analysis we used the software CTPA (Change and Trend Problem Analysis) (Procházka et al., 2001). The CTPA software offers tools for testing the mean of the analysed series in terms of its possible gradual change, time occurrence of this change and possible change in the parameters of the detected change. These tests include four tests:

- T*est of trend existence in the analysed series.* (The null hypothesis "the mean of the analysed series does not change" is tested against an alternative assuming that the analysed series involves a linear trend);
- *Test of trend appearance of upward or downward trend*. (The null hypothesis "the mean of the analysed series does not change" is tested against an alternative assuming that the analysed series involves a trend since observation (time) k, whose position is estimated);
- *Test for change in trend slope*. (The null hypothesis "the analysed series involves a constant trend" is tested against an alternative assuming a change in the parameters of the trend line at time which is estimated);
- T*est for change in trend slope.* (The null hypothesis "the analysed series involves a constant trend" is tested against an alternative assuming a change in the trend slope at time which is estimated).

The assumptions are: the residuals are independent equally distributed random variables with normal distribution and zero mean.

4.3.2 Non parametric tests

There are two non-parametric tests for trend analysis: the Mann-Kendall test based on the statistic S, and the Spearman's ρ (rho) test. For the non-parametric trend analysis we used the software AnClim (Štepánek, 2005). The Mann–Kendall trend test (Mann, 1945; Kendall, 1975) is one of the widely used distribution-free tests of trend in time series. Distribution-free

tests have the advantage that their power and significance are not affected by the actual distribution of the data. This is in contrast to parametric trend tests, such as the regression coefficient test, which assume that the data follow the Normal distribution, and whose power can be greatly reduced in the case of skewed data (Yue et al., 2002a,b). The Mann–Kendall trend test has therefore been widely used for testing trends in many natural time series that deviate significantly from the Normal distribution, such as temperature, rainfall, river flow, and water quality time series. The Mann-Kendall test estimates the gradients between each datum and all the subsequent data in a sequence and tests the null hypothesis based on the standardized sum of the number of positive gradients minus the sum of the number of negative gradients. This test is the result of the development of the nonparametric trend test first proposed by Mann (1945). This test was further studied by Kendall (1975) and improved by Hirsch et al (1982, 1984) who allowed taking into account seasonality.
For n (number of tested values) ≥ 10, the statistic S is approximately normally distributed with the mean and variance as follows

$$E(S) = 0 \tag{4.6}$$

$$VAR(S) = \frac{1}{18}\left[n(n-1)(n-2) - \sum_{p=1}^{q} t_p(t_p-1)(2t_p+5)\right] \tag{4.7}$$

where:
q – is the number of tied groups,
t_p – the number of data values in the p group.

The standard test statistic Z is computed as follows

$$Z = \begin{cases} \dfrac{S-1}{\sqrt{VAR(S)}} & if \quad S \rangle 0 \\ 0 & if \quad S = 0 \\ \dfrac{S+1}{\sqrt{VAR(S)}} & if \quad S \langle 0 \end{cases} \tag{4.8}$$

The presence of a statistically significant trend is evaluated using the Z value. A positive (negative) value of Z indicates an upward (downward) trend. The statistic Z has a normal distribution. To test for either an upward or downward monotone trend (a two-tailed test) at α level of significance, hypothesis H_0 (no trend) is rejected if the absolute value of Z is greater than Z_1-α/2, where Z_1-α/2 is obtained from the standard normal cumulative distribution tables. The M-K test detects trends at four levels of significance: α = 0.001, 0.01, 0.05, and α = 0.1. Significance level of 0.001 means that there is a 0.1% probability that the value of x_i is from a random distribution and are likely to make a mistake if we reject the hypothesis H_0; Significance level of 0.1 means that there is a 10% probability that we make a mistake if we reject the hypothesis H_0. If the absolute value of Z is less than the level of significance, there is no trend.
For the four tested significance levels the following symbols are used in the template:

*** if trend at α = 0.001 level of significance - H_0 seems to be impossible
** if trend at α = 0.01 level of significance
* if trend at α = 0.05 level of significance - 5% mistake if we reject the H_0
+ if trend at α = 0.1 level of significance

Blank: the significance level is greater than 0.1, cannot be excluded that the H_0 is true.
The Mann-Kendall (as well as Spearman) tests for trends assess a sequence of data and assume a null hypothesis that there is no trend in the sequence. The Spearman test determines the difference between the actual position of each datum in the sequence, and its position in the sequence when it is sorted in ascending order, and tests the null hypothesis based on the standardized sum of these differences. To estimate the true slope b of an existing trend (as change per year) the Sen's nonparametric method can be used.

4.4 Trend analysis of the average annual Danube discharge

The homogeneity tests showed that the series of mean annual discharges of the Danube River for the period 1876–2006 are homogeneous. The length of the discharge series is unique in Europe. The X^2 and the Kolmogorov- Smirnov tests confirmed that the examined data series satisfies the normality requirement at the chosen significance level. To detect and estimate trends in time series of annual mean discharge we used EXCEL file MEKESENS 1.0 developed at the Finish Meteorological Institute (Salmi et al, 2002). We used the non-parametric Mann-Kendall test to test the presence of the monotonic increasing or decreasing trend, and the nonparametric Sen's method to estimate the slope of a linear trend. The Mann-Kendall test requires at least 4 values, and calculation of the confidence intervals for Sen's slope estimates requires at least 10 values in a time series.

Fig. 4.3 illustrates the longest average annual discharge time series of the Danube River. Results of the trend analysis from the rest of the stations are presented in the Table 4.1. Generally, no significant trend, from the statistical point of view, was detected in the discharges series within the 75-year period 1931–2005 (Pekárová et al., 2016).

4.4.1 Trend analysis of the average annual and extreme annual Danube discharge series

The period 1931–2005 is not representative in terms of annual maxima of discharge. The last two decades of the 19-th century were extremely rich in catastrophic floods in the whole Danube basin. In the Upper Danube, on the other hand, the period 1900–1953 was poor in floods. After 1954, the variability of annual maxima increased again, similarly to the period 1876–1899. Therefore we tested the long-term trends only for the period 1876–2005 for five stations along the Danube River.

In general, in the Danube River basin, the years 1915, 1940, 1965, and 1980 were extremely rich with runoff. In contrast, the period around 1947 and the 90s of the twentieth (last) century were extremely dry. But the period around the year 1863 was even drier. Therefore the trends determined on data from the periods 1901–2005 or 1931–2005 cannot be considered conclusive.

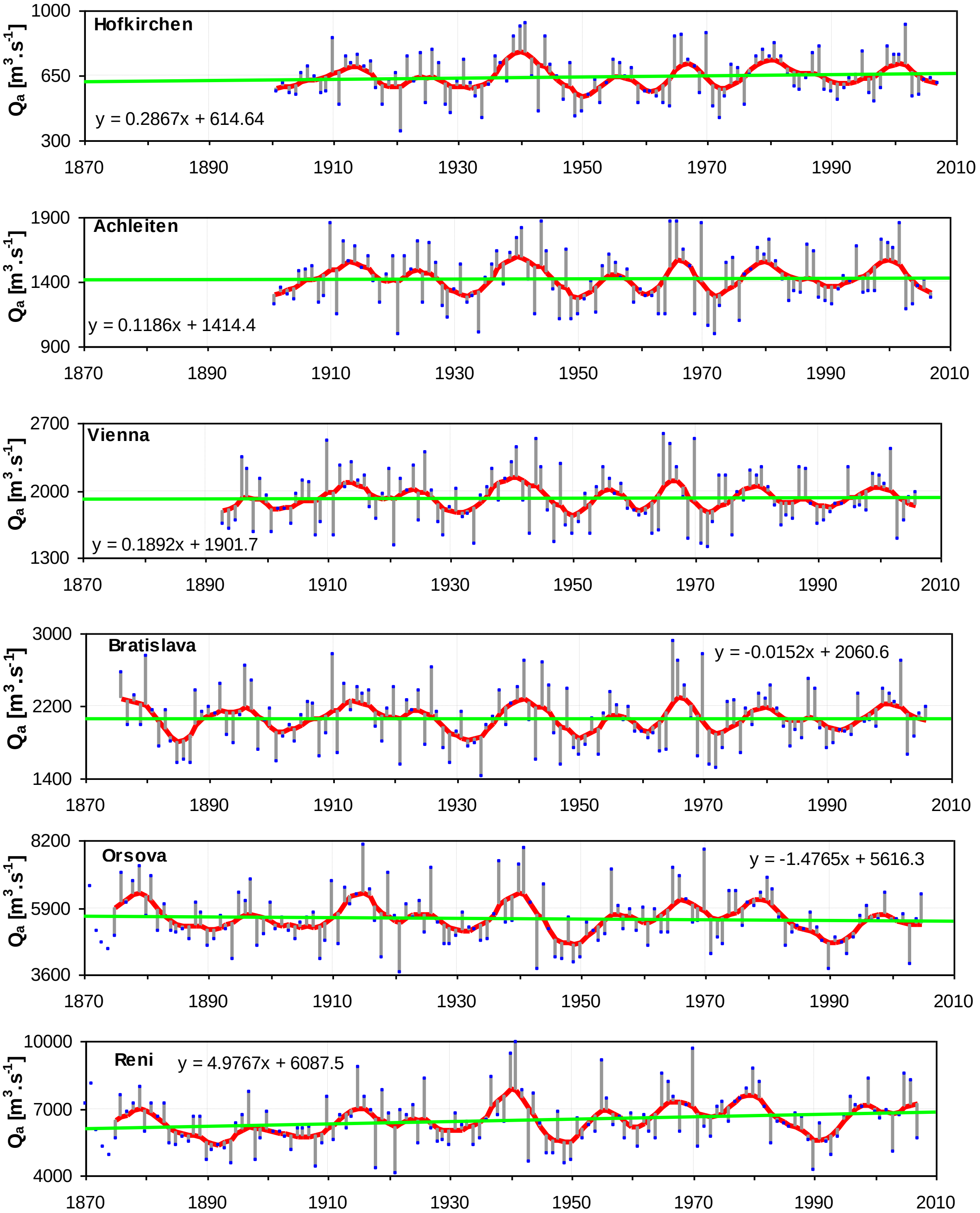

Fig. 4.3 *Long term linear trends of the mean annual discharge in the selected stations on the Danube River.*

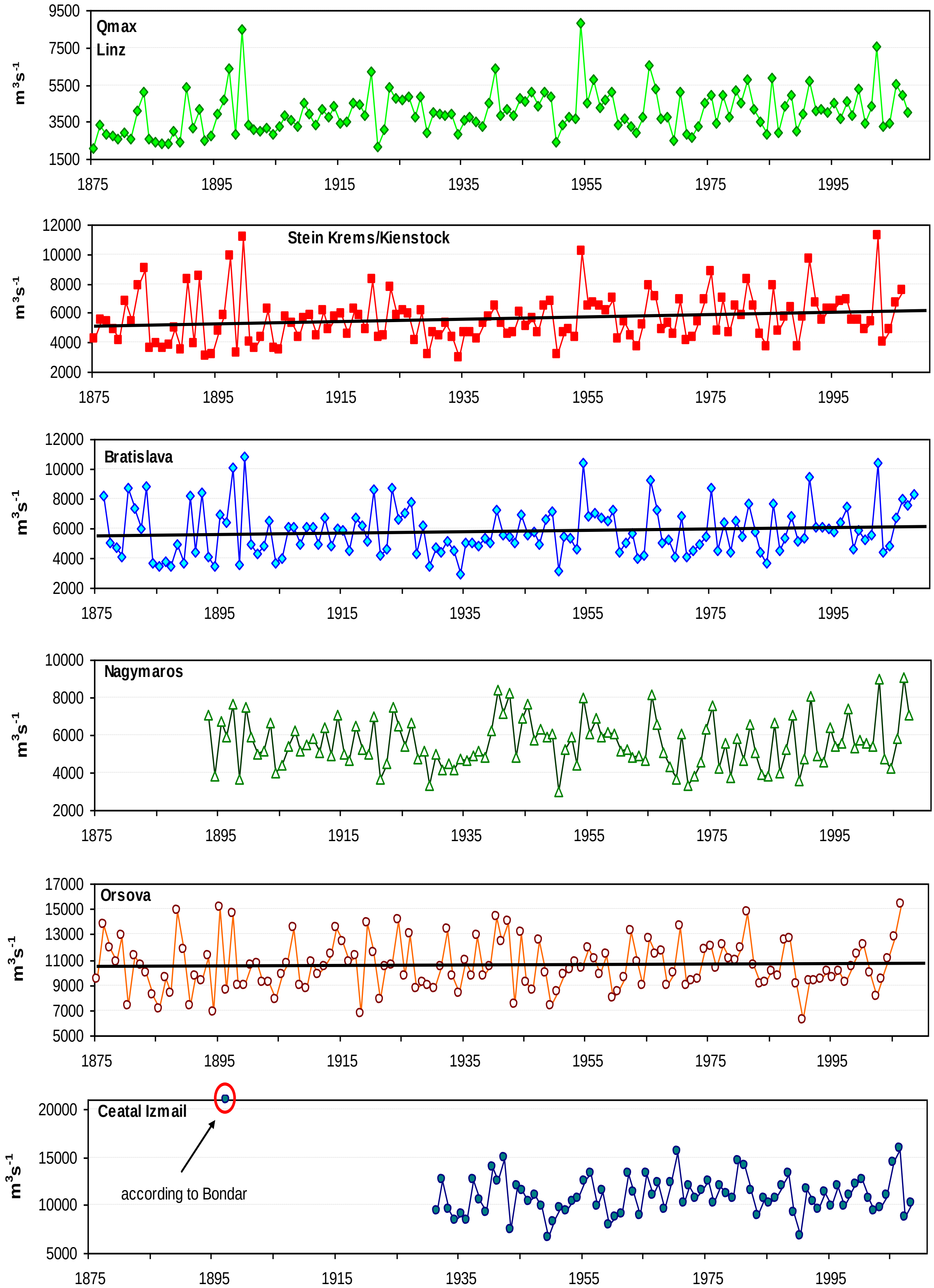

Fig. 4.4 Long term linear trends of the maximum annual discharge in the selected stations on the Danube River.

Table 4.1 Summary table of the results, trend analysis of the average annual discharge; b - the Sen's estimator for the true slope of linear trend; a - estimate of the constant a in equation f(year)=a+b*(year-firstYear), period 1931–2005

Danube	**1931-2005**							
Annual	**Mann-Kendall trend**		**Sen's slope**		**estimate**			
discharge	**Test Z**	**Signific.**	**b**	**b min99**	**b max99**	**a**	**a min99**	**a max99**
Berg	1.51		0.1	-0.069	0.277	34	40	27
Ingolstadt	0.8		0.24	-0.658	1.329	297	329	266
Regensburg	0.95		0.57	-0.924	2.046	412	476	368
Pfeling	0.72		0.43	-1.105	1.989	429	493	385
Hofkirchen	0.48		0.35	-1.712	2.203	614	693	572
Achleiten	0.38		0.58	-3.166	3.98	1386	1537	1278
Linz	-1.29		-1.78	-5.556	1.849	1502	1657	1397
Stein	0.69		1.28	-3.53	5.368	1790	1993	1663
Wien	-0.12		-0.19	-4.654	4.347	1898	2097	1744
Bratislava	0.52		1.05	-3.659	5.837	1967	2148	1805
Nagymaros	-0.1		-0.23	-6.499	5.666	2289	2511	2037
Mohacs	0.29		0.65	-5.999	7.18	2277	2520	2052
Bezdan	-1.71	+	-3.96	-10.776	2.281	2458	2731	2236
Bogojevo	-2.76	**	-7.55	-15.206	-0.438	3140	3427	2902
Pancevo	-1.07		-5.06	-18.724	6.733	5365	5842	4961
Gradiste	-1.23		-6.56	-19.102	6.501	5623	6098	5069
Orsova	-0.76		-3.15	-17.06	9.537	5613	6023	5045
Zimnicea	-0.57		-2.8	-16.759	11.191	6116	6495	5439
Reni	0.59		3.92	-14.243	20.983	6384	7030	5645
Ceatal	0.6		3.21	-12.81	19.349	6261	6921	5605

For the four tested significance levels the following symbols are used
*** trend at $\alpha = 0.001$ level of significance; ** trend at $\alpha = 0.01$ level of significance
* trend at $\alpha = 0.05$ level of significance; + trend at $\alpha = 0.1$ level of significance

Table 4.2 Summary table of the results, trend analysis of the maximum annual discharge

Danube	**1876-2005**							
Maximal annual	**Mann-Kendall trend**		**Sen's slope**		**estimate**			
discharge	**Test Z**	**Signific.**	**b**	**b min99**	**b max99**	**a**	**a min99**	**a max99**
Linz	3.80	***	9.444	3.261	15.613	3212	3645	2854
Stein-Krems (Kienstock)	2.76	**	9.310	0.677	17.460	4636	5339	4149
Wien-Nussdorf	3.16	**	10.158	2.006	17.631	4623	5201	4238
Devin/Bratislava	1.36		4.956	-5.106	13.615	5021	5935	4505
Orsova	0.38		1.657	-10.709	13.772	10111	10983	9310

The combined periodogram method revealed periods of 2.4, 3.6, 4.2, and 7 years, as well as long periods of 14, 22, 30 and 44 years (Fig. 4). The cycle of 2.4 years is probably connected to the QBO phenomena. The cycle of about 3.6 years probably depends on the Southern Oscillation (SO) represented by the SO index. The 44, 22, and 11 years' cycles are connected to the solar activity. The cycle length of approx. 28–31 years is related to the Arctic oscillation (AO), expressed by the AO index. Finally, the cycle of about 13 years is connected to the North Atlantic Oscillation (NAO), represented by the NAO index.

4.5 Linkage between NAO, QBO, SO indices and discharge series

This chapter deals with the analysis of the long-term trends and possibilities of the long-term forecasts of discharge in the Danube River basin using the winter North-Atlantic Oscillation Index. The value of the winter NAO index in the year 2010, calculated as an average of the months December 2009 – March 2010, was extraordinary low, only –2.85. The statistical analyses show, that discharge is lower during the periods with positive winter NAOI. The years with negative winter NAOI are usually wet. The mean annual discharge and precipitation series are considered to be random. We can estimate the occurrence of maxima and minima with certain probability, but we cannot estimate their timing. In this chapter we show that there is significant negative relation between the discharge series of the rivers in the Danube basin and the winter NAO index. This relation makes it possible to predict the wetness of a particular year by the winter NAO index value. At the same time this relation indicates that the floods of 2010 that hit Central Europe coincided with the extraordinary low value of the winter NAO index, and that the index interrelated with extraordinary high sea water temperature near Iceland during that winter. The other important information following from the cross-correlation analysis is that extraordinary a dry year should come approximately 5-6 years after the extremely low NAO index.

4.5.1 Index NAO

After the 2010 flood in Central Europe much attention was given predictions of such extremely wet year. Are there any indicators that would allow us to expect that the next year would be rich in precipitation with a higher risk of floods, or will the next year be dry?
The variability of streamflow is associated with the global system of oceanic currents, the global circulation of the atmosphere, and the transport of precipitation. In the recent years, many scientists have studied relationships between the atmospheric phenomena such as Quasi Biennial Oscillation (QBO), Southern Oscillation (SO), North Atlantic Oscillation (NAO), and Arctic Oscillation (AO)) and hydro-climatic characteristics such as total precipitation, air temperature, discharge, snow and ice cover, flood risk, see stage series, or coral oxygen isotope records, dendrochronological series etc. Jevrejeva and Moore (2001) and Jevrejeva et al. (2003) studied the temporal variability of ice conditions in the Baltic Sea within the context of NAO and AO winter indices using the Singular Spectrum Analysis (SSA) and wavelet approach. According to these authors, cross-wavelet power for the time series indicates that the times of largest variance in ice conditions are in excellent agreement with a significant power in the AO at 2.2–3.5-, 5.7–7.8-, and 12–20-yr periods, similar patterns have been also seen with the Southern Oscillation Index (SOI) and Niño-3 sea surface temperature series. Wavelet coherence shows in-phase linkages between the 2.2–7.8- and 12–20-yr period signals in both the tropical and Arctic atmospheric circulations and with ice conditions in the Baltic Sea. Anctil and Coulibaly (2003) described the local inter-annual variability in southern Québec streamflow based on wavelet analysis, and identified plausible climatic teleconnections that could explain these local variations. The span of available observations, 1938–2000, allows depicting the variance for periods up to about 12 yr. Turkes and Erlet (2003) and Uvo (2003) studied the teleconnection of NAO variability with precipitation variability in Turkey, and in Northern Europe, respectively. Felis et al. (2000) studied a 245-yr coral oxygen isotope record from the northern Red Sea with bimonthly resolution. A similar oscillation with a period of 70-yrs, which is probably of North Atlantic origin, dominates the coral time series. The inter-annual to inter-decadal variability is correlated with climate variability expressed as the NAO, the El Niño-Southern Oscillation (ENSO), and

North Pacific climate variability. The results suggest that these modes contributed consistently to Middle East climate variability after 1750, preferentially at a period close to 5.7 years. Yang et al. (2000) investigated the ENSO teleconnection with annual precipitation series (Tiberian Plateau, China) from 1690 to 1987 (nearly 300 years). Their investigations showed that negative precipitation anomalies are significantly associated with El Niño years. Tardif et al. (2003) studied variations in periodicities of the radial growth response of black ash exposed to yearly spring flooding in relation to hydrological fluctuations at Lake Duparquet in north western Québec. They detected 3.5-, 3.75-, and 7.5-yr periodicities in all the dendrochronological series. According to authors, the 3.75- and 7.5-yr components are harmonics of a 15-yr periodicity. Youn (2005) quantified major periodicities in surface air temperature variations over the Korean Peninsula. Using spectral analysis he found the most dominant pattern centred at 2.3 yrs.

Inter-annual to decadal variability of the atmosphere over the North Atlantic region is characterized by the NAO teleconnection pattern (Fig. 4.5). The NAO refers to swings in the atmospheric sea-level pressure difference between the Artic and subtropical Atlantic that are associated with changes in the mean wind speed and direction (Hurrell et al., 2003, 2009). Whereas runoff in western and northern Europe increases with positive values of the NAO and AO indices during the period 1901–2000, in the middle and lower parts of the Danube basin the annual precipitation totals and runoff decrease with positive NAO values (Adler et al., 1999; Rimbu et al., 2002; Pekárová and Miklánek, 2004a,b).

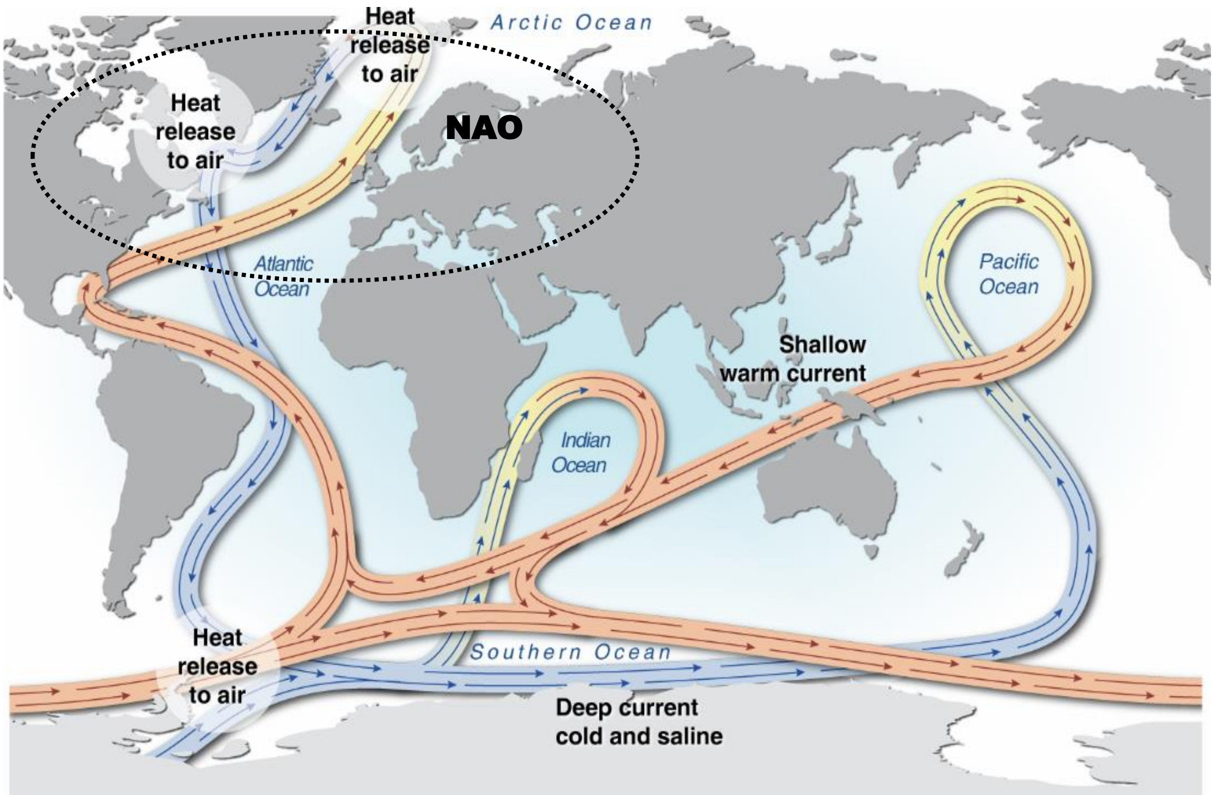

Fig. 4.5 World ocean thermohaline circulation. NAO – North-Atlantic Oscillation. http://maps.grida.no/go/graphic/world-ocean-thermohaline-circulation1

The role of the NAO on multi-annual variability of the Danube was investigated with cross-correlation analysis of the mean annual Danube discharge time series from 20 stations located along the river and NAO winter indices.

The North Atlantic Oscillation (NAO) is one of the major modes of variability of the Northern Hemisphere atmosphere. It is particularly important in winter when it exerts a strong control on the climate of the Northern Hemisphere. The difference between the normalised sea level pressure over Gibraltar and the normalised sea level pressure over Southwest Iceland is a useful index indicating the magnitude of NAO for the winter season which exhibits the strongest inter-decadal variability. Jones et al. (1997) used early instrumental data to extend this index back to 1823.

The winter values of the North Atlantic Oscillation Index (NAOI,w) are shown in Fig. 4.6a. In our analysis we used the winter NAO index (December through March) based on the difference of normalized sea level pressure (SLP) between Lisbon, Portugal and Stykkisholmur/Reykjavik, Iceland since 1864 (according to Osborn, 2011).

The SLP anomalies at each station were normalized by dividing seasonal mean pressure by the long-term mean (1864-1983) standard deviation. Positive values of the NAO index indicate stronger-than-average westerlies over the middle latitudes.
The significant increase in precipitation in Slovakia after the dry period 1981–1994 is directly related to higher number of floods since 1996. In the last 10 years (2000–2010), precipitation in Slovakia increased by almost 150 mm compared to the period 1981–1990 (Fig. 4.6b).

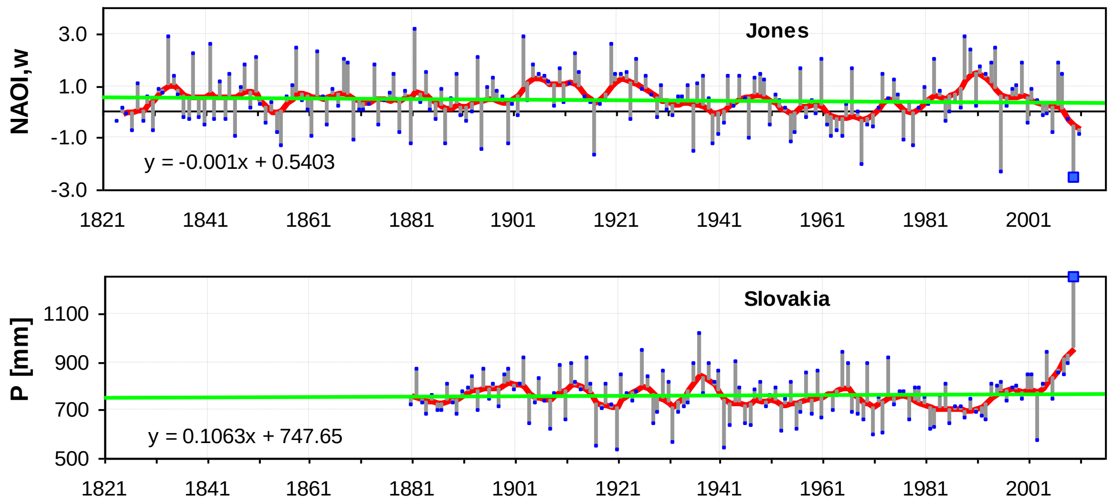

Fig. 4.6 a) Winter NAO index (average Dec, Jan, Feb, Mar) calculated according to Jones's methodology (1824–2011). http://www.cru.uea.ac.uk/~timo/datapages/naoi.htm
b) Mean annual precipitation depths in Slovakia since 1881.

Annual discharge

The primary quantity analysed in this chapter is the annual mean of the Danube's discharge. The time series of annual average flows were calculated from daily mean flows of the Danube River measured at twenty hydrological stations located along the Danube River.

Statistical test was carried out to detect homogeneity and trends. The annual averages were calculated from average daily discharges. To illustrate the multiannual component of the series, Fig. 4.7 shows the double 5-year moving averages of discharge. Trend analysis revealed that there is no trend in the annual discharge at the analysed stations, except for Bezdan and Bogojevo stations (Fig. 4.8). The annual discharge is subject only to multiannual variability.

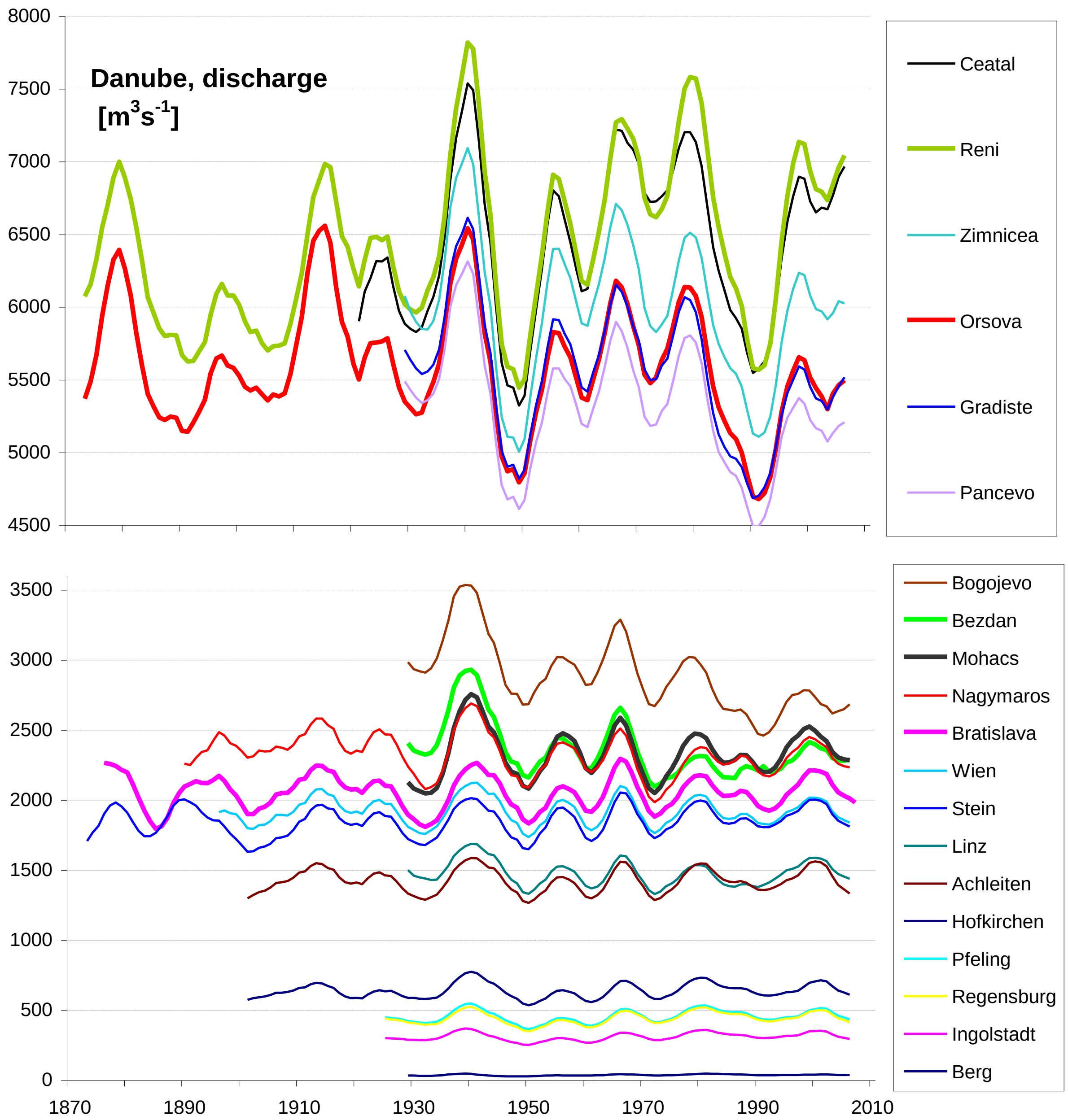

Fig. 4.7 *Double 5-year moving averages of annual discharge at 20 stations located on the Danube River.*

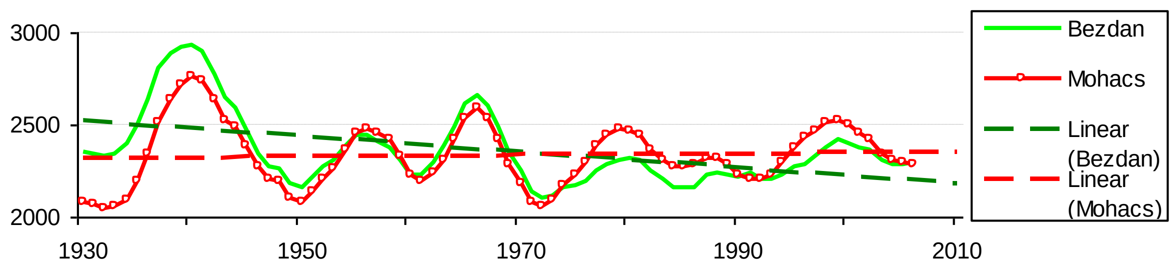

Fig. 4.8 *Non homogeneity of the Danube discharge series: stations Mohac and Bezdan. Linear long-term trend for 1931–2005.*

4.5.2 Cross-correlation analysis

The time shift between the winter NAO index and annual discharge series of selected rivers was identified by cross-correlation for the period 1931–2005. The results from the selected Danube stations for three different periods (15-, 30-, and 45-years) are presented in Fig. 4.9. In general, the lowland streams are more influenced by the North-Atlantic oscillation. This implies that dry years should be expected when the winter NAO index value is high. Similar results were obtained by Rimbu et al. (2002). The negative relation between the winter NAO index and discharge has been observed also at a time shift of one year (Table 4.3). At the shift of about 5-6 years the correlation coefficients are positive. **The mean annual discharge should be lowest five to six years after a low of the NAO index**.

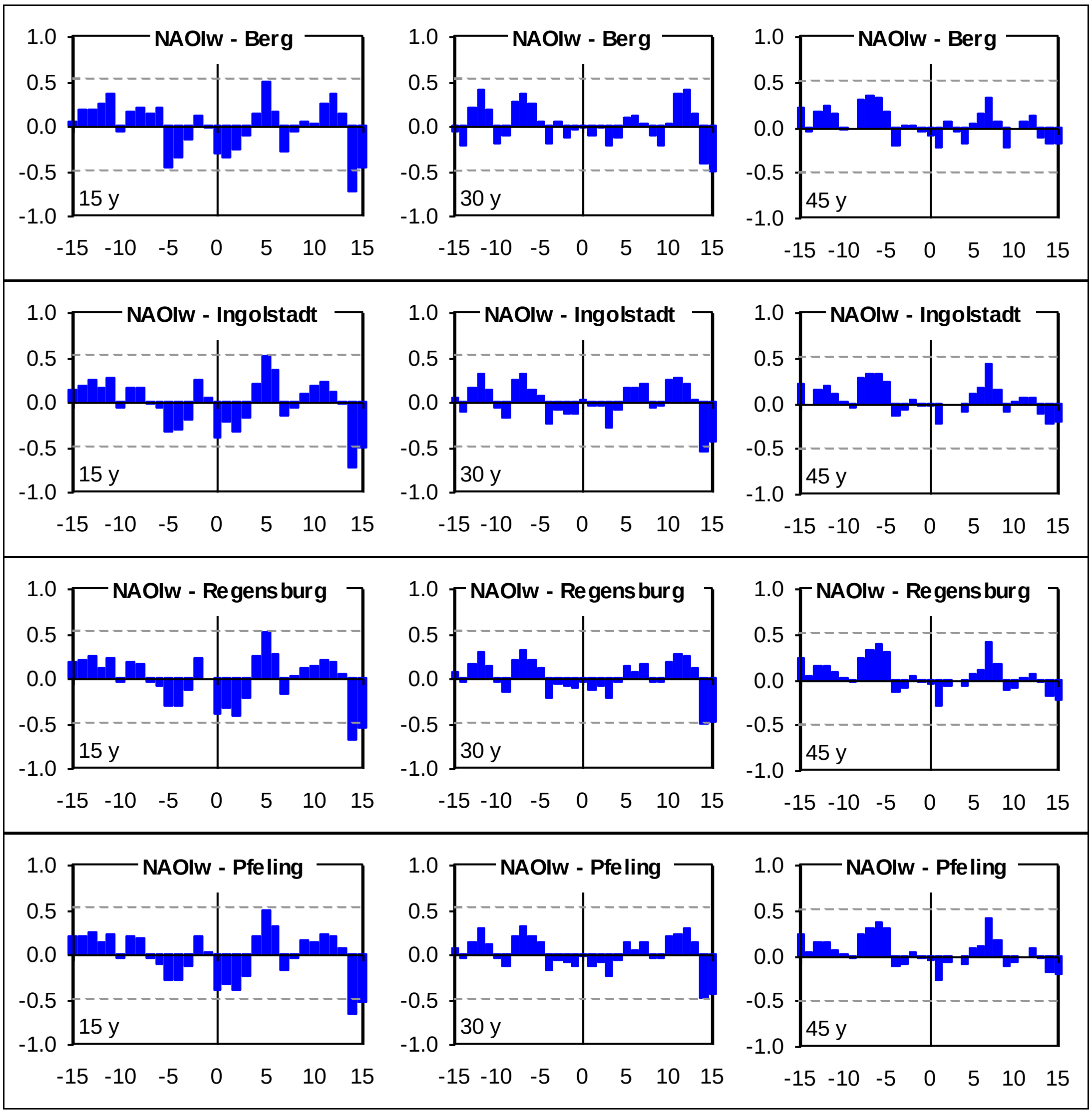

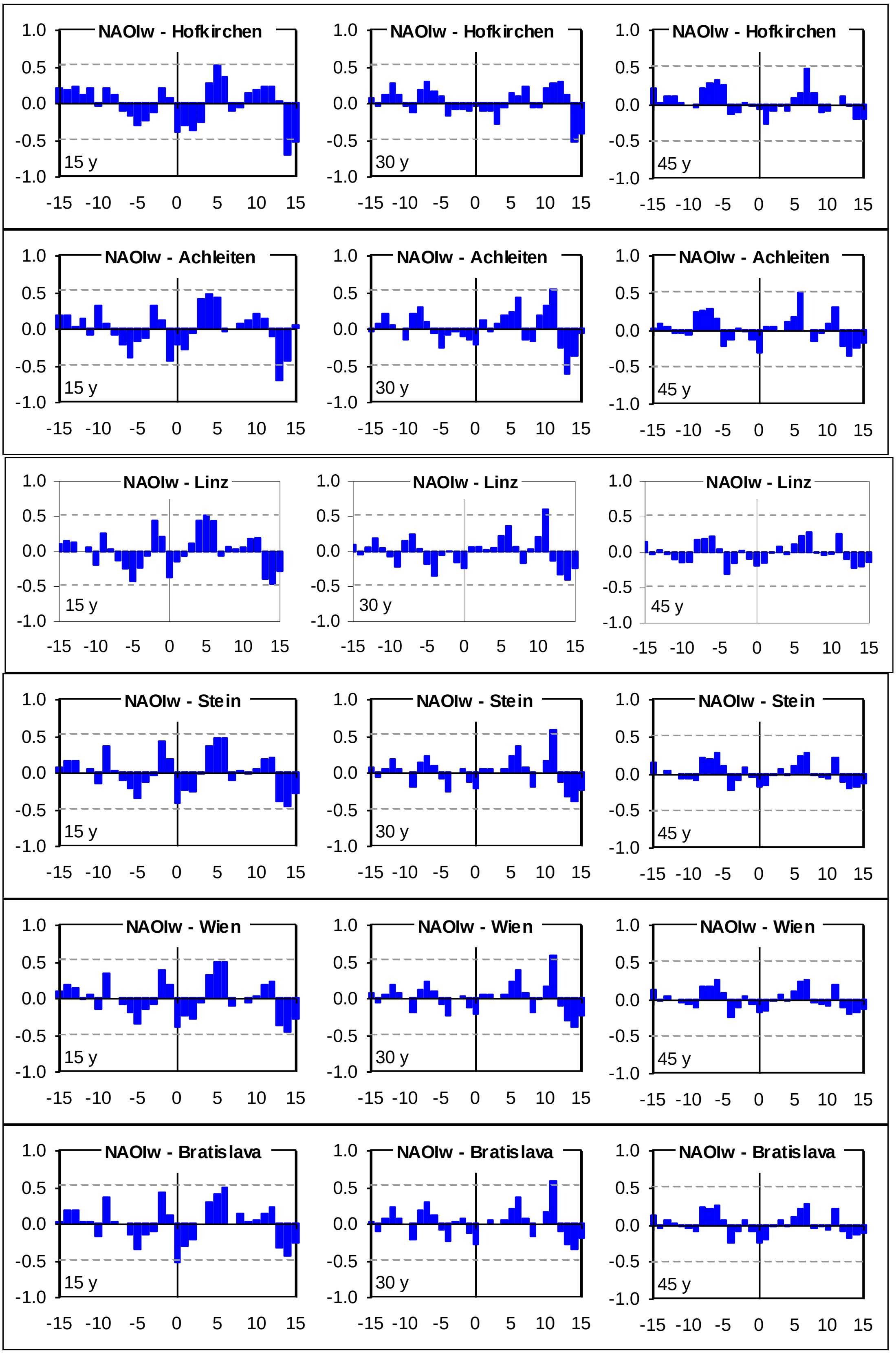
NAOIw - Hofkirchen
15 y
NAOIw - Hofkirchen
30 y
NAOIw - Hofkirchen
45 y
NAOIw - Achleiten
15 y
NAOIw - Achleiten
30 y
NAOIw - Achleiten
45 y
NAOIw - Linz
15 y
NAOIw - Linz
30 y
NAOIw - Linz
45 y
NAOIw - Stein
15 y
NAOIw - Stein
30 y
NAOIw - Stein
45 y
NAOIw - Wien
15 y
NAOIw - Wien
30 y
NAOIw - Wien
45 y
NAOIw - Bratislava
15 y
NAOIw - Bratislava
30 y
NAOIw - Bratislava
45 y

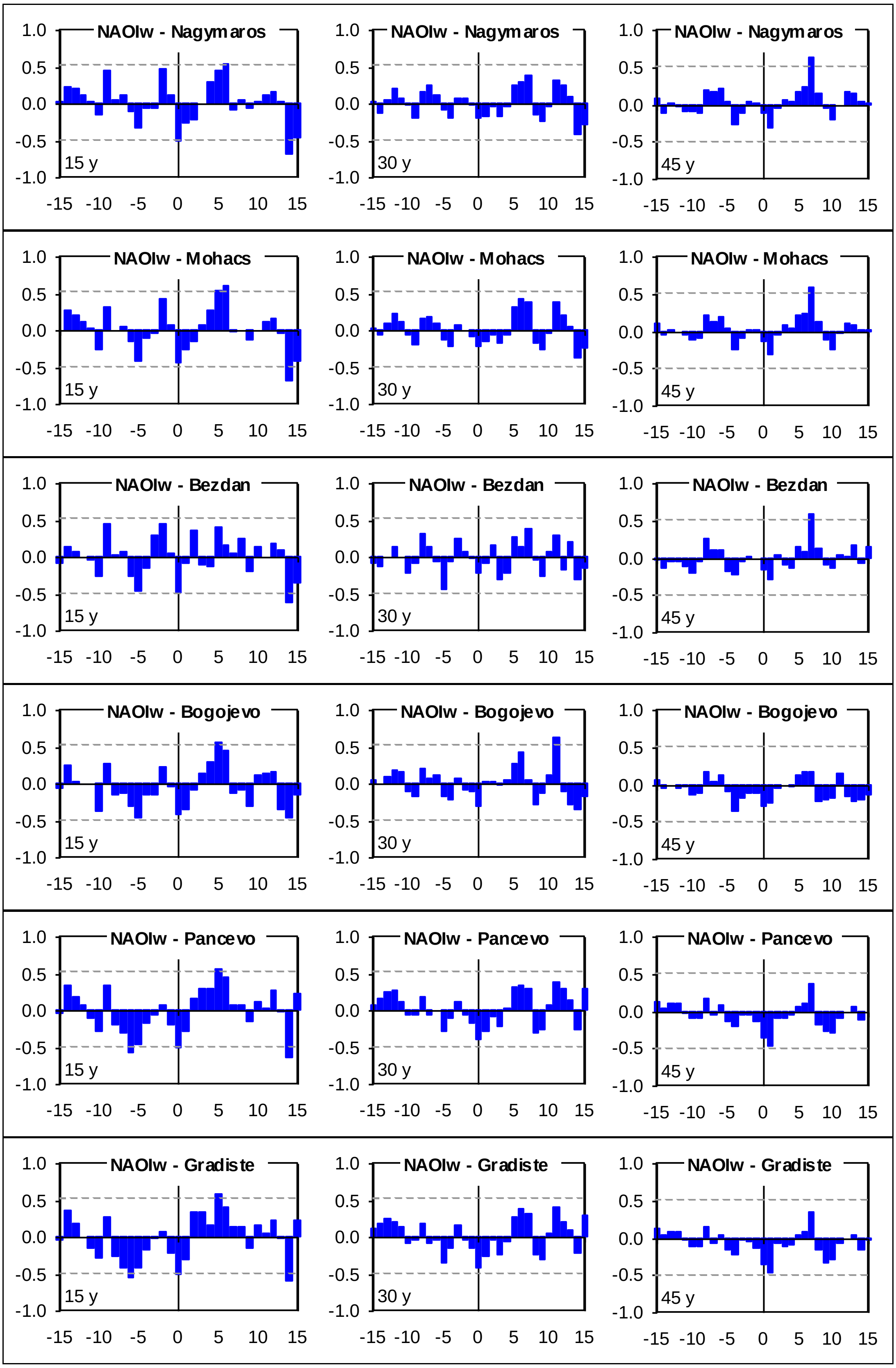
NAOIw - Nagymaros
15 y
30 y
45 y
NAOIw - Mohacs
NAOIw - Bezdan
NAOIw - Bogojevo
NAOIw - Pancevo
NAOIw - Gradiste
1.0
0.5
0.0
-0.5
-1.0
-15 -10 -5 0 5 10 15

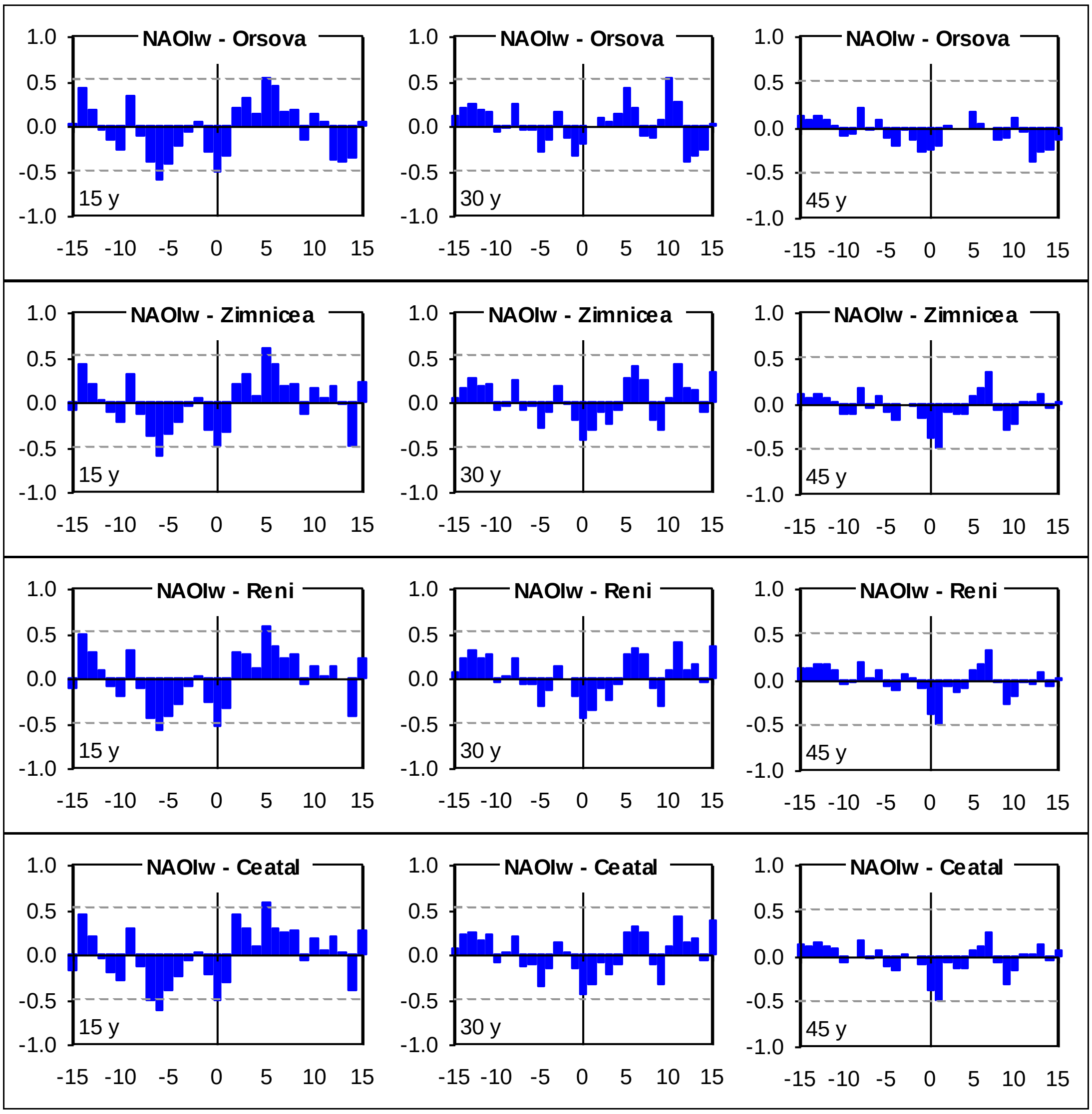

Fig. 4.9 *Cross-correlation between winter NAO index (NAOI,w) and mean annual Danube discharge at selected stations for three periods: 15-, 30-, and 45- years.*

4.6 Conclusion

The proponents of the hypothesis of long-term variability of the hydrological series did demonstrate already 60 years ago (Hurst, 1951) or recently e.g. (Kane, 1997; Jevrejeva et al., 2003; Pekárová, 2009) that the climatic system is subject to multi-annual dry and wet cycles. It has been shown that the cycles may be caused by thermohaline circulation of the oceanic water and in the northern Atlantic Ocean by its local demonstration – the North Atlantic Oscillation. This chapter dealt with the possibilities of the long-term runoff forecast of rivers in the Danube basin using the winter North-Atlantic Oscillation Index. The value of the winter NAO index in year 2010 (average of the months December 2009 – March 2010) was extraordinary low, only –2.85. The cross-correlation analyses showed that the periods of positive winter NAOI are accompanied with low discharge in the Danube River. On the other hand, the years with negative winter NAOI are much moister.

Table 4.3. Correlation coefficients between winter NAO index (NAOI,w) and mean annual Danube discharge at selected stations for 3 periods: 15-, 30-, and 45- years, columns indicate lag times [years].

15y	0	1	2	3	4	5	6	7	8	9	10	11	12	13	14	15
Berg	-0.30	-0.35	-0.26	-0.10	0.13	0.50	0.16	-0.29	-0.07	0.05	0.03	0.25	0.35	0.14	-0.73	-0.48
Ingolstadt	-0.39	-0.23	-0.33	-0.17	0.21	0.50	0.36	-0.15	-0.07	0.10	0.18	0.22	0.12	-0.03	-0.73	-0.52
Regensburg	-0.39	-0.34	-0.42	-0.21	0.26	0.52	0.27	-0.18	0.01	0.12	0.14	0.20	0.17	0.05	-0.69	-0.56
Pfeling	-0.41	-0.33	-0.40	-0.24	0.20	0.49	0.32	-0.18	-0.04	0.14	0.14	0.22	0.21	0.08	-0.67	-0.53
Hofkirchen	-0.40	-0.31	-0.39	-0.26	0.26	0.50	0.36	-0.11	-0.07	0.13	0.19	0.21	0.23	0.02	-0.70	-0.53
Achleiten	-0.22	-0.29	-0.07	0.40	0.47	0.43	-0.05	-0.01	0.07	0.12	0.20	0.14	-0.12	-0.70	-0.45	0.04
Linz	-0.40	-0.46	-0.65	-0.50	-0.22	-0.22	-0.11	-0.07	-0.26	-0.23	-0.19	-	-	-	-	-
Stein	-0.42	-0.25	-0.26	-0.03	0.35	0.46	0.46	-0.11	0.02	-0.02	0.04	0.18	0.19	-0.39	-0.47	-0.28
Wien	-0.39	-0.25	-0.28	-0.07	0.30	0.49	0.49	-0.11	-0.01	-0.07	0.01	0.19	0.22	-0.38	-0.46	-0.28
Bratislava	-0.54	-0.31	-0.23	0	0.3	0.4	0.49	-0.01	0.12	0.03	0.04	0.14	0.21	-0.34	-0.45	-0.27
Nagymaros	-0.51	-0.27	-0.23	0	0.28	0.45	0.54	-0.08	0.04	-0.08	0.02	0.11	0.16	0.03	-0.7	-0.46
Mohacs	-0.45	-0.26	-0.15	0.07	0.27	0.53	0.6	-0.02	0	-0.13	0	0.11	0.16	-0.04	-0.69	-0.42
Bezdan	-0.49	-0.10	0.35	-0.11	-0.12	0.39	0.16	0.04	0.24	-0.19	0.13	0.00	0.17	0.09	-0.62	-0.36
Bogojevo	-0.43	-0.35	-0.09	0.14	0.28	0.55	0.45	-0.13	-0.09	-0.3	0.12	0.14	0.16	-0.35	-0.47	-0.16
Pancevo	-0.5	-0.29	0.16	0.29	0.28	0.55	0.45	0.07	0.08	-0.15	0.11	0.02	0.26	-0.01	-0.65	0.21
Gradiste	-0.5	-0.31	0.34	0.33	0.16	0.57	0.4	0.14	0.14	-0.16	0.16	0.03	0.23	-0.02	-0.59	0.22
Orsova	-0.51	-0.33	0.19	0.32	0.14	0.54	0.43	0.16	0.17	-0.15	0.14	0.03	-0.38	-0.4	-0.35	0.03
Zimnicea	-0.50	-0.33	0.21	0.31	0.08	0.59	0.42	0.18	0.20	-0.13	0.16	0.05	0.19	-0.03	-0.49	0.22
Reni	-0.53	-0.33	0.29	0.28	0.1	0.57	0.35	0.23	0.27	-0.07	0.14	0.02	0.13	0.01	-0.41	0.22
Ceatal	-0.52	-0.32	0.44	0.28	0.09	0.57	0.3	0.24	0.27	-0.07	0.17	0.05	0.21	0.03	-0.39	0.26

30y	0	1	2	3	4	5	6	7	8	9	10	11	12	13	14	15
Berg	-0.01	-0.12	-0.02	-0.23	-0.14	0.09	0.12	0.02	-0.12	-0.21	0.03	0.36	0.41	0.13	-0.43	-0.51
Ingolstadt	0.02	-0.03	-0.04	-0.29	-0.08	0.16	0.15	0.19	-0.07	-0.05	0.24	0.27	0.19	0.02	-0.55	-0.44
Regensburg	-0.05	-0.14	-0.09	-0.21	-0.03	0.13	0.06	0.16	-0.04	-0.05	0.19	0.27	0.24	0.12	-0.51	-0.49
Pfeling	-0.02	-0.13	-0.10	-0.23	-0.07	0.12	0.04	0.14	-0.05	-0.06	0.19	0.22	0.30	0.14	-0.49	-0.44
Hofkirchen	-0.05	-0.10	-0.11	-0.28	-0.08	0.13	0.10	0.21	-0.07	-0.06	0.20	0.26	0.30	0.11	-0.54	-0.42
Achleiten	-0.22	0.12	-0.05	0.07	0.17	0.22	0.42	-0.16	-0.17	0.18	0.31	0.53	-0.26	-0.62	-0.39	-0.08
Linz	-0.03	-0.06	-0.19	-0.22	-0.07	-0.10	-0.08	-0.17	-0.32	-0.31	-0.42	-0.38	-	-	-	-
Stein	-0.23	0.04	0.04	0.01	0.05	0.22	0.36	0.06	-0.19	0.00	0.17	0.58	-0.13	-0.32	-0.41	-0.24
Wien	-0.23	0.04	0.04	0.00	0.04	0.23	0.37	0.06	-0.20	-0.02	0.15	0.58	-0.12	-0.31	-0.39	-0.24
Bratislava	-0.3	0.01	0.04	0	0.03	0.2	0.35	0.08	-0.19	-0.01	0.16	0.58	-0.11	-0.28	-0.35	-0.20
Nagymaros	-0.2	-0.17	-0.05	-0.18	-0.05	0.24	0.29	0.38	-0.16	-0.25	-0.04	0.32	0.24	0.1	-0.41	-0.29
Mohacs	-0.23	-0.16	-0.06	-0.19	-0.06	0.3	0.42	0.37	-0.18	-0.27	-0.04	0.37	0.21	0.06	-0.37	-0.25
Bezdan	-0.21	-0.08	0.17	-0.30	-0.22	0.27	0.14	0.38	-0.04	-0.27	0.07	0.29	-0.18	0.21	-0.31	-0.17
Bogojevo	-0.31	0.03	0.03	-0.03	0.05	0.28	0.41	0.04	-0.29	-0.13	0.11	0.62	-0.12	-0.28	-0.35	-0.18
Pancevo	-0.41	-0.28	-0.08	-0.22	0.03	0.3	0.34	0.28	-0.3	-0.27	0.07	0.37	0.28	0.12	-0.27	0.28
Gradiste	-0.42	-0.28	-0.06	-0.24	-0.07	0.26	0.37	0.32	-0.24	-0.31	0.05	0.39	0.2	0.09	-0.23	0.29
Orsova	-0.19	0	0.09	0.04	0.14	0.43	0.21	-0.11	-0.12	0.07	0.54	0.26	-0.41	-0.33	-0.26	0.02
Zimnicea	-0.42	-0.31	-0.11	-0.24	-0.08	0.27	0.40	0.25	-0.20	-0.31	0.05	0.41	0.15	0.13	-0.11	0.34
Reni	-0.45	-0.35	-0.11	-0.25	-0.08	0.27	0.33	0.26	-0.12	-0.31	0.09	0.4	0.09	0.16	-0.04	0.35
Ceatal	-0.45	-0.33	-0.08	-0.23	-0.11	0.24	0.31	0.25	-0.11	-0.34	0.1	0.42	0.13	0.17	-0.06	0.37

45y	0	1	2	3	4	5	6	7	8	9	10	11	12	13	14	15
Berg	-0.10	-0.24	0.06	-0.06	-0.18	0.03	0.15	0.32	0.05	-0.23	-0.01	0.07	0.13	-0.11	-0.19	-0.18
Ingolstadt	-0.03	-0.23	-0.02	-0.01	-0.10	0.09	0.16	0.43	0.15	-0.10	0.01	0.06	0.06	-0.11	-0.23	-0.21
Regensburg	-0.06	-0.30	-0.07	-0.01	-0.08	0.06	0.10	0.41	0.17	-0.12	-0.09	0.01	0.05	-0.04	-0.18	-0.24
Pfeling	-0.05	-0.29	-0.08	-0.01	-0.09	0.07	0.10	0.41	0.16	-0.11	-0.08	-0.02	0.08	-0.02	-0.18	-0.22
Hofkirchen	-0.07	-0.28	-0.10	-0.03	-0.10	0.08	0.14	0.47	0.15	-0.11	-0.09	0.00	0.09	-0.04	-0.20	-0.20
Achleiten	-0.31	0.02	0.03	-0.02	0.09	0.16	0.50	-0.01	-0.17	-0.05	0.07	0.29	-0.22	-0.36	-0.26	-0.18
Linz	-0.19	-0.26	-0.30	-0.25	-0.25	-0.26	-0.26	-0.23	-0.35	-0.38	-0.41	-0.43	-0.44	-0.39	-0.24	-0.27
Stein	-0.18	-0.16	-0.03	0.06	-0.03	0.11	0.22	0.27	-0.04	-0.06	-0.08	0.21	-0.12	-0.21	-0.19	-0.15
Wien	-0.18	-0.16	-0.03	0.05	-0.04	0.11	0.22	0.26	-0.05	-0.08	-0.10	0.20	-0.13	-0.22	-0.19	-0.14
Bratislava	-0.24	-0.2	-0.03	0.06	-0.03	0.1	0.21	0.27	-0.05	-0.04	-0.08	0.21	-0.1	-0.18	-0.15	-0.11
Nagymaros	-0.13	-0.31	-0.04	0.06	0.03	0.17	0.23	0.62	0.14	-0.05	-0.22	-0.01	0.16	0.14	0.03	0
Mohacs	-0.15	0.07	-0.32	-0.05	0.08	0.04	0.20	0.22	0.58	0.11	-0.11	-0.25	-0.04	0.09	0.02	0.01
Bezdan	-0.17	-0.31	0.02	-0.09	-0.15	0.14	0.08	0.58	0.13	-0.10	-0.14	0.03	0.01	0.16	-0.08	0.14
Bogojevo	-0.29	-0.24	-0.06	-0.02	-0.03	0.12	0.15	0.16	-0.23	-0.21	-0.18	0.14	-0.17	-0.23	-0.2	-0.15
Pancevo	-0.36	-0.46	-0.09	-0.10	-0.06	0.06	0.09	0.37	-0.20	-0.27	-0.29	-0.10	-0.01	0.04	-0.12	-0.01
Gradiste	-0.37	-0.47	-0.08	-0.12	-0.10	0.03	0.08	0.34	-0.17	-0.33	-0.30	-0.08	-0.01	0.04	-0.16	-0.03
Orsova	-0.25	-0.21	0.00	-0.01	-0.01	0.16	0.04	-0.02	-0.14	-0.11	0.10	-0.06	-0.38	-0.27	-0.24	-0.15
Zimnicea	-0.39	-0.49	-0.09	-0.12	-0.12	0.07	0.16	0.34	-0.07	-0.29	-0.22	0.01	0.00	0.09	-0.07	0.01
Reni	-0.39	-0.07	-0.13	-0.11	0.09	0.16	0.31	-0.03	-0.27	-0.18	-0.02	-0.05	0.07	-0.07	-0.5	0.01
Ceatal	-0.39	-0.49	-0.07	-0.14	-0.14	0.05	0.1	0.26	-0.07	-0.32	-0.17	0	0.01	0.12	-0.06	0.05

We have shown that there is significant negative relation between the discharge series in the Danube basin and the winter NAO index. This relation allows us to forecast the wetness of a particular year by the winter NAO index. Another important information arising from the cross-correlation analysis is that an extraordinary dry year should follow extremely low NAO index with a time lag of approximately 5-6 years.

References

Adler MJ, Busuioc A, Ghioca M, Stefan S. 1999. Atmospheric processes leading to drought periods in Romania. In Hydrological Extremes: Understanding, Predicting, Mitigating, Gottschalk L, Olivoy J-C, Reed D, Rosbjerg D (eds). IAHS Publication No. 255. IAHS Press: Wallingford; 37–47.

Anctil F, Coulibaly P. 2003. Wavelet Analysis of the Interannual Variability in Southern Québec Streamflow. J. Climate, 17(1), 163–173.

Belz JU, Goda L, Buzás Z, Domokos M, Engel H, Weber J. 2004. Runoff Regimes in the Danube Basin. The Danube and its catchment – A hydrological monograph, Follow-up volume VIII/2, Koblenz & Baja, 152 p.

Brázdil R, Tran N Tam. 1990. Climatic changes in the instrumental period in Central Europe. In Climatic change in the historical and the instrumental periods. Brázdil R (ed). Masaryk University, Brno, 223–230.

Brilly M. 2010. Hydrological Processes of the Danube River Basin. Springer, 328 s.

Brockwell PJ, Davis RA. 2003. Introduction to Time Series and Forecasting. Springer-Verlag: New York; 434.

Charvátová I, Střeštík J. 2004. Periodicities between 6 and 16 years in the surface air temperature in possible relation to solar inertial motion. J of Atmospheric and Solar-Terrestrial Physics 66: 219–227.

Charvátová I. 2000. Can origin of the 2400-year cycle of solar activity be caused by solar inertial motion? Ann Geophys.-Atmosph. Hydrosph. and Space Scienc. 18: 399–405.

Currie RG. 1996. Variance contribution of luni-solar (Mn) and solar cycle (Sc) signals to climate data. Int. J. of Climatology 16: 1343–1364.

Directive 2007. Directive 2007/60/EC of the European Parliament and of the Council of 23 October 2007 on the assessment and management of flood risks.

Esper J, Cook ER, Schweingruber FH. 2002. Low-frequency signals in long tree-ring chronologies for reconstructing past temperature variability. Science 295: 2250–2253.

Felis T, Patzold J, Loya Y, Fine M, Nawar AH, Wefer G. 2000. A coral oxygen isotope record from the northern Red Sea documenting NAO, ENSO, and North Pacific teleconnections on Middle East climate variability since the year 1750. Paleoceanography,15(6), 679–694.

Hirsch RM, Slack JR. 1984. A nonparametric trend test for seasonal data with serial dependence. Water Resources Research v. 20, p. 727–732.

Hirsch RM, Slack JR, Smith RA. 1982. Techniques of trend analysis for monthly water quality data. Water Resources Research v. 18, p.107–121.

Hurrell JW, Deser C. 2009. North Atlantic climate variability: The role of the North Atlantic Oscillation. J. Mar. Syst., 78, No. 1, 28-41, DOI:10.1016/j.jmarsys.2008.11.026.

Hurst HE. 1951. Long term storage capacity of reservoirs. Trans. Am. Soc. Civ. Eng., 116, 770–808.

Jevrejeva S, Moore JC, Grinsted A. 2003. Influence of the Arctic oscillation and El Nino–southern oscillation (ENSO) on ice conditions in the Baltic Sea: the wavelet approach. Journal of Geophysical Research–Atmospheres 108(D21): art. no. 4677.

Jevrejeva S, Moore JC. 2001. Singular Spectrum Analysis of Baltic Sea ice conditions and large-scale atmospheric patterns since 1708. Geoph. Res. Letters, 28, 23, 4503-4506.

Jones PD, Jónsson T, Wheeler D. 1997. Extension to the North Atlantic Oscillation using early instrumental pressure observations from Gibraltar and South-West Iceland. Int. J. Climatol. 17, 1433–1450.

Kane RP. 1997. Prediction of droughts in north-east Brazil: role of ENSO and use of periodicities. International Journal of Climatology 17: 655–665.

Kendall MG. 1975. Rank Correlation Methods. Griffin, London.

Labat D, Goddéris Y, Probst JL, Guzot JL. 2004. Evidence for global runoff increase related to climate warming. Adv. Water Resour., 27, 631–642.

Liritzis I, Fairbridge R. 2003. Remarks on astrochronology and time series analysis of Lake Sake varved sediments. J. Balkan Geoph. Soc. 6: 165–172.

Lohre M, Sibbertsen P, Konnig T. 2003. Modeling water flow of the Rhine River using seasonal long memory. Watre Resour. Res. 39: 1132.

Mann HB. 1945. Nonparametric tests against trend. Econometrica, 13, 245-259.

Osborn TJ. 2011. Winter 2009/2010 temperatures and a record-breaking North Atlantic Oscillation index. Weather 66, 19-21.

Pekárová P, Miklánek P. 2004a. Abflusstrends slowakischer Flüsse und mögliche Zusammenhänge mit ENSO/NAO - Erscheinungen. Österreichische Wasser- und Abfalllwirtschaft, Springer, 1-2: 17–25.

Pekárová P, Miklánek P. 2004b. Occurrence of the dry periods in European runoff series. In CD ROM - XXII. Conference of the Danubian Countries. Brno, 12p.

Pekárová P. 2009. Multiannual runoff variability in the upper Danube region. DrSc. thesis, Bratislava, IH SAS, 151 pp.° http://pavla.pekarova.sk

Pekárová P, Miklánek P, Halmová D. 2009. Flood Regime of Rivers on the Danube River Basin, Phase I. Objective O1 - Average daily discharge and annual peak discharge series collection. Report December 2009 on activities of the Project No. 9, Bratislava, Institute of Hydrology, 16 s.

Pekárová P, Miklánek P, Pekár J. 2003. Spatial and temporal runoff oscillation analysis of the main rivers of the world during the 19th-20th centuries. In Journal of Hydrology. 2003, vol. 274, no. 1, pp. 62-79

Pekárová P, Onderka M, Pekár J, Miklánek P, Halmová D, Škoda P, Bačová Mitková V. 2008. Hydrologic scenarios for the Danube River at Bratislava. Key Publishing, Ostrava, 160 s., <http://www.ih.savba.sk/danubeflood>.

Pekárová P, Pekár J. 2006. Long-term discharge prediction for the Turnu Severin station (the Danube) using a linear autoregressive model. Hydrological Processes, 20, 5, 1217–1228.

Pekárová P, Pramuk B, Halmová D, Miklánek P, Prohaska S. 2016. Identification of long-term high-flow regime changes in selected stations along the Danube River. J. of Hydrol. Hydromech., 64, 4, 393–403.

Popa R, Bosce C. 2002. Fuzzy nearest neighbour method for monthly inflows forecasting into “Iron Gates I” reservoir. In CD ROM - XXI Conference of the Danubian Countries. Bucharest, ISBN 973-0-02759-5, 7p.

Probst J, Tardy Y. 1987. Long range streamflow and world continental runoff fluctuation since the beginning of this century. J. Hydrol. 94: 289–311.

Procházka M, Deyl M, Novický O. 2001. Technology for Detecting Trends and Changes in Time Series of Hydrological and Meteorological Variables - Change and Trend Problem Analysis (CTPA). User’s Guide. CHMI, Prague; 25 pp.

Prohaska S, Isailović D, Srna P, Marčetić I. 1999. Coincidence of flood flow of the Danube River and its tributaries. The Danube and its catchment – A hydrological monograph, Follow-up volume IV, Bratislava, 187 s.

Rao AR, Hamed KH. 2000. Flood frequency analysis. CRC Press LLC, N. W. Corporate Blvd., Boca Raton, Florida.

Rimbu N, Boroneant C, Buta C, Dima M. 2002. Decadal variability of Danube River flow in the lower basin and its relation with the North Atlantic oscillation. Int. Journal of Climatology 22: 1169–1179

Salmi T, Määttä A, Anttila P, Ruoho-Airola T, Amnell T. 2002. Detecting trends of annual values of atmospheric pollutants by the Mann-Kendall test and Sen's slope estimates - the excel template application MAKESENS. Finnish Meteorological Institute, Helsinki, Publications on Air Quality No. 31, 35 pp.

Solanki SK, Usoskin IG, Kromer B, Schüssler M, Beer J. 2004. Unusual activity of the Sun during recent decades compared to the previous 11,000 years. Nature 431: 1084–1087.

Sosedko M. 1997. Regular alternation of high and low streamflow periods in the river basin of the Carpathians. Annales Geophysicae, Part II, Supplement II to Vol. 15, C 310.

Stănescu VA, Ungureanu V, Mătreaţă M. 2004. Regional analysis of the annual peak discharges in the Danube catchment. The Danube and its catchment – A hydrological monograph, follow-up volume VII, Bucharest, 64 s.

Štěpánek P. 2005. AnClim - software for time series analysis. Dept. of Geography, Fac. of Natural Sciences, MU, Brno. 1.47 MB.

Tardif J, Dutilleul P, Bergeron Y. 2003. Variations in Periodicities of the Ring Width of Black Ash (Fraxinus nigra Marsh.) in Relation to Flooding and Ecological Site Factors at Lake Duparquet in Northwestern Québec. Biologic. Rhythm Res. 29: 1–29.

Turkes M, Erlat E. 2003. Precipitation changes and variability in Turkey linked to the North Atlantic oscillation during the period 1930–2000. Intern. J. Climat., 23 (14), 1771–1796.

Uvo CB. 2003. Analysis and regionalization of Northern European winter precipitation based on its relationship with the North Atlantic oscillation. Intern. J. Climat., 23(10), 1185–1194.

Van Gelder PHAJM, Kuzmin VA, Visser PJ. 2000. Analysis and statistical forecasting of trends in river discharges under uncertain climate changes. In: River Flood Defence. Booklet 9. Tönsmann, F, Koch M. (eds). ISBN-Nr.: 3-930150-20-4. 10 p.

Vasiliev SS, Dergachev VA. 2002. The approximate to 2400-year cycle in atmospheric radiocarbon concentration: bispectrum of C-14 data over the last 8000 years. Annales Geoph. 20: 115–120.

Walanus A, Soja R. 1995. The 3.5 yr period in river runoff – is it random fluctuation? In Proccced. Hydrological Processes in the Catchment, Wiezik B. (ed). Cracow; 141–148.

Williams GR. 1961. Cyclical variations in the world-wide hydrological data. J. of Hydraulic division, 6: 71–88.

World ocean thermohaline circulation. (June 2007). In UNEP/GRID-Arendal Maps and Graphics Library. Retrieved 14:33, November 19, 2010 from http://maps.grida.no/go/graphic/world-ocean-thermohaline-circulation1

Yang M, Yao T, He Y, Thompson LG. 2000. ENSO events recorded in the Guliya ice core. Climatic Change, 47, 401–409.

Youn YH. 2005: The climate variabilities of air temperature around the Korean Penisula. Adv. Atmos. Sci., 22(4), 575–584.

Yue S, Pilon P, Cavadias G. 2002a. Power of the Mann–Kendall and Spearman's rho tests for detecting monotonic trends in hydrological series. J. Hydrol. 259, 254–271.

Yue S, Pilon P, Phinney B, Cavadias G. 2002b. The influence of autocorrelation on the ability to detect trend in hydrological series. Hydrol. Process. 16, 1807– 1829.

5 Analysis of the intra-annual regime of flood flow and its changes in the Danube basin

Ole Rössler,, Jörg Uwe Belz, Michael Mürlebach, Maria Larina-Pooth,
Dana Halmová, Marcel Garaj, and Pavla Pekárová

The main objective of this chapter is to analyse the seasonality of selected runoff characteristics in the Danube Basin and its change during the 20th century. First, the mean annual runoff characteristics at selected gauges along the Danube River were analysed, followed by a flood seasonality examination.

Figs. 5.1a-d presents the basic monthly and seasonal runoff characteristics for four Danube gauges: Hofkirchen (DE), Bratislava (SK), Orsova (RO) and Reni (UKR). Likewise, the runoff characteristics for further stations along the Danube are listed in the APPENDIX V. This summary table presents the long-term characteristics (top two panels) such as *Qma* – long-term average monthly, annual and seasonal discharge in m^3s^{-1}; *Qmin*/*Qmax* – minimal/maximal monthly discharge, *Vm* – long-term monthly runoff volume in 10^9 m^3; *Rm* – long-term monthly runoff depth in mm, *Vm/Va* – long-term monthly share on yearly runoff in %, *tr* – long-term trend of monthly discharges, c_s – coefficient of asymmetry, and c_v is coefficient of variability of the monthly discharges, *P1956–1980* and *P1981–2005* – Pardé coefficients.

Furthermore, long-term runoff time-series and comparisons of two different time periods displayed changes during the past almost 150 years. The figures document the length of discharge measurements on the Danube River, enabling a detailed spatial characterization of the Danube runoff, a robust determination of possible trends, and classification of recent data in terms of long-term temporal evolution.

In the subsequent analysis we focus on the period 1956-2005 for practical reasons (e.g. equal availiabilty of data at the majority of gauges in order to allow a broad, comparable overview of the entire catchment area). As discharge characteristics often change over time, a classification of this relatively short time period into longer time periods is appropriate to avoid misinterpretations. Figures 5.1a-d nicely display the basic statistical characteristics of monthly and seasonal discharges; subplots: Long-term monthly runoff, monthly discharge series, Pardé coefficient for two periods 1956–1980 and 1981–2005, moving averages of seasonal discharge, share of the summer-autumn discharge and percentiles (log-normal distribution) of monthly discharges. Monthly discharge characteristics of the time period 1951–2005 show very similar monthly values compared to the time period 1931–2005. Those changes in the intra-annual monthly flow regime as well as changes in the flood regime are the subject of the following chapter.

5.1 Intra-annual flow-regime analysis according to PARDÉ

Analysis of the mean annual runoff variability and its change in time are typically performed by applying the common classification method by PARDÉ (1964). This analysis is based on the ratio of each of the twelve long-term monthly MQs with the associated long-term annual MQ, the so-called PARDÉ-coefficient. The calculation of PARDÉ-coefficients has always the effect of a standardization that facilitates the direct comparison between different annual flow hydrographs.

The PARDÉ flow coefficient k_i is defined as:

$$k_i = \overline{mMQi} / \overline{MQ} \qquad (5.1)$$

with $\overline{mMQ}\,i$ – long-term mean monthly streamflow in the single month *i*, *(i=I, XII)* [m³/s], and MQ being the long-term annual streamflow [m³/s].

Mean Monthly and Seasonal Discharges in m³/s

		Elevation:	300 m
Station	**Danube - Hofkirchen**	**Longitude:**	13.12
Catchment	47496 km²	**Latitude:**	48.68

	I	II	III	IV	V	VI	VII	VIII	IX	X	XI	XII	Year	XI-IV	V-X
Qma	623	654	744	758	725	734	684	600	541	500	521	579	**638**	646	631
Qmin	269.65	220.00	271.74	311.87	312.19	338.13	293.42	258.10	211.50	220.03	260.10	232.90	**342.64**	338.68	348.10
Qmax	1660	1474	1525	1430	1545	1943	1410	1277	1171	1251	1479	1323	**924**	1015	983
Vm	1.67	1.58	1.99	1.96	1.94	1.90	1.83	1.61	1.40	1.34	1.35	1.55	**20.13**	10.11	10.03
Rm	35.1	33.3	41.9	41.3	40.9	40.1	38.6	33.9	29.5	28.2	28.4	32.7	**424**	212.8	211.1
Vm/Va	8.3	7.9	9.9	9.8	9.6	9.5	9.1	8.0	7.0	6.6	6.7	7.7	**100**	50	50
tr	0.001	0.017	0.022	0.007	-0.014	-0.003	-0.010	-0.004	-0.015	0.000	0.014	0.024	**0.016**	0.043	-0.017
cs	1.36	0.87	0.83	0.57	1.07	1.79	0.90	0.74	0.89	1.41	1.92	1.18	**0.22**	0.33	0.38
cv	0.387	0.383	0.354	0.291	0.287	0.327	0.350	0.332	0.340	0.360	0.431	0.402	**0.194**	0.215	0.223

	I	II	III	IV	V	VI	VII	VIII	IX	X	XI	XII	Year	XI-IV	V-X
1841-1870															
1856-1885															
1871-1900															
1886-1915															
1901-1930	643	569	665	740	763	723	675	604	569	490	484	544	**623**	608	637
1916-1945	651	641	679	755	745	756	667	628	584	548	567	538	**646**	639	654
1931-1960	604	687	777	741	677	724	733	605	534	515	542	530	**639**	647	631
1946-1975	577	657	712	716	681	719	722	589	482	450	471	545	**610**	613	607
1961-1990	610	716	739	789	755	782	689	615	526	496	498	619	**652**	662	644
1976-2005	678	723	812	779	724	719	652	581	539	523	560	649	**661**	700	623
1991-2013	696	659	796	741	679	731	611	555	534	502	569	647	**643**	685	602
1876-2010	623	654	744	758	725	734	684	600	541	500	521	579	**638**	646	631
P1956-1980	0.88	1.11	1.13	1.17	1.16	1.21	1.10	0.99	0.81	0.76	0.77	0.90	1.00	0.99	1.01
P1981-2005	1.06	1.06	1.24	1.18	1.08	1.08	0.96	0.86	0.82	0.80	0.86	1.01	1.00	1.07	0.93

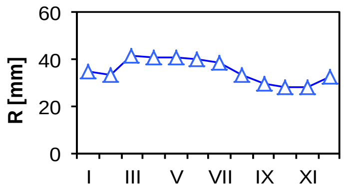

Long-term monthly runoff.

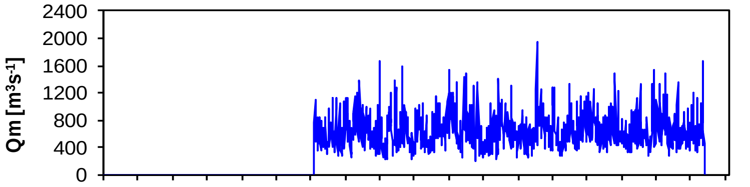

Course of monthly discharges.

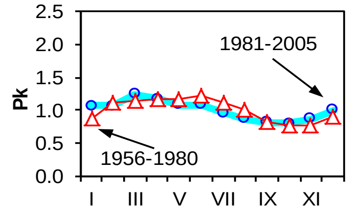

Parde coefficient - two periods.

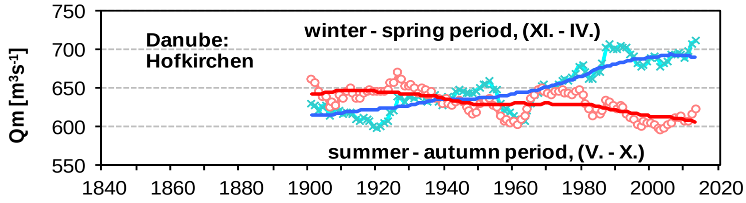

Course of moving averges of seasonal discharges.

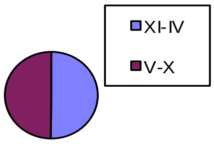

Share of the summer-autumn discharge.

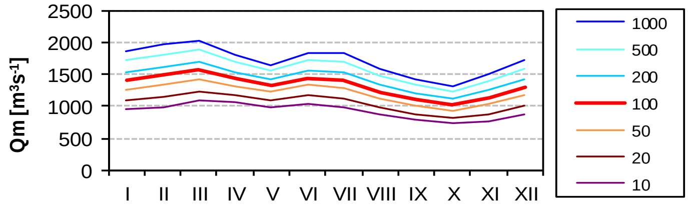

T-year monthly discharges, (log-normal distribution).

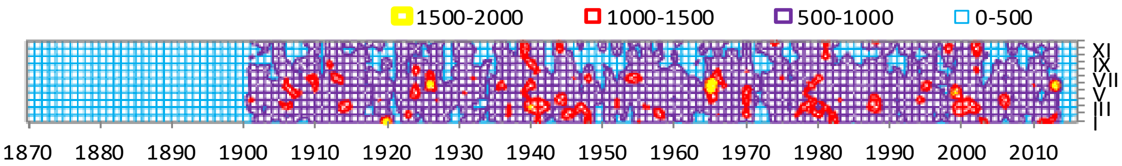

Monthly discharge, 2D plot.

Fig. 5.1a Basic statistical characteristics of monthly and seasonal discharges at Hofkirchen; subplots: Long-term monthly runoff, Pardé coefficient, moving averages of seasonal discharges, Share of the summer-autumn discharge, T-years monthly discharge (long-normal distribution), and 2D picture of the monthly discharges.

Mean Monthly and Seasonal Discharges in m³/s

		Elevation:	128 m
Station	**Danube - Bratislava**	**Longitude:**	17.11
Catchment	131338 km²	**Latitude:**	48.14

	I	II	III	IV	V	VI	VII	VIII	IX	X	XI	XII	Year	XI-IV	V-X
Qma	1630	1721	2097	2389	2680	2793	2627	2285	1909	1548	1476	1527	**2059**	1807	2307
Qmin	770.23	744.57	937.03	1020.33	1275.13	1492.77	1325.99	1090.42	736.87	632.55	812.37	664.32	**1419.61**	1208.85	1284.51
Qmax	5117	4366	4900	4855	5283	7324	5424	5007	4594	2919	3684	3686	**2910**	3057	3774
Vm	4.36	4.16	5.62	6.19	7.18	7.24	7.04	6.12	4.95	4.15	3.83	4.09	**64.92**	28.25	36.67
Rm	33.2	31.7	42.8	47.1	54.7	55.1	53.6	46.6	37.7	31.6	29.1	31.1	**494**	215.1	279.2
Vm/Va	6.7	6.4	8.6	9.5	11.1	11.2	10.8	9.4	7.6	6.4	5.9	6.3	**100**	44	56
tr	-0.006	-0.001	0.007	0.009	-0.001	-0.001	-0.002	-0.006	-0.009	-0.005	0.008	0.012	**-0.001**	0.014	-0.010
cs	1.94	1.34	0.86	0.81	0.92	2.02	1.13	1.05	1.48	0.64	1.54	1.25	**0.32**	0.73	0.69
cv	0.427	0.397	0.329	0.284	0.256	0.274	0.293	0.302	0.352	0.294	0.340	0.357	**0.157**	0.195	0.184

	I	II	III	IV	V	VI	VII	VIII	IX	X	XI	XII	Year	XI-IV	V-X
1841-1870															
1856-1885															
1871-1900	1842	1923	2125	2204	2624	2780	2552	2437	2102	1578	1406	1412	**2083**	1819	2345
1886-1915	1489	1566	2035	2411	2863	2852	2717	2408	2177	1581	1354	1366	**2071**	1703	2433
1901-1930	1676	1528	1868	2318	2846	2801	2707	2323	2067	1592	1443	1485	**2058**	1720	2389
1916-1945	1644	1652	1925	2375	2721	2917	2579	2345	2004	1675	1585	1445	**2074**	1771	2373
1931-1960	1458	1673	2150	2422	2521	2792	2762	2286	1765	1554	1514	1418	**2028**	1773	2280
1946-1975	1490	1682	2014	2365	2638	2826	2867	2276	1639	1383	1381	1501	**2007**	1739	2272
1961-1990	1585	1813	2044	2485	2759	2918	2631	2236	1733	1456	1408	1669	**2063**	1834	2289
1976-2005	1720	1864	2306	2486	2626	2605	2432	2135	1816	1568	1559	1717	**2071**	1942	2197
1991-2006	1709	1721	2252	2373	2567	2664	2312	2060	1900	1590	1617	1624	**2034**	1883	2182
1876-2010	1630	1721	2097	2389	2680	2793	2627	2285	1909	1548	1476	1527	**2059**	1807	2307
P1956-1980	0.71	0.86	0.98	1.16	1.33	1.45	1.34	1.14	0.84	0.72	0.69	0.77	1.00	0.86	1.14
P1981-2005	0.85	0.88	1.13	1.21	1.26	1.24	1.16	1.02	0.88	0.76	0.76	0.84	1.00	0.94	1.05

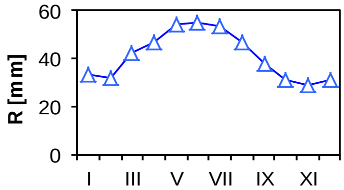

Long-term monthly runoff.

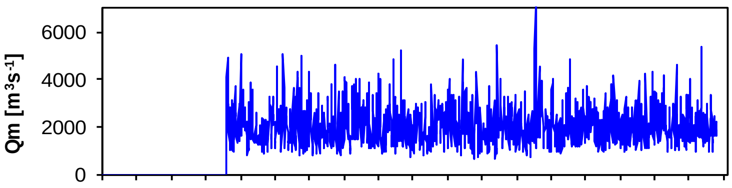

Course of monthly discharges.

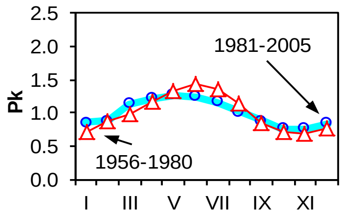

Parde coefficient - two periods.

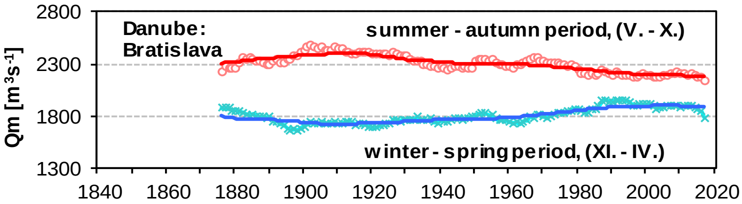

Course of moving averges of seasonal discharges.

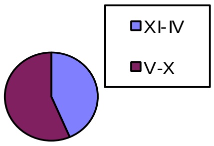

Share of the summer-autumn discharge.

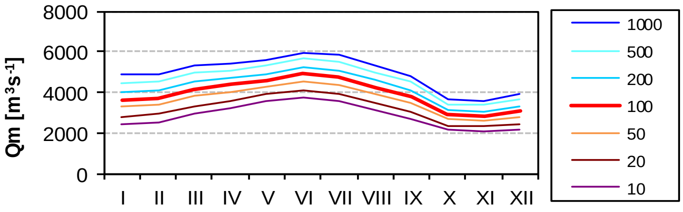

T-year monthly discharges, (log-normal distribution).

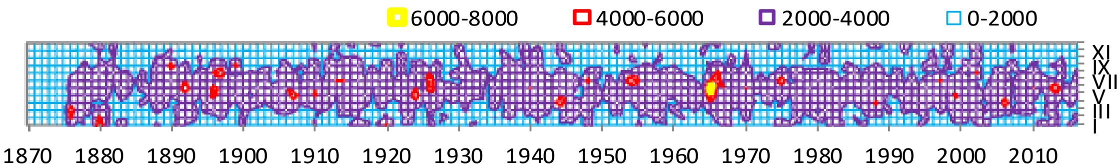

Monthly discharge, 2D plot.

Fig. 5.1b *Basic statistical characteristics of monthly and seasonal discharges at Bratislava; subplots: Long-term monthly runoff, Pardé coefficient, moving averages of seasonal discharges, Share of the summer-autumn discharge, T-years monthly discharge (long-normal distribution), and 2D picture of the monthly discharges.*

Mean Monthly and Seasonal Discharges in m³/s

			Elevation:	44 m
Station	**Danube - Orsova**		**Longitude:**	22.00
Catchment	576232	km²	**Latitude:**	44.70

	I	II	III	IV	V	VI	VII	VIII	IX	X	XI	XII	**Year**	XI-IV	V-X
Qma	4796	5126	6653	7913	7644	6627	5540	4498	3994	4052	4831	5156	**5570**	5746	5392
Qmin	1675	1859	3144	3978	3944	3129	2328	1923	1917	1672	2036	1927	**3472**	3356	2865
Qmax	10187	10157	11555	13289	12996	13324	12273	10558	8290	8006	9704	10890	**8291**	9501	8461
Vm	12.8	12.4	17.8	20.5	20.5	17.2	14.8	12.0	10.4	10.9	12.5	13.8	**176**	89.9	85.7
Rm	22.3	21.5	30.9	35.6	35.5	29.8	25.8	20.9	18.0	18.8	21.7	24.0	**305**	156.0	148.8
Vm/Va	7.3	7.1	10.1	11.7	11.7	9.8	8.4	6.9	5.9	6.2	7.1	7.9	**100**	51	49
tr	0.004	0.005	0.002	0.001	-0.004	-0.005	-0.005	-0.006	-0.005	-0.003	-0.002	0.001	**-0.003**	0.006	-0.009
cs	0.63	0.41	0.36	0.42	0.52	0.76	1.02	1.17	0.82	0.77	0.75	0.64	**0.44**	0.38	0.39
cv	0.387	0.327	0.283	0.272	0.260	0.263	0.286	0.305	0.305	0.328	0.371	0.345	**0.168**	0.185	0.204

	I	II	III	IV	V	VI	VII	VIII	IX	X	XI	XII	**Year**	XI-IV	V-X
1841-1870	4393	4957	6417	7590	7785	6772	5544	4701	4187	4032	4814	4965	**5514**	5523	5503
1856-1885	4730	4703	6187	7319	7556	6596	5440	4416	3957	3834	4736	5222	**5394**	5483	5300
1871-1900	4362	4595	6263	7954	8051	7156	5935	4644	4029	4201	4810	4972	**5585**	5493	5669
1886-1915	4108	4560	6599	8288	8041	7144	5894	4706	4112	4332	4596	4791	**5601**	5490	5705
1901-1930	5181	4768	6702	7911	8070	6682	5707	4671	4159	4325	5038	5278	**5713**	5813	5602
1916-1945	5118	5043	7028	8115	8180	6731	5459	4422	4077	4264	5563	5309	**5777**	6029	5522
1931-1960	4712	5277	7327	8087	7408	6603	5480	4426	3747	3863	5183	5274	**5615**	5977	5254
1946-1975	5036	5513	6751	7800	7196	6505	5799	4581	3774	3609	4443	5183	**5514**	5788	5244
1961-1990	5050	5932	6765	8098	7601	6695	5555	4369	3919	3844	4257	5203	**5603**	5884	5330
1976-2005	5223	5667	6606	7958	7045	5872	4823	4013	3751	4006	4558	5250	**5394**	5877	4918
1991-2009	5278	5232	6494	7972	6679	5474	4704	3907	3810	4026	4841	5285	**5307**	5850	4767
1876-2010	4800	5120	6672	7933	7659	6635	5538	4488	3986	4050	4823	5155	**5572**	5750	5393
P1956-1980	0.89	1.04	1.20	1.38	1.35	1.19	1.03	0.82	0.70	0.68	0.79	0.94	1.00	1.04	0.96
P1981-2005	0.99	1.00	1.22	1.51	1.30	1.08	0.89	0.73	0.71	0.75	0.85	0.97	1.00	1.09	0.91

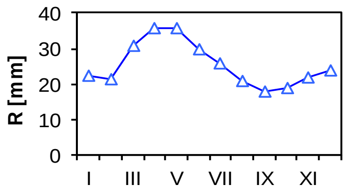

Long-term monthly runoff.

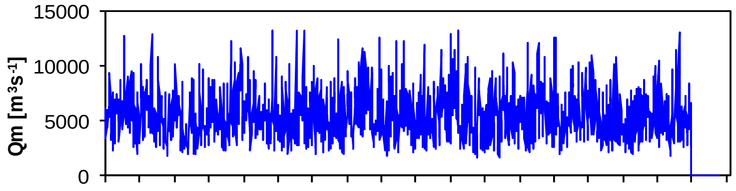

Course of monthly discharges.

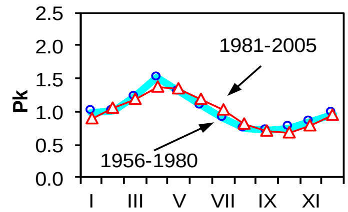

Parde coefficient - two periods.

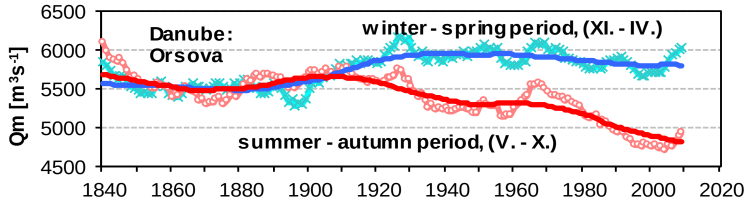

Course of moving averges of seasonal discharges.

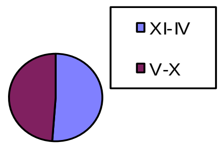

Share of the summer-autumn discharge.

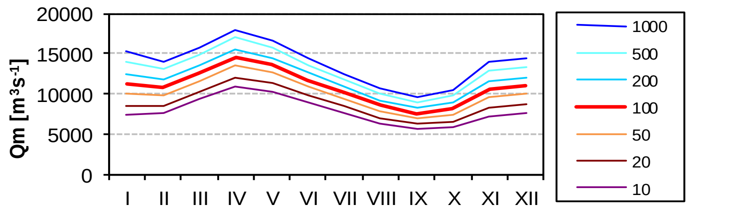

T-year monthly discharges, (log-normal distribution).

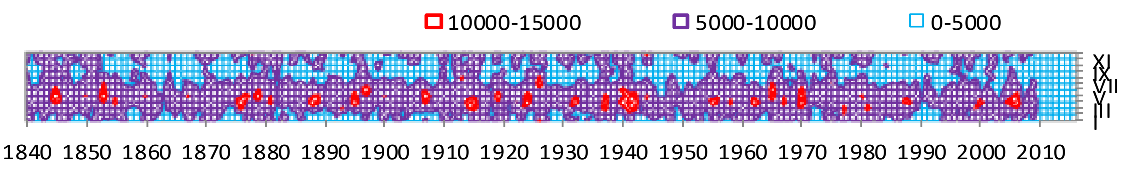

Monthly discharge, 2D plot.

Fig. 5.1c *Basic statistical characteristics of monthly and seasonal discharges at Orsova; subplots: Long-term monthly runoff, Pardé coefficient, moving averages of seasonal discharges, Share of the summer-autumn discharge, T-years monthly discharge (long-normal distribution), and 2D picture of the monthly discharges.*

Mean Monthly and Seasonal Discharges in m³/s

			Elevation:	4 m
Station	**Danube-Reni**		**Longitude:**	28.13
Catchment	805700	km²	**Latitude:**	45.28

	I	II	III	IV	V	VI	VII	VIII	IX	X	XI	XII	**Year**	XI-IV	V-X
Qma	6132	6371	7550	8945	9130	8302	6965	5378	4594	4438	5019	5950	**6564**	6661	6468
Qmin	1805.48	2162.14	2608.71	3907.00	4662.90	3867.00	2705.48	2423.87	2129.00	1583.87	2048.00	1972.90	**3906.00**	3558.82	3212.92
Qmax	11934	11761	12639	14103	15158	14820	12955	12235	9663	8973	11417	10695	**9916**	10266	10368
Vm	16.42	15.41	20.22	23.19	24.45	21.52	18.65	14.40	11.91	11.89	13.01	15.94	**207.01**	104.19	102.82
Rm	20.4	19.1	25.1	28.8	30.4	26.7	23.2	17.9	14.8	14.8	16.1	19.8	**257**	129.3	127.6
Vm/Va	7.9	7.4	9.8	11.2	11.8	10.4	9.0	7.0	5.8	5.7	6.3	7.7	**100**	50	50
tr	0.002	0.002	0.002	0.003	0.001	-0.001	-0.001	0.001	0.002	0.004	0.001	0.002	**0.003**	0.005	0.001
cs	0.46	0.38	0.30	-0.06	0.20	0.40	0.64	0.93	0.91	0.66	1.00	0.30	**0.48**	0.24	0.37
cv	0.341	0.285	0.288	0.277	0.255	0.283	0.326	0.366	0.356	0.357	0.378	0.327	**0.194**	0.193	0.243

	I	II	III	IV	V	VI	VII	VIII	IX	X	XI	XII	**Year**	XI-IV	V-X
1841-1870															
1856-1885															
1871-1900															
1886-1915															
1901-1930															
1916-1945	5718	6128	7167	8233	9242	8912	7230	5266	4523	4430	5443	5971	**6522**	6443	6600
1931-1960	5811	6287	7646	8478	8871	8488	7181	5465	4308	4067	5021	5732	**6446**	6496	6397
1946-1975	6070	6355	7603	8590	8859	8156	7231	5555	4522	4000	4486	5622	**6421**	6454	6387
1961-1990	6274	6732	7837	9493	9605	8635	7205	5417	4767	4533	4711	5850	**6753**	6816	6694
1976-2007	6410	6504	7516	9655	9373	7879	6359	5258	4670	4839	5175	6107	**6644**	6894	6396
1991-2010	6672	6535	7721	9417	8989	7706	6305	5276	4693	4967	5435	6272	**6665**	7009	6323
1876-2010	6132	6371	7550	8945	9130	8302	6965	5378	4594	4438	5019	5950	**6564**	6661	6468
P1956-1980	0.91	0.99	1.16	1.33	1.41	1.29	1.10	0.85	0.72	0.66	0.71	0.88	1.00	0.99	1.01
P1981-2005	1.00	0.95	1.12	1.47	1.41	1.17	0.95	0.78	0.71	0.74	0.79	0.91	1.00	1.04	0.96

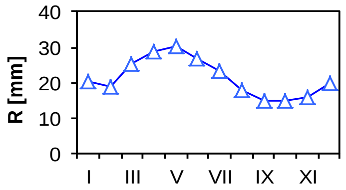

Long-term monthly runoff.

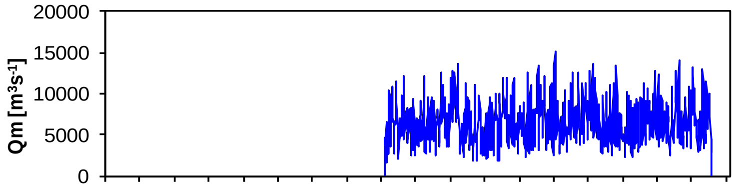

Course of monthly discharges.

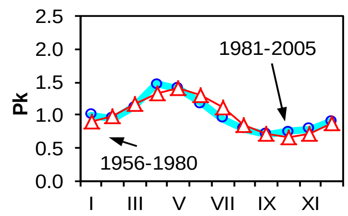

Parde coefficient - two periods.

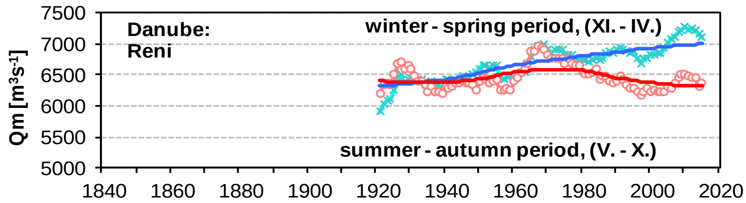

Course of moving averges of seasonal discharges.

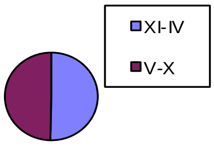

Share of the summer-autumn discharge.

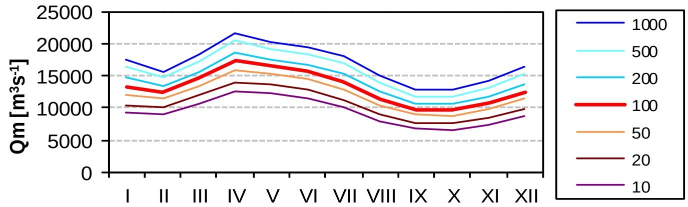

T-year monthly discharges, (log-normal distribution).

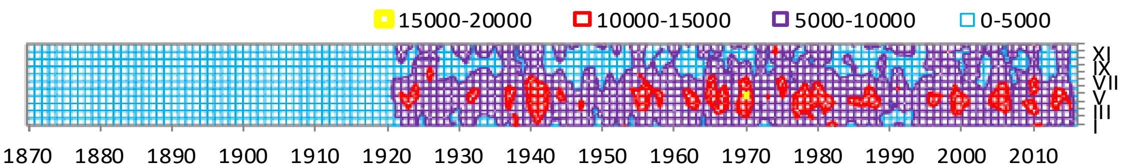

Monthly discharge, 2D plot.

Fig. 5.1d *Basic statistical characteristics of monthly and seasonal discharges at Reni; subplots: Long-term monthly runoff, Pardé coefficient, moving averages of seasonal discharges, Share of the summer-autumn discharge, T-years monthly discharge (long-normal distribution), and 2D picture of the monthly discharges.*

The twelve standardized monthly Pardé-coefficients may be used to construct the so-called regime-curves (Figure 5.2). They are essentially determined by the monthly water balances in the catchments, as well as by intra-annual storage effects such as snow accumulation and snowmelt. PARDÉ originally distinguished a multitude of types of flow regimes that are not discussed in detail here. A distinction is made according to the number and position of monthly maxima and minima within a year, the feeding/origin of flow (see below), and the variability range of the coefficient values. Simple type regimes (one-peak) can be separated from complex multi-peak regimes that arise from superposition of several processes. The flow maxima are typically fed either by glacier-meltwater (glacial regime), snow-meltwater (nival regime) or by rainfall (pluvial regime), or weighted combination of these.
Concerning the Danube basin, major types of the Pardé flow regime (acc. to PARDÉ) are shown in the Figure 5.2:

- **the nival** (= snowmelt-dominated) runoff regime of mountainous areas, illustrated with the example of Austrian gauge Achleiten (Danube River), displaying a very wide amplitude of the coefficient values, single-peak with a maximum in early summer due to snowmelt in the Alps and a minimum in winter when the water is retained as ice and snow;
- **the pluvial** (= rain dominated) oceanic regime, represented here by the example of German gauge Berg (Danube River), with a wide range of amplitude, single-peak, with a maximum in the mild rainy winter months and a minimum in summer resulting from intensive evapotranspiration (Berg: subperiod 1956-1980 only, the subsequent period 1981-2005 represents the transition to a mixed regime with two discharge peaks every year);
- **the balanced pluvial mixed regime** („complex regime 2nd order") of the rain-snow type, shown by the example of Sava at Zagreb (HR), two-peaks, with the main maximum in late autumn and a minimum in summer.

The Pardé-method is a very illustrative way how to show monthly discharge by comparing different runoff periods. The gauge Bratislava is given here as an example (Fig. 5.3) with 2 periods with a length of 30 years. The example shows changes in the flow regime shown by the intra-annual variations of streamflow. A time-shift in maximum discharge of 1-2 months from early summer toward spring is evident. At the same time the winter discharge (month 12) increased, whereas late summer runoff decreases. This pattern is quite typical for nival regimes under the effect of climate warming: earlier snowmelt, higher evapotranspiration increases the water deficit in late summer, and rain dominate precipitation in winter.

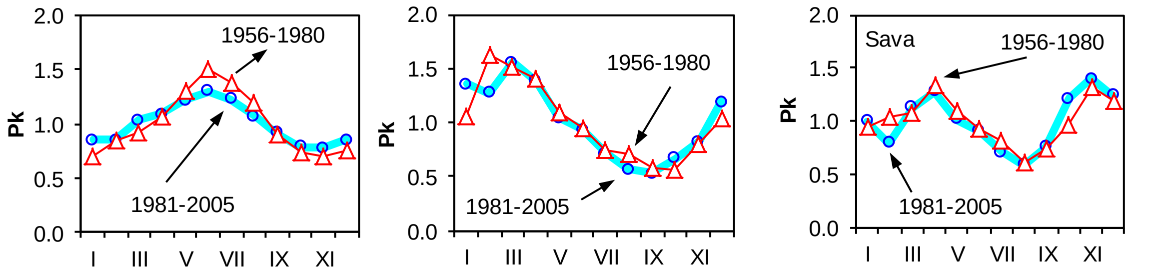

Danube: Achleiten, nival | Danube: Berg, pluvial, oceanic (subperiod 1956-1980 only) | Sava: Zagreb, mixed, two peaks

Fig. 5.2 Examples of Pardé-regime curves using data from the Danube basin, characteristic types of flow regimes in the Danube-basin, period 1956-2005.

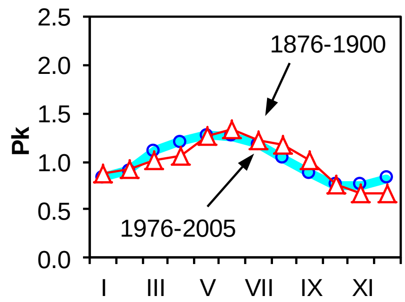

Fig. 5.3 *Gauge Bratislava, Middle Danube: Changes in the flow regime shown by the intra-annual variations of streamflow in the 1876–2005 period. Blue: 1976-2005, red: 1876-1900.*

5.1.1 Monthly flow-regime characterization

To understand the monthly flow-regime characterization and its evolution on the Danube River, it is necessary to understand the inflow structure. Strahler (1968) invented the so-called Strahler-diagram to illustrate the location and inflow quantity along a river. Figure 5.4 depicts the Strahler-diagram of the Danube River and illustrates that left-side tributaries are numerous, but weaker in terms of their contributing volume of water. Furthermore is illustrated, that, in the course of Danube River, from the confluence of River Tisza downstream occurs a change from a more right-sided inflow to an overweight of left-sided river tributaries. In terms of discharge, the Danube is mainly fed by right-side tributaries coming from the Alps and the Dinaric Mountains. Left-side tributaries – excluding the river Tisa (Theiß) – individually contribute to a much smaller extent, although they are of considerable length and drain a large basin area. Their low specific discharge is determined by lower mountain ranges and a semi-humid continental climate in contrast to the Mediterranean and Alpine humid climate and higher mountain areas of the right-side tributaries.

The Danube runoff regime is comprehensively described in Belz et al. (2004). The following description of the Danube River regime is adopted from this publication. The Danube River is mainly influenced by three inflow sections shaping the runoff characteristics of the main river. The first section encompasses the alpine rivers Isar, Inn, and Enns that multiply the discharge of the upstream Danube and change the very balanced, complex runoff regime typical for mid-range mountains (represented by the gauge Hofkirchen, Germany) to a nival regime (represented by Vienna, Austria). Influences of glacier-melt and summer precipitation lead to a prolongation of high flows into the summer. This glacio-nival regime is balanced again to a more complex pluvial-nival regime on its way through the Hungarian low lands (cp. gauge: Mohács). This regime curve has two maxima in April and June. The first runoff maximum corresponds to the midrange-mountain inflows, while the June maximum is related to the alpine snowmelt peak of the previous Danube sections.

The second important inflow section encloses the mouth of river Sava, Drava, Tisa and Velika Morava. Within a river stretch of only ~270 km, these inflows contribute more than double the runoff of the Danube itself. The Drava brings water from the Alps and the Dinaric Mountains and shows an alpine regime type. The Sava originates in the Alps, too, but is mainly influenced by the Dinaric Mountain chain with its karstic environment and Mediterranean climate. The latter leads to a strong increase of runoff in late autumn/early winter. The Tisa on the contrary, drains large parts of the precipitous Western, Northern and Inner Carpathians with a pluvio-nival runoff regime. Finally, the comparatively small Velika Morava contributes with a nivo-pluvial runoff regime characterized by March maximum and September minimum. All these rivers also show a strong annual variability (Figure 5.5).

These four different runoff regimes overlap and mutually influence each other and are further combined with the rather balanced runoff of the Danube at Mohács. The result is a more distinct annual variability (in comparison to the Danube at Mohács), with slightly earlier runoff peak (April) and an earlier runoff minimum (September, gauge Veliko Gradiste). Furthermore, the Mediterranean influence leads to a strong increase in early winter.

Finally, the third section corresponding to the Lower Danube is characterized by the inflow of several left-side tributaries draining the Eastern and Southern Carpathian Mountains. However, the relatively small inflows to the Danube cannot overshape the runoff regime of the Danube which therefore remains quite unchanged. This Lower Danube runoff regime can be characterized as a continental nivo-pluvial, with a long snow melting period from March to June.

The annual variability of the Danube and their tributaries is shown in Figure 5.5 reviving the structure of the Danube as indicated by the regime types. The upstream Danube is characterized by relatively low variability up to the gauge of Hofkirchen that shows a more seasonally shaped runoff. The increased variability of the Danube River does not further change before the inflow of Drava, Sava, and Tisa. This constancy proves that smaller tributaries like the Raba or Morava cannot overshape, yet alter the regime of the Danube due to their smaller discharge volumes. After the inflow of Drava, Sava and Tisa, all characterized by highly seasonal runoff distributions, the annual variability of the Danube increases and remains on this level up to its mouthing into the Black Sea. The several, left-sided tributaries discharging the southern and eastern Carpathian Mountains do not alter the variability of the Danube.

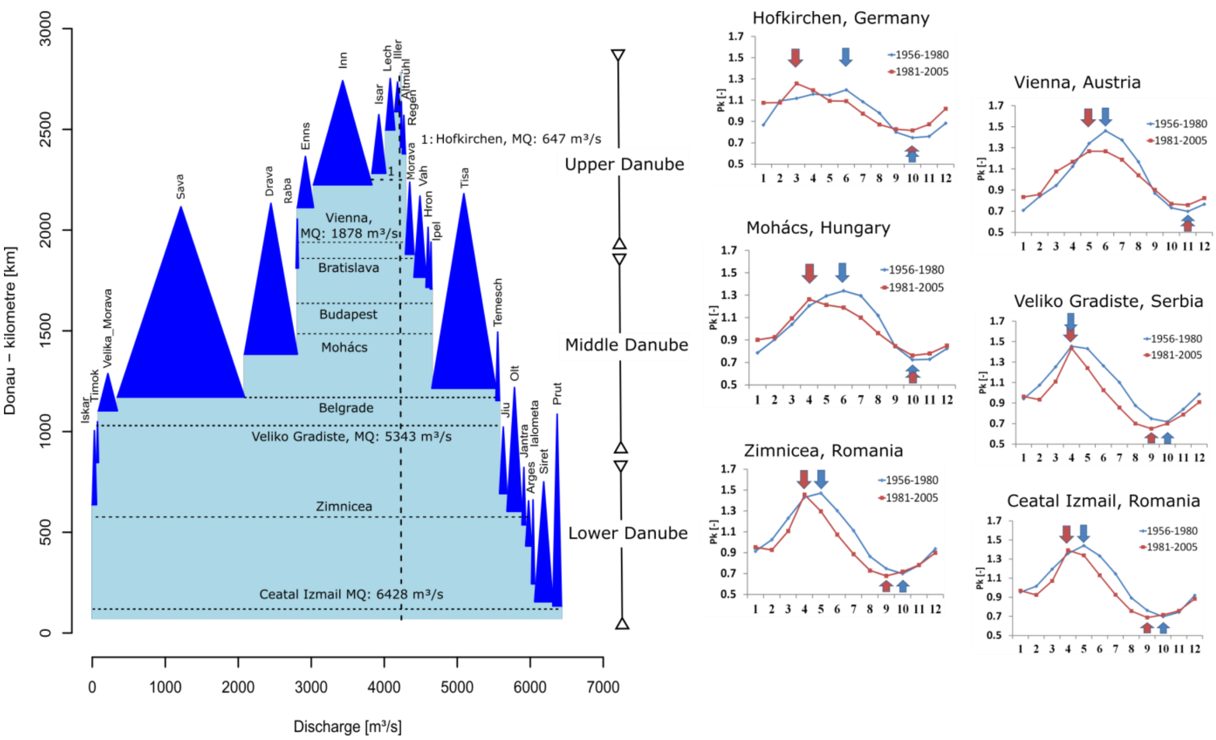

Fig. 5.4 *The Strahler diagram of the Danube illustrating the locations and distribution of tributaries and discharge (left), as well as annual runoff characteristics expressed as Pardé-coefficient for selected gauges along the Danube River (right). Downward arrows in the Pardé curve graphics indicate the month with the highest relative runoff, upward arrows indicate the month with the lowest runoff – color-coded for both considered time slices.*

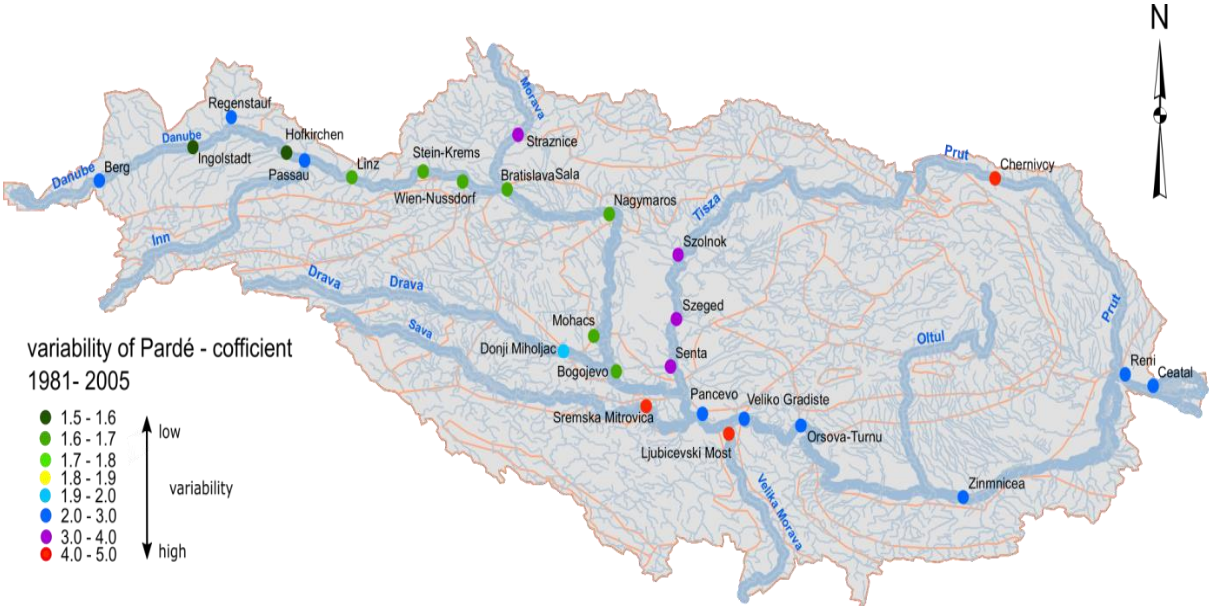

Fig. 5.5 *Variability (kmax/kmin) of Pardé-coefficient illustrates the increasing variability along the Danube, as a result of tributary's inflow with high Pardé variabilities.*

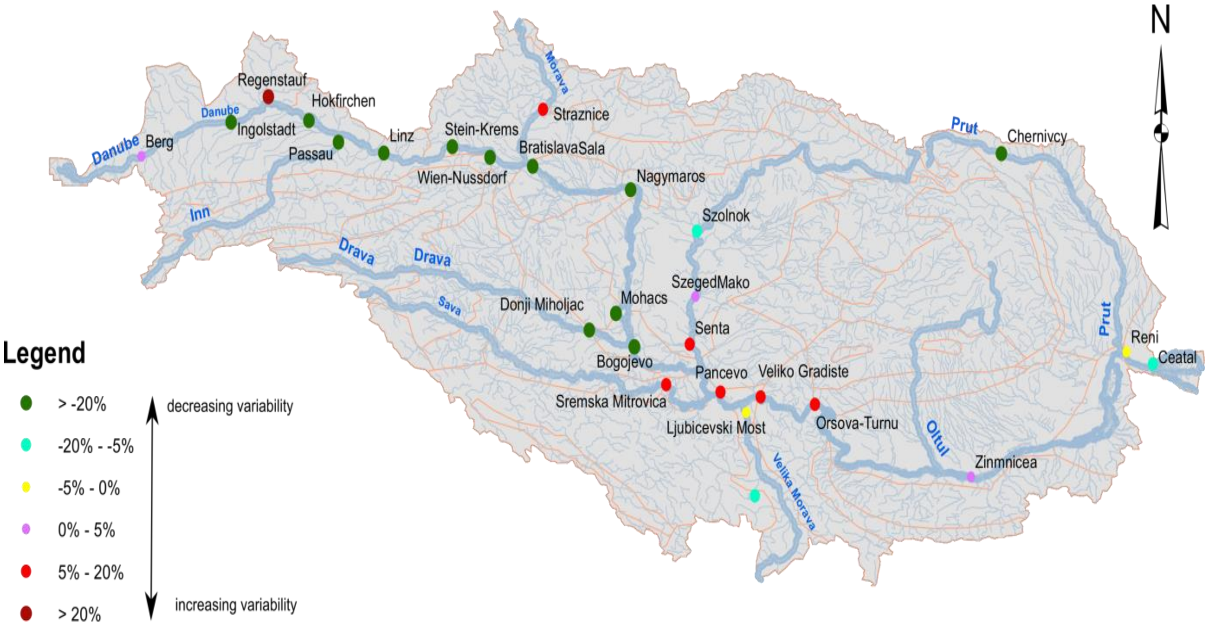

Fig. 5.6 *Percentage changes of the Pardé-variability between 1981-2005 and 1956-1980. Negative values indicate a loss in variability, positive values an increase.*

5.1.2 Changes in the intra-annual flow-regime

Regime types based on Pardé-coefficients are regularly used to detect changes in the regime-defining processes by comparing coefficients of two (or more) time slices. Here, we compared the reference regime (1981-2005) to a previous regime (1956-1980). Thereby, we compare the rather cold time period of the past mid-century to the recent, time slice affected by climate warming. Figure 5.4 (right) visually compares these two slices for six selected stations along the Danube River. The runoff regime in Hofkirchen in the upper Danube shows a shift of the regime peak from June to March. Thereby, the snowmelt runoff part in the predominant complex regime type loses importance at the gain of winter rainfall runoff. At the same time, the late autumn low flow in 1956-1980 occurs earlier, though not with an equal intensity. The runoff regime in Vienna remarkably changes its variability and shifts from a distinct glacio-nival regime to a more complex regime in which snowmelt and glacier-melt still dominate, but in which stronger influences of winter rainfall in February and March occur. Presumably, this rainfall influence is a result of the change signal found at gauge Hofkirchen. The regime changes found in Vienna are further passed on the regime at gauge Mohács. Here, however, an even stronger rain signal can be found in winter. As described before, with the inflow of Drava, Sava, and Tisa, the runoff regime is overshaped by Mediterranean and continental mountain runoff patterns. Likewise, the change patterns alter as well: While, at Veliko Gradiste, the general regime (spring peak, autumn low) remains unchanged, the runoff volume decreases resulting in lower, and slightly earlier minima. In addition, the maximum runoff occurrence in spring decreased from two to one month, probably as a result of a shorter snow melt season due to fewer snow (see change signals upstream). This pattern of change continues downstream, which might either be a result of unchanged climatological conditions or the relatively small influence the downstream tributaries have on the Danube regime.

The elaborated change pattern can also be seen in Figure 5.6 that quantifies the ratio of variability. Runoff regimes along the Upper and Middle Danube (i.e. Ingolstadt to Bogojevo) are subject to decreasing regime curve variability that relates to an increase of complexity. In contrast, downstream of Bogojevo the runoff shows increasing variability, apart from the Danube estuary. This increase is smaller than the decrease in the upstream part and likely relates to the small change found for the low runoff in autumn (cp. gauge Veliko Gradiste, Figure 5.4).

The reason for either the decreasing signal in the upstream or the increasing change signal in the downstream Danube are unclear and need to be elucidated using at least meteorological data and information on anthropogenic influences. Here, we can only speculate:

- Increasing (winter) temperatures result in higher fractions of rainfall during winter that cause both increasing winter runoff and less snow melt later in the year. Both effects can be seen in the changed regime types of the upstream Danube. The decrease in runoff volume and the lower runoff in late summer might also be an effect of less snow melt in upstream areas, be it the Alps, the Dinaric or the Carpathian Mountains. A similar effect of changed climate on runoff regime at the downstream area of the Danube cannot be found at this stage. However, changes to the runoff – if present at all – are less prominent than in the Upper Danube. These conclusions are just first hypotheses that need to be validated or falsified in a separate investigation.

5.2 Flood seasonality

5.2.1 Maximum annual flood seasonality analysis according to BURN index

The seasonality index according to BURN (1994) allows to estimate the date and probability of the occurrence of a (flood or low-flow) extreme in the calendar year. The result is the most probable date of the occurrence of an extreme event along with the stability index $\bar{r}$ (expressing the probability that the event will actually occur on this day). D_i is defined as the date of the occurrence of the *i*-th event in the Julian day format, with D=1 standing for 1 January and D=366 for 31 December. Results of a Burn analysis are typically graphed on an unit circle and D is to be understood as polar coordinate on the unit circle with the angle θ. The direction of the mean vector of all events gives the mean date of the occurrence *MD*, and the length r of the mean vectors is a measure of the variability of the date of the occurrence. Values of $\bar{r}$ range between 0 (events occur with equal probability on all days of the year) and 1 (all events occur on one single day in the year). *MD* and $\bar{r}$ are calculated as follows:

Angle on the unit circle based on the Julian calendar day:

$$\theta_i = D_i\left(\frac{2\pi}{366}\right), i = 1, n \tag{5.4}$$

Calculation of the average flood occurrence day (MD) follows these terms and equations:

$$\bar{x} = \frac{1}{n}\sum_{i=1}^{n}\cos(\theta_i), \quad \bar{y} = \frac{1}{n}\sum_{i=1}^{n}\sin(\theta_i) \tag{5.5}$$

$$\bar{\theta} = \tan^{-1}\left(\frac{\bar{y}}{\bar{x}}\right) \text{ for } x \geq 0 \text{ and} \tag{5.6}$$

$$\bar{\theta} = \tan^{-1}\left(\frac{\bar{y}}{\bar{x}}\right) + \pi \text{ for } x < 0 \tag{5.7}$$

$$MD = \bar{\theta}\,\frac{366}{2\pi} \tag{5.8}$$

And finally, the seasonality vector is calculated as:

$$\bar{r} = \sqrt{\bar{x}^2 + \bar{y}^2} \tag{5.9}$$

It should be noted that MD should be regarded as a probability statement and should not be misinterpreted as a true or exact predicted value/prediction.

5.2.2 Flood seasonality along the Danube River and its tributaries

To understand the reasons for the spatial and temporal patterns of flood seasonality, it is helpful to apply the concept of disposition: The flood favouring conditions can be classified into two dispositions: The basis disposition, and the variable disposition. The basic disposition represents literally invariable conditions like catchment shape, location in a climate zone, or river morphology. In contrast, the variable disposition comprises of changeable conditions like sum or time distribution of precipitation, or storage level. The higher the total disposition level rises, the likelier a triggering event (rainfall) can cause an extreme event like a flood. In our case, different climate zones and mountain areas contribute to the basic disposition, and glaciermelt, snowmelt, or regular rainfalls contribute to an increase of the variable disposition. That is the reason for floods to occur typically during months with high runoff, hence high river water stages and likely filled water storages within the landscape. The previous chapter was elaborated on the runoff regime and its change over time and thereby it sets the scene to the flood seasonality analysis.

For calculation of the Burn indexes in this capture, the mean daily discharge time series were used. Figure 5.7 depicts the Burn vectors for all selected gauges along the Danube and its tributaries. The arrows thereby mark the calculated day of average flood occurrence (MD), indicated by the direction of the arrow, and the severity of the seasonality, indicated by the scale of the arrow. Furthermore, Figure 5.8 summarizes the average flood day (MD) and the *r*-value, the seasonality index for different time periods. Looking at the figures, the already elaborated subdivision of the Danube River with respect to regime type reappears: The upper reach up to the gauge of Hofkirchen shows winter floods in March or February (corresponding to Julian dates 40-80 in Figure 5.8). In combination with the strong summer flood seasonality of the alpine right-sided tributaries, and the spring flood prone left-sided tributaries up to the gauge of Bratislava, this leads to a very unspecified flood seasonality, meaning that floods can occur throughout the year.

Keeping this low seasonality level in mind, the Middle Danube at its beginning is characterized by a shift from high to early summer floods (Julian Date ~180) and later on – from the inflow of the Morava to the gauge of Bogojevo – to spring (March-April/Julian Date ~90). With the inflow of Drava and Sava, the flood regime of the Danube alters again and regains more pronounced flood seasonality with an occurrence day in spring. This type of regime persists from here on downstream to the Lower Danube. As on this section of the Danube the stream shares its seasonality pattern with the Tisza and the Velika Morava, the influence of these two major tributaries is not detectable within the regime characteristics.

The tributary rivers of the Danube group in terms of flood seasonality as a function of catchment characteristics, namely topography and climate zone (Figure 5.7), that is to say runoff regime. Alpine rivers like Isar, Inn, Enns, and Drava show a typical summer flood season. The nivo-pluvial rivers Morava, Vah, Hron, Ipel originating from the Carpathian and Tatra Mountains, and the right-sided Raba too, experience mainly flood events in spring (March or April). The mediterranean winter rainfall influence on the flood seasonality is recognizable at the Sava River, with a slight west – east pattern: November and December floods in the west, January and February average flood days in the east. Interestingly, the runoff regime and the peak flood month correspond well, however, with the tendency that floods occur approximately one month later than the regime maximum.

Despite the general similarity between flood season maximum and monthly runoff peak, it needs to be highlighted that the flood seasonality along the Danube is not very pronounced. The *r*-value exceeds the low value 0.4 (i.e. 40% probability) only at the upstream most gauge Berg, shortly after the inflow of the Inn, and downstream of the Drava, Sava, and Tisa (Figure 5.7 and 5.8). In between these sections the flood seasonality shows locally a strong decrease (i.e. gauge Nagymaros). The decrease in the *r*-value thereby corresponds to occurrence of a complex runoff regimes and hence to a longer time of increased variable disposition. For the tributaries the seasonality *r*-values lie in general higher than those of the Danube as complex regime types occur fewer.

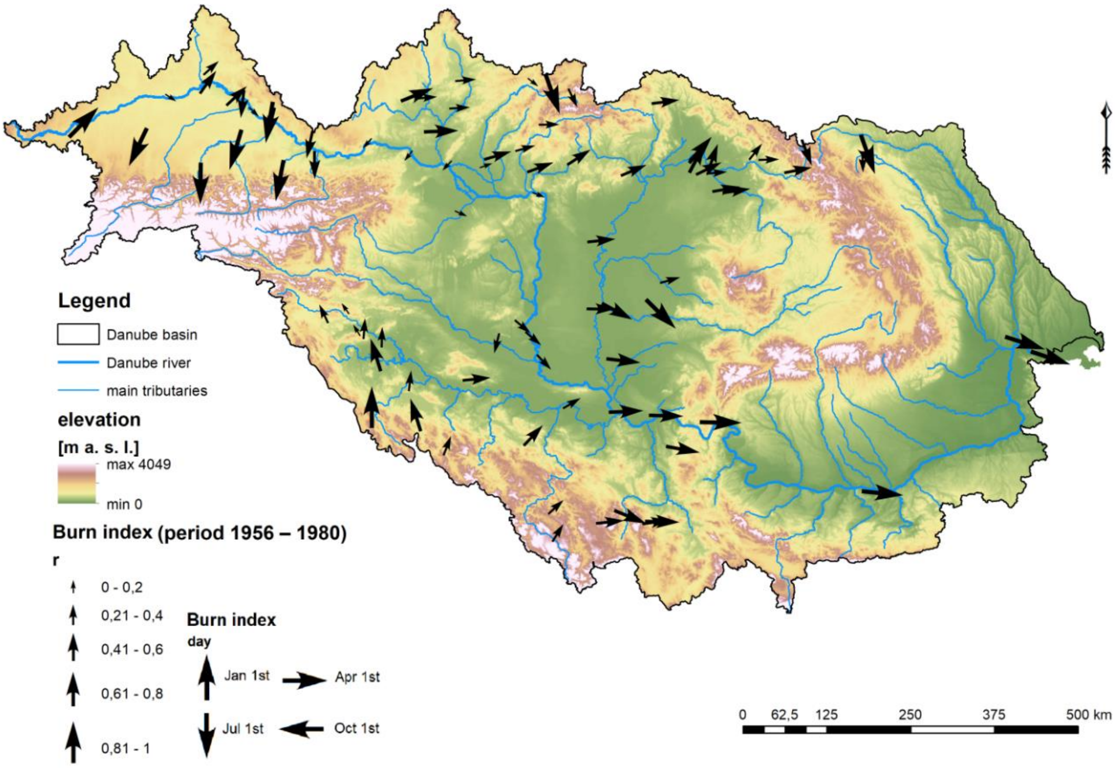

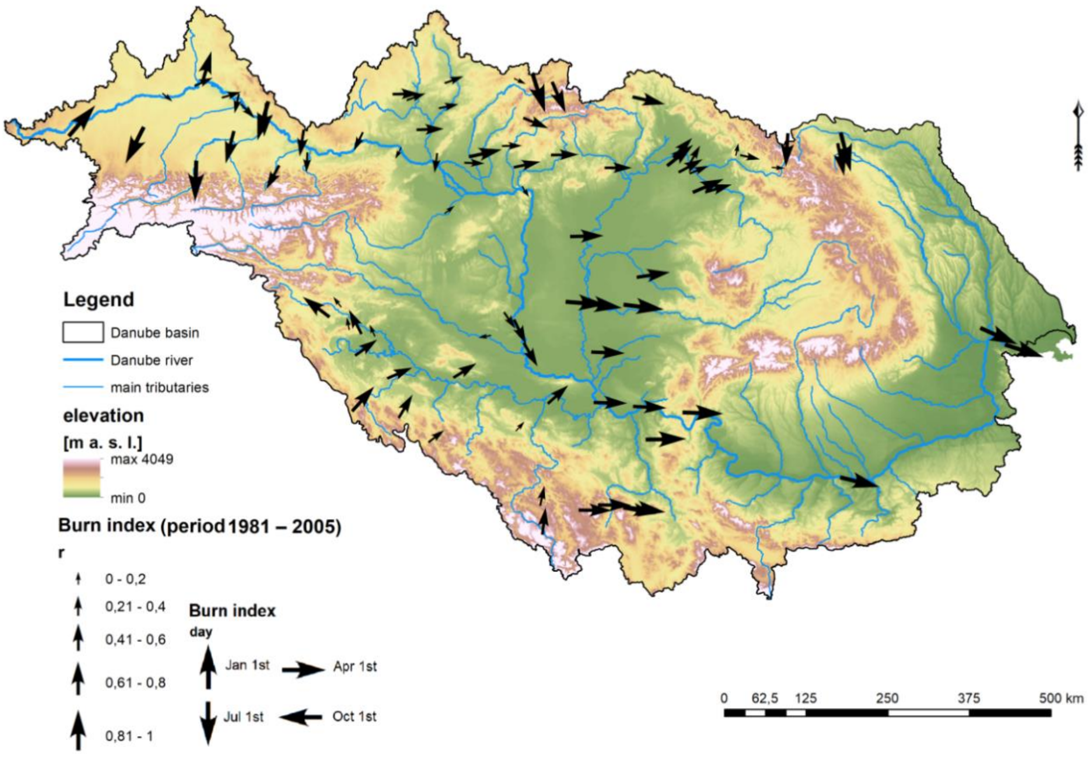

Fig. 5.7 Illustration of the Burn flood seasonality vector date (up), as well as the Burn r-value (down) as an indicator of the seasonality strength, for both: the Danube River, and tributaries in two periods (1956-1980, 1981-2005).

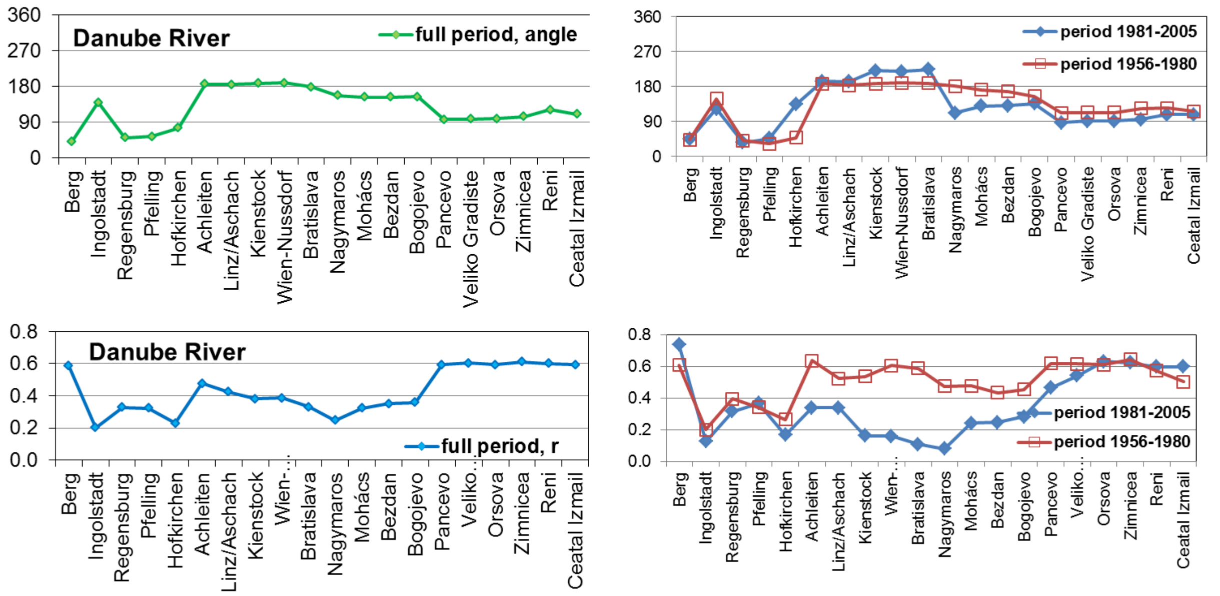

Figure 5.8 Average flood day (upper charts) and the Burn r-value as an indication of the seasonality strength (lower charts) and their change over time for 20 gauges along the river Danube (1956–1980 vs. 1981–2005).

Thereby, spring floods show a quite high regularity, which was expected as variations in winter precipitation are even out due to the temporal storage of water in snow. In contrast, the low *r*-values in the Sava result from timely unreliable heavy precipitation events in the winter half of the year. Gauges located at higher altitudes are exception, as the snow accumulation and melting effect comes back in play.

Figure 5.9 finally provides a more detailed look into the Burn statistics and its change over time for four selected gauges. For each gauge a unit circle is drawn with red lines marking flood events and related magnitudes. Furthermore, the annual maximum time series and the related day of the year are given, allowing for a temporal framing of the date of occurrence and the flood magnitude. We will first explore the unit circle and come back later to the temporal framing.

For the gauge Achleiten at the Upper Danube (shortly after the inflow of the Inn) a concentration of high flood during the summer (June to September) is recorded. In addition, a second phase of the year – in winter to spring– is depicted with floods of smaller magnitudes. These floods likely originate from the mid-range mountain part of the upper most Danube experiencing winter rainfall, or widespread snowmelt, or special alpine flood generating processes like rain-on-snow conditions. However, they do not occur at the same level of magnitude as summer floods, when high runoff from snow and glacier melt are amplified by intense summer rainfall.

For the gauge Bratislava, the same general pattern holds, however, the difference between winter and summer floods in terms of magnitude are much fewer, and floods can occur almost anytime. Accordingly, the *r*-value is low (Figure 5.7, and 5.8). The reason for the less pronounced flood season are likely the attenuated snow melt regime, and an increased inflow of floods from the upstream left-sided rivers that show a clear spring flood occurrence signal (cp. Figure 5.7).

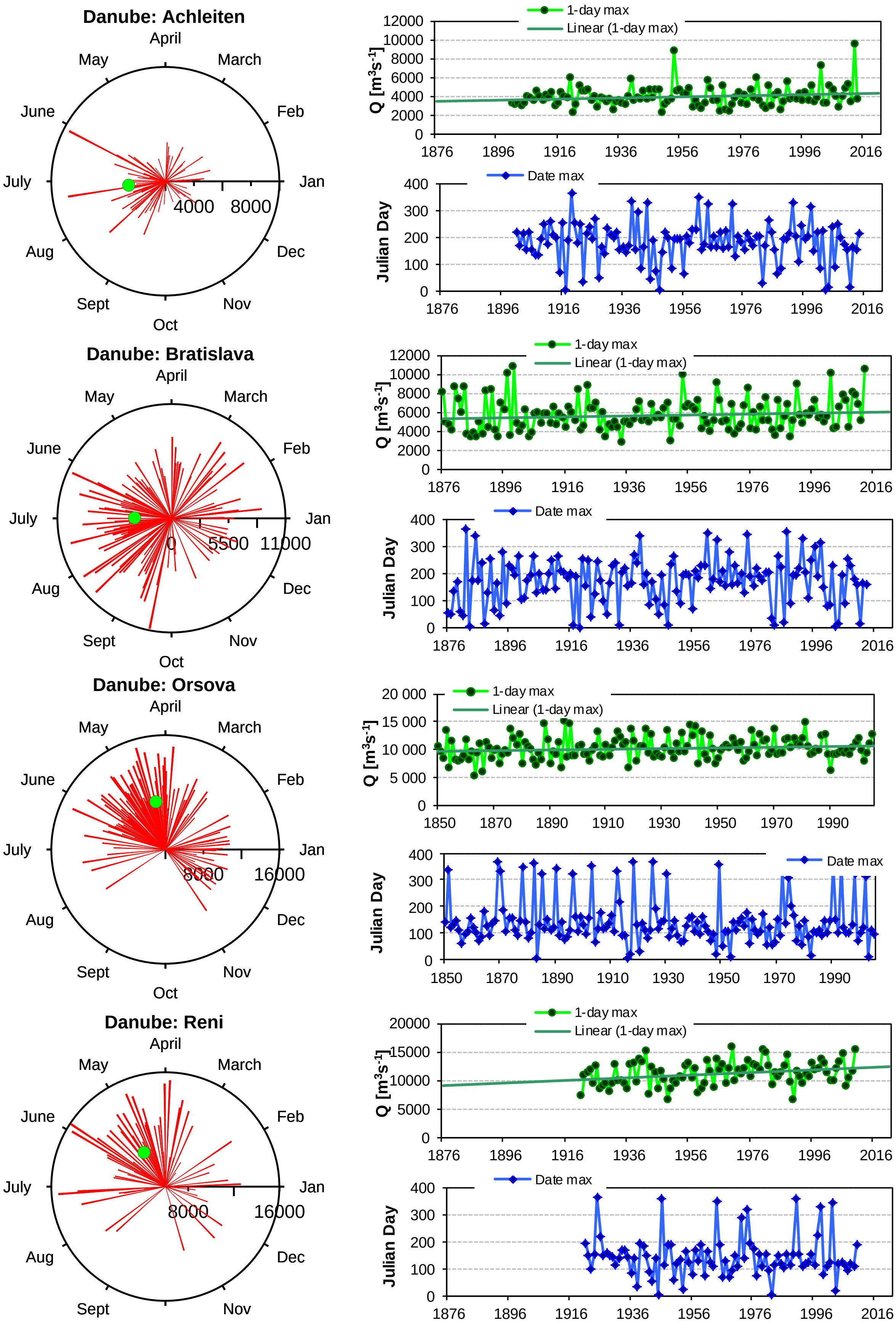

Figs. 5.9 *Changes in the flow regime shown by the intra-annual variations of streamflow in the 1840–2015 period of gauges along the Danube River.*

The gauge Orsova documents a complete shift in the flood seasonality: Again, two flood seasons can be derived. The major season occurs from April to August, and a smaller one occurs during winter (November-January). Consulting the Burn analysis for the tributaries (Figure 5.7), it becomes apparent that these two seasons are rather a mixture of three different flood types and seasons of the contributing rivers that intersect in the Danube: The alpine Drava shows a summer flood signal in agreement with other rivers origin from the Alps. On the contrary, the Sava springing in the Dinaric Mountain Chain, experiences Mediterranean winter rainfall and thus exhibits a winter flood season. The flood season of the Tisa and the Velika Morava, finally, is stimulated by the snow melt season of the Carpathian and lies accordingly in spring, completing the compound flood season pattern found at the gauge Orsova, situated downstream of these tributaries.

Finally, the question arises if the flood season underwent changes likewise the runoff regimes. Figure 5.8 illustrates the change of the flood date and the Burn *r*-value as an indication of the seasonality strength from the 1956-1980 vs. the 1981–2005. While the average flood date showed only marginal changes, the seasonality strength in the Middle Danube decreased strongly. The *r*-values from the gauges Hofkirchen to Bogojevo decreased 0.6 to at least 0.4, and partly to 0.1 (Nagymaros).This loss of flood seasonality corresponds to the decrease of monthly mean flows and the shift to a spring peak runoff regime, thus indicating a loss of summer snow and glacier melt water. Accordingly the variable disposition for a summer flood in this Middle Danube section decreases and thereby aggravates the flood generation by a triggering event. As a further side effect of this seasonality decrease, the slight changes in flood dates should not be overinterpreted.

In terms of tributaries and their change in seasonality and flood dates, revealed rather unchanged characteristics for most of the rivers (Figure 5.10a-b): While the alpine rivers, the rivers discharging the Carpathian Mountains and the Tatra Mountains, as well as lower Sava, Drava, and upper Tisza showed almost unchanged flood dates and seasonality values, gauges situated at the upper Sava river, showed a shift from early to late winter with similar seasonality values. However, given the diversity of catchments considered this stability of flood seasons was unexpected. Future studies might consider even longer time series to do this change detection.

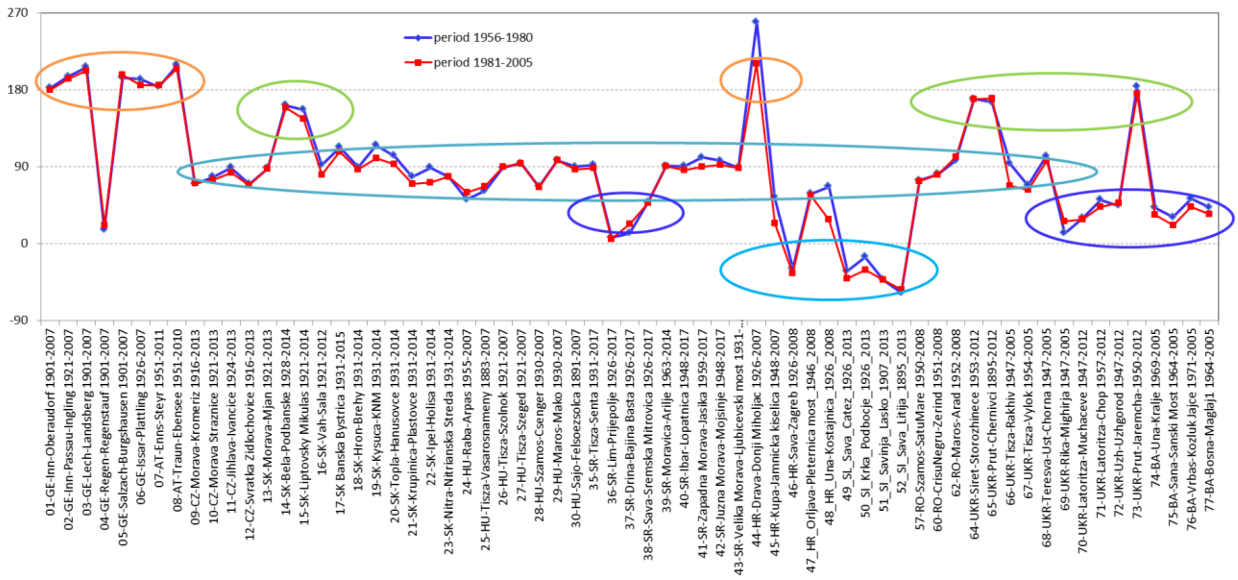

Fig. 5.10a Burn indexes for 65 gauges of the Danube tributary rivers, changes of the mean flood day, period 1956–1980 and 1981–2005.(minus 1 is 359, minus 2 is 358).

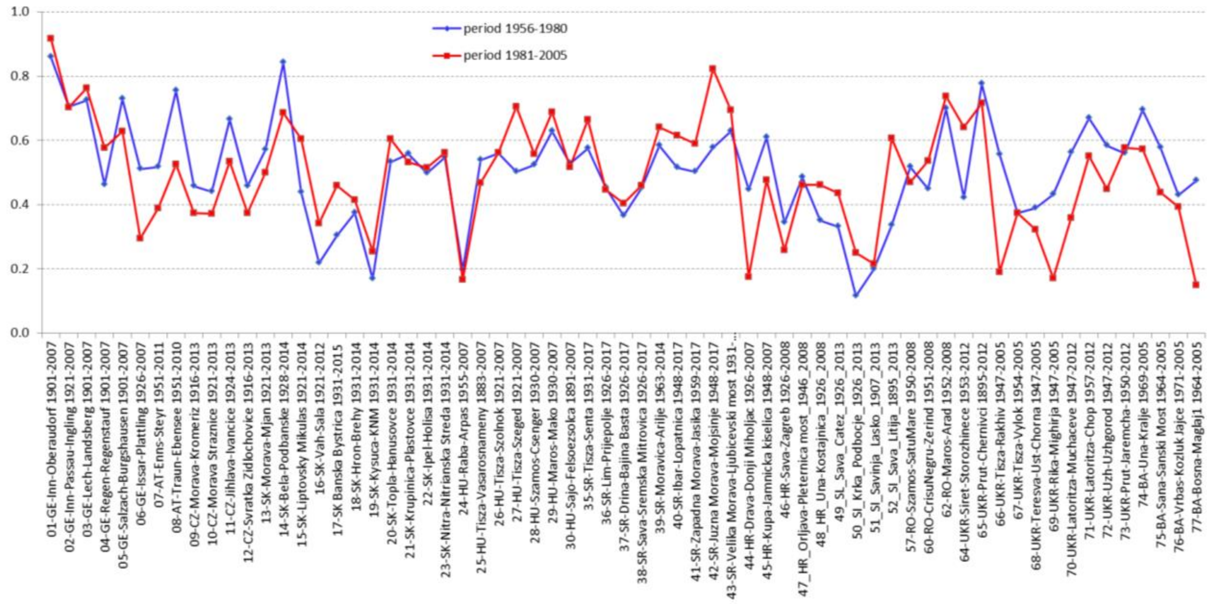

Fig. 10b *The Burn r-value as an indication of the seasonality strength and its change over time for 65 gauges of the Danube tributary rivers, period 1956–1980 and 1981–2005.*

5.2.2.1 Long term trends of the time series of the Burn indexes

Finally, increasing the considered time span of the analysis for the Danube, it reveals that the found tendency to earlier, but less pronounced flood dates especially from the eastern part of the Upper Danube (Pfelling) to the western part of the Middle Danube (Bratislava), and the rather unchanged flood seasonality for the Upper and Lower part of the Danube, is accompanied by an overall tendency (fig. 9) to higher flood magnitudes.

We have used time series of the Burn index to analyse the significance of the long-term trends of the Burn index. The series were calculated in successive steps for 25-years periods. The Burn index value of the period 1901–1925 was assigned to the year 1913, of the period 1981–2005 to the year 1993, etc. The Burn index series were calculated for the stations on the Danube and for the tributaries as well, with the longest daily discharge series. For detecting and estimating trend in time series of the Burn indexes we used the non-parametric Mann-Kendall test (see paragraph 4.3). Figure 5.11 displays the selected stations series.

Table 5.1 presents the results of trend significance analysis for selected stations along the Danube and the tributaries, with the longest daily discharge series

Table 5.1 Trend significance analysis for selected stations with the longest series

	Mann-Kendall trend					Sen's slope estimate	
Time series *Burn index, Julian day*	**First year**	**Last Year**	**n**	**Test Z**	**Signific.**	**A**	**B**
Danube: Hofkirchen	1913	2004	92	7.92	***	1.078	1.41
Danube: Achleiten	1913	2004	92	-0.35		-0.022	188.44
Danube Bratislava	1888	2005	118	5.47	***	0.208	172.90
Danube Orsova	1888	1995	108	-2.11	*	-0.048	103.80
Danube: Reni	1933	2005	73	2.17	*	0.406	126.56
Salzach: Burgshausen	1901	2005	93	-4.70	***	-0.153	209.18
Sajo: Felsoezsolca	1903	2005	103	9.11	***	0.373	43.88
Tisza: Vasarosnameny	1895	2005	111	-2.83	**	-0.089	71.37
Sava: Litija	1908	2005	98	-3.33	***	-0.162	332.25

For the four tested significance levels the following symbols are used
*** if trend at α = 0.001 level of significance; ** if trend at α = 0.01 level of significance

* if trend at α = 0.05 level of significance; + if trend at α = 0.1 level of significance

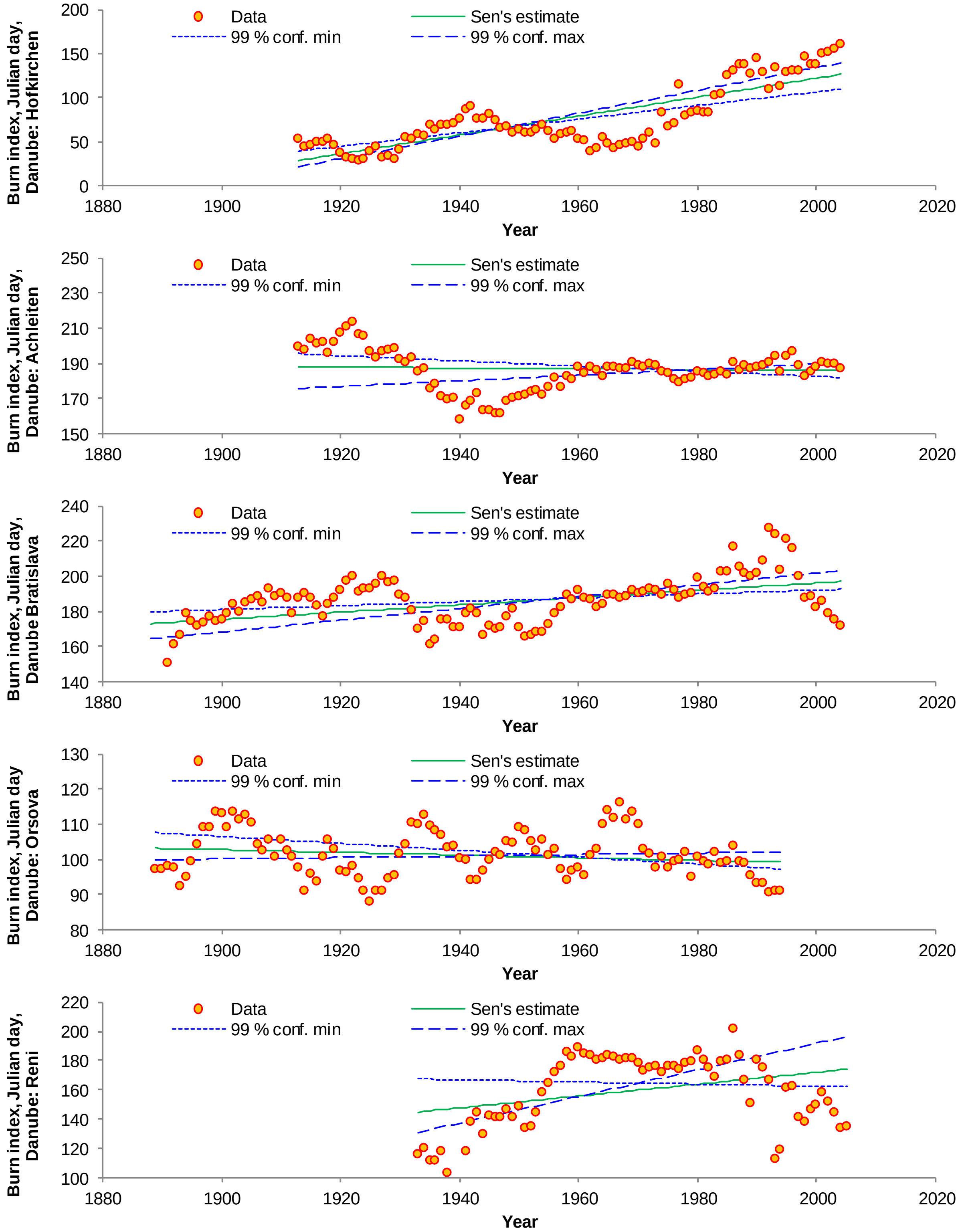

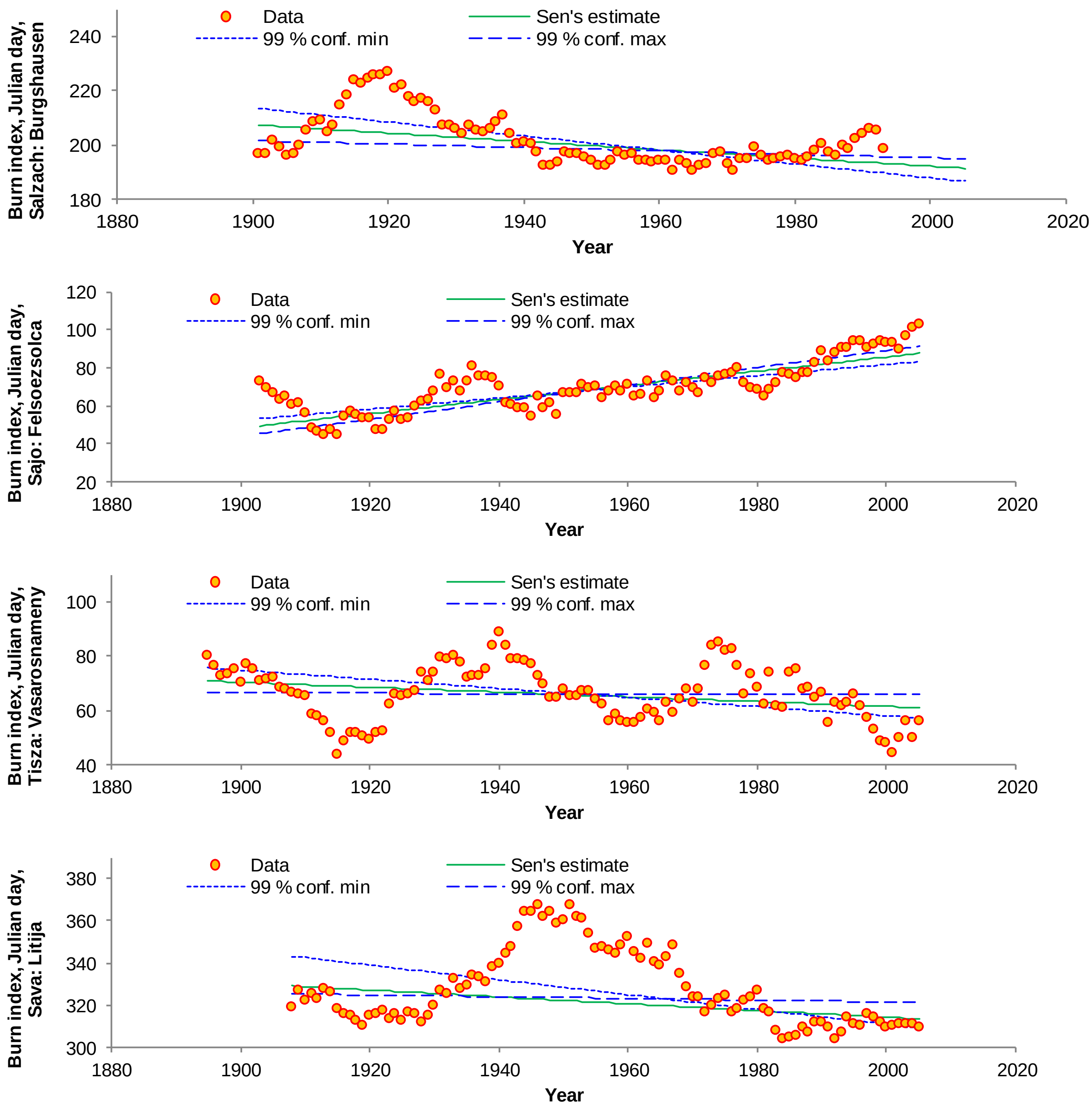

Fig. 5.11 Long term trends of the Burn index time series for selected gauges along the Danube River calculated for 25-year periods.

The analysis of trend significance of the Burn index shows variable results. The trends in different stations were decreasing, stable or increasing.

Very interesting are the results of the Danube at Orsova station as a strong variability of the Burn index time series is displayed. The Burn indexes vary from 90 to 115. The similar variability we can see from the results for Tisza at Vasarosnameny station; but Burn indexes vary from 40 to 90 and the wave amplitude is two times longer.

Increasing trend of the Burn index is evident for Danube: Hofkirchen, and Sajo: Felsoezsolca stations. At the Danube: Reni station, looking at the length of the observed series, we cannot clearly speak about an increasing trend.

5.2.2.2 Regionalization of the flood regime in the Danube basin

Regions with the same vector / Burn index can be derived from the analysis of results shown in Figure 5.7 and are shown for period 1981–2005 for water gauging stations of the river Danube and main tributaries on Fig. 5.12.

More detailed regionalization of runoff in the Danube basin using copula functions is discussed in Chapter 9 of this monograph.

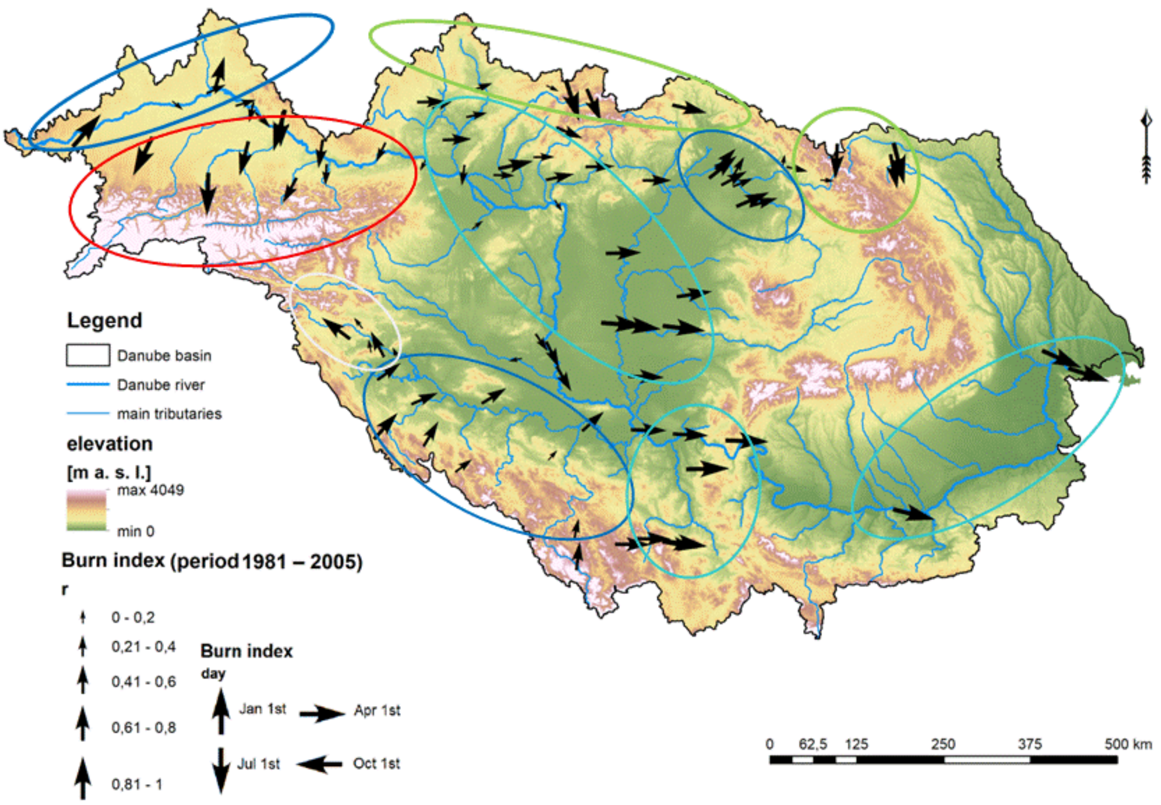

Fig. 5.12 Water gauging stations of the river Danube and main tributaries: regions with the same Burn index for period 1981–2005.

5.3 Conclusions

Along the 2780 km the Danube River changes its runoff character repeatedly: starting from the mid-mountain ranges making up the complex regime and flood season in the uppermost reach, over the glacier- and snowmelt determined sections that lose its alpine character as it flows through the Pannonial planes, to the mixed runoff characteristics of the Lower Danube, the runoff regime as well as the flood seasonality changes. Tributaries like Inn, Sava, Tisa, or Drava play a superior role in understanding the Danube River characteristics. That is because they represent the regional water balance and hydrometeorological conditions, and due to their pure amount of discharging water, partly overshaping the upstream runoff signals. Runoff regimes and flood seasons correspond very well.

Particularly the upper reaches of the Danube show shifts in the regime types during the last decades. This is likely caused by the increasing temperature and the shift of the discharge maxima due to earlier snowmelt. In the lower reaches, on the other hand, the general characteristic remains largely intact. However, spring and summer deficits compared to earlier time periods suggest losses in snow melting and increased evapotranspiration, which also explain the lower discharge quantities in general. Floods, on the other hand, show hardly any change over the last centuries, especially for the average date of occurrence and thereby partly deviate from the corresponding pattern shown above. However, some gauges record an increase in the flood magnitude. Future studies will have to show whether and how this is related to global warming or rather the expression of climate variability, or human activity.

The annual variability of the Danube River and their tributaries is indicated by the regime types. The upstream Danube is characterized by relatively low variability up to the gauge of Hofkirchen that shows a more seasonally shaped runoff. The increased variability of the Danube River does not further change before the inflow of Drava, Sava, and Tisa. This constancy proves that smaller tributaries like the Raba or Morava cannot overshape, yet alter the regime of the Danube due to their smaller discharge volumes. After the inflow of Drava, Sava and Tisa, all characterized by highly seasonal runoff distributions, the annual variability of the Danube increases and remains on this level up to its mouthing into the Black Sea. The several, left-sided tributaries discharging the southern and eastern Carpathian Mountains do not alter the variability of the Danube.

Defining temporal change in river discharge is a fundamental part of establishing hydrological variability, and crucially important for identifying climate–streamflow linkages, water resource planning, flood and drought management and for assessing geomorphological and hydro-ecological responses. The implications of analytical decisions on the interpretations of hydrological change are important and impact on planning and development in many fields including water resources, flood defence, hydro-ecology and climate-flow analysis.

References:

Belz J.U., Goda L, Buzás Z, Domokos M, Engel H, Weber J. 2004. Runoff Regimes in the Danube Basin. The Danube and its catchment – A hydrological monograph, Follow-up volume VIII/2, Regional Cooperation of the Danube Countries, Koblenz & Baja, 152 p.r

Burn D.H. 1994. Hydrological effects of climatic change in west-central Canada. In: Journal of Hydrology 160, p. 53-70.

Burn, D.H., Elnur M.A.H. 2002. Detection of hydrologic trends and variability. Journal of Hydrology 255, p. 107-122.

Pardé M. 1947. Fleuves et Riviéres. Paris.

Stănescu V.A. 2004. Regional analysis of the annual peak discharges in the Danube catchment. The Danube and its catchment – A hydrological monograph, Follow-up volume No.VII, Regional Cooperation of the Danube Countries, Bucharest, 64 p.

Yulianti J.S., Burn, D.H. 1998. Investigating links between climatic warming and low streamflow in the Prairies region of Canada. Canadian Water Resources Journal, 23:1, 45-60, DOI: 10.4296/cwrj2301045

6 Statistical analysis of extreme discharges

Pavla Pekárová, Radu Drobot, Veronika Bačová Mitková, Jakub Mészáros, and
Aurelian Florentin Draghia

One of the basic problems in flood hydrology is the relationship between peak discharge of flood waves and the probability of their exceedance. Importance of extrapolating these variables (so called frequency curve) is especially necessary for proper water management and flood control plans. The European Parliament's Directive 2007/60/ EC concerning the assessment and management of flood risks requires member States to create flood hazard maps of floods with very long return periods *T* (*500* to *1000* years).

The main steps of the statistical processing are the following:

1) *Selection of time series with maximum discharges*:

a) the maximum average daily discharge exceeding a certain threshold value, or

b) the maximum annual discharge Q_{max}.

2) Fitting the empirical data can be based on:

a) a set of distribution functions, or

b) only one distribution function.

All methods used to estimate floods with a very long return period are associated with great uncertainties. Determining the specific value of a *500*- or *1000*-year flood for engineering practice is extremely complex. Nowadays, hydrologists are required to determine not only the specific design value of the flood, but it is also necessary to specify confidence intervals in which the flow of a given *100*-, *500*-, or *1000*-year flood may occur with probability, for example, 90%.

In this chapter, we will present two methods of calculating the design values of *T*-year discharges:

1) Statistical processing of series of maximum discharges based on a set of distribution functions; and

2) Estimation of the *T*-year design discharges based on log Pearson type III distribution with the inclusion of historical floods into the $Q_{ma}x$ time series.

6.1 Statistical processing of the maximum discharges and flood volumes based on a set of distribution functions

6.1.1 Introduction

Different statistical distributions can be selected for fitting the empirical distributions (Bobée et al., 1993; Koutsoyiannis, 2005; Maidment, 1992). Malamud and Turcotte cited in El Adlouni et all (2008) showed that the most common distributions in hydrology can be divided into four groups: the normal family (normal, Lognormal), the general extreme value family (GEV, Gumbel, Fréchet, reverse Weibull), the Pearson type III family (Gamma, Pearson type III, Log-Pearson type III), and the Generalized Pareto distribution. In practice, all these models are fitted to data and compared using conventional goodness-of-fit tests. Having a data set of discharge annual maxima different statistical tests such as the Kolmogorov-Smirnov, Anderson-Darling and Chi-Squared tests (Ang and Tang, 2007) are used to select the suitable continuous distribution. When the sample size is not sufficiently long it can be extended by numerical simulations of a random variable based on the inverse method. The maximum discharges Qp% corresponding to the probability of exceedance P% are not unique values as they depend on aleatory and epistemic uncertainty (Merz and Thieken, 2009). Aleatory uncertainty is mainly due to the temporal variability and the length of the series, while the epistemic uncertainty is the consequence of the incomplete knowledge of the hydrological system.

6.1.2 Processing the annual maximum discharges

A set of distributions (Drobot et al., 2017; Danube Floodrisk, 2012) were considered to analyse the discharge maxima from different gauging stations along the Danube. As an example, the discharges registered at Bratislava and Turnu-Măgurele were processed to estimate the interval of uncertainty (Fig. 6.1). The statistical distributions were then ordered according to their adequacy based on statistical tests (Kolmogorov-Smirnov, Anderson-Darling and Chi-Squared tests) (Fig. 6.2).

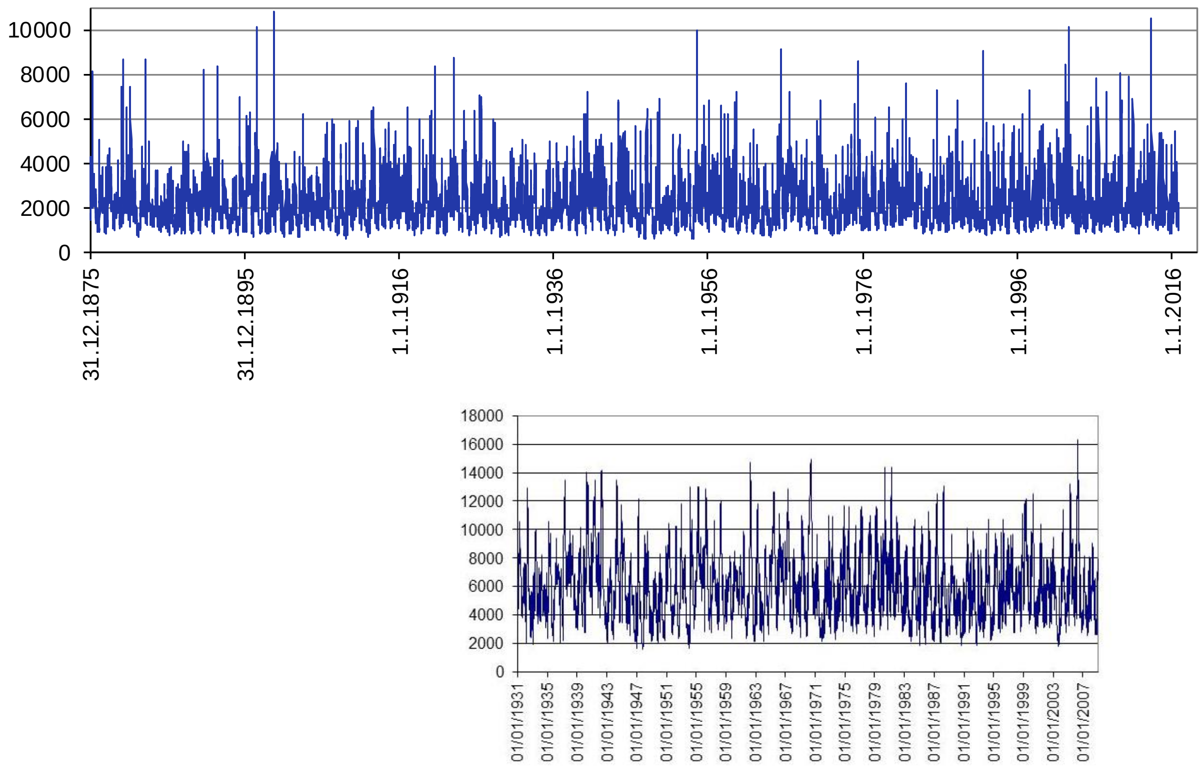

Fig. 6.1 *Complete time series of discharges registered at Bratislava (up, from 1876 till 2016) and Turnu-Măgurele (down, from 1931 till 2007), (Slovak Hydrometeorological Institute, National Institute of Hydrology and Water Management, Romania).*

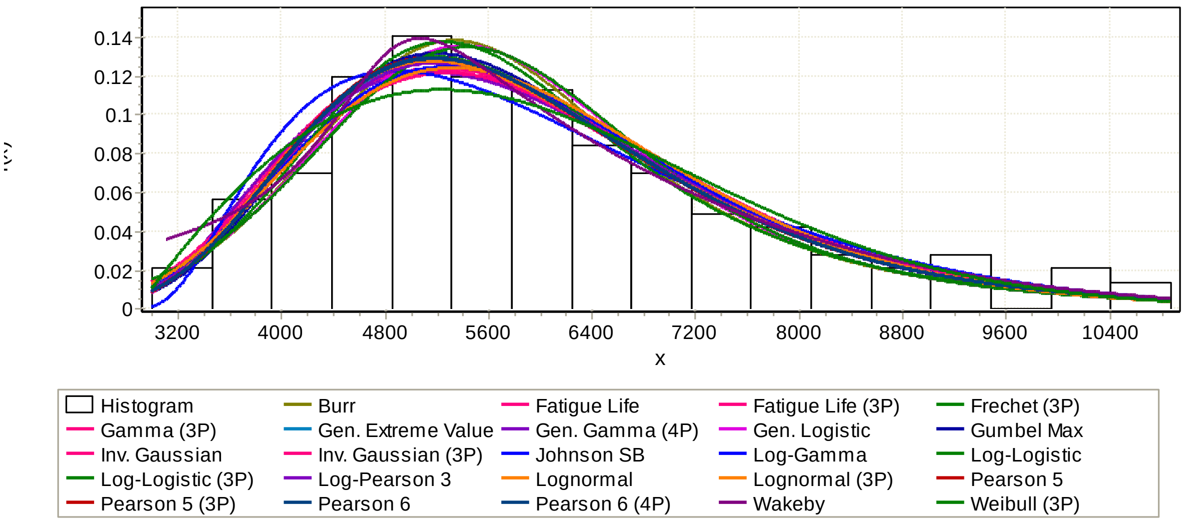

Fig. 6.2 *The best 24 Probability Density Functions of Q_{max} time series, Danube: Bratislava.*

The results for the first 9 ranked distributions are presented in Table 6.1a,b and Fig. 6.3 where, besides the empirical distribution, the lower and the upper limits of the uncertainty interval are presented (Drobot et al., 2017).

Table 6.1a Results of the statistical processing, Danube: Bratislava

T	P	m^3s^{-1}									Uncert. interval	
years	%	Gen. Extreme Value	Log normal (3P)	Inv. Gaussian (3P)	Fatigue Life (3P)	Pearson 5	Pearson 6	Pearson 5 (3P)	Pearson 6 (4P)	Log Pearson type III	m^3s^{-1}	m^3s^{-1}
1000	0.1	14242	14229	13825	13781	14816	14734	14587	14590	14139	13781	14816
200	0.5	12156	12098	11925	11905	12368	12322	12241	12243	12021	11905	12368
100	1	11251	11194	11091	11079	11367	11334	11276	11277	11129	11079	11367
50	2	10339	10293	10242	10237	10391	10368	10329	10330	10241	10237	10391
33	3	9800	9763	9737	9734	9827	9810	9780	9781	9721	9721	9827
20	5	9116	9091	9086	9085	9120	9109	9090	9091	9060	9060	9120
10	10	8168	8158	8169	8171	8156	8152	8145	8146	8144	8144	8171
5	20	7175	7176	7190	7193	7160	7161	7162	7163	7178	7160	7193
4	25	6839	6841	6853	6855	6824	6826	6829	6830	6847	6824	6855
3.33	30	6554	6556	6566	6568	6540	6542	6546	6547	6566	6540	6568
2.50	40	6076	6077	6083	6084	6065	6068	6074	6074	6092	6065	6092
2.00	50	5670	5669	5670	5670	5661	5664	5670	5671	5685	5661	5685
1.67	60	5298	5296	5293	5292	5292	5296	5301	5302	5311	5292	5311
1.43	70	4933	4931	4925	4924	4933	4936	4939	4941	4944	4924	4944
1.28	78	4627	4627	4619	4618	4632	4634	4636	4637	4635	4618	4637
1.25	80	4545	4546	4538	4537	4553	4554	4556	4556	4553	4537	4556
1.11	90	4065	4077	4072	4070	4087	4087	4084	4085	4070	4065	4087
1.05	95	3712	3741	3740	3740	3750	3748	3742	3743	3720	3712	3750
1.03	97	3501	3545	3418	3548	3552	3548	3539	3540	3512	3418	3552
1.01	99	3135	3215	3229	3232	3213	3207	3193	3194	3157	3135	3232
1.001	99.9	2589	2756	2793	2801	2728	2717	2694	2695	2648	2589	2801

Table 6.1b Results of the statistical processing, Danube: Turnu-Măgurele

T	P%	m^3s^{-1}									Uncert. interval	
years	m^3s^{-1}	Log-Gamma	Fatigue Life	Log normal (3P)	Pearson 6	Pearson 5	Gen. Extreme Value	Gamma	Gen Gamma	Pearson 5 (3P)	m^3s^{-1}	m^3s^{-1}
1000	0.1	19117	18715	18808	19626	19884	17632	18041	18006	18118	17632	19884
200	0.5	17364	17111	17152	17632	17798	16889	16682	16653	16707	16589	17798
100	1	16577	16377	16403	16788	16888	16042	16047	16022	16088	16022	16888
33	3	15263	15138	15144	15330	15410	15022	14982	14933	14942	14933	15410
20	5	14613	14516	14818	14636	14696	14472	14393	14376	14378	14376	14696
10	10	13670	13606	13603	13648	13679	13626	13588	13546	13541	13541	13679
5	20	12613	12576	12572	12666	12568	12625	12591	12583	12577	12666	12625
4	25	12235	12204	12202	12171	12177	12256	12236	12229	12224	12171	12256
3.33	30	11906	11880	11878	11839	11840	11931	11922	11917	11913	11839	11931
2.50	40	11338	11318	11315	11267	11261	11361	11370	11368	11366	11261	11370
2.00	50	10828	10811	10813	10764	10754	10848	10870	10869	10871	10754	10871
1.67	60	10346	10330	10333	10290	10277	10354	10384	10386	10390	10277	10390
1.43	70	9855	9838	9844	9812	9798	9848	9881	9884	9892	9798	9892
1.28	78	9594	9577	9582	9589	9545	9578	9609	9614	9623	9545	9623
1.25	80	9311	9294	9300	9287	9273	9284	9313	9319	9329	9273	9329
1.11	90	8611	8590	8595	8618	8607	8547	8563	8571	8582	8547	8618
1.05	95	8075	808l	8054	8111	8104	7977	7978	7988	7993	7978	8111
1.03	97	7746	7721	7720	7802	7799	7623	7608	7620	7624	7608	7802
1.01	99	7163	7137	7128	7259	7263	6987	6948	6961	6983	6948	7263
1.001	99.9	6272	6245	6217	6438	6455	5984	5911	5926	5879	5879	6455

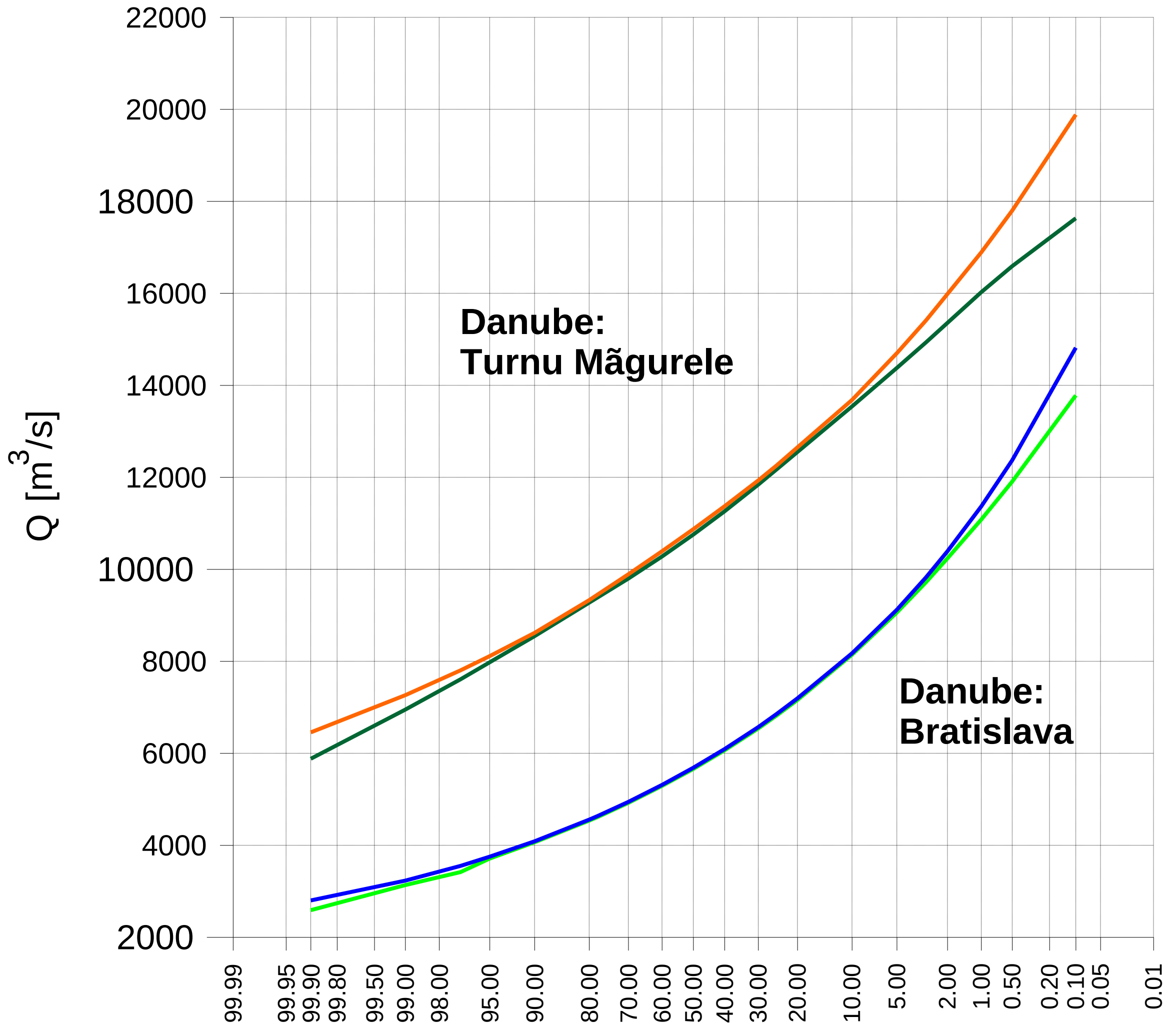

Fig. 6.3 *Uncertainty interval of the discharge maxima at the Bratislava and Turnu Măgurele gauge stations.*

The epistemic uncertainty was proved by analysing 50–60 statistical distributions and selecting the first nine to fit the registered discharges according to Kolmogorov-Smirnov statistical test. The uncertainty interval for 1% probability of exceedance at Turnu Măgurele is in the range (16,022–16,888) m^3s^{-1}. The maximum discharge registered at Turnu Măgurele on 23-24 of April 2006 was 16,300 m^3s^{-1}, being the highest registered value since 1898. The maximum discharge of this flood corresponded to 1% probability of exceedance. As depicted in Fig. 6.3, the maximum discharge in 2006 is located in the central part of the interval of uncertainty for a 1% flood. The results show that the maximum discharges corresponding to a given probability of exceedance are not unique values, as is the current practice, but they belong to an interval of uncertainty. This interval can be determined by using a single suitable distribution or by analyzing more statistical distributions, in the latter case the selection being based on Kolmogorov-Smirnov, Anderson-Darling or Chi-Squared tests. The interval of uncertainty should be considered when defining the design flood.

6.1.3 Processing the flood volumes

The flood volume is obtained based on a POT (Peak Over Threshold) approach. The number of selected floods should be equal with the number n of years of the discharge series. Consequently, a threshold discharge Q_{thr1} is arbitrarily chosen for this purpose, and the floods whit discharge overpassing this threshold are selected. For these floods a second threshold $Q_{thr2} = a\, Q_{thr1}$, where $a < 0.9$ is chosen to derive distinct floods. The flood duration $T = t_k - t_1$ corresponds to all discharges $Q(t_i)_{t_i \epsilon (t_1, t_k)} > Q_{thr2}$. The volume over the threshold Q_{thr2} is added to the volume under the threshold for the same duration T in order to obtain the flood volume (Drobot and Draghia, 2012).
The n flood volumes are statistically processed in the same way as in the case of maximum discharges, obtaining the uncertainty interval for volume.

6.1.4 Uncertainty intervals for the maximum discharge and floods volume on the Middle and Lower Danube

Following the statistical processing of the maximum discharges and floods volume two intervals of uncertainty have to be considered (Danube Floodrisk, 2012):

- An uncertainty interval for maximum discharges $Q_{P\%}^{max} \epsilon\, (Q_{P\%}^{lower};\ Q_{P\%}^{upper})$;
- An uncertainty interval for flood volume $V_{P\%}\, \epsilon\, (V_{P\%}^{lower};\ V_{P\%}^{upper})$.

Middle Danube

P%	01. Batina			
	Q lower	Q upper	V lower	V upper
0.1%	10045	11416	35083	43360
1%	8207	8585	24507	26097
3%	7332	7544	19962	20199
10%	6239	6400	14885	15267

P%	02. Aljmaš			
	Q lower	Q upper	V lower	V upper
0.1%	9149	10072	59866	73061
1%	8112	8543	50959	55585
3%	7544	7804	42439	46191
10%	6821	6901	32466	35024

P%	03. Bogajevo			
	Q lower	Q upper	V lower	V upper
0.1%	10688	12045	76893	93757
1%	8991	9243	48097	52928
3%	8023	8210	36694	39086
10%	6896	7074	25625	26807

P%	04. Dalj			
	Q lower	Q upper	V lower	V upper
0.1%	8676	9712	71466	90125
1%	7962	8335	46744	51918
3%	7429	7622	36055	38043
10%	6665	6784	25096	26203

P%	05. Vukovar			
	Q lower	Q upper	V lower	V upper
0.1%	9409	11088	67173	86583
1%	8198	8783	50277	60072
3%	7565	7888	41731	47163
10%	6741	6879	31706	33435

P%	06. Ilok			
	Q lower	Q upper	V lower	V upper
0.1%	9010	10003	79300	104444
1%	8148	8516	55016	62713
3%	7621	7808	43762	47253
10%	6811	6931	30997	32538

Lower Danube

Stretch 1

P%	1.1. Bazias			
	Q lower (m^3/s)	Q upper (m^3/s)	V lower (10^9 m^3)	V upper (10^9 m^3)
0.1%	18258	20231	170.0	199.6
0.5%	16604	17719	126.9	132.9
1%	15848	16635	106.7	114.1
3%	14571	14907	76.1	85.8
5%	13932	14133	64.0	73.4
10%	12973	13072	49.4	57.1

P%	1.2. Moldova Veche			
	Q lower (m^3/s)	Q upper (m^3/s)	V lower (10^9 m^3)	V upper (10^9 m^3)
0.1%	18253	20236	169.7	199.7
0.5%	16603	17724	132.1	138.7
1%	15849	16639	110.2	120.0
3%	14574	14911	78.6	90.9
5%	13935	14136	65.8	77.7
10%	12976	13077	50.2	61.1

P%	1.3. Drencova			
	Q lower (m^3/s)	Q upper (m^3/s)	V lower (10^9 m^3)	V upper (10^9 m^3)
0.1%	18455	20253	174.8	203.3
0.5%	16726	17744	133.8	152.1
1%	15943	16661	116.4	130.5
3%	14630	14935	89.0	96.9
5%	13978	14156	76.3	81.8
10%	13003	13101	59.1	61.8

P%	1.4. Svinita			
	Q lower (m^3/s)	Q upper (m^3/s)	V lower (10^9 m^3)	V upper (10^9 m^3)
0.1%	18522	20341	175.6	202.0
0.5%	16746	17829	140.6	148.5
1%	15951	16745	120.4	126.5
3%	14629	15017	89.8	93.5
5%	13977	14241	76.3	79.0
10%	13033	13277	58.6	59.6

P%	1.5. Orsova			
	Q lower (m^3/s)	Q upper (m^3/s)	V lower (10^9 m^3)	V upper (10^9 m^3)
0.1%	18376	20374	179.4	206.5
0.5%	16636	17861	135.9	153.7
1%	15855	16776	117.5	131.4
3%	14554	15047	88.8	97.1
5%	13911	14263	75.7	83.0
10%	12978	13299	56.9	63.9

P%	1.6. Drobeta			
	Q lower (m^3/s)	Q upper (m^3/s)	V lower (10^9 m^3)	V upper (10^9 m^3)
0.1%	18437	20303	176.5	207.4
0.5%	16737	17817	137.9	150.4
1%	15968	16744	119.6	127.2
3%	14684	15034	89.4	94.4
5%	14042	14230	75.8	80.4
10%	13106	13216	57.5	61.5

P%	1.7. Tiganasi			
	Q lower (m^3/s)	Q upper (m^3/s)	V lower (10^9 m^3)	V upper (10^9 m^3)
0.1%	16879	18381	185.9	206.3
0.5%	15729	16560	143.9	155.4
1%	15130	15761	125.8	133.8
3%	14106	14468	97.1	100.3
5%	13587	13881	83.6	86.3
10%	12815	13026	64.9	67.3

P%	1.8. Gruia			
	Q lower (m^3/s)	Q upper (m^3/s)	V lower (10^9 m^3)	V upper (10^9 m^3)
0.1%	16715	18344	184.2	208.3
0.5%	15588	16517	150.9	157.1
1%	15014	15716	129.6	135.5
3%	14024	14408	95.1	101.9
5%	13478	13773	79.9	86.6
10%	12646	12865	60.5	66.5

Stretch 2

P%	2.1. Calafat			
	Q lower (m^3/s)	Q upper (m^3/s)	V lower (10^9 m^3)	V upper (10^9 m^3)
0.1%	16734	17946	190.3	206.7
0.5%	15741	16365	144.2	145.6
1%	15173	15652	121.6	126.6
3%	14187	14461	89.9	96.9
5%	13680	13869	76.8	83.2
10%	12915	13009	60.3	65.0

P%	2.2. Bechet			
	Q lower (m^3/s)	Q upper (m^3/s)	V lower (10^9 m^3)	V upper (10^9 m^3)
0.1%	17108	19205	190.3	210.0
0.5%	16195	17366	147.3	149.6
1%	15709	16543	127.1	128.8
3%	14781	15174	95.2	99.3
5%	14235	14499	81.6	85.6
10%	13346	13521	64.2	66.9

P%	2.3. Corabia			
	Q lower (m^3/s)	Q upper (m^3/s)	V lower (10^9 m^3)	V upper (10^9 m^3)
0.1%	17017	19203	183.3	213.8
0.5%	16442	17360	147.5	168.3
1%	15921	16534	131.7	148.1
3%	14779	15228	106.0	115.4
5%	14197	14703	93.7	99.9
10%	13329	13811	76.5	78.7

P%	2.4. Turnu Magurele			
	Q lower (m^3/s)	Q upper (m^3/s)	V lower (10^9 m^3)	V upper (10^9 m^3)
0.1%	17632	19884	191.5	220.5
0.5%	16589	17798	158.4	175.5
1%	16022	16888	140.9	155.8
3%	14933	15410	112.3	124.1
5%	14376	14696	98.3	109.1
10%	13541	13679	78.9	88.2

P%	2.5. Zimnicea			
	Q lower (m^3/s)	Q upper (m^3/s)	V lower (10^9 m^3)	V upper (10^9 m^3)
0.1%	18205	19504	191.2	219.8
0.5%	16940	17704	161.9	173.3
1%	16260	16896	143.9	152.8
3%	15097	15549	114.7	121.6
5%	14502	14882	100.8	106.1
10%	13624	13915	80.8	83.6

P%	2.6. Giurgiu			
	Q lower (m^3/s)	Q upper (m^3/s)	V lower (10^9 m^3)	V upper (10^9 m^3)
0.1%	18442	20107	193.2	220.0
0.5%	17120	17951	155.9	175.0
1%	16456	17014	139.4	154.8
3%	15223	15493	112.5	121.6
5%	14584	14759	99.6	105.7
10%	13646	13716	81.4	83.7

P%	2.7. Oltenita			
	Q lower (m^3/s)	Q upper (m^3/s)	V lower (10^9 m^3)	V upper (10^9 m^3)
0.1%	18495	20369	192.2	223.5
0.5%	17208	18168	168.4	175.4
1%	16556	17212	149.2	154.5
3%	15335	15662	115.5	125.5
5%	14665	14915	99.8	109.8
10%	13693	13854	78.5	86.5

P%	2.8. Br. Borcea Calarasi - Chiciu			
	Q lower (m^3/s)	Q upper (m^3/s)	V lower (10^9 m^3)	V upper (10^9 m^3)
0.1%	18533	20227	195.3	221.1
0.5%	17179	18046	163.6	175.4
1%	16502	17098	146.2	158.5
3%	15174	15562	117.8	129.9
5%	14511	14821	104.2	113.8
10%	13550	13768	85.1	89.7

Stretch 3

P%	3.1. Cernavoda			
	Q lower (m^3/s)	Q upper (m^3/s)	V lower (10^9 m^3)	V upper (10^9 m^3)
0.1%	7962	8685	93.4	112.6
0.5%	7385	7784	74.4	84.7
1%	7084	7382	66.0	73.9
3%	6550	6714	52.4	57.1
5%	6273	6385	45.7	49.2
10%	5859	5911	36.2	38.6

P%	3.2. Harsova			
	Q lower (m^3/s)	Q upper (m^3/s)	V lower (10^9 m^3)	V upper (10^9 m^3)
0.1%	7542	8355	83.1	107.0
0.5%	6999	7461	71.8	81.0
1%	6706	7065	64.1	70.4
3%	6196	6413	51.8	55.8
5%	5937	6094	45.9	49.2
10%	5551	5636	37.6	39.7

P%	3.3. Vadu oii			
	Q lower (m^3/s)	Q upper (m^3/s)	V lower (10^9 m^3)	V upper (10^9 m^3)
0.1%	18490	20547	204.1	228.0
0.5%	16927	18085	173.1	178.1
1%	16213	17021	154.3	161.2
3%	14979	15327	123.2	130.8
5%	14360	14530	107.6	114.5
10%	13430	13517	86.6	90.8

P%	3.4. Braila			
	Q lower (m^3/s)	Q upper (m^3/s)	V lower (10^9 m^3)	V upper (10^9 m^3)
0.1%	17944	20281	196.1	229.9
0.5%	16394	17340	182.3	184.2
1%	15691	16344	164.1	172.1
3%	14510	14902	131.4	147.4
5%	13804	14206	115.8	131.2
10%	12838	13256	93.9	104.2

Stretch 4

P%	4.1. Grindu			
	Q lower (m^3/s)	Q upper (m^3/s)	V lower (10^9 m^3)	V upper (10^9 m^3)
0.1%	18369	20485	187.1	236.7
0.5%	16836	17561	180.9	189.3
1%	16139	16429	168.5	175.3
3%	14765	15052	134.8	158.0
5%	14035	14408	118.7	144.0
10%	13069	13522	96.3	116.0

P%	4.2. Isacea			
	Q lower (m^3/s)	Q upper (m^3/s)	V lower (10^9 m^3)	V upper (10^9 m^3)
0.1%	18841	20185	189.4	237.6
0.5%	17304	18102	183.9	190.9
1%	16597	17193	170.4	178.6
3%	15383	15712	136.9	161.1
5%	14736	14995	120.9	146.3
10%	13796	13976	98.6	116.1

P%	4.3. Ceatal Izmail			
	Q lower (m^3/s)	Q upper (m^3/s)	V lower (10^9 m^3)	V upper (10^9 m^3)
0.1%	18608	20895	193.3	239.4
0.5%	17216	18376	183.9	190.9
1%	16497	17289	170.4	178.6
3%	15230	15556	136.9	161.1
5%	14595	14849	120.9	146.3
10%	13617	13875	85.4	90.8

6.1.5 Uncertainty intervals for the maximum discharge and flood volume on the tributaries

Statistical processing was carried out for the Romanian tributaries of the lower Danube: Jiu (Podari), Olt (Stoienești), Argeș (Budești), Ialomița (Țăndărei), Siret (Lungoci) and Prut (Oancea). The uncertainty intervals for the maximum discharges and the flood volumes are presented in the following tables (Danube Floodrisk Project, 2009-2012).

P%	1. Jiu – Podari gauge station			
	Q lower (m^3/s)	Q upper (m^3/s)	V lower (10^6 m^3)	V upper (10^6 m^3)
0.1%	1545	1801	428	602
0.5%	1384	1564	376	464
1%	1306	1451	352	412
3%	1167	1258	311	336
5%	1093	1159	289	303
10%	980	1015	257	260

P%	2. Olt – Stoienești gauge station			
	Q lower (m^3/s)	Q upper (m^3/s)	V lower (10^6 m^3)	V upper (10^6 m^3)
0.1%	4437	5294	3950	4934
0.5%	3469	3885	2914	3271
1%	3061	3344	2488	2681
3%	2425	2561	1833	1883
5%	2134	2231	1531	1572
10%	1744	1801	1161	1196

P%	3. Arges – Budești gauge station			
	Q lower (m^3/s)	Q upper (m^3/s)	V lower (10^6 m^3)	V upper (10^6 m^3)
0.1%	1549	1736	702	888
0.5%	1161	1243	540	635
1%	997	1048	470	532
3%	742	761	360	381
5%	626	637	309	316
10%	474	480	234	240

P%	4. Ialomița – Țăndărei gauge station			
	Q lower (m^3/s)	Q upper (m^3/s)	V lower (10^6 m^3)	V upper (10^6 m^3)
0.1%	665	823	863	1063
0.5%	582	690	540	585
1%	543	629	436	459
3%	474	526	292	308
5%	438	475	241	254
10%	384	402	184	192

P%	5. Siret – Lungoci gauge station			
	Q lower (m^3/s)	Q upper (m^3/s)	V lower (10^6 m^3)	V upper (10^6 m^3)
0.1%	5937	7449	2245	2608
0.5%	4846	5481	1879	2070
1%	4363	4734	1712	1840
3%	3578	3667	1430	1477
5%	3194	3255	1290	1317
10%	2597	2685	1078	1094

P%	6. Prut – Oancea gauge station			
	Q lower (m^3/s)	Q upper (m^3/s)	V lower (10^6 m^3)	V upper (10^6 m^3)
0.1%	1596	1701	2234	2428
0.5%	1246	1311	1882	1982
1%	1096	1144	1725	1801
3%	856	881	1464	1523
5%	745	760	1337	1386
10%	595	596	1154	1189

6.2 Estimation of the *T*-year design flows with the inclusion of historical floods based on log Pearson III distribution

Stănescu et al (2001, 2004) summarized the regionalisation of distribution functions estimated for annual peak discharges in the Danube basin. The aim of their project coordinated by Rumanian hydrologists, executed within the scope of the hydrological cooperation of the 13 Countries of the Danube Catchment, IHP/UNESCO, was to produce regional empirical relationships from sufficiently long and reliable series of annual peak discharges available for 176 water gauging stations of the Danube Catchment. The aim was to facilitate the estimation of the quantile of annual peak discharge and related specific flood discharge in the ungauged river sections of that catchment.

Here we present another possible approach to determine the values of design values of the *T*-year floods with very long return period in river basins with short series of observations. This approach is based on the determination of the historical skew coefficient G_h of the LP3 distribution calculated using historical floods.

It is known that the extrapolation of data is very sensitive not only to the length of the data series, but also to the inclusion of the historic extremes to data series. The correctly estimate the potential flood magnitude requires to include the longest data series of observations and historic pre-instrumental data (Merz and Blöschl 2008a; Merz and Blöschl 2008b; Elleder 2010; Gaal et al. 2010; Elleder et al. 2013; Kjeldsen et al., 2014). Brazdil et al. (2006) studied historic hydrological materials in order to estimate flood threat in Europe. Estimation of the uncertainty at the design discharges was investigated for example by Merz and Thieken (2009) or Rogger et al. (2012).

The long-term maximum annual discharges from more than 20 water gauging stations along the Danube River and 62 series from Danube tributaries were analysed and used to estimate discharges with different return period. We present a concrete example of the use of flood marks and historical descriptions of the water level during extreme historical floods to estimate *T*-year floods with a long return period.

6.2.1 Methods

We used log Pearson Type III distribution (LP3) to estimate Q_{max} discharge series distribution function. The LP3 distribution is used to estimate the extremes in many natural processes and is the most common frequency distribution used especially in hydrology. Pilon and Adamowski (1993) developed the Log Likelihood function of LP3 and estimated its parameters. Cheng et al. (2007) presented a frequency factor based method in hydrological frequency analysis for random generation of five distributions (normal, lognormal, extreme value type 1, Pearson Type III and log-Pearson Type III). Griffis and Stendinger (2007 and 2009) used LP3 distribution in flood frequency analysis.

Using one type of distribution also allows estimating the value of the *T*-year maximum discharges in ungauged sections of the river, only on the basis of long-term average of maximum annual discharge and distribution parameters obtained from the neighbouring gauging stations.

To estimate the distribution parameters, the method described in Bulletin17B was used. Bulletin 17B was issued in USA in 1981, and re-issued with minor corrections in 1982 by the Center for Research in Water Resources of the University of Texas at Austin (IACWD, 1982). Bulletin 17B provided revised procedures for weighting station skew values with results from a generalized skew study, detecting and treating outliers, making two station comparisons, and computing confidence limits about a frequency curve. Bulletin 17B is based on Bulletins 15, 17, 17A (http://acwi.gov/hydrology/ Frequency/minutes/index.html). Design flood estimation procedures in the United States have traditionally focused on two primary methods: frequency analysis of peak flows for floodplain management and levee design; and deterministic – Probable Maximum Flood estimates – for design of dams and nuclear facilities.

6.2.1.1 Log Pearson Type III distribution

The log-Pearson Type III distribution is a three-parameter Gamma distribution with a logarithmic transform of the variable. This distribution is widely used for flood analyses because the data often easily fit the assumed annual maximum discharge series. The probability density function of the Pearson Type III distribution is of the form:

$$f(x|\tau,\alpha,\beta) = \frac{\left(\frac{x-\tau}{\beta}\right)^{\alpha-1} exp\left(-\frac{x-\tau}{\beta}\right)}{|\beta|\Gamma(\alpha)} \qquad (6.1)$$

with $\frac{x-\tau}{\beta} \geq 0$, where τ, α, β are parameters:

τ – is the location parameter;
α – is the shape parameter;
β – is the scale parameter;

and $\Gamma(\alpha)$ is the Gamma function given by:

$$\Gamma(\alpha) = \int_0^\infty t^{\alpha-1} exp(-t)dt. \qquad (6.2)$$

The Pearson type III distribution is sometimes called three-parameter Gamma distribution, since it can be obtained from the two-parameter Gamma distribution by introducing the location parameter τ. It is very flexible since it has three parameters which can produce a wide variety of shapes of density function.
A random variable X follows log-Pearson type III distribution if random variable $Y = lnX$ or $Y = logX$ follows the Pearson type III distribution.

Q_{max} series conditions
The basic assumptions in frequency analysis of maximum annual discharge are:

1. Maximum annual discharges must be independent and stochastic;
2. Processes influencing the runoff process are stationary with respect to time (homogeneity of the series);
3. Statistical characteristics of the measured data series (series of maximum annual discharge) represent the past, presence and future.

$$logQ = \bar{X} + KS \qquad (6.3)$$

where:

$\bar{X}$ is the mean,
S is the standard deviation, and
K is a factor of the skew coefficient at selected exceedance probability.

The formulas for these parameters are provided below.

Mean $$\bar{X} = \frac{1}{n}\sum_{i=1}^{n} X_i. \qquad (6.4)$$

Standard Deviation $$S = \sqrt{\frac{1}{n-1}\sum_{i=1}^{n}(X_i - \bar{X})^2}. \qquad (6.5)$$

Skew Coefficient $$G = \frac{n}{(n-1)(n-2)S^3}\sum_{i=1}^{n}(X_i - \bar{X})^3. \qquad (6.6)$$

Probability estimates are calculated for chosen plotting positions. A basic plotting position formula for symmetrical distributions is given by (Stedinger et al., 1993)

$$p_i = \frac{i-a}{n+1-2a}, \tag{6.7}$$

where p_i is the exceedance probability of flood observations Q_i ranked from largest (i = 1) to smallest (i = n), and a is a plotting position parameter, $(0 \leq a \leq 0.5)$.

6.2.1.2 Parameter Estimation: Simple Case

The method of moments uses the logarithms of flood flows to estimate the distribution parameters. The first three sample moments are used to estimate the LP3 parameters. These include the mean ($\hat{\mu}$), standard deviation ($\hat{\sigma}$), and skewness coefficient ($\hat{\gamma}$).

Moments and Parameters

If only systematic data are available, with no historical information, the mean, standard deviation and skewness coefficient of station data may be computed using the following equations:

$$\hat{\mu} = \frac{1}{n}\sum_{i=1}^{n} X_i \tag{6.8}$$

$$\hat{\sigma} = \sqrt{\frac{1}{n-1}\sum_{i=1}^{n}(X_i - \hat{\mu})^2} \tag{6.9}$$

$$\hat{\gamma} = \frac{n}{(n-1)(n-2)\hat{\sigma}^3}\sum_{i=1}^{n}(X_i - \hat{\mu})^3. \tag{6.10}$$

where n is the number of flood observations and (ˆ) represents a sample estimate. The sample standard deviation and skewness coefficient include bias correction factors (n-1) and (n-1)(n-2) for small samples, respectively.

6.2.1.3 Historical floods

Historical flood peaks reflect the frequency of large floods and thus should be incorporated into flood frequency analysis. They can also be used to judge the adequacy of estimated flood frequency relationships. For this latter purpose, appropriate plotting positions or estimates of the average exceedance probabilities associated with the historical peaks and the remainder of the data are desired. Hirsch and Stedinger (1987) and Hirsch (1987) provide an algorithm for assigning plotting positions to censored data such as historical floods.

6.2.1.4 Weighted Skew Coefficient

There is relatively large uncertainty in the sample skewness coefficient (third moment) because it is sensitive to extreme events in modest length records (Griffis and Stedinger, 2007). The station skew coefficient and regional skew coefficient can be combined to form a better estimate of skew for a given watershed. Under the assumption that the regional skew coefficient is unbiased and independent of the station skew, the mean-square errors (MSEs) of the station skew and the regional skew can be used to estimate a **weighted skew coefficient**.

If the regional and station skews differ by more than 0.5, a careful examination of the data and the flood-producing characteristics of the watershed should be made. Possibly greater weight may be given to the station skew, depending on the length of record, the largest floods within the gauging record and watershed, and watershed characteristics. Large deviations between the regional skew and station skew may indicate that the flood frequency characteristics of the watershed of interest are different from those used to develop the regional skew estimate. It is thought that station skew is a function of rainfall skew, channel storage, and basin storage. There is considerable variability of response among different basins with similar observable characteristics, in addition to the random sampling variability in estimating skew from a short record. It is considered reasonable to give greater weight to the station skew, after due consideration of the data and flood-producing characteristics of the basin.

Uniform technique for determining flood discharge frequencies

We added the historic floods to the measured series of Q_{max}, and recalculated the parameters of the distribution curves for individual stations having included the historic floods.

6.2.2 Regionalization of the skew coefficients of the LP3 probability curves in Danube basin

6.2.2.1 Estimation of the skew coefficients G_h for the stations along the Danube River

The landscape geomorphology of the Danube River Basin is characterised by a diversity of morphological patterns. Fig. 6.6 shows examples of the maximum annual discharge series Q_{max} in the upper (Hofkirchen gauge), in the middle (Bratislava and Nagymaros gauges) and lower Danube (Orsova/Turnu Severin gauge, and Reni gauge) from 95 to 170 years.

It is interesting that at the Bratislava station similar maximum discharges observed over the last 20 years did occur also at the end of the 19th century. The other situation is at Nagymaros station. While the peak discharges did not exceed 8000 m^3s^{-1} during the floods of 1895–1900, the floods after 2000 peak above 8700 m^3s^{-1}, in 2013 the maximum discharge reached 9505 m^3s^{-1}. During the floods of 1893, 1897, 1899, 1954 and 1965, the Danube dams in the Vienna - Nagymaros river section breached. No damage to dams within this section of the river was observed during the recent years that would negatively affect the transformation/reduction of flood waves. This section of the Danube is an example of how the construction of dams on the upper river reaches has an impact on the increase of peak flood waves at lower stations.

Very high floods occurred on the lower Danube in 2006 (peak discharge 14 900 m^3s^{-1} at Reni), and 2010 (peak discharge 15400 m^3s^{-1} at Reni).

To estimate regional skew coefficient of the LP3 distribution for Danube River we use 20 Q_{max} observations from water gauges along the Danube River from Germany to Ukraine (Fig. 6.7). Basic statistical characteristics of the stations are presented in Table 6.2.

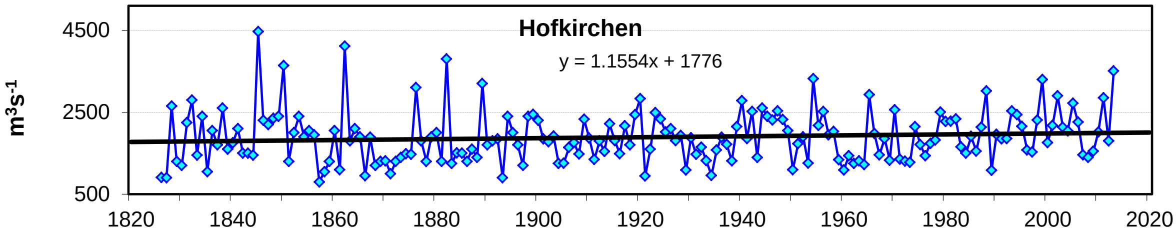

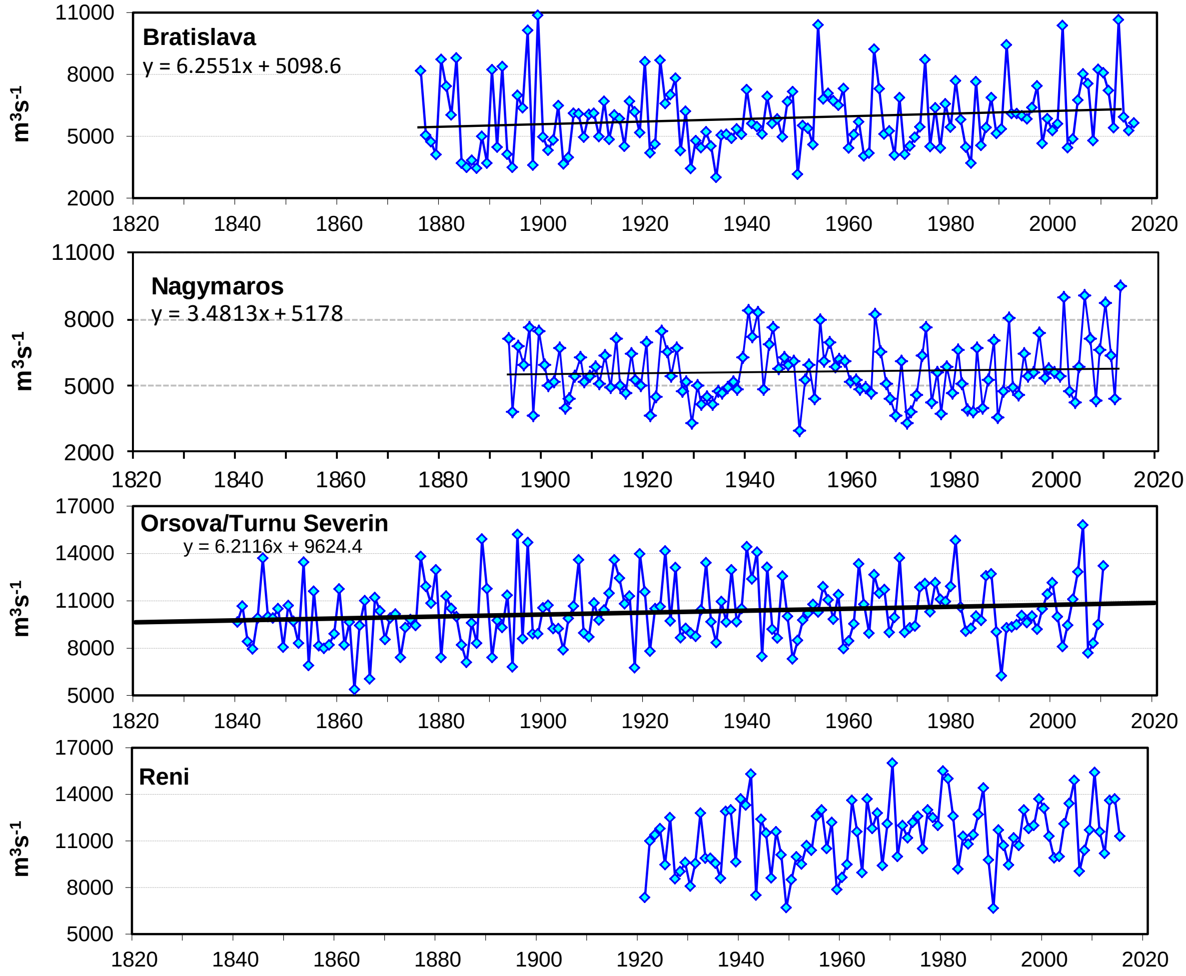

Fig. 6.6 Maximum annual discharges series at selected stations along the Danube River.

The design values for 20 gauge station along the Danube River were calculated. The Frequency curve spreadsheet version 3.06 was used to estimate the parameters of distribution functions and to calculate the design values with inclusion of the historical floods into calculation. As the first step we estimated the LP3 distribution function parameters (mean Q, standard deviation S, and station skewness coefficient G) for each of the stations separately and computed Q_{max} design values. In the case of gauges with historic floods, we added historic floods into the measured Q_{max} series (see Fig. 6.8), and recalculated the parameters of the distribution curves for individual stations. The inclusion of the historic floods in the calculations has increased the skew coefficient G_h on average by 0.2. Other stations along the Danube River and its tributaries are presented in APPENDIX VI.

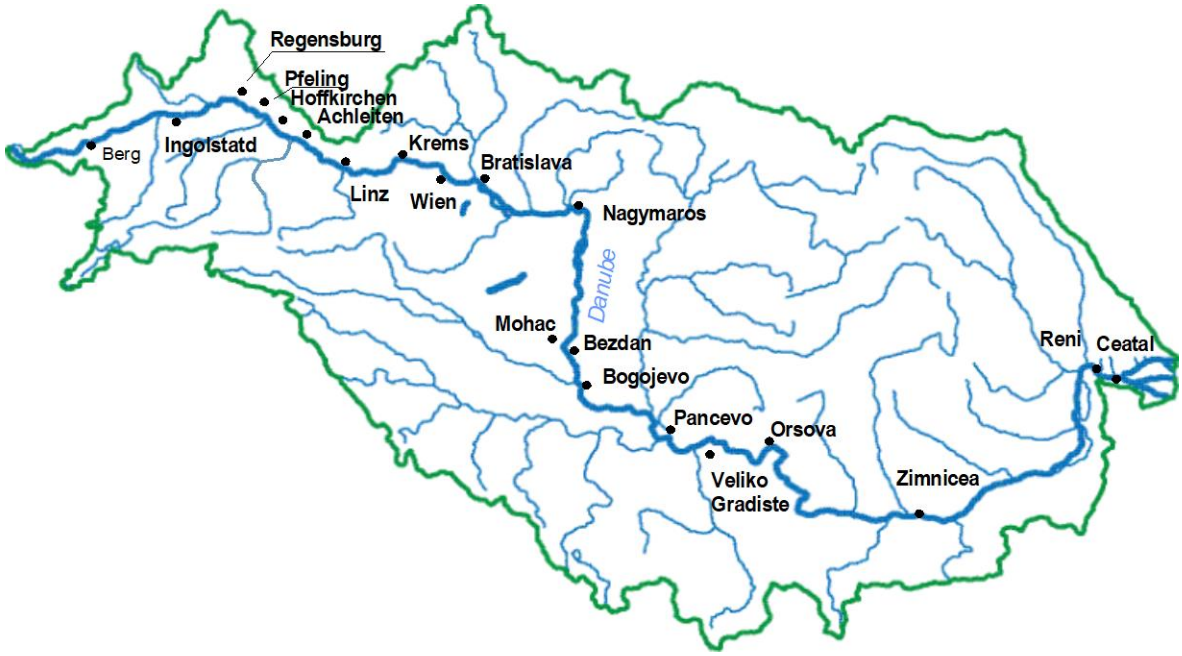

Fig. 6.7 Scheme of the Danube River basin and water gauging stations along the Danube River.

Table 6.2 List of the gauging stations along the Danube River, basic characteristics and *Qamax* – long-term average of the maximum annual discharge

No.	River kilometer	Gauge	Period	Country	Area [km^2]	Elevation [m a.s.l.]	Runoff [mm]	Q_{amax} [m^{3}s^{-1}]
1	2613	Berg	1930–2007	GE	4047	489.48	296	204
2	2458.3	Ingolstadt	1940–2007	GE	20001	359.97	494	1110
3	2376.1	Regensburg-Schwabelweis	1924–2007	GE	35399	324.06	396	1532
4	2300	Pfelling	1926–2007	GE	37757	307.73	392	1516
5	2256.9	Hofkirchen	1826–2013	GE	47496	299.17	425	1896
6	2150	Achleiten	1901–2007	GE	76653	287.27	587	4146
7	2135.2	Linz*	1821–2013	AT	79490	247.06	581	3670
8	2002.7	Stein-Krems (Kienstock)	1828–2006	AT	96045	193.32	621	5372
9	1934.1	Wien-Nussdorf	1828–2006	AT	101731	157.0	595	5301
10	1868.8	Devin/Bratislava	1876–2013	SK	131338	132.86	492	5884
11	1694.6	Nagymaros	1893–2007	HU	183534	99.37	401	5598
12	1446.8	Mohács	1930–2007	HU	209064	79.19	355	5063
13	1425.5	Bezdan	1940–2006	SR	210250	79.29	354	4974
14	1367.4	Bogojevo	1940–2006	SR	251593	76.11	363	5675
15	1153.3	Pancevo	1940–2006	SR	525009	65.98	320	10147
16	1060	Veliko Gradiste	1931–2007	SR	570375	60.83	307	10529
17	955	Orsova-Turnu Severin	1840–2006	RO	576232	44.76	307	10295
18	554	Zimnicea	1931–2010	RO	658400	16.06	287	11087
19	132	Reni	1921–2010	UKR	805700	0.2	257	11217
20	72	Ceatal Izmail	1931–2010	RO	807000		251	11173

River - Station:	**Danube - Bratislava**	mean log =	3.752833	
Country	SK	n =	138	years of record
Area [km^2]	131 338	S =	0.1205	standard deviation
Runoff [mm]	492	G =	0.1800	station skew
		Gw =	0.1800	weighted skew

log-Pearson type III distribution			Confidence limits	
T [years]	p [-]	Q_{max} [m^{3}s^{-1}]	Q(5)	Q(95)
10	0.1	8116	8591	7723
50	0.02	10273	11100	9622
100	0.01	11192	12192	10415
200	0.005	12119	13305	11207
500	0.002	13365	14818	12262
1000	0.001	14328	15999	13072

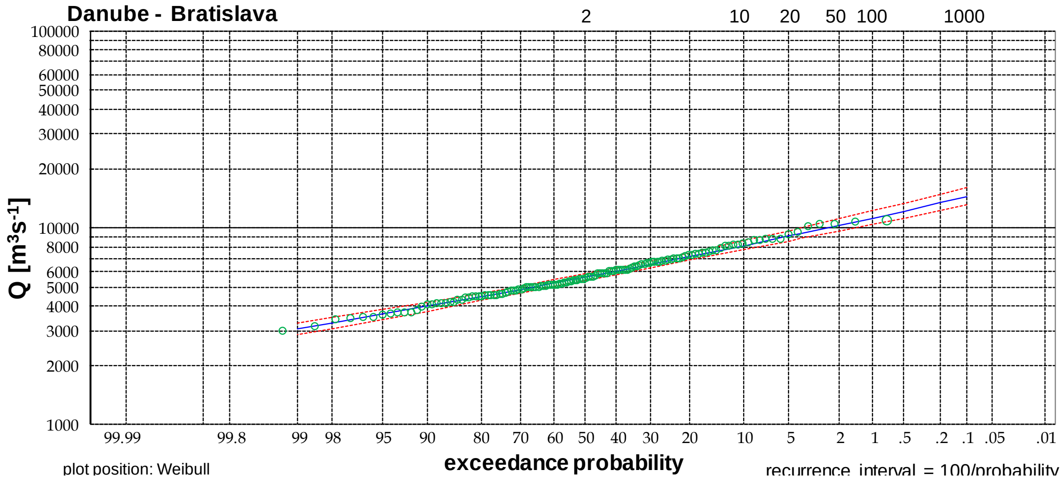

a)

River - Station:	**Danube - Bratislava**	mean log =	3.7542499	
Country	SK	n =	140	years of record
Area [km^2]	131 338	S =	0.1221	standard deviation
Runoff [mm]	492	G =	0.1800	station skew
		Gw =	0.2431	weighted skew

log-Pearson type III distribution			Confidence limits	
T [years]	p [-]	Q_{max} [m^{3}s^{-1}]	Q(5)	Q(95)
10	0.1	8194	8677	7794
50	0.02	10485	11343	9809
100	0.01	11477	12524	10665
200	0.005	12487	13739	11527
500	0.002	13860	15409	12687
1000	0.001	14931	16726	13585

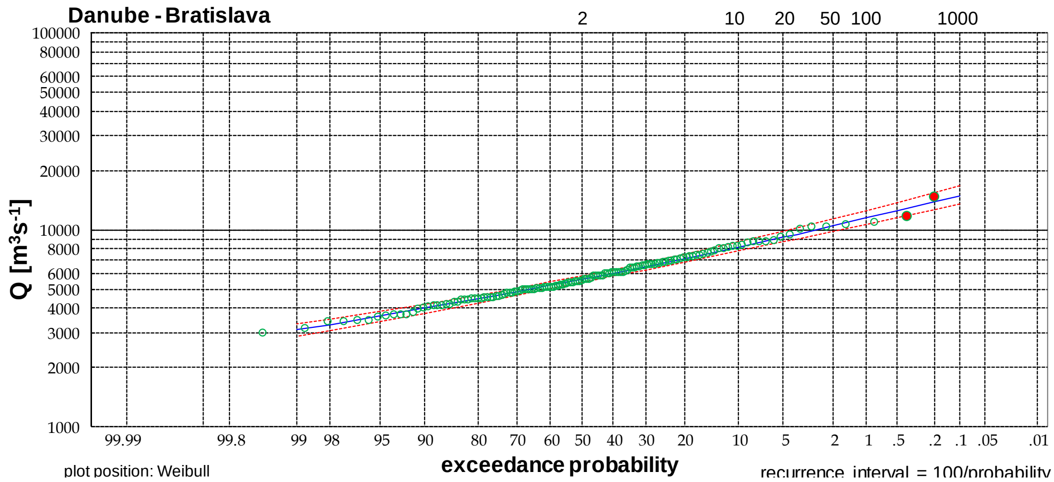

b)

Fig. 6.8 Example of the computations for the Danube at Bratislava/Devín station a) without historical data; b) with historical data. Distribution curve with confidence limits, design values.

Tables 6.3 Design values of selected *T*-year annual maximum discharges along the Danube River, without and with historical maxima, *G* – skew coefficient

Station/*T*-year	***G***	***10***	***50***	***100***	***200***	***500***	***1000***
Berg	-0.30	324	432	476	518	573	613
Ingolstadt	0.15	1526	2002	2222	2453	2779	3043
Regensburg-Schwabelweis	-0.46	2125	2530	2675	2809	2969	3081
Pfelling	-0.23	2144	2649	2846	3034	3273	3447
Hofkirchen	0.12	2765	3840	4353	4905	5701	6359
Achleiten	0.39	5512	7155	7925	8744	9913	10869
Linz	0.26	5455	7352	8205	9092	10323	11304
Stein-Krems (Kienstock)	0.39	7397	9605	10592	11613	13028	14154
Wien-Nussdorf	0.27	7187	9046	9847	10658	11756	12610
Devin/Bratislava	0.18	8116	10273	11192	12119	13365	14328
Nagymaros	-0.05	7325	8712	9257	9783	10457	10955
Mohács	-0.08	6548	7708	8157	8589	9138	9541
Bezdan	0.30	6452	7847	8437	9029	9823	10435
Bogojevo	0.19	7334	8810	9418	10020	10815	11418
Pancevo	0.15	12611	14661	15483	16285	17326	18105
Veliko Gradiste	0.02	13128	15167	15962	16728	17708	18430
Orsova-Turnu Severin	-0.19	12901	14754	15445	16094	16901	17481
Zimnicea	-0.09	13776	15769	16528	17248	18155	18815
Reni	-0.40	13918	15596	16183	16715	17352	17793
Ceatal Izmail	-0.21	13677	15492	16161	16785	17557	18108
With historical maxima							
Station/*T*-year	***G_h***	***10***	***50***	***100***	***200***	***500***	***1000***
Regensburg-Schwabelweis*	0.26	2298	3065	3407	3761	4249	4637
Pfelling*	0.2	2306	3089	3437	3795	4289	4680
Achleiten*	0.86	5776	7748	8701	9730	11226	12472
Linz*	0.6	5453	7717	8818	10014	11758	13218
Stein-Krems (Kienstock)*	0.59	7535	10096	11295	12569	14384	15869
Wien-Nussdorf*	0.58	7329	9623	10682	11798	13374	14652
Devin/Bratislava*	0.24	8194.4	10485	11477	12487	13860	14931
Nagymaros*	0.11	7431	9020	9671	10314	11159	11799
Reni*	-0.19	14102	16118	16869	17575	18452	19081
Ceatal Izmail*	0.02	13830	15973	16808	17612	18640	19397

**T*-year discharges were estimated both excluding extreme historical data as well as including historical data (eg. from years at 1501, 1682, and 1787 at Achleiten – Bratislava, and 1897 at Reni and Ceatal Izmail)

Several hydrological characteristics were analysed along the Danube River. Fig. 6.9a shows how Q_T design values change along the Danube. The coefficients $k=Q_T/Q_a$, (Q_a is long term mean discharge) are presented in Fig. 6.9b. The *1000*-year discharge is 16-times higher than the mean annual discharge at station Berg, while its is only 7-times higher at station Bratislava, and only 3-times higher at station Reni.

As shown in Fig. 6.10, both, the skew coefficients G and G_h , and long term runoff depth at the analysed stations have the similar course along the Danube. The following two best fitted relationships between the historical skew coefficient G_h and the runoff depth at the station were estimated (Fig. 6.11):

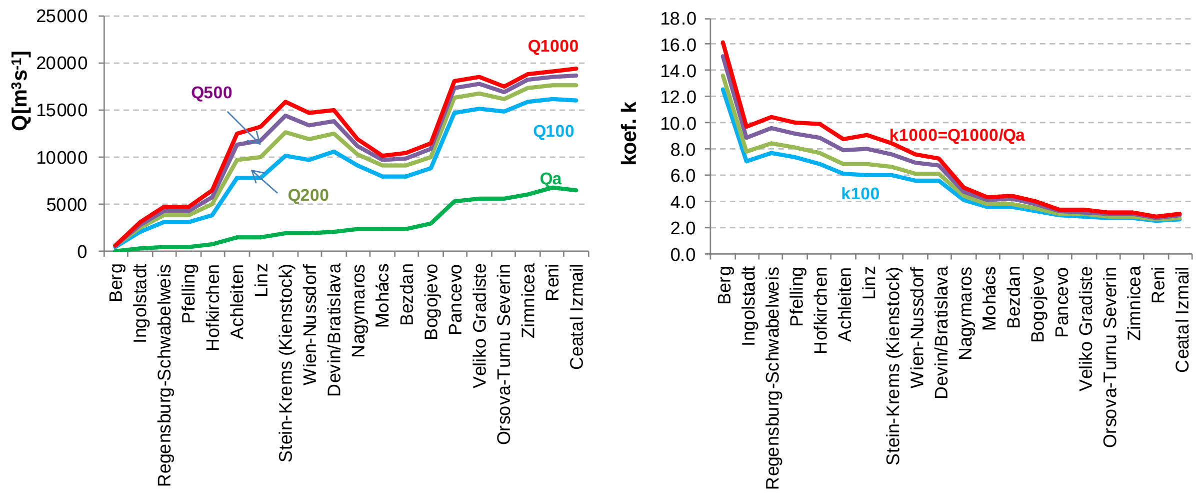

Fig. 6.9 T design discharges (left); coefficient k (right) at stations along the Danube River.

$G_h = 0.977*\ln(R) - 5.595$ (6.11)

$r^2 = 0.786$;

$G_h = 0.00234*R - 0.719$ (6.12)

$r^2 = 0.779$;

where: R – long-term average annual runoff depth in mm (from 240 mm to 640 mm).

We propose to use the regional skew G_r coefficient calculated according to the simple linear relationship (6.12) for estimations of the *T*-year discharges at gauges on the Danube River.

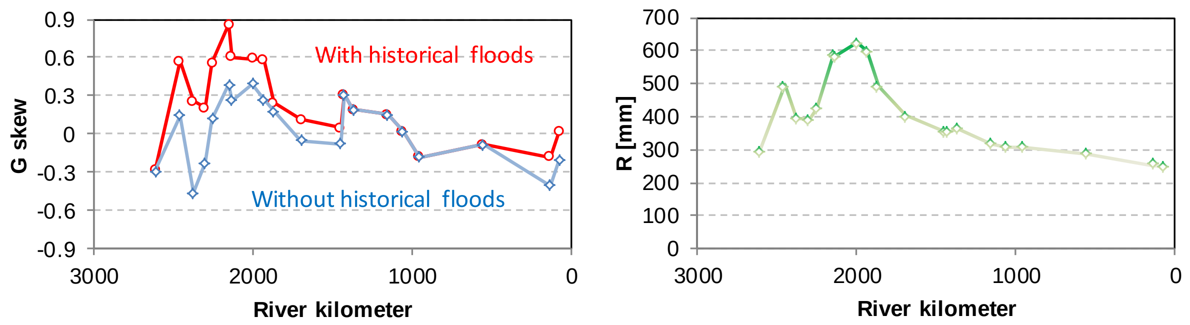

Fig. 6.10 Skew coefficients G with and without historical maxima (left), long term mean runoff R (right) along the Danube River.

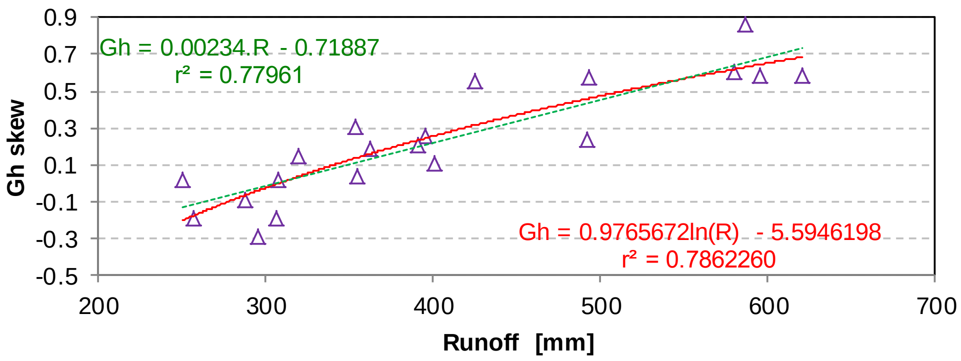

Fig. 6.11 Dependence of skew coefficient G_h on the runoff depth at Danube River gauges.

6.2.2.2 Estimation of the design discharge in small mountainous basins with short observations

Inclusion of historical floods and regionalization of the *G* skewness parameter of the LP3 distribution can change and raise the accuracy of design discharge. As an example we present some distribution functions for the Jalovecky creek, Slovakia, High Tatra Mountainous, with only 23-years of record. The design discharge, without and with the inclusion of historical floods, between 1813 and 1894 years is presented in Fig. 6.12.

We used the LP3 distribution of the annual peak flows for determining peak-flow frequency estimates in the region of the High Tatra mountains region for six gauges in small mountainous basins:

1. First, we estimated the distribution function parameters (mean Q_{max}, standard deviation *S*, and skewness *G*), for each of the stations separately (Table 6.4);
2. Then we included the historical floods into the observation series and calculated the skewness coefficient G_h, for each of the station;
3. Finally we estimated a generalized (regional) skewness coefficient G_r using dependence of the skew coefficient on altitude:

Table 6.4 Basic statistical characteristics, area, altitude of the selected gauging stations, station skew coefficient *G*

River	Area km^2	Elevation	Skew coef. *G*
Jalovecky creek: L. Ondrasova	45.00	566	0.45
Smrecianka: Ziarska valey	17.99	872	0.69
Koprovsky creek	31.24	989	1.00
Tichy creek	57.45	978	1.02
Dovalovec: Dovalovo	21.68	627	0.53
Bela: Podbanske	93.49	922	0.52

$$G_r = 0.001062 * \text{Alt} - 0.175 \quad (6.13)$$
$r^2 = 0.599$

where: Alt – altitude of the station (500<Alt<1000).

Including the historical flood records into the observation series and using of the regional skew coefficient increased the *1000*-year discharge estimate almost 4-times.

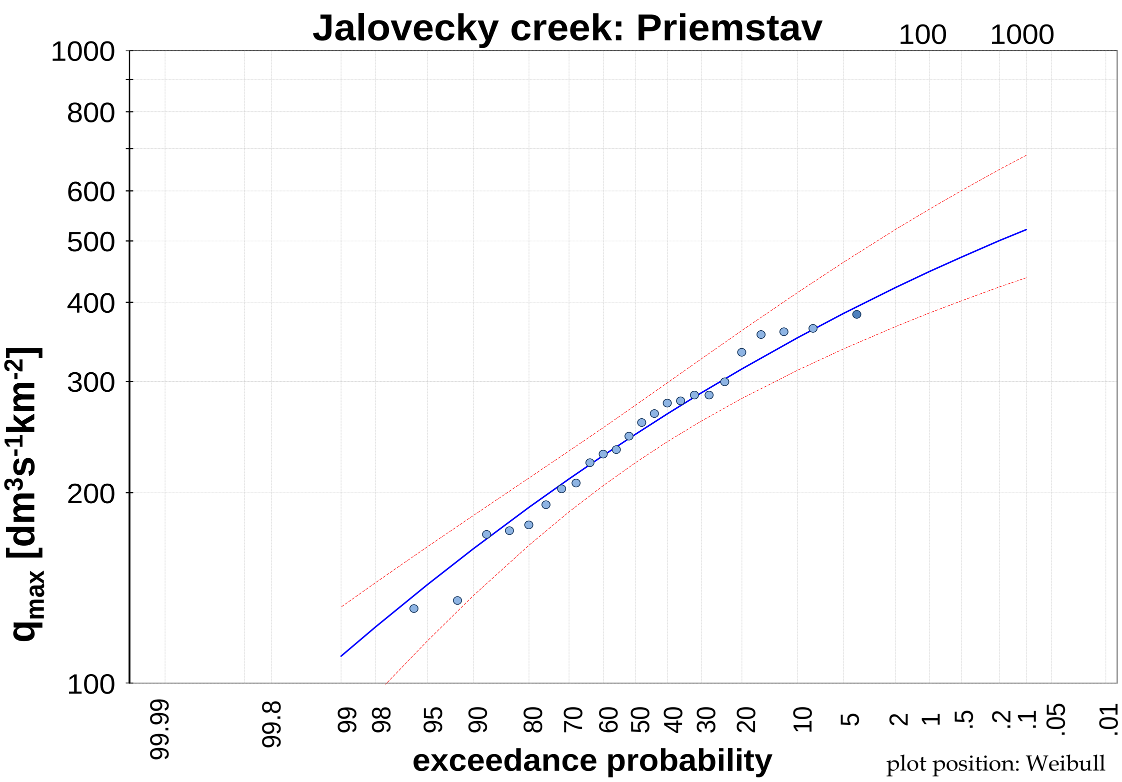

a)

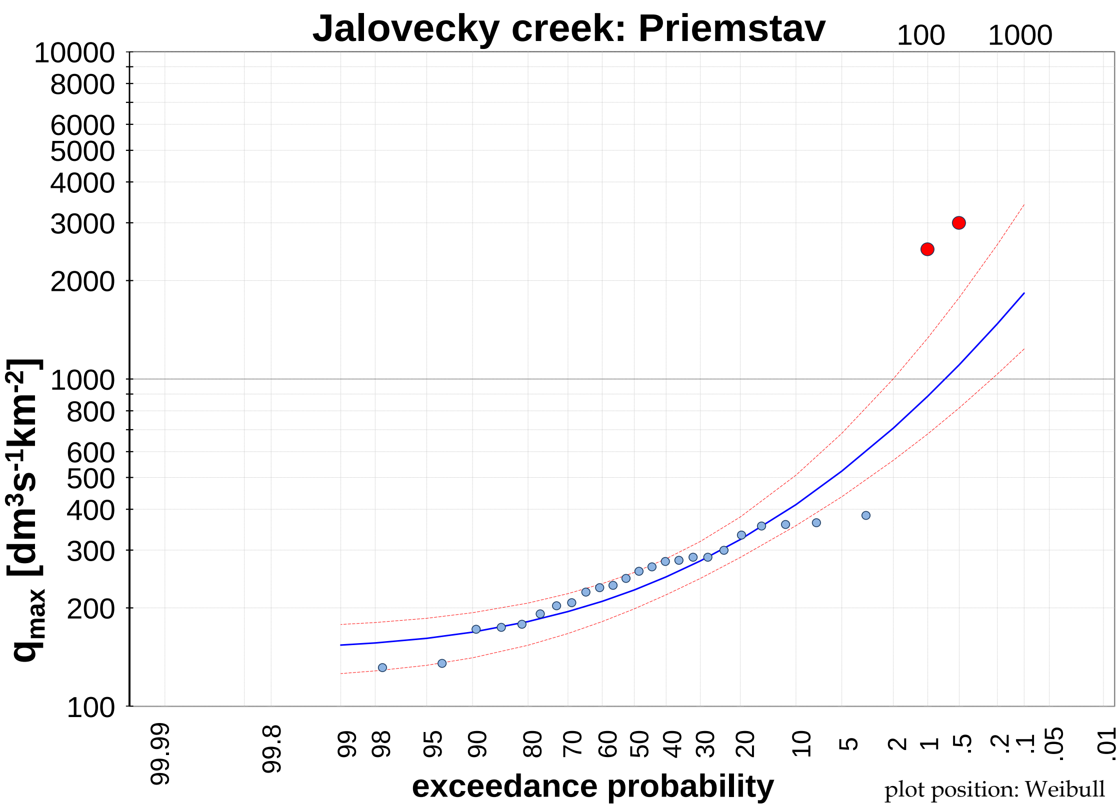

b)

Fig. 6.12 *Theoretical log Pearson probability exceedance curve type III., of the maximum annual runoff of the Jalovecky creek at the outlet of the Jalovecka valley for the period 1988–2011, 5% and 95% confidence intervals. a) without historical flood; b) with 1958 and 1813 historical floods and G_r skewness coefficient.*

Table 6.5 Design values of selected *T*-year annual maximum discharges on the Danube tributaries, *G* – skew coefficient

No	River	Station	*G*	*10*	*50*	*100*	*200*	*500*	*1000*
1	Inn	Oberaudorf	0.19	1686	2078	2243	2407	2626	2794
2	Inn	Passau-Ingling	0.81	4285	6010	6863	7799	9179	10347
3	Lech	Landsberg	0.32	740	1054	1201	1358	1583	1766
4	Regen	Regenstauf	-0.30	489	652	718	781	863	924
5	Salzach	Burghausen	0.64	2029	2854	3255	3691	4327	4859
6	Issar	Plattling	0.92	814	1195	1392	1614	1949	2241
7	Enns	Steyr	0.24	2016	2790	3143	3513	4030	4446
8	Traun	Ebensee	0.24	732	1009	1135	1266	1450	1597
9	Morava	Kromeriz	0.20	586	794	887	983	1116	1221
10	Morava	Straznice	-0.42	621	774	831	884	949	996
11	Jihlava	Ivancice	-0.09	233	378	446	520	623	707
12	Svratka	Zidlochovice	0.07	242	382	450	523	628	715
13	Morava	Mor.Sv.Jan	0.17	961	1428	1648	1884	2220	2495
14	Bela	Podbanske	0.81	76	149	195	252	349	444
15	Vah	L. Mikulas	0.40	258	403	477	558	680	784
16	Vah	Sala	-0.25	1430	1821	1975	2123	2313	2452
17	Hron	B. Bystrica	0.43	275	409	475	548	654	744
18	Hron	Brehy	0.17	627	838	921	1002	1106	1182
19	Kysuca	Kysucke N. Mesto	0.30	493	729	843	965	1142	1288
20	Topla	Hanusovce	0.27	250	403	481	567	695	804
21	Krupinica	Plastovce	-0.53	84	125	141	157	178	192
22	Ipel	Holisa	-0.82	94	132	145	157	171	181
23	Nitra	Nitrianska Streda	-0.53	268	358	392	424	463	491
24	Raba	Arpas	-0.15	379	561	642	725	838	927
25	Tisza	Vasarosnameny	-0.25	2958	3799	4132	4455	4868	5173
27	Tisza	Szeged	0.05	3206	3997	4323	4647	5073	5397
28	Szamos	Csenger	0.18	1676	2544	2961	3408	4052	4582
29	Maros	Mako	0.58	1179	1799	2115	2468	2998	3453
30	Sajo	Felsoezsolca	-0.49	422	496	548	598	661	706
31	Tisza	Senta	0.38	2820	3445	3703	3958	4294	4548
32	Lim	Prijepolje	0.74	737	1085	1262	1458	1753	2006
33	Drina	Bajina Basta	1.13	2952	4620	5537	6606	8297	9826
34	Sava	Sremska Mitrovica	0.44	5172	6141	6552	6965	7519	7947
35	Moravica	Arilje	0.70	233	452	584	746	1019	1280
36	Ibar	Lopatnica Lakat	0.64	652	1068	1292	1549	1949	2304
38	Juzna Morava	Mojsinje	-0.27	1222	1757	1984	2210	2511	2739
39	Velika Morava	Ljubicevski most	-0.49	1881	2348	2519	2678	2871	3006
40	Drava	Donji Miholjac	-0.10	1745	2069	2195	2316	2470	2583
41	Kupa	Jamnicka Kiselica	0.11	1221	1474	1577	1678	1811	1912
42	Sava	Zagreb (incl. Catez)	-0.07	2378	2880	3079	3272	3520	3704
43	Orljava	Pleternica Most	-0.89	96	118	125	131	137	141
44	Una	Kostajnica	-0.55	1462	1650	1714	1771	1837	1881
45	Sava	Čatež	0.16	2768	3569	3913	4262	4732	5098
46	Krka	Podbočje	-0.12	396	459	483	506	534	555
47	Savinja	Laško	-0.04	952	1309	1463	1620	1832	1996
48	Sava	Litija	-0.30	1789	2239	2412	2577	2785	2936
49	Szamos	Satu Mare	0.16	1696	2528	2921	3340	3937	4425
52	Siret	Storozhinec	0.27	351	673	854	1068	1408	1715
53	Prut	Chernivcy	-0.23	2700	4464	5290	6157	7368	8333
54	Tisza	Rakhiv	0.18	560	919	1100	1301	1598	1849
55	Tisza	Vylok	-0.23	2906	3812	4178	4535	4996	5339
56	Teresva	Ust-Chorna	0.27	316	490	576	669	807	922
57	Rika	Mizhhirya	-0.32	474	657	733	807	903	975
58	Latorycya	Mucacheve	0.10	942	1519	1803	2113	2566	2943
59	Latorycya	Chop	-0.36	486	688	771	853	959	1037
60	Uzh	Uzhhorod	-0.43	1178	1667	1864	2055	2299	2478
61	Prut	Jaremcha	0.43	617	1195	1533	1938	2600	3215
62	Una	Kralje	0.60	593	778	863	953	1080	1183
63	Sana	Sanski Most	-0.58	544	629	657	683	713	733
64	Vrbas	Kozluk Jajce	0.63	189	268	306	347	407	458
65	Bosna	Maglaj	0.56	1560	2184	2484	2807	3275	3664

6.2.2.3 Skew coefficients of the LP3 distributions for Danube tributaries

Using the procedure described above, we estimated the skew coefficient G of the LP3 distribution for 62 time series of maximum annual discharge from Danube tributaries. The values of estimated skew coefficients G are presented in Fig. 6.13, and are given in Table 6.5. The estimated T-year flood design values are also shown in Table 6.5. The primary objective was not to carry out runoff regionalization, but rather to assessment the runoff characteristics from the long-term point of view. Nevertheless, we visualized the regional distribution of skewness coefficient in those parts of the basin where data were available. These regions can be compared with the zones identified by Stănescu (2004).

Stănescu et al (2001, 2004) proposed the following zonation of the Danube Basin (see Fig. 6.14) to identify regions with the same water outflow regime:

- Zone 1: The right-side tributaries of the Danube in Germany flowing from the Alps and tributaries in the Austrian Alps and the mountainous area of Slovenia.
- Zone 2: The right-side tributaries of the Danube coming from the mountains in Schwarzwald and the left-size tributaries in Germany.
- Zone 3: The left-size tributaries of the Danube flowing from the Czech Republic (Morava River Basin), Slovakia, the Tisza Upper basin from Ukraine and Hungary (Sajo River, Bodva and Hornád), the Somes and Mures basins (Romania), the Olt Upper basin (Romania), the upper and middle basins of Siret and Prut Rivers from Romania and Ukraine including their tributaries from the Republic of Moldova.
- Zone 4: Both righ-side and left-size tributaries of the Danube in Hungary including the tributaries of the Tisa River coming from the western slopes of the Carpathians (Romania) and Zagyva River (Hungary).
- Zone 5: The left-size tributaries of the Danube coming from the Southern Carpathians, and those on the right side from Serbia and Bosna and Herzegovina (Sava - Drina Rivers and Morava River) and from Bulgaria.

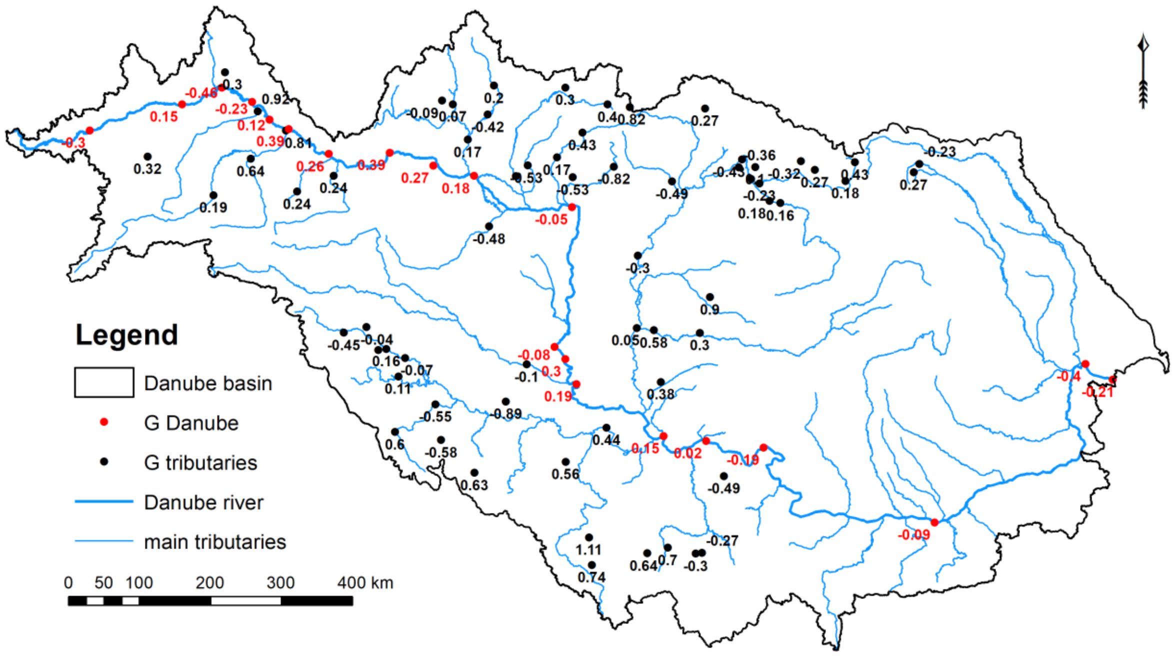

Fig. 6.13 Estimated values of the G_r coefficient in stations on the Danube and its tributaries.

Stănescu (2004) processed 176 time series and considered these as insuficient for the whole Danube basin zonation. Our analysis is based on “only” 82 time series (Fig. 6.15) of the annual maximum discharges. Our goal was to estimate the *T*-year design discharge by processing the longest available time series with included historical floods.

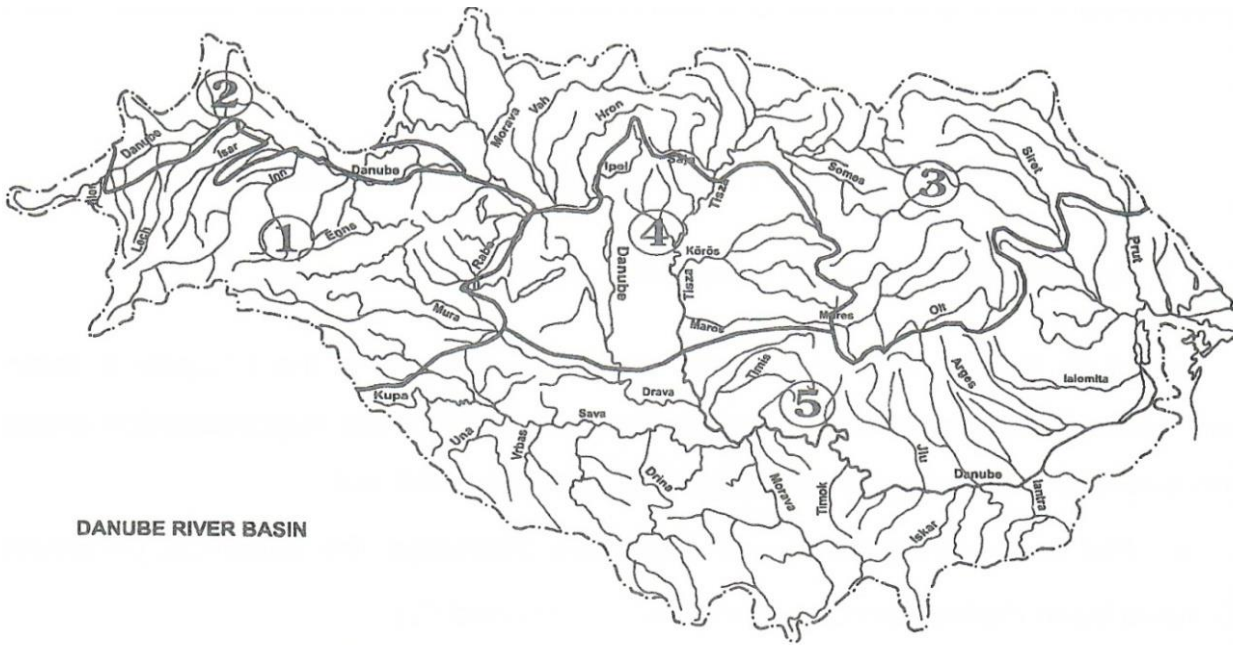

Fig. 6.14 Water gauging stations of the river Danube and main tributaries: a) regions with the same water runoff regime (the zonation of the Danube Basin according Stănescu (2004).

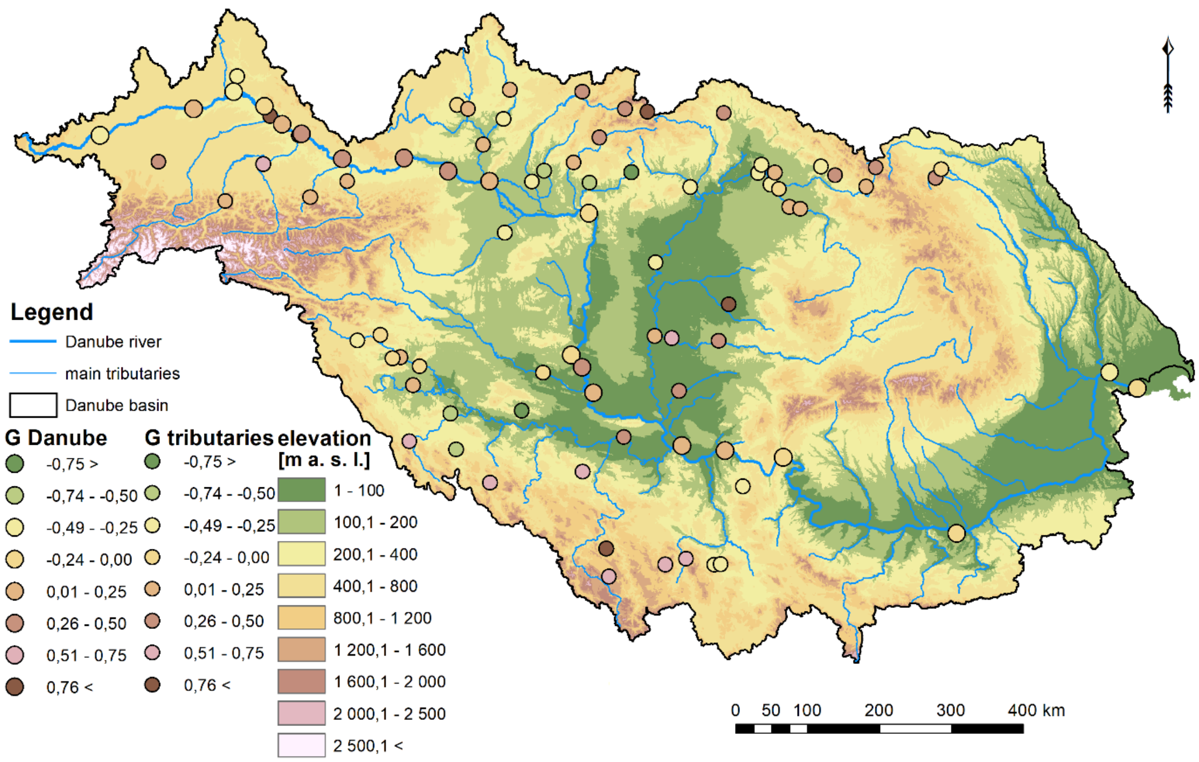

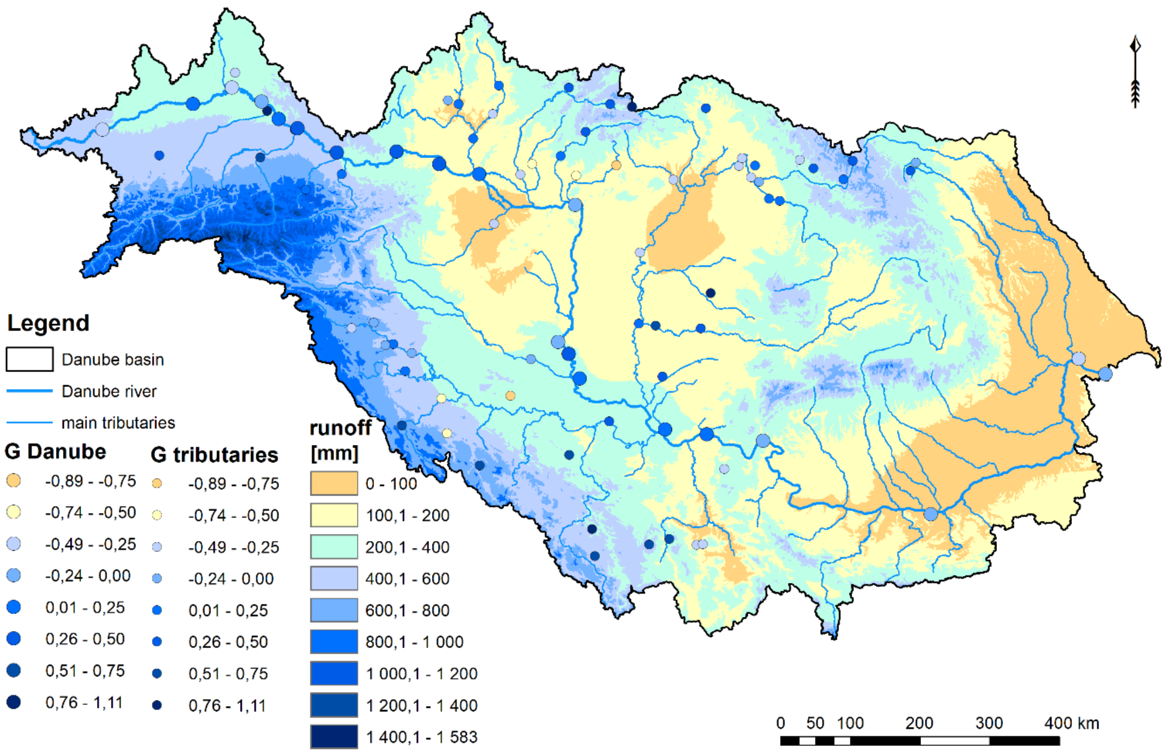

Fig. 6.15 Estimated values of the G_h coefficient in stations on the Danube and its tributaries.

6.3 Conclusions

The Danube River flows through and connects the highest number of countries in the world. Close international cooperation is needed for acquisition and subsequent processing of national data by uniform methodologies. Validation of underlying assumptions is needed in order to obtain reliable statistics (IACWD, 1982). Significant changes in the river basins such as urbanization or construction of flood protection structures may affect discharge maxima and thus bias the results of frequency analysis. Since forecasts of the maximum flows are based on observations made in the past, changes in land cover and/or significant regulation of peak flows violate the stationarity assumption of hydrological time series. Statistical measures such as mean, variation and skewness must be selected properly for the whole period of observations in order to reliably estimate flood characteristics. It is necessary to recalculate the distribution functions if any of the conditions of the Q_{max} series 1-3 have changed.

Due to climate change, statistical processing of observed data can be carried out only after checking the mutual independence and identical distribution, the homogeneity and the lack of trend of the sample.

The maximum discharges $Q_{p\%}$ corresponding to the probability of exceedance $P\%$ depend on aleatory and epistemic uncertainty. Consequently, the maximum discharges $Q_{p\%}$ and the floods volume are not unique values and should always be associated with an interval of uncertainty. When using a unique distribution function, this interval can be derived by varying the length of the sample data or generating new data based on the entire length of observation.

The confidence interval can also be used as a measure of uncertainty of estimated flood parameters.

After constructing a set of statistical distributions, only the best ones should be retained, based on statistical tests like chi-square, Kolmogorov or Anderson-Darling. The lower and the upper limits of the selected distributions define the interval of uncertainty. In defining design flood, the upper limit of the maximum discharge and the lower limit of the volume are coupled for each probability of exceedance, and vice versa. The flood characterized by the couple ($Q_{P\%}^{upper}$; $V_{P\%}^{lower}$) is mainly used in the design of spillways and the height of dam crests, while the combination ($Q_{P\%}^{lower}$; $V_{P\%}^{upper}$) is necessary for establishing the temporary floodwater storage capacity of the reservoirs.

In the second part of this chapter, only one type of peak probability distribution, namely the log-Pearson type III distribution (LP3) was tested for extreme floods design values. This type of distribution is flexible to cover extreme values depending to the coefficient of skewness (G). Coefficient of skewness calculated from observed data affects the shape of frequency curve. Steep slopes in catchments, low infiltrated areas, quick propagation of flood waves and one or more extremely high peak flows contribute high positive values of skewness (G). On the other hand, flat slopes, high infiltrated areas and runoff from catchment regulated by lakes and wetlands indicate negative values of skewness.

We incorporated the information form historic floods into the observed Q_{max} series and recalculated the parameters of the LP3 distribution curves for the individual stations. The inclusion of the historical floods has increased the skew coefficient G to G_h on average by 0.2. The coefficients of skewness (G_h) of the LP3 distribution curves range from –0.404 to 0.861 along the Danube River.

We propose that for stations along the Danube River the regional skew coefficient G_r estimated according to relation (6.12) should be applied. Using only one type of distribution allows us to generalize the skewness coefficients. We are able to estimate T-year discharges at gauges with short length of observations.

The calculated *1000*-year discharge is 16-times higher than the mean annual discharge at station Berg, while it is only 7-times higher at station Bratislava, and only 3-times higher at station Reni.

The estimation of T-year discharges is a never-ending process. Urbanization, channel regulation, flood protection measures and many other interventions can change maximum discharges and negatively affect the application of frequency analysis. The future prediction of peak annual discharges should include historical records. Land use changes and massive regulations of river beds can violate the stationarity assumption of hydrological time series. Selected statistical variables, namely as the mean, median, skew, variation, have to be estimated appropriately from the entire observation series. It is necessary to recalculate distribution curves and define new T-year discharges in particular stations after any changes in their basins.

References

Danube Floodrisk 2012. SEE/A/077/2.1/X, Stakeholder oriented flood risk assessment for the Danube floodplains. South East Europe (SEE). Transnational Cooperation Programme. 2009-2012.

Ang, A. H-S. & Tang W. H. 2007. Probability Concepts in Engineering, Emphasis on Application to Civil and Environmental Engineering, John Wiley & Sons.

Bobée, B., Cavadias G., Ashkar F., Bernier J. & Rasmussen P. 1993. Towards a systematic approach to comparing distributions used in flood frequency analysis. J. of Hydrol., 142, 1–4, 121–136.

Brazdil, R., Kundzewicz Z., W., Benito, G. 2006. Historical hydrology for studying flood risk in Europe. Hydrological Science Journal, 51, 5, 739–764. DOI:10.1623/hysj.51.5.739.

Cheng, K.S. Chiang, J.L., Hsu, C.W. 2007. Simulation of probability distributions commonly used in hydrological frequency analysis. Hydrological Process, 21, 1, 51–60.

Drobot, R., Draghia, A.F. 2012. Design Floods Obtained by Statistical Processing. 24th Congress on Large Dams. Q94-R11, Kyoto, Japan, 142–159.

Drobot, R., Draghia, A.F., Trandafir, R., Ciuiu, D. 2017. The uncertainty interval of the maximum discharges with high return period. XXVII Conference of the Danubian Countries on Hydrological Forecasting and Hydrological Bases of Water Management, 26-28 September 2017, Golden Sands, Bulgaria, e-book pages 124–131.

El Adlouni S., Bobée, B., Ouarda T.B.M.J. 2008. On the tails of extreme event distributions in hydrology. J. of Hydrol. 355, 1–4, 16–33.

Elleder, L. 2010. Reconstruction of the 1784 flood hydrograph for the Vltava River in Prague, Czech Republic, Global and Planetary Change, 70, 117–124.

Elleder, L., Herget, J., Roggenkamp, T., Nießen, A. 2013 Historic floods in the city of Prague – a reconstruction of peak discharges for 1481–1825 based on documentary sources, Hydrology Research, 44, 2, 202–214.

Gaal, L., Szolgay, J., Kohnova, S., Hlavcova, K., Viglione, A. 2010. Inclusion of historical information in flood frequency analysis using a Bayesian MCMC technique: A case study for the power dam Orlik, Czech Republic, Contributions to Geophysics and Geodesy, 40, 2, 121–147.

Griffis, V. W. and Stedinger, J. R. 2007. The log-Pearson type III distribution and its application in flood frequency analysis. 1: Distribution characteristics, J. of Hydrologic Engineering, 12, 5, 482–491.

Griffis, V.W. and Stedinger, J.R. 2009 Log-Pearson type 3distribution and its application in flood frequency analysis, III—sample skew and weighted skew estimators, J. Hydrol., 14, 2, 121–130.

Hirsch, R., M. 1987. Probability plotting position formulas for flood records with historical information. J. Hydrol., 96, 185–199.

Hirsch, R., M., Stedinger, J., R. 1987. Plotting position for historical floods and their precision. WRR 23, 4, 715–727.

IACWD 1982. Guidelines for determining flood flow frequency, Bulletin 17-B. Technical report, Interagency Committee on Water Data, Hydrology Subcommittee. 194 pp.

Kjeldsen, T. R., Macdonald, N., Lang, M., Mediero, L., Albuquerque, T., Bogdanowicz, E., Brazdil, R., Castellarin, A., David, V., Fleig, A., Gul, G. O., Kriauciuniene, J., Kohnova, S., Merz, B., Nicholson, O., Roald, L. A., Salinas, J. L., Sarauskiene, D., Sraj, M., Strupczewski, W., Szolgay, J., Toumazis, A., Vanneuville, W., Veijalainen, N. Wilson, D. 2014. Documentary evidence of past floods in Europe and their utility in flood frequency estimation, J. Hydrol., 517, 963–973. ISSN 0022-1694.

Koutsoyiannis, D. 2005. Uncertainty, entropy, scaling and hydrological statistics. Hydrological Sciences Journal, 50, 3, 381–404.

Maidment, D., R. 1992. Handbook of Hydrology. Ch. 18. Frequency analysis of extreme events, McGraw-Hill, 18.12–18.13.

Merz, B., Thieken, A., H. 2009. Flood risk curves and uncertainty bounds. Natural Hazards, 51, 3, 437–458.

Merz, R., Blöschl, G. 2008b. Flood frequency hydrology: 1. Temporal, spatial, and causal expansion of information, Water Resources Research, 44, W08432.

Merz, R., Blöschl, G. 2008a. Flood frequency hydrology: 2. Combining data evidence, Water Resources Research, 44, W08433.

Pilon, P. J. and Adamowski, K. 1993. Asymptotic variance of flood quantile in log Pearson type III distribution with historical information, J. Hydrol., 143 (3-4), 481–503.

Rogger M., Kohl B., Pirkl H., Viglione A., Komma J., Kirnbauer R., Merz R. Blöschl G. 2012. Runoff models and flood frequency statistics for design flood estimation in Austria – Do they tell a consistent story? J. Hydrol., 456–457.

Stănescu, V., A., Ungureanu, V., Domokos, M. 2001. Regionalization of the Danube catchment for the estimation of the distribution functions of annual peak discharges. J. Hydrol. Hydromech., 49, 6, 407–427.

Stănescu, V., A., 2004. Regional analysis of the annual peak discharges in the Danube catchment. Follow-up volume No.VII to the Danube Monograph. Regional Cooperation of the Danube Countries. Bucharest. 64 p.

Stedinger, J., Vogel, R., M., Foufoula-Georgiou, E. 1993. Frequency analysis of extreme events. Chapter 18, Handbook of Hydrology, D. Maidment (ed.), McGraw-Hill, Inc., New York.

7 Coincidence of the flood flow of the Danube River and its main tributaries

Stevan Prohaska and Aleksandra Ilić

7.1 Introductory comments

The conventional approach to flood risk assessment is to determine the probability that a flood will exceed a predefined flood wave parameter. This is, in fact, equivalent to estimating the return period of a flood event. The procedure involves statistical analysis of hydrological data from a near gauging station. From an engineering perspective, this approach provides satisfactory results for a large number of tasks, especially in the case of flood protection problems that involve relatively simple circumstances or, more precisely, where there are no tributaries in the flood-protected area.

However, the above approach does not ensure a reliable assessment of the considered flood wave parameter if there is a mouth of a tributary in the protected area. Namely, as a rule, the onset and development of flood waves on two rivers differ, such that maximum flood wave parameters do not occur simultaneously on both. Further, the flood wave on one of the rivers can have a considerable impact on the flow regime of the other. In addition, hydrological data is generally collected at gauging stations located beyond the zone of mutual influence of the rivers. In such cases it is especially important to assess the coincidence of flood waves on the recipient and the tributary, and to size flood protection measures for a discharge of a certain return period, defined by bivariate probability analysis.

7.2 Methodology for estimating flood coincidence

7.2.1 Theoretical background

To determine design water levels within the zone of mutual influence of the recipient and its tributaries, the probability of simultaneous occurrence, or coincidence, of flood waves on the considered rivers needs to be defined (Prohaska, Marjanović and Čabrić, 1978).

The term “coincidence” means the probability of simultaneous occurrence of two random variables, X and Y, which represent random events on the main river and its tributary (Prohaska, 2006).

If the two-dimensional random variables are normally distributed, the probability distribution function may be written as (Prohaska and Ilić, 2009):

$$f(x,y)=\frac{1}{2\pi\cdot\sigma_x\cdot\sigma_y\cdot\sqrt{1-R^2}}\cdot e^{-\frac{1}{2\cdot\left(1-R^2\right)}\cdot\left[\frac{(x-\overline{X})^2}{\sigma_x^2}-\frac{2\rho\cdot(x-\overline{X})\cdot(y-\overline{Y})}{\sigma_x\cdot\sigma_y}+\frac{(y-\overline{Y})^2}{\sigma_y^2}\right]} \qquad (7.1)$$

where:

x and y	– current values of random variables X and Y,
$\overline{X}$ and $\overline{Y}$	– average values of random variables X and Y,
σ_x and σ_y	– standard deviations of X and Y,
R	– coefficient of correlation between X and Y.

The cumulative distribution function of a two-dimensional random variable is defined by:

$$\Phi(x,y)=P[X\geq x;Y\geq y], \qquad (7.2)$$

where:
X and Y are the random variables (flood wave parameters) of the recipient and the tributary, while x and y are corresponding values simultaneously exceeded by X and Y, respectively.

Given that, as a rule, the considered variables are not subject to normal distribution, they need to be logarithmed and partially standardized, as follows:

$$u = log\ X \qquad w = log\, Y$$
$$\psi = u - \bar{u} \qquad \xi = w - \bar{w}$$

Consequently, the distribution function of the transformed variables may be written as:

$$f(\psi,\xi) = \frac{1}{2\pi \cdot (1-\rho^2)} exp\left\{-\frac{1}{2 \cdot (1-\rho^2)} \cdot \left[\psi^2 - 2 \cdot \rho \cdot \psi \cdot \xi + \xi^2\right]\right\} \qquad (7.3)$$

The variances σ_ξ^2 and σ_ψ^2, and the correlation coefficient ρ, can be estimated using observed time-series. Based on the calculated coefficient of correlation ρ between variables ξ and ψ, equation:

$$\Phi(\lambda) = 1 - \int_{-\infty}^{\lambda} e^{\frac{-t^2}{2 \cdot (1-\rho^2)}} dt \qquad (7.4)$$

can be used to determine the value of λ for any given $\Phi(\lambda)$. Namely, the value of λ is clearly defined by:

$$\psi^2 - 2\rho\psi\xi + \xi^2 = \lambda^2 \qquad (7.5)$$

from which

$$\xi^2 = 2\rho\psi\xi + (\psi^2 - \lambda^2) = 0 \qquad (7.6)$$

follows.

The solution to quadratic Eq. (7.6) for any ψ provides a corresponding pair of values $\xi_{1,2}$. In other words, for each standardized variable $\psi = \log X - \overline{\log X}$, there are two standardized values $\xi_{1,2} = \log Y - \overline{\log Y}$.

When the corresponding quantities of ξ_1 and ξ_2 are entered for each selected value of ψ in the coordinate system, ellipses that represent the desired probability $f(\lambda)$ can be constructed. These ellipses are referred to as correlation ellipses and they actually represent the intersection of the horizontal plane and the surface that defines the bivariate normal distribution. Then, using the inverse procedure, antilogarithming can provide the quantities of the natural, non-standardized variables X and Y.

When the corresponding values of X and Y determined in this way are entered into the rectangular coordinate system, the ellipses are clearly transformed into closed curves of irregular shape.

The next step is to assess the probability of simultaneous occurrence of X less than or equal to a given value of x, and simultaneously Y less than or equal to a given value of y. In the previous consideration the initial assumption was that two-dimensional random variables ψ and ξ are subject to the bivariate distribution law, with mean values m_ψ and m_ξ, variances σ_ξ^2 and σ_ψ^2, and correlation coefficient ρ. If the assumption holds, the required probability may be expressed as:

$$P_r(X \le h_o; Y \le k_o) = \int_{-\infty}^{\frac{h_o - m_\psi}{\sigma_\psi}} \int_{-\infty}^{\frac{k_o - m_\xi}{\sigma_\xi}} g(s,t,\rho)\cdot ds \cdot dt = L\left[-\left(\frac{h_o - m_\psi}{\sigma_\psi}\right); -\left(\frac{k_o - m_\xi}{\sigma_\xi}\right); \rho\right] \tag{7.7}$$

The answer to the basic question: what is the probability that variable X will be greater than a given h_0, and that at the same time Y will be greater than a given k_0, can be defined as:

$$P\{X \ge h_o, Y \ge k_o\} = 1 - P_r\{X \le h_o, Y \le k_o\} \tag{7.8}$$

The probability density function is therefore:

$$\frac{1}{2\cdot\sigma_\psi\cdot\sigma_\xi\cdot\sqrt{1-\rho^2}}\, exp\left[-\frac{G}{2\cdot(1-\rho^2)}\right] = \frac{1}{\sigma_\psi\cdot\sigma_\xi}\cdot g\left(\frac{\psi - m_\psi}{\sigma_\psi}; \frac{\xi - m_\xi}{\sigma_\xi}; \rho\right) \tag{7.9}$$

where:

$$G = \frac{(\psi - m_\psi)^2}{\sigma_\psi^2} - \frac{2\rho\cdot(\psi - m_\psi)\cdot(\xi - m_\xi)}{\sigma_\psi\cdot\sigma_\xi} + \frac{(\xi - m_\xi)^2}{\sigma_\xi^2} \tag{7.10}$$

The way in which the required probability is calculated is described by Eqs. (7.7) and (7.8). In fact, the solutions are derived from Eq. (7.9), whose solution is graphically represented in the literature (Abramowitz and Stegun, 1972).

The graphical solution is based on the equation:

$$L(h,k,\rho) = L\left(h, 0, \frac{(\rho\cdot h - k)\cdot \mathrm{sgn}h}{\sqrt{h^2 - 2\rho\cdot h\cdot k + k^2}}\right) + L\left(k, 0, \frac{(\rho\cdot h - k)\cdot \mathrm{sgn}k}{\sqrt{h^2 - 2\rho\cdot h\cdot k + k^2}}\right) - \begin{cases} 0; \text{if } h\cdot k \ge 0 \text{ and } h + k \ge 0 \\ \frac{1}{2}; \text{for all other val.} \end{cases} \tag{7.11}$$

where: (*sgnh*) and (*sgnk*) are equal to unity when *h* and *k* are greater than or equal to zero, or –1 for negative values of *h* and *k*. Corresponding probabilities are calculated as follows: $\log X$ and $\log Y$ are entered into the *XY* coordinate system, and threshold values of h_0 for variable *X* and k_0 for variable *Y* are selected. Then the probability of a common event is determined, that is, the probability that variables *X* and *Y* will exceed predefined values of h_0 and k_0. The mean variances of *X* and *Y* and the coefficient of correlation need to be calculated first, and then *h* and *k* are determined from equations:

$$h = \frac{h_o - m_\psi}{\sigma_\psi}\ ;\ k = \frac{k_o - m_\xi}{\sigma_\xi}, \tag{7.12}$$

where: h_0 and k_0 are the threshold values of $\log X$ and $\log Y$. Then all the necessary elements for Eq. (7.11) are calculated and the probabilities given by Eq. (7.12) are read out from nomograms presented in the literature (Abramowitz and Sregun, 1972), for calculated *h*, *k* and ρ.

The probability estimated in this way is actually the probability of exceedance of a combination of *X* and *Y*, such that the points determined by the abscissa *X* and ordinate *Y* fall to the right side of h_0 and above k_0. The procedure is repeated for all points near the intersection of *X* and *Y*. This results in a grid of points, each of which is characterized by the probability of occurrence of a combination of *X* and *Y* less than these coordinate points. Lines of the same probabilities are calculated on the basis of the probability at the point of intersection of the targeted *X* and *Y*, as follows: One of the variables, say *X*, is taken as the abscissa in the probability grid. Then, for a constant quantity $X=X_1$ the probabilities P_i are read out for different values of $Y=Y_1$, such that a *P*-*Y* plot is produced for the selected quantity X_1. The procedure is repeated for a sufficiently large number of points X_1, to define a family of *P*-*Y* curves, where each curve stands for a single value of *X*. Then, for the selected value, *Y* is read out from each plot for every *X*. This results in a series of *X*-*Y* pairs whose probabilities *P* are the same.

The procedure described above is repeated for each of the desired quantities.

The significance of the resulting correlation coefficients is assessed by calculating their error using the formula (Yevjevich, 1972):

$$\sigma_R = \frac{1-R^2}{\sqrt{N}}, \tag{7.13}$$

where:
σ_R – error of correlation coefficient *R*,
N – total number of data points.

The most commonly used criterion for correlation coefficient assessment was adopted in the present study – that the correlation coefficient significantly differs from zero if its absolute value exceeds three times its error:

$$|R| \geq 3 \cdot \sigma_R\ . \tag{7.14}$$

7.2.2 Defining relevant variables

Flood wave coincidence analysis of the recipient and a tributary is based on defining a two-parameter distribution of the following combinations of variables (Prohaska et al., 2009):

1. maximum annual value of the selected flood wave parameter of the recipient X – maximum annual value of the same flood wave parameter of the tributary Y,
2. maximum annual value of the selected flood wave parameter of the recipient X – corresponding value of the same flood wave parameter of the tributary Y_{cor},
3. maximum annual value of the selected flood wave parameter of the tributary Y – corresponding value of the same flood wave parameter of the recipient X_{cor}.

The result of coincidence calculations is a line of the same probabilities of the above combinations of the selected flood wave parameter (differential distribution law), as well as a line that defines the exceedance probability of the same constellations of variables, i.e.:

$$P\left[X > X_1; Y > Y_1\right] = \int_{X_1}^{\infty}\int_{Y_1}^{\infty} g\left(X, Y, R\right) dx dy \tag{7.15a}$$

$$P\left[X > X_1; Y_{cor} > Y_1\right] = \int_{X_1}^{\infty}\int_{Y_1}^{\infty} g\left(X, Y_{cor}, R\right) dx dy_{cor} \tag{7.15b}$$

$$P\left[X_{cor} > X_1; Y > Y_1\right] = \int_{X_1}^{\infty}\int_{Y_1}^{\infty} g\left(X_{cor}, Y, R\right) dx_{cor} dy \tag{7.15c}$$

The flood wave is represented by a hydrograph whose maximum exceeds a predefined quantity. That quantity can be selected from the average flow duration line or in another way. The following characteristic flood wave parameters can be analyzed:

- maximum discharge – Q_{max},
- flood wave volume above predefined discharge – W,
- flood wave duration above predefined discharge – T,
- time difference between maximum discharges at two river points – τ_{max}.

Depending on hydrologic conditions, the predefined discharge may be exceeded several times during a calendar year. This means that the number of predefined events may change from year to year. Hence, the annual flood frequency is a very important characteristic that needs to be defined through prior analysis. Further, it is of interest to examine the period during the year in which flooding might occur.

In flood coincidence analyses of the recipient and a tributary, or two cross-sections of the same river upstream and downstream of the tributary, due attention needs to be paid to flood wave origin. In this regard the following flood wave parameters are important: snow melt, precipitation intensity, concentration time, and the like. The time delay between the considered events also needs to be assessed. The flood coincidence analysis should be based on the nearest gauging stations on the recipient upstream and downstream of the tributary. The most important characteristics of flood wave coincidence are described in Fig. 7.1 (Prohaska et al., 1999).

The symbols in Fig. 7.1 stand for:

QIN_{max} – maximum annual discharge of the recipient at the input cross-section in the considered river sector,

$QOUT_{max}$ – maximum annual discharge of the recipient at the output cross-section in the considered river sector,

qTR_{max} – maximum annual discharge of the tributary in the considered river sector,

QIN_{corr1} – corresponding discharge of the recipient at the input cross-section at the time of occurrence of maximum annual discharge at the output cross-section of the recipient in the considered river sector,

$QOUT_{corr1}$ – corresponding discharge of the recipient at the output cross-section at the time of occurrence of maximum annual discharge at the input cross-section of the recipient in the considered river sector,

qTR_{corr1} – corresponding discharge of the tributary at the time of occurrence of maximum annual discharge at the input cross-section of the recipient in the considered river sector,

QIN_{corr2} – corresponding discharge of the recipient at the input cross-section at the time of occurrence of maximum annual discharge of the tributary,

$QOUT_{cor2}$ – corresponding discharge of the recipient at the output cross-section at the time of occurrence of maximum annual discharge of the tributary,

qTR_{corr2} – corresponding discharge of the tributary at the time of occurrence of maximum annual discharge at the output cross-section of the recipient in the considered sector,

QIN_1 – maximum discharge peak of the flood wave on the recipient at the input cross-section at the time of occurrence of maximum annual discharge at the output cross-section of the recipient in the considered river sector,

$QOUT_1$ – maximum flood wave peak of the recipient at the output cross-section at the time of occurrence of maximum annual discharge at the input cross-section of the recipient in the considered river sector,

qTR_1 – maximum flood wave peak of the tributary at the time of occurrence of maximum annual discharge at the input cross-section of the recipient in the considered river sector,

QIN_2 – maximum flood wave peak of the recipient at the input cross-section at the time of occurrence of maximum annual discharge of the tributary,

$QOUT_2$ – maximum flood wave peak of the recipient at the output cross-section at the time of occurrence of maximum annual discharge of the tributary, and

qTR_2 – maximum flood wave peak of the tributary at the time of occurrence of maximum annual discharge at the output cross-section of the recipient in the considered river sector.

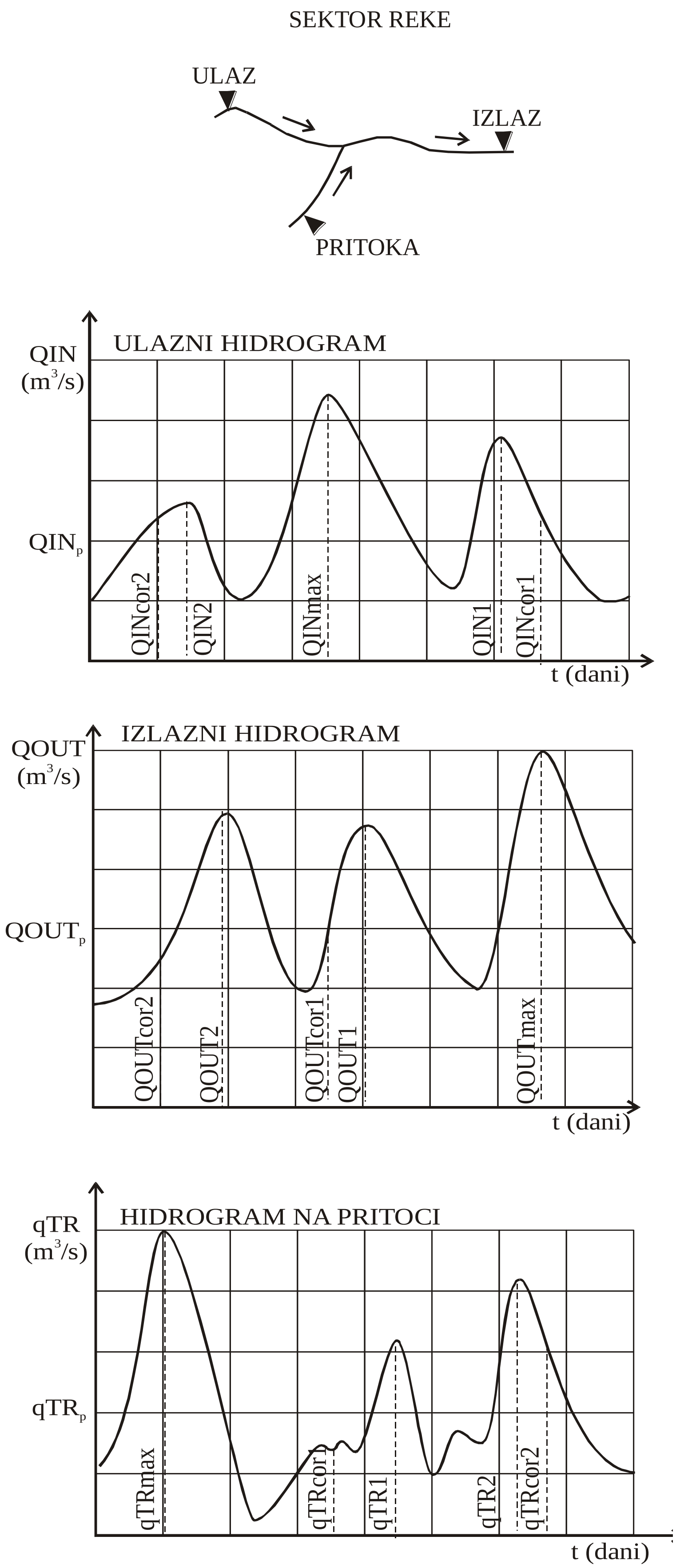

Fig. 7.1. Schematic representation of typical symbols for flow coincidence analysis.

7.2.3 Combinations of variables

The most relevant combinations of variables for flood wave coincidence analysis of the Danube River and its tributaries are as follows:

a) Simultaneous/synchronous occurrences

I.a.1 Maximum annual discharge of the Danube upstream from the mouth of the tributary – corresponding discharge of the Danube downstream from the mouth of the tributary (QIN_{max}; $QOUT_{cor1}$),
I.a.2 Maximum annual discharge of the Danube upstream from the mouth of the tributary – corresponding discharge of the tributary (QIN_{max}; qTR_{cor1})
I.a.3 Maximum annual discharge of the Danube downstream from the mouth of the tributary – corresponding discharge of the Danube upstream from the mouth of the tributary ($QOUT_{max}$; QIN_{cor1}),
I.a.4 Maximum annual discharge of the Danube downstream from the mouth of the tributary – corresponding discharge of the tributary ($QOUT_{max}$; qTR_{cor2}),
I.a.5 Maximum annual discharge of the tributary – corresponding discharge of the Danube downstream from the mouth of the tributary (qTR_{max}; $QOUT_{cor2}$),
I.a.6 Maximum annual discharge of the tributary – corresponding discharge of the Danube upstream from the mouth of the tributary (qTR_{max}; QIN_{cor2}).

b) Genetic – simultaneous

I.b.1 Maximum annual discharge of the Danube upstream from the mouth of the tributary – maximum discharge of the Danube downstream from the mouth of the tributary, of genetically the same flood wave (QIN_{max}; $QOUT_1$),
I.b.2 Maximum annual discharge of the Danube upstream from the mouth of the tributary – maximum discharge of the tributary, of the genetically the same flood wave (QIN_{max}; qTR_1),
I.b.3 Maximum annual discharge of the Danube downstream from the mouth of the tributary – maximum discharge of the Danube upstream from the mouth of the tributary, of genetically the same flood wave ($QOUT_{max}$; QIN_1)
I.b.4 Maximum annual discharge of the Danube downstream from the mouth of the tributary – maximum discharge of the tributary, of genetically the same flood wave ($QOUT_{max}$; qTR_2),
I.b.5 Maximum annual discharge of the tributary – maximum discharge of the Danube upstream from the mouth of the tributary, of genetically the same flood wave (qTR_{max}; QIN_2),
I.b.6 Maximum annual discharge of the tributary – maximum discharge of the Danube downstream from the tributary, of genetically the same flood wave (qTR_{max}; $QOUT_2$).

c) Macro-annual – simultaneous

I.c.1 Maximum annual discharge of the Danube upstream from the mouth of the tributary – maximum annual discharge of the Danube downstream from the mouth of the tributary (QIN_{max}; $QOUT_{max}$),
I.c.2 Maximum annual discharge of the Danube upstream from the mouth of the tributary – maximum annual discharge of the tributary (QIN_{max}; qTR_{max}),

I.c.3 Maximum annual discharge of the Danube downstream from the mouth of the tributary – maximum annual discharge of the tributary ($QOUT_{max}$; qTR_{max}).

7.2.4 Recommended uses of the results

The results of flood calculations for confluences of the recipient and its tributaries can be used for the following practical purposes:

1. to define maximum design water levels at a gauged confluence of a recipient and tributary,
2. to define maximum design water levels at an insufficiently gauged (undergauged) confluence of a recipient and tributary (data on the downstream reach of the recipient not available), and
3. to assess the statistical significance of the coincidence of characteristic parameters of recorded (historic) and future flood hydrographs at the confluence of a recipient and tributary.

The theoretical background for all the practical aspects of the results of flood wave coincidence analysis at the confluence of a recipient and tributary is briefly discussed below.

7.2.4.1 Flood coincidence calculations for defining design water stages at gauged confluences

The extended area of the confluence of a recipient and tributary is a river reach where all the required hydrological data (hydrological stations) are available at the input cross-sections (of the recipient and the tributary) and the output cross-section (of the recipient downstream from the confluence). The following data are needed to define design water levels:

- Time-series of maximum annual discharges at the input cross-sections (of the recipient and the tributary) and the output cross-section (of the recipient), and
- Results of flood wave coincidence calculations for the following combinations of variables:
  - maximum annual discharge of the recipient – maximum annual discharge of the tributary,
  - maximum annual discharge of the recipient – corresponding discharge of the tributary, and
  - maximum annual discharge of the tributary – corresponding discharge of the recipient.

The design water levels in the extended area of the confluence are derived from hydraulic analyses of water level lines, based on adopted boundary conditions and adopted design discharges. If the confluence is gauged, the design discharges are adopted as follows:

- For the reach of the recipient downstream from the confluence – the design water levels are those based on the theoretical maximum annual discharge $QOUT_{max,p}$ for the adopted probability of occurrence p, at the hydrological station on the recipient downstream from the mouth of the tributary;
- For the reach of the recipient upstream from the confluence and within the zone of mutual influence of the recipient and the tributary – the design water level is an

envelope of maximum water levels derived from calculations of water level lines, based on discharges and certain combinations of variables:

  - maximum annual discharge of the recipient downstream from the confluence, of the adopted probability of occurrence p, and corresponding discharge of the recipient upstream from the confluence, of the same coincidence probability $(QOUT_{max}; QIN_{cor1})_p$,
  - corresponding discharge of the recipient downstream from the confluence and maximum annual discharge of the recipient upstream from the confluence, of the adopted probability of occurrence p, based on the coincidence of the same probability $(QIN_{max}; QOUT_{cor1})_p$.

- For the tributary upstream from the confluence and within the zone of mutual influence of the recipient and the tributary – the design water level is an envelope of maximum water levels derived from calculations of water level lines, based on the following combinations of variables:
  - maximum annual discharge of the recipient downstream from the confluence, of the adopted probability of occurrence p, and corresponding discharge of the recipient upstream from the confluence, of the same coincidence probability $(QOUT_{max}; qTR_{cor2})_p$,
  - corresponding discharge of the recipient downstream from the confluence and maximum annual discharge of the tributary upstream from the confluence, of the adopted probability p, based on the coincidence of the same probability $(qTR_{max}; QOUT_{cor2})_p$.
- For the recipient upstream from the zone of mutual influence of the recipient and the tributary – the design water levels correspond to the maximum annual discharge of the recipient (at the input hydrological station), of the adopted probability of occurrence, $QIN_{max,p}$.
- For the tributary upstream from the zone of mutual influence of the recipient and the tributary – the design water levels correspond to the maximum annual discharge of the tributary (at the input hydrological station), of the adopted probability of occurrence p, $qTR_{max,p}$.

The determination of design water level lines for the zone of mutual influence of the recipient and a tributary is schematically represented in Fig. 7.2. The selected level of protection corresponds to the adopted probability of occurrence p.

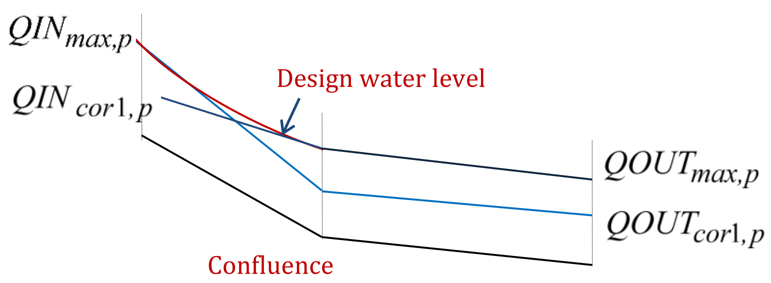

Fig. 7.2. Schematic representation of the selection of the design water level for a river confluence zone

7.2.4.2 Flood coincidence calculations aimed at defining design water stages for undergauged confluences

An undergauged (insufficiently gauged) confluence is the extended area of the confluence, as defined in Section 7.2.2, where the required data from one input station or the output station is missing. Available data are used to define the necessary probabilities and coincidences of variables as described in Section 7.2.3.

To simplify the procedure, in the case discussed below no data are available for the input cross-section of the recipient. This practically means that time-series of daily discharges are available for:

- the output cross-section of the recipient, $QOUT_{max,}$ and
- the input cross-section of the tributary, qTR_{max}.

In this case it is necessary to define the coincidences (lines of the same probabilities of occurrence $f(x,y)$ and the cumulative line of exceedance probability $\Phi(x,y)$) for the following constellations of variables, defined in Section 2.3, and only for simultaneous/synchronous occurrences of:

a.2 Maximum annual discharge of the recipient upstream from the mouth of the tributary – corresponding discharge of the tributary (QIN_{max}; QTR_{cor1}) ($QOUT_{max}$; QTR_{cor2}), and

a.6 Maximum annual discharge of the tributary – corresponding discharge of the recipient upstream from the mouth of the tributary (QTR_{max}; QIN_{cor2}) (qTR_{max}; $QOUT_{cor2}$).

Only two points of intersection each (1 and 2) on the coincidence lines on the two coincidence plots are considered in this specific case, to assess the maximum annual discharge of a certain probability of occurrence – $QOUT_{max,p}$:

1. $P[(OUT_{max} > qOUT_{max}) \cap (QTR_{cor1} > qTR_{cor1})] = p$ and $f(QOUT_{max}, QTR_{cor1}) = p$

2. $P[(QTR_{max} > qTR_{max}) \cap (QOUT_{cor2} > qOUT_{cor2})] = p$ and $f(QTR_{max}, QOUT_{cor2}) = p$

where:
p – probability of occurrence.

The coordinates of the intersected points are:

1. Graphic 1:
   - Point 1 $(QOUT^1_{max}: QTR^1_{cor1})_p$
   - Point 2 $(QOUT^2_{max}: QTR^2_{cor1})_p$
2. Graphic 2:
   - Point 1 $(QTR^1_{max} : QOUT^1_{cor2})_p$
   - Point 2 $(QTR^2_{max} : QOUT^2_{cor2})_p$

The maximum design discharge on the downstream reach of the recipient, after the mouth of the tributary, of occurrence probability p – $QIN_{max,p}$, is equal to the average sum of the differences between the coordinates of the two points in both graphics, i.e.

$$QOUT_{max,p}=[(\sum_{1}^{2}(QIN^{1}_{max,p}-QTR^{1}_{cor1,p})+\sum_{1}^{2}(QIN^{2}_{max,p}-QTR^{2}_{cor1,p}))+(\sum_{1}^{2}(QTR^{1}_{max,p}-QIN^{1}_{cor2,p})++\sum_{1}^{2}(QTR^{2}_{max,p}-QIN^{2}_{cor2,p})]/2$$

The main assumption here is that the intermediate catchment in the considered sector between the input cross-sections and the output cross-section has no significant contribution to the formation of a flood wave at the output cross-section of the recipient.

7.2.4.3 Flood coincidence calculations aimed at assessing the statistical significance of flood waves

The main purpose of graphical representations of calculated coincidences of flood hydrograph parameters is to assess the statistical significance of flood waves on the recipient and the tributary, both historic and future.

The statistical significance assessment approach consists of entering the characteristic parameters/desired combinations of variables into appropriate diagrams. The resulting empirical points are then compared with coincidence exceedance lines of different probabilities of occurrence. The exceedance probability of an entered empirical point is determined by logarithmic (or linear) interpolation. The reciprocal value of the probability is the return period, or the statistical significance of the considered flood hydrograph parameters at the confluence of the recipient and the tributary.

7.3 Results of flood coincidence calculations for the Danube and its tributaries

7.3.1 Selection of constellations of variables for gauged cross-sections

The main assumption is that structural flood protection measures in river confluence zones need to be sized optimally and economically. In the specific case, the primary structural measures are levees. As a rule, river levees are longer than the zone of mutual influence of the rivers at flood stages, for example from the input gauging stations on the recipient and the tributary to the output cross-section on the recipient (Prohaska and Ilić, 2008). The river sector is schematically represented in Fig. 7.3.

The monograph discusses the sector of the Danube from the hydrological station (HS) at Hofkirchen in Germany (catchment size A=47496 km^2) to HS Veliko Gradište in Serbia (catchment size A=570375 km^2). The studied sectors of the Danube, along with input and output cross-sections, are shown in Table 7.1.

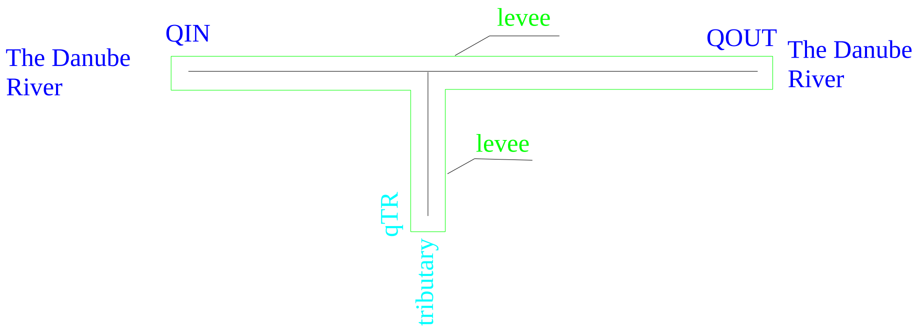

Fig. 7.3. Schematic representation of a flood protection sector in the extended zone of the confluence of the Danube and a tributary.

Table 7.1 Sectors of the Danube with tributaries

Node	Recipient	Hydrological station		Tributary	Hydrological station
		QIN	QOUT		qTR
1	Danube	Hofkirchen	Achleiten	Inn	P-Ingling
2		Vienna	Bratislava	Morava	Moravsky Jan
3		Bezdan	Bogojevo	Drava	Donji Miholjac
4		Bogojevo	Slankamen	Tisa	Senta
5		Slankamen	Smederevo	Sava	Sremska Mitrovica
6		Smederevo	Veliko Gradište	Velika Morava	Ljubičevski Most

Applying the conventional procedure, and disregarding flood coincidence, the basis for sizing levees would be the theoretical maximum annual discharges of different return periods, derived by means of the corresponding theoretical distribution functions. These values at the gauging stations, based on available data from 1931 to 2007, are shown in Tables 7.2a through 2f.

Table 7.2a Theoretical maximum annual discharges of the Danube and the Inn of different probabilities of occurrence – $Q_{\max,p}$ (m3/s) - NODE 1

p(%)	R. Danube		R. Inn
	$Q^{H}_{max,p}$	$Q^{A}_{max,p}$	$Q^{I}_{max,p}$
0.1	6359	10869	8440
1.0	4353	7925	6138
2.0	3840	7155	5517
5.0	2944	6274	4734

Table 7.2b Theoretical maximum annual discharges of the Danube and the Morava of different probabilities of occurrence – $Q_{\max,p}$ (m3/s) - NODE 2

p(%)	R. Danube		R. Morava
	$Q^{W}_{max,p}$	$Q^{B}_{max,p}$	$Q^{MJ}_{max,p}$
0.1	12610	14328	2170
1.0	9847	11192	1541
2.0	9046	10274	1362
5.0	8463	8890	1131

Table 7.2c Theoretical maximum annual discharges of the Danube and the Drava of different probabilities of occurrence – $Q_{\max,p}$ (m3/s) - NODE 3

p(%)	R. Danube		R. Drava
	$Q^{Bez}_{max,p}$	$Q^{Bog}_{max,p}$	$Q^{DM}_{max,p}$
0.1	10435	11418	3258
1.0	8437	9418	2542
2.0	7847	8810	2336
5.0	7029	7912	2064

Table 7.2d Theoretical maximum annual discharges of the Danube and the Tisa of different probabilities of occurrence – $Q_{\max,p}$ (m3/s) - NODE 4

p(%)	R. Danube		R. Tisa
	$Q^{Bog}_{max,p}$	$Q^{Sla}_{max,p}$	$Q^{St}_{max,p}$
0.1	10799	12940	4611
1.0	9172	10869	3847
2.0	8650	10236	3598
5.0	7918	9374	3248

Table 7.2 Theoretical maximum annual discharges of the Danube and the Sava of different probabilities of occurrence – $Q_{\max,p}$ (m3/s) - NODE 5

p(%)	R. Danube		R. Sava
	$Q^{Sla}_{max,p}$	$Q^{SD}_{max,p}$	$Q^{SM}_{max,p}$
0.1	13203	17381	7813/7781
1.0	11043	15128	6589/6581
2.0	10385	14395	6211/6209
5.0	9492	13360	5695/5699

Table 7.2f Theoretical maximum annual discharges of the Danube and the Velika Morava of different probabilities of occurrence – $Q_{max,p}$ (m3/s) - NODE 6

p(%)	R. Danube		R. Velika Morava
	$Q^{SD}_{max,p}$	$Q^{VG}_{max,p}$	$Q^{LjM}_{max,p}$
0.1	17381	18809	2829
1.0	15128	16351	2356
2.0	14395	15549	2198
5.0	13360	14416	1971

However, upstream from the confluence, within the zone of mutual influence of the two rivers, the design discharges for levee sizing are not those defined in Tables 7.2a-7.2f, but are derived quantities that depend on the strength of flood coincidence of the Danube and its tributaries. In principle, the best approach is to adopt the most probable constellation of variable coincidences of the discharges of the Danube and the tributary, from the coincidence exceedance curve, for the selected safety level (i.e. return period).

In the specific case, flood coincidences of the Danube and the tributaries were calculated for the following constellations of variables:

a) The Danube upstream from the mouth of a tributary:

- maximum annual discharge at the HS upstream from the confluence – maximum annual discharge at the HS downstream from the confluence (QIN_{max}; $QOUT_{max}$) ≡ (*IMOM*),
- maximum annual discharge at the HS upstream from the confluence – corresponding discharge at the HS downstream from the confluence (QIN_{max}; $QOUT_{cor1}$) ≡ (*IMOC*),
- corresponding discharge at the HS upstream from the confluence – maximum annual discharge at the HS downstream from the confluence (QIN_{cor1}; $QOUT_{max}$) ≡ (*ICOM*).

b) A reach of the Danube that includes a tributary:

- maximum annual discharge at the HS upstream from the confluence – maximum annual discharge at the HS on the tributary (QIN_{max}; qTR_{max}) ≡ (*IMTM*),
- maximum annual discharge at the HS upstream from the confluence – corresponding discharge at the HS on the tributary (QIN_{max}; qTR_{cor1}) ≡ (*IMTC*),
- corresponding discharge at the HS upstream from the confluence – maximum annual discharge at the HS on the tributary (QIN_{cor2}; qTR_{max}) ≡ (*ICTM*),
- maximum annual discharge at the HS downstream from the confluence – maximum annual discharge at the HS on the tributary ($QOUT_{max}$; qTR_{max}) ≡ (*OMTM*),
- maximum annual discharge at the HS downstream from the confluence – corresponding discharge at the HS on the tributary ($QOUT_{max}$; qTR_{cor2}) ≡ (*OMTC*),
- corresponding discharge at the HS downstream from the confluence – maximum annual discharge at the HS on the tributary ($QOUT_{cor2}$; qTR_{max}) ≡ (*OCTM*).

The results of flood coincidence calculations relating to the Danube and its considered tributaries are graphically represented, by node, in Appendices 7.1.1 through 7.6.3. The graphics show the lines of the same probabilities of occurrence (density functions), lines of exceedance probabilities (distribution functions), and empirical points.

For an assessment of the statistical significance of the calculated variable flood coincidences of the Danube and the tributaries, Tables 7.3a through 7.3f show the main indicators of the strength of the established coincidence correlations by node, including the coefficient of linear correlation and standard correlation coefficient error.

Table 7.3a Statistical significance of the considered constellations of variables: NODE 1

HS	Constellation of variables	R	N	σ	3σ	Statistical significance
Hofkirchen – Achleiten	max – max	0.73588	77	0.052249	0.156746	YES
	max – cor	0.80014	77	0.041000	0.123001	YES
	cor – max	0.52810	77	0.082178	0.246534	YES
Hofkirchen – P-Ingling	max – max	0.38154	77	0.097371	0.292113	YES
	max – cor	0.32281	77	0.102085	0.306256	YES
	cor – max	0.47562	77	0.088181	0.264543	YES
P-Ingling – Achleiten	max – max	0.8228	77	0.036809	0.110428	YES
	cor – max	0.71332	77	0.055975	0.167924	YES
	max –cor	0.88298	77	0.025111	0.075332	YES

Table 7.3b Statistical significance of the considered constellations of variables: NODE 2

HS	Constellation of variables	R	N	σ	3σ	Statistical significance
Vienna – Bratislava	max – max	0.94317	76	0.012667	0.03800	YES
	max – cor	0.92648	76	0.016247	0.04874	YES
	cor – max	0.90409	76	0.020948	0.062844	YES
Vienna – Moravsky Jan	max – max	0.28541	76	0.105364	0.316092	NO
	max – cor	-0.12899	76	0.112799	0.338398	NO
	cor – max	0.20391	76	0.109938	0.329815	NO
Moravsky Jan – Bratislava	max – max	0.32463	77	0.101951	0.305853	YES
	cor – max	0.02115	77	0.11391	0.341729	NO
	max –cor	0.18261	84	0.105471	0.316412	NO

Table 7.3c Statistical significance of the considered constellations of variables: NODE 3

HS	Constellation of variables	R	N	σ	3σ	Statistical significance
Bezdan – Bogojevo	max – max	0.9371	79	0.013708	0.041125	YES
	max – cor	0.91809	79	0.017676	0.053029	YES
	cor – max	0.8561	79	0.03005	0.090151	YES
Bezdan – Donji Miholjac	max – max	0.18000	79	0.10886	0.32659	NO
	max – cor	0.15869	79	0.10968	0.32903	NO
	cor – max	0.45369	79	0.08935	0.26805	YES
Donji Miholjac – Bogojevo	max – max	0.33104	79	0.10018	0.30054	YES
	cor – max	0.24087	79	0.10598	0.31794	NO
	max –cor	0.45362	79	0.089358	0.268073	YES

Table 7.3d Statistical significance of the considered constellations of variables: NODE 4

HS	Constellation of variables	*R*	*N*	σ	3σ	Statistical significance
Bogojevo – Slankamen	max – max	0.86771	82	0.02729	0.08186	YES
	max – cor	0.79096	82	0.04134	0.12403	YES
	cor – max	0.80042	82	0.03968	0.11904	YES
Bogojevo – Senta	max – max	0.59386	82	0.07149	0.21446	YES
	max – cor	0.43787	82	0.08926	0.26778	YES
	cor – max	0.68209	82	0.05905	0.17716	YES
Senta – Slankamen	max – max	0.33375	82	0.09813	0.29439	YES
	cor – max	0.23267	82	0.10445	0.31336	NO
	max –cor	0.37304	82	0.09506	0.28519	YES

Table 7.3e Statistical significance of the considered constellations of variables: NODE 5

HS	Constellation of variables	*R*	*N*	σ	3σ	Statistical significance
Slankamen – Smederevo	max – max	0.74211	84	0.04902	0.14706	YES
	max – cor	0.73926	84	0.04948	0.14844	YES
	cor – max	0.81051	84	0.03743	0.11230	YES
Slankamen – Sremska Mitrovica	max – max	0.40038	84	0.09162	0.27485	YES
	max – cor	0.16693	84	0.10607	0.31821	NO
	cor – max	0.16444	83	0.10680	0.32039	NO
Sremska Mitrovica - Smederevo	max – max	0.73926	84	0.04948	0.14844	YES
	cor – max	0.43624	84	0.08834	0.26503	YES
	max –cor	0.44814	84	0.08720	0.26159	YES

Table 7.3f Statistical significance of the considered constellations of variables: NODE 6

HS	Constellation of variables	*R*	*N*	σ	3σ	Statistical significance
Smederevo – Veliko Gradište	max – max	0.96989	84	0.006472	0.019415	YES
	max – cor	0.91679	84	0.017402	0.052207	YES
	cor – max	0.96331	84	0.00786	0.023579	YES
Smederevo – Ljubičevski Most	max – max	0.55763	84	0.075181	0.225544	YES
	max – cor	0.36099	84	0.094891	0.284672	YES
	cor – max	0.40062	84	0.091597	0.274792	YES
Ljubičevski Most – Veliko Gradište	max – max	0.55411	84	0.075608	0.226825	YES
	cor – max	0.43426	84	0.088533	0.265599	YES
	max –cor	0.46185	84	0.085835	0.257506	YES

The general conclusion is that in 78% of the cases there are statistically significant flood coincidences of the Danube and its tributaries. A coincidence is statistically significant in all constellations between the input (*IN*) and output (*OUT*) cross-sections, as well as in constellations of maximum discharges at the output (*OUT*) cross-sections and the tributaries (*TR*). In the constellations of maximum discharges at input (*IN*) cross-sections and of the tributaries (TR), as well as maximum discharges of the tributaries (*TR*) and corresponding discharges at the output (*OUT*) cross-sections of the Danube, the coincidences are statistically significant in 67% of the cases. In the constellations of maximum discharges of the Danube at the input (*IN*) and output (*OUT*) cross-sections, and the corresponding discharges of the tributaries (*TR*), the coincidences are statistically significant in 50% of the cases.

7.3.2 Selection of design discharges for water level lines when data are available from all three gauging stations

The quantitative indicators of the calculated discharges of different flood coincidence probabilities for the Danube and the tributaries, needed for defining design water levels in the extended zone of the confluence (Section 7.2.3), are shown in Tables 7.4a through 7.4f.

Table 7.4a Design discharges of different flood coincidence probabilities for the Danube and the Inn – NODE 1

p(%)	HS Hofkirchen			HS Achleiten			HS Ingling		
	$Q^{H}_{max,p}$	$Q^{A}_{cor1,p}$	$Q^{I}_{cor1,p}$	$Q^{A}_{max,p}$	$Q^{H}_{cor1,p}$	$Q^{I}_{cor2,p}$	$Q^{I}_{max,p}$	$Q^{H}_{cor2,p}$	$Q^{A}_{cor2,p}$
0.1	6359	6000	1800	10869	1500	5500	8440	1000	6200
1.0	4353	4700	1150	7925	1200	3100	6138	800	4600
2.0	3840	4200	1000	7155	1100	2500	5517	700	4000
5.0	2944	3300	800	6274	950	2050	4734	600	3500

Table 7.4b Design discharges of different flood coincidence probabilities for the Danube and the Morava – NODE 2

p(%)	HS Wien			HS Bratislava			HS Moravsky Jan		
	$Q^{W}_{max,p}$	$Q^{B}_{cor1,p}$	$Q^{MJ}_{cor1,p}$	$Q^{B}_{max,p}$	$Q^{W}_{cor1,p}$	$Q^{MJ}_{cor2,p}$	$Q^{MJ}_{max,p}$	$Q^{W}_{cor2,p}$	$Q^{B}_{cor2,p}$
0.1	12610	6000	31	14328	6500	22	2170	2100	2500
1.0	9847	5800	30	11192	6100	19	1541	1700	1800
2.0	9046	5500	29	10273	5700	17.5	1362	1550	1600
5.0	8463	5300	28	8890	5100	16	1131	1250	1500

Table 7.4c Design discharges of different flood coincidence probabilities for the Danube and the Drava – NODE 3

p%	HS Bezdan			HS Bogojevo			HS Donji Miholjac		
	$Q^{Bez}_{max,p}$	$Q^{Bog}_{cor1,p}$	$Q^{DM}_{cor1,p}$	$Q^{Bog}_{max,p}$	$Q^{Bez}_{cor1,p}$	$Q^{DM}_{cor2,p}$	$Q^{DM}_{max,p}$	$Q^{Bog}_{cor2,p}$	$Q^{Bez}_{cor2,p}$
0.1	10435	9500	1000	11418	7800	1100	3258	5700	4000
1.0	8437	7300	500	9418	6500	700	2542	4000	3000
2.0	7847	6750	460	8810	6150	600	2336	3500	2800
5.0	7029	6000	400	7912	5800	500	2064	3000	2500

Table 7.4d Design discharges of different flood coincidence probabilities for the Danube and the Tisa – NODE 4

p%	HS Bogojevo			HS Slankamen			HS Senta		
	$Q^{Bog}_{max,p}$	$Q^{Sla}_{cor1,p}$	$Q^{St}_{cor1,p}$	$Q^{Sla}_{max,p}$	$Q^{Bez}_{cor1,p}$	$Q^{St}_{cor2,p}$	$Q^{St}_{max,p}$	$Q^{Bog}_{cor2,p}$	$Q^{Sla}_{cor2,p}$
0.1	11418	10000	1450	12940	6000	1340	4611	6600	10200
1.0	9418	8600	1000	10869	5000	1200	3847	4650	8500
2.0	8810	8100	910	10236	4650	1160	3598	4000	7900
5.0	7918	7500	900	9374	4500	1110	3248	3630	7100

Table 7.4e Design discharges of different flood coincidence probabilities for the Danube and the Sava – NODE 5

p%	HS Slankamen			HS Smederevo			HS Sremska Mitrovica		
	$Q^{Sla}_{max,p}$	$Q^{SD}_{cor1,p}$	$Q^{SM}_{cor1,p}$	$Q^{SD}_{max,p}$	$Q^{Sla}_{cor1,p}$	$Q^{SM}_{cor2,p}$	$Q^{SM}_{max,p}$	$Q^{Sla}_{cor2,p}$	$Q^{SD}_{cor2,p}$
0.1	13203	12000	1850	17381	12200	3800	7813/7781	8300	5800
1.0	11043	9700	1310	15128	9000	3200	6589/6581	7700	4000
2.0	10385	9250	1150	14395	8200	3000	6211/6209	7100	3500
5.0	9492	9000	1000	13360	7100	2800	5695/5699	6800	3000

Table 7.4f Design discharges of different flood coincidence probabilities for the Danube and the Velika Morava – NODE 6

p(%)	HS Smederevo			HS Veliko Gradište			HS Ljubičevski most		
	$Q^{SD}_{max,p}$	$Q^{VG}_{cor1,p}$	$Q^{LjM}_{cor1,p}$	$Q^{VG}_{max,p}$	$Q^{SD}_{cor1,p}$	$Q^{LjM}_{cor2,p}$	$Q^{LjM}_{max,p}$	$Q^{SD}_{cor2,p}$	$Q^{VG}_{cor2,p}$
0.1	17381	17200	650	18809	15000	700	2829	14000	15000
1.0	15128	15200	400	16351	13000	500	2356	11200	12000
2.0	14395	14400	350	15549	12500	400	2198	9500	10500
5.0	13360	12500	300	14416	11500	330	1971	7500	8500

In practical terms, the results of probability coincidence analysis (Tables 7.4a – 7.4f), in the case of sizing of levees in the extended area of the confluence of the Danube and a tributary, for example NODE 2 and a safety level that corresponds to a 100-year return period, are used as follows:

For the reach of *the Danube from HS Bratislava to the mouth of the Morava*, the design discharge is $Q^{B}_{max,p=1\%} = 11192$ m^3/s
The selection of design discharges within the zone of mutual influence of flood discharges of the Danube and the Morava depends on the degree of their coincidence.

For the reach of *the Danube upstream from the mouth of the Morava*, within the zone of influence of the Danube and the Morava, the design water level is an envelope of maximum water levels obtained by calculations of the water level line, based on the following combinations of variables:

- 100-year maximum discharge of the Danube downstream from the mouth of the Morava, or $Q^{B}_{max,p} = 11192$ m^3/s in this specific case, and the corresponding discharge of the Danube upstream from the mouth of the Morava, for the same 100-year exceedance probability (coincidence), from the graphic of (Q^{W}_{cor}; Q^{B}_{max}), which amounts to $Q^{W}_{cor1,p=1\%} = 6100$ m^3/s, and

- corresponding discharge of the Danube downstream from the mouth of the Morava and maximum annual discharge of the Danube upstream from the mouth of the Morava, for a 100-year coincidence probability from the graphic (Q^B_{cor}; Q^W_{max}), which amount to (Q^B_{cor} = 5800 m^3/s and ($Q^W_{max,1\%}$ = 9847 m^3/s) in the specific case.

The adopted design discharges for calculating the 100-year water level for the entire sector of the Danube from HS Bratislava to the mouth of the Morava and upstream from the mouth of the Morava to HS Vienna are shown in Fig. 7.4/1.

For the sector of the *Morava River upstream from its mouth*, within the zone of mutual influence of the Danube and the Morava, the design water level is an envelope of maximum water levels obtained by calculations of the water level line, based on the following combinations of discharge variables:

- 100-year maximum discharge of the Danube upstream from the mouth of the Morava, which is $Q^B_{max,p}$ = 11192 m^3/s, and corresponding discharge of the Morava upstream from its mouth, for the same 100-year exceedance (coincidence) probability, from the graphic of (Q^{MJ}_{cor}; Q^B_{max}), amounting to (Q^{MJ}_{cor} = 19 m^3/s), and
- corresponding discharge of the Danube downstream from the mouth of the Morava and maximum annual discharge of the Morava upstream from its mouth, for a 100-year coincidence probability, from the graphic (Q^{MJ}_{max}; Q^B_{cor}), or in the specific case ($Q^{MJ}_{max,1\%}$ = 1541 m^3/s) and (Q^B_{cor} = 1800 m^3/s).

The adopted design discharges for calculating the 100-year water surface of the Morava upstream from its mouth, at HS Moravsky Jan, are schematically represented in Fig. 7.4/2.

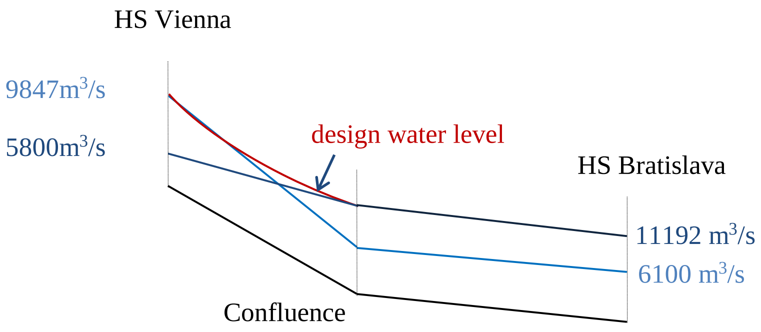

Fig. 7.4/1. Maximum design discharges for calculating the 100-year water level of the Danube within the zone of the mouth of the Morava.

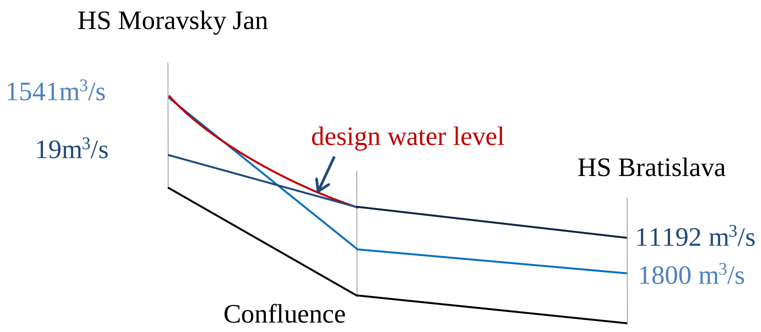

Fig. 7.4/2 Maximum design discharges for calculating 100-year water stages along the Danube to the mouth of the Morava and up the Morava to HS Moravsky Jan.

7.3.3 Calculation of the design flood discharge at an undergauged cross-section of the recipient

An example of flood calculations for undergauged river cross-sections is described below, only for Node 2. In the specific case, applying the proposed procedure for calculating the coincidence of flood waves to define design water levels at an undergauged cross-section, the assumption is that there are only two hydrological stations in the considered sector of the Danube and its tributary, the Morava – at Bratislava and Moravsky Jan, and that for the downstream reach, after the mouth of the Inn, there are no observation data from HS Vienna.

Given these conditions, the results of coincidence calculations only for those constellations of variables that pertain to HS Bratislava and HS Moravsky Jan are used. In the specific case, the coincidences are:

- maximum annual discharge of the Danube at HS Bratislava – corresponding discharge of the Morava at HS Moravsky Jan, (Q^{B}_{max}; Q^{MJ}_{cor2}), and
- maximum annual discharge of the Morava at HS Moravsky Jan – corresponding discharge of the Danube at HS Bratislava, (Q^{MJ}_{max} ; Q^{B}_{cor2}).

The analysis of the theoretical values of maximum design discharges of the Danube at the "non-existent" HS Vienna, for the probabilities of occurrence p = 0.1, 1.0 and 5.0 %, is shown in Table 7.4.

The results lead to the conclusion that the proposed methodology for flood coincidence calculations is also suitable for defining theoretical maximum discharges, of certain probabilities of occurrence, in the downstream sector of the recipient, after the mouth of the tributary, if time-series of daily and maximum annual discharges are available from both input cross-sections, in the upstream sector.

In the following example of maximum annual discharges of the Danube at "non-existent" HS Vienna (Table 7.5, Figs. 7.2.3/2. and 7.2.3/3. in Appendix 7.2.3), the assumption is that data are available only from HS Bratislava on the Danube and HS Moravsky Jan on the Morava. The theoretical values of maximum annual discharges of the Danube at "non-existent" HS Vienna were derived using the defined coincidence functions and they agree relatively well with the results of the conventional probabilistic analysis whose results are shown in Table 7.1. The differences between the theoretical values via coincidence and the statistical analysis are minimal; the errors range from 1.6% (20-year return period) to +6.1% (100-year return period).

Table 7.5 Theoretical discharges of the Danube at "non-existent" HS Vienna for different probabilities of occurrence

Constellation	Variables	5%			1%			0.1%		
		Points		∑∑	Points		∑∑	Points		∑∑
		1	2		1	2		1	2	
(Q^{B}_{max};$Q^{MJ}_{cor.1}$)	Q^{B}_{max}	8890	4600	13490	11192	5200	16392	14328	6000	20328
	$Q^{MJ}_{cor.1}$	16	239	255	19	404	423	22	732	754
	(-)			13235			15969			19574
(Q^{MJ}_{max};$Q^{B}_{cor.2}$)	Q^{MJI}_{max}	1131	200	1331	1549	300	1849	2170	400	2570
	$Q^{B}_{cor.2}$	1500	3796	5296	1800	5030	6830	2500	6963	9463
	(-)			3965			4931			6893
	∑(-)			17200			20900			26467
	∑(-)/2			**8600**			**10450**			**13233**
Vienna										
	$Q^{V}_{max,gauged}$			**8463**			**9847**			**12610**
	$\Delta Q_{max,p}$ (%)			**+1.6**			**+6.1**			**+4.9**

7.3.4 Calculations of flood coincidence and assessment of statistical significance of historic floods

As part of this project, it was interesting to analyze the return periods of exceedance probabilities of the July 1954 and June 2013 floods in Bratislava.

The probability of exceedance of the constellation of maximum annual discharges of the Danube at Bratislava and the corresponding discharge of the Morava at HS Moravsky Jan in 2013 is (Fig. 7.5):

$$P\{(Q^{B}_{max}\geq 10640)\cap (Q^{MJ}_{cor2}\geq 52.34)\} = 0.009,$$

or the return period is:

$$T = \frac{1}{P} = \frac{1}{0.009} = 111 \text{ years}$$

The probability of exceedance of the constellation of maximum annual discharges of the Danube at Bratislava and the corresponding discharge of the Morava at Moravsky Jan in 1954 is (Fig. 7.5):

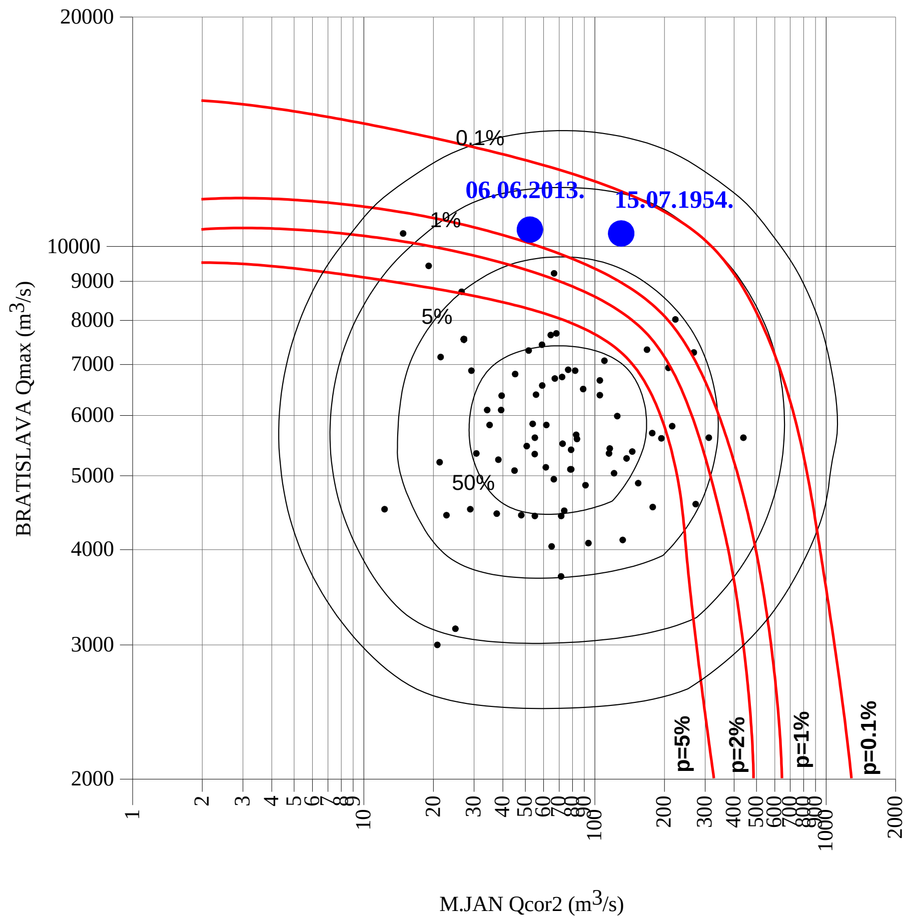

Fig. 7.5. *Coincidence of maximum annual discharge of the Danube at HS Bratislava and corresponding discharges of the Morava at HS Moravsky Jan, for two flood events at HS Bratislava on the Danube.*

$P\{(Q^{B}_{max}\geq 10400)\cap(Q^{MJ}_{cor2}\geq 130)\} = 0.005$,

or the return period is:

$$T = \frac{1}{P} = \frac{1}{0.005} = 200 \text{ years}$$

Consequently, from a statistical significance perspective, considering a simultaneous occurrence of maximum annual discharges of the Danube at HS Bratislava and corresponding discharge of the Morava at HS Moravsky Jan, which is important for flood protection, the most significant flood waves were recorded in July 1954 (200-year event) and June 2013 (100-year event), even though when viewed individually, both maximum discharges of the Danube at HS Bratislava are below the 100-year return period level.

7.4 Conclusions

The importance of the results of coincidence analyses is multi-faceted. First, they can be used to **assess the statistical significance of the coincidence of different flood hydrograph parameters** in the extended zone of a river confluence, and thereby of the flood event as a whole, on both the recipient and its main tributaries. The practical importance of these results is that if there is no coincidence, the level of flood protection in the zone of mutual influence of the recipient and the tributary can be reduced, relative to the conventional one-dimensional structural sizing procedure, while retaining the same level of protection from a flood risk perspective. Second, the proposed methodology for coincidence calculations **provides quantitative design indicators of optimal combinations of the considered random variables,** from economic and structural safety standpoints. Third, the results can be used to **define design water levels at river confluences,** in cases where there is no (appropriate) data from an input or the output gauging station.

References

Abramowitz, M., Stegun, A., I., 1972: *Handbook of Mathematical Functions with Formulas*, Graphs and Mathematical Tables, Dover Publications, INC., New York.

Prohaska, S., Marjanović, N., Čabrić, M., 1978: *Dvoparametarsko definiranje velikih voda,* Vode Vojvodine, Novi Sad.

Prohaska S., Isailović D., Srna P., Marčetić I. (1999): *The Danube and its Basin – A Hydrological Monograph Follow-up volume IV,* Coincidence of Flood Flow of the Danube River and its Tributaries, Regional Co-operation of the Danube Countries in the Frame of the International Hydrological Programme of UNESCO, pp 1-187, Water Research Institute Bratislava, Slovakia.

Prohaska S. (2006) *Hidrologija II deo*, Institut za vodoprivredu "Jaroslav Černi", Rudarsko-geološki fakultet i RHMZ Srbije, Beograd.

Prohaska S., Ilić A.: *Coincidence of the Probability of Flood Waves*, International Conference "Planning and Management of Water Resources Systems", Organized to celebrate the 50th anniversary of the scientific and educational work, and the 75th birthday of Prof. Dr. Milorad Miloradov, 25-27 September 2008, Novi Sad, pp. 171-183, 2008.

Prohaska S., Ilic A.: *Coincidence of Flood Flow of the Danube River and Its Tributaries*, (In: Mitja Brilly (Ed.): Hydrological Processes of the Danube River Basin - Perspectives from the Danubian Countries), Publisher: Springer, ISBN 978-90-481-3422-9, Book Chapter 6, p. 175-226, 2010. DOI: 10.1007/978-90-481-3423-6_6

Yevjevich, V., 1972: *Probability and Statistics in Hydrology*; Water Resources Publications, Fort Collins, Colo. U.S.A.

8 Theoretical design hydrographs at the hydrological gauging stations along the Danube River

Stevan Prohaska, and Aleksandra Ilić

8.1 Introduction

Design flood hydrographs of different probabilities of occurrence at river gauging stations, where long-term time-series are available, are a very important consideration in hydrological engineering. Various approaches have been used to date in Serbia and elsewhere, with no clear position as to which approach is the most effective in practice. The essence of all these approaches is to first define the maximum hydrograph ordinate (flood wave peak) on the basis of available time-series of maximum annual flows, applying different theoretical probability distribution functions. Various procedures are used to assess the second very important parameter of flood hydrographs (flood wave volume), often derived from the calculated time to the maximum hydrograph ordinate, precipitation retention time in the basin, time of concentration, and the like. These temporal parameters are generally calculated using empirical equations from literature, which are often not verified for the climate, physical and geographic characteristics of the considered basin.

Estimation of the design river flood is the first step in flood risk assessment, design of hydraulic structures, and development of flood risk management strategies.

Risk management requires a multi-dimensional analysis and a trade-off between the cost, benefit and risk. There is an aspiration to come up with new metrics for risk assessment, founded upon multiple probabilistic analysis, in addition to the approach based on expectations, which has been the only measure of risk in the past (Haimes, Lambert, Li, 1992). To determine a value that must not be exceeded, in the case of flood flow, the standard procedure has been one-dimensional probabilistic analysis of extreme events (flood wave peak). This approach is justifiable where only one variable is important for the structural design or where there is no apparent correlation between the considered parameters (Chebana, 2013).

A review of available methods leads to the conclusion that larger strides have been made in data collection and description of processes that cause floods, so it is safe to say that more progress has been made in the analytical sense than in the assessment of floods as a complex phenomenon (Singh and Strupczewsky, 2002).

Problems related to extreme events in nature are multi-dimensional and procedures that maximize the use of data and at the same time assess parameters of a complex phenomenon, as well as their correlation and ultimately the probability of occurrence, have not been developed to a level that enables relatively easy application in practice. As a result, the World Meteorological Organization proposed in 1988 the transformation of marginal probabilities, which usually do not follow normal distribution, in order to form a normal multiple distribution of probabilities. This approach has been followed in many studies that address common probabilities (conditional probabilities) of flood hydrograph parameters, particularly peak and volume (Adamson, Metcalfe, Parmentier, 1999). The concept of conditional probability distribution is also presented in detail in (Yue and Rasmussen, 2002).

Subsequently, Singh and Strupczewsky (2007) emphasized the need to consider common exceedance probabilities of different flood hydrograph parameters. They discuss the role of assessing the correlation between flood wave peak and volume in modeling of urban flood protection systems. Many attempts have been made to show in the most adequate way the correlations between runoff hydrograph parameters and construct probability distributions in multidimensional space.

Probability distribution quantile calculations in multidimensional space allow different combinations of variables that yield the same risk (Chebana, Ouarda, 2011).

In view of all the above, the authors of this Chapter have developed a comprehensive approach for assessing theoretical flood hydrographs at river gauging stations, where all the parameters are calibrated based on recorded data, in the specific case time-series of maximum annual flows and maximum flood wave volumes, as well as observed flood wave shapes. In essence, the "limited runoff intensity method" (LRIM) is used to produce theoretical flood hydrographs. LRIM parameters are calibrated with equated theoretical maximum annual flows and maximum annual volumes of the same probability of occurrence, that is, the standard procedure for fitting time-series to theoretical distribution functions, commonly used in hydrological engineering. Characteristic points of the selected exceedance probability from the predefined two-dimensional probability distribution (or coincidence of the main parameters of the flood hydrograph) are used to select the best combinations of the hydrograph parameters, maximum ordinates and volumes of flood waves.

The Chapter describes the methods applied to assess flood hydrographs and coincidence of parameters. A practical example is presented, where the proposed approach is applied to assess theoretical flood hydrographs of the Danube River at several selected official gauging stations.

8.2 Theoretical background of the proposed approach in the case of gauged watersheds

Design flood hydrographs are theoretical hydrographs of different probabilities of occurrence, whose parameters (maximum ordinate and maximum flood wave volume) correspond to different and/or the same theoretical values of these parameters derived by applying the conventional statistical-probabilistic approach.

Design flood hydrographs at gauging stations are defined where perennial time-series are available for maximum annual flows, maximum flood wave volumes, and recorded hydrograph shapes. The flow and volume time-series are used to define the theoretical values of these parameters for different probabilities of occurrence (return periods). Flood hydrograph records from limnigraph stations (continuous monitoring) or gauging stations (one-day time step) are used to define hydrograph shapes.

The main flood hydrograph parameters and the hydrograph shape are basically determined applying the *limited runoff intensity method* (LRIM). The LRIM procedure is described in more detail in the literature (Prohaska, 2006).

The LRIM starting point is the application of the rational theory of river runoff, according to which the maximum flow of probability of occurrence $p(Q_{max,p})$ is computed from the formula:

$$Q_{\max,p} = 16{,}67 \cdot \bar{i}_{\max,p}(\tau) \cdot \varphi \cdot F \tag{8.1}$$

where:
$Q_{max,p}$ – maximum hydrograph ordinate of probability p in m^3/s,
$\bar{i}_{\max,p}(\tau)$ – maximum average rainfall intensity of design rainfall duration τ,
φ – total runoff coefficient,
F – catchment area in km^2.
τ – time of concentration, in minutes.

According to the LRIM theory, the design rainfall duration τ is equal to the time of concentration τ_p, which is in a causal relationship with the maximum hydrograph ordinate $Q_{max,p}$ in the form of:

$$\tau_p = \frac{16.67 \cdot K \cdot L}{a \cdot I_{ur}^{1/3} \cdot Q_{\max,p}^{1/4}} \tag{8.2}$$

where:
τ_p – time of concentration in minutes,
K – rising to falling limb time ratio,
a – coefficient dependent on riverbed roughness and weighted channel slope,
L – length of main stream in km,
I_{ur} – weighted channel slope in ‰.

Maximum daily precipitation data and the main properties of heavy-rainfall duration curves from pluviograph stations are used to calculate the maximum average rainfall intensity $\bar{i}_{\max,p}(\tau)$, as:

$$\bar{i}_{\max,p}(\tau) = \frac{\psi_p(\tau)}{\tau} \cdot H_{\max,dn,p} = \overline{\psi_p}(\tau) \cdot H_{\max,dn,p} \tag{8.3}$$

where:
τ – rainfall duration in minutes, and
$\psi_p(\tau)$ – maximum rainfall depth reduction curve ordinate of probability p for rainfall duration τ, calculated from:

$$\psi_p(\tau) = \frac{H(\tau)_p}{H_{\max,dn,p}} \tag{8.4}$$

where:
$H(\tau)_p$ – theoretical rainfall depth for rainfall duration of probability p,
$H_{max,dy,p}$ – theoretical maximum daily precipitation total of probability p,
$\overline{\psi_p}(\tau)$ – maximum average rainfall reduction curve ordinate for rainfall duration τ.
The flood wave volume is estimated applying the equation:

$$W_p = 1000 \cdot h_p \cdot F \tag{8.5}$$

where:

W_p – flood wave hydrograph volume of probability p,

h_p – runoff depth in (mm),

$$h_p = (\varphi H)_p \cdot \psi_p(\tau) . \tag{8.6}$$

The flood hydrograph ordinates $Q_{p,i}$ (i=1,2,3,...,T_B, T_B – hydrograph time base) are calculated according to the Goodrich law of distribution:

$$Q_{p,i} = Q_{\max,p} \cdot 10^{-a\frac{1-X_i}{X_i}} \tag{8.7}$$

$$T_p = B_p \cdot \frac{0.278 \cdot \lambda^* \cdot h_p}{q_{\max,p}} \tag{8.8}$$

where:

$X_i = \frac{t_i}{T_p}$ – relative abscissa of the hydrograph,

T_p – conditional hydrograph rising limb time of probability p,

$q_{max,p}$ – maximum runoff modulus (m^3/s/km^2),

$q_{\max,p} = \frac{Q_{\max,p}}{F}$,

a – parameter that depends on the skewness coefficient of the hydrograph K_s, or the coefficient of the hydrograph shape λ^*,

$K_S = \frac{1}{1+K}$,

$\lambda^* = \frac{Q_{\max,p} \cdot T_P}{W_{por}}$

B_p – coefficient to be calibrated,

W_{por}– volume under rising hydrograph limb.

The correlations among a, λ^* and K_s are discussed in the literature (Prohaska and Ristić, 2002).

According to the theoretical background, the conclusion is that the main parameters calibrated applying LRIM are: ***K*** – rising to falling limb time ratio, ***a*** – coefficient that depends on riverbed roughness and weighted channel slope, and B_p– coefficient.

A predefined bivariate (two-dimensional) probability distribution of the main hydrograph parameters – flood wave peak and volume – serves as a basis for selecting the combinations of characteristic parameters for which the design hydrographs are defined. The hydrograph shape parameters are determined from flood hydrographs actually recorded by the considered gauging station. In the present case, the bivariate distribution function was defined applying the grapho-analytical procedure (Abramowitz and Stegun, 1972); details are available in the literature (Prohaska et al., 1999) and (Prohaska and Ilić, 2010).

The theory is based on practical application of bivariate normal distribution functions of two random variables, X and Y. In essence, the bivariate normal distribution is a distribution whose probability density is defined as (Prohaska et al., 1978):

$$f(x,y) = \frac{1}{2\pi \cdot \sigma_x \cdot \sigma_y \cdot \sqrt{1-\rho^2}} \cdot e^{-\frac{1}{2\cdot\left(1-\rho^2\right)}\cdot\left[\frac{(x-\mu_x)^2}{\sigma_x^2} - \frac{2\rho\cdot(x-\mu_x)\cdot(y-\mu_y)}{\sigma_x\cdot\sigma_y} + \frac{(y-\mu_y)^2}{\sigma_y^2}\right]} \quad (8.9)$$

where:

x and y – instantaneous occurrence of random variables X and Y, respectively;

μ_x and μ_y – mathematical expectations of X and Y;

σ_x and σ_y – standard deviations of X and Y;

ρ – coefficient of correlation of X and Y.

To determine the distribution density function, $f(x, y)$, the first step is to derive marginal probabilities $f(x,\bullet)$ and $f(\bullet,y)$ as:

$$f(x,\bullet) = \int_{y=-\infty}^{y=\infty} f(x,y)dy \tag{8.10}$$

$$f(\bullet,y) = \int_{x=-\infty}^{x=\infty} f(x,y)dx \tag{8.11}$$

Then their cumulative probabilities are:

$$F(x,\bullet) = \int_{t=-\infty}^{t=x} f(t,\bullet)dt \tag{8.12}$$

and

$$F(x,\bullet) = \int_{t=-\infty}^{t=x} f(t,\bullet)dt \tag{8.13}$$

The cumulative probability distribution function, $F(x, y)$, is defined as:

$$F(x,y) = P[X \le x \cap Y \le y] = \int_{t=-\infty}^{t=x} \int_{z=-\infty}^{z=y} f(t,z)dtdz \tag{8.14}$$

The subsequent step is to determine the exceedance probability $\Phi(x, y)$ in bivariate probability space (Prohaska et al., 1978):

$$\begin{aligned}\Phi(x,y) &= \int_{t=x}^{t=+\infty} \int_{z=y}^{z=+\infty} f(t,z)dtdz = P[X > x \cap Y > y] = 1 - P[X < x \cup Y < y] = \\ &= 1 - F(x,\bullet) - F(\bullet,y) + F(x,y)\end{aligned} \tag{8.15}$$

Bivariate probability distribution in statistical analysis of various flood hydrograph parameters requires simplification for the above-described procedure to be applicable.

The main simplification pertains to the assumption that each of the considered hydrograph parameters follows the normal (log-normal) distribution law, which may not be the case.

The established bivariate distribution function, or the coincidence of the main flood hydrograph parameters, is statistically significant if the inequality (Yevjevich, 1972):

$|R| \ge 3\sigma_R$ is true. (8.16)

8.3 Selection of hydrological stations for defining the theoretical flood hydrographs along the Danube River

In order to practically apply the elaborated methodology for defining the theoretical flood hydrographs, the main hydrological stations along the Danube River were selected from the spring to the dam "Djerdap 1". An overview of selected hydrological stations with information on the position, basin size and length of the observation period for which the necessary hydrological data have been collected is given in Table 8.1.

Table 8.1 Selected hydrological stations with information on the position, basin size and observation period length along the Danube River

No.	Hydrological station	Kilometers	Basin size in km^2	Observation period	Country
1.	Berg	2613	4047	1930-2007	GE
2.	Ingolstadt	2458.3	20001	1940-2007	GE
3.	Regensburg	2376.1	35599	1924-2007	GE
4.	Hofkirchen	2256.9	47496	1826-2013	GE
5.	Achleiten	2150	76653	1901-2007	GE
6.	Wien	1934.1	101731	1828-2006	AT
7.	Bratislava	1868.8	131338	1876-2013	SK
8.	Bezdan	1425.5	210250	1940-2006	SR
9.	Bogojevo	1367.4	251593	1940-2006	SR
10.	Pančevo	1153.3	525009	1940-2006	SR
11.	Oršava	955	576232	1840-2007	RO

Data on mean daily flows and absolute maximum annual flows have been collected for all the mentioned hydrological stations. Based on the data on mean daily flows, corresponding flood wave hydrographs have been identified and their volumes were calculated. In this way were formed the time series of maximum annual flows and the volumes of flood waves. Also, the ratio of increase and the parameters of hydrograph was determined at all the hydrological stations. The exact position of the selected hydrological stations in the Danube River Basin is shown in Figure 8.1.

Fig. 8.1 Sheme of water gauging stations along the Danube River (Fig. 6.2 in "Flood Regime of Rivers in the Danube River Basin").

8.4 Review of the calculation results of theoretical flood hydrographs at the considered profiles of hydrological stations

The exposed theoretical basis for the calculation of theoretical flood hydrographs was carried out at all the mentioned hydrological stations. The time series of maximum annual flows and maximum annual volumes were used, as well as the registered forms of historical flood waves. The theoretical values of random variables for different probability of occurrence are calculated using the conventional procedure of adjusting the theoretical probability distribution functions. The following distribution laws were used: Pirson III, Log Pirson III, Gumbel, Ln Normal 3, and Ln Normal 2. Adjustment quality was tested using the χ^2 test, the Kolmogorov-Smirnov and $n\omega^2$ test.

In order to define the coincidence of the considered main flood hydrograph parameters and to define the bivariate law of distribution of two random variables - the maximum annual flow and the maximum annual flood wave volume, the procedure shown in Section 8.2 of this chapter was used. The results of these calculations are presented graphically in the form of lines of the same probability of occurrence (bivariate density function) and lines of exceedance probability (bivariate distribution functions). The necessary hydrograph shape parameters were determined on the basis of the observed flood hydrographs.

8.4.1 Probability of occurrence of main flood hydrograph parameters

Regarding the analyzed distribution functions Log Pirson III and Pirson III for further analysis have been adopted the results (theoretical values) from distribution functions that better adapt to the empirical distributions (according to Alekseev), both for the series of maximum annual flows and maximum flood wave volumes. The results of these calculations are shown numerically in Table 8.2, as well as graphically in Appendix 8.1 (Figures 8.1.1/a-8.1.11/b), in which are presented the theoretical values, empirical probabilities and theoretical values of maximum annual flows taken from the Chapter 7.2.2 of project "Flood Regime of Rivers in the Danube River Basin" and marked with the FRDRB.

Table 8.2. Theoretical maximum annual flows and maximum flood wave volumes in the Danube River Basin

No	H. S.	Variable	Probability of occurrence p (%)					
			0.1	0.5	1.0	2.0	10.0	Distribution function
1	Berg	$Q_{max,p}$(m^3/s)	613	518	476	432	324	LPIII
			613	518	476	432	324	FRDRB
			626	522	479	435	323	LRIM
		$W_{max,p}$(10^6m^3)	642	550	509	466	357	LPIII
			642	550	509	449	357	LRIM

2	Inglostadt	$Q_{max,p(}m^3/s)$	2483	2142	1996	1850	1496	LPIII
			3043	2453	2222	2002	1526	FRDRB
			3044	2396	2160	1986	1498	LRIM
		$W_{max,p}(10^6m^3)$	3270	2723	2492	2263	1724	LPIII
			3268	2730	2501	2264	1733	LRIM
3	Regensburg	$Q_{max,p(}m^3/s)$	3081	2809	2675	2530	2125	LPIII
			4637	3761	3407	3065	2298	FRDRB
			4634	3758	3406	3063	2298	LRIM
		$W_{max,p}(10^6m^3)$	6191	5063	4594	4131	3061	PIII
			6186	5100	4594	4130	3085	LRIM
4	Hofkirchen	$Q_{max,p(}m^3/s)$	4222	3701	3469	3231	2631	LPIII
			6359	4905	4353	3840	2765	FRDRB
			6358	4979	4442	3859	2723	LRIM
		$W_{max,p}(10^6m^3)$	8487	7157	6576	5986	4608	PIII
			8499	7172	6620	5997	4528	LRIM
5	Achleiten	$Q_{max,p(}m^3/s)$	10810	8809	8022	7271	5632	LPIII
			10869	8744	7925	7155	5512	FRDRB
			10916	8763	7929	7183	5514	LRIM
		$W_{max,p}(10^6m^3)$	13786	12335	11651	10923	8975	LPIII
			14063	12623	11835	10862	8971	LRIM
6	Wien	$Q_{max,p(}m^3/s)$	12610	10658	9847	9046	7187	PLIII
			12610	10658	9847	9046	7187	FRDRB
			12626	10830	9776	9134	7253	LRIM
		$W_{max,p}(10^6m^3)$	18528	16194	15149	14069	11341	LPIII
			18603	16097	15143	14105	11395	LRIM
7	Bratislava	$Q_{max,p(}m^3/s)$	14190	12054	11154	10259	8149	LPIII
			14328	12119	11192	10273	8116	FRDRB
			14383	11953	11077	10263	8192	LRIM
		$W_{max,p}(10^6m^3)$	22304	19693	18501	17252	14013	PIII
			22307	19699	18509	17250	14003	LRIM
8	Bezdan	$Q_{max,p(}m^3/s)$	14490	9223	8656	8072	6614	PIII
			10435	9029	8437	7847	6452	FRDRB
			10421	9080	8445	7833	6455	LRIM
		$W_{max,p}(10^6m^3)$	36292	31980	30007	27939	22567	PIII
			36671	32067	30095	28027	22572	LRIM

9	Bogojevo	$Q_{max,p}$(m^3/s)	11137	9911	9358	8785	7332	PIII
			11418	10020	9418	8810	7334	FRDRB
			11410	10028	9405	8811	7328	LRIM
		$W_{max,p}$(10^6m^3)	39899	35692	33741	31674	26185	PIII
			39632	35320	33554	31310	25542	LRIM
10	Pančevo	$Q_{max,p}$(m^3/s)	17353	15753	15035	14289	12383	LPIII
			18105	16285	15483	14661	12611	FRDRB
			17986	16302	15406	14566	12724	LRIM
		$W_{max,p}$(10^6m^3)	86015	79232	75884	72182	61446	PIII
			88709	80570	75631	71940	61721	LRIM
11	Orsova	$Q_{max,p}$(m^3/s)	17550	16126	15463	14759	12879	LPIII
			17481	16094	15445	14754	12901	FRDRB
			17457	16095	15532	14805	12849	LRIM
		$W_{max,p}$(10^6m^3)	89343	83514	80556	77224	67208	PIII
			89466	83636	80684	77360	67124	LRIM

8.4.2 Bivariate probability (coincidence) of main flood hydrograph parameters

The bivariate probability law (coincidence) of the main flood hydrograph parameters (maximum annual flow and flood wave volume) at all the considered profiles of the gauging stations is defined with synchronous data of the same time series used in Section 8.4.1. The following functions were defined:
• Density functions (lines of the same bivariate probabilities of occurrence)

$$F(Q_{max}; W_{max}) = p$$

for probability p = 0.1, 1.0, 5.0 and 50%.
• Distribution functions (lines of bivariate exceedance probabilities)

$$P\{(Q_{max} \geq q_{max,P}) \cap (W_{max} \geq w_{max,P})\} = P \qquad (9.17)$$

for the exceedance probability P = 0.1, 1.0, 2.0 and 5.0%.

Graphical presentations of the calculated bivariate distribution function of the main flood hydrograph parameters at all the considered profiles of hydrological stations are shown in Appendix 8.2 in Figures 8.2.1-8.2.11.

Based on the graphs shown in Appendix 8.2, it can be concluded that for a certain exceedance probability $P\{(Q_{max} \geq q_{max,P}) \cap (W_{max} \geq w_{max,P}) = P$ exists a very wide range of possibilities for choosing the corresponding values of the considered flood wave hydrograph parameters.

Statistical significance of the established correlation dependences of the main flood hydrograph parameters, the maximum annual flows and the flood waves volumes at all the considered profiles of hydrological stations along the Danube River according to the equation (8.16), are shown in Table 8.3.

Table 8.3. Statistical significance of Q_{max} and W_{max} waves coincidence at the considered profiles of hydrological stations along the Danube River

No.	H. S.	R	N	σ	σ_R	Statistical significance
1.	Berg	0.659	78	0.064	0.192	+
2.	Ingolstadt	0.603	90	0.067	0.201	+
3.	Regensburg	0.652	90	0.061	0.182	+
4.	Hofkirchen	0.662	113	0.053	0.159	+
5.	Achleiten	0.472	113	0.073	0.219	+
6.	Wien	0.405	107	0.081	0.242	+
7.	Bratislava	0.612	137	0.051	0.160	+
8.	Bezdan	0.432	85	0.088	0.265	+
9.	Bogojevo	0.562	83	0.075	0.225	+
10.	Pančevo	0.728	86	0.051	0.152	+
11.	Oršava	0.640	173	0.045	0.135	+

Based on the results shown in Table 8.3 it can be concluded that flood coincidences at the Danube River and its tributaries are statistically significant at the level of hypothesis acceptance 95%, in all the considered sectors.

8.4.3 Calculation of theoretical flood hydrographs by the “limited runoff intensity” method

The proposed new approach in defining theoretical flood hydrographs at the profiles of hydrological stations, combined with the application of the “limited runoff intensity” method and defined bivariate distribution functions probabilities of the main hydrograph parameters, indicates the great possibilities of its practical application, as presented below. The elaborated procedure gives wide possibilities to choose combinations of main hydrograph parameters, both for the selected probability of occurrence p and for the exceedance probability P.

For the purposes of illustrating the practical application of the presented procedure, it is assumed that there is a very strong correlation (R=1.0) between the main flood hydrograph parameters. This practically means that the maximum annual flow of a certain probability of occurrence always coincides with the maximum annual volume of the same probability of occurrence, which basically, taking into account the results shown in Table 9.3 and in Appendix 8.2 in Figures 8.2.1-8.2.11, does not correspond to reality. However, this constellation of hydrograph parameters makes sense, because it essentially represents the “maximum possible” combination, which in the concrete case has the exceedance probability $P\{(Q_{max} \geq q_{max,\,P})\cap(W_{max} \geq w_{max,\,P})\} > P$.
The first calculation of theoretical flood hydrographs by the “limited runoff intensity” method (LRIM) was made for the “maximum possible” constellation of the main flood hydrograph parameters – a combination: maximum annual flow and maximum volume of the flood wave. For these assumptions, the parameters of the LRIM method are calibrated to the empirical

distribution functions of the maximum annual flood wave flows and volumes, as shown in Appendix 8.1 in Figures 8.1.1/a-8.1.11/b. The results of the calculation of the main flood hydrograph parameters according to the LRIM method are shown numerically, also in Table 8.2.

In order to verify the LRIM method in the drawings (Appendix 8.1, Figures 8.1.1/a-8.1.11/b), theoretical values of the maximum annual flood wave flows and volumes obtained by the LRIM method have also been applied. As seen in these figures, a very good match between the valuescalculated using the classic statistic-probabilistic analysis and the values obtained by the LRIM method is achieved.

Graphical interpretations of calculated theoretical flood hydrographs of different probabilities of occurrence at all the selected profiles of hydrological stations along the Danube according to the LRIM method, under the assumption that there is a very strong correlation (R=1.0) between the considered main flood hydrograph parameters are given in Appendix 8.3 in Figures 8.3.1-8.3.11.

8.4.4 Calculation of theoretical flood hydrographs by the "limited runoff intensity" method for different combinations of main flood hydrograph parameters

Defined bivariate distribution functions of the main flood hydrograph parameters indicate that for a certain exceeding probability $P\{(Q_{max} \geq q_{max, P}) \cap (W_{max} \geq w_{max, P})\} > P$ exists a wide range of possible combinations of maximum annual flows and maximum flood wave volumes. This practically means that there are many combinations (constellations) of the main flood hydrograph parameters that correspond to the same exceedance probability P. Therefore, it is necessary to find a procedure that, from the viewpoint of the users of the results, will define the most optimal combinations.

Authors of this paper suggest that in the field of flood protection, for the predefined exceedance probability P, it is best for users to work with the following combinations of parameters of the same marginal probabilities:

- Maximum annual flow - maximum flood wave volume of the same marginal probabilities – $P(Q_{max, P}, W_{max, P})$
- Maximum annual flow of the same marginal probability – the corresponding flood wave volume for the selected exceedance probability – $P(Q_{max, P}, W_{cor, P})$
- The corresponding maximum annual flow for the selected exceedance probability – the maximum flood wave volume of the same marginal probability – $P(Q_{cor,P}, W_{max,P})$
- The most probable combination (Mod) of the maximum annual flow and maximum flood wave volume for the selected exceedance probability – $P(Q_{Mod, P}, W_{Mod, P})$.

The values of the flood hydrograph parameters are taken from the results obtained by the LRIM method for the "maximum possible" constellation (Section 8.4.3), and the correspondant values of other mentioned constellations for the same exceedance probability P are taken from the bivariate distribution diagram shown in Figures 8.2.1-8.2.11 in Appendix 8.2. The numerical values of the selected constellations of the flood hydrograph parameters at all the studied profiles of hydrological stations along the Danube River are given in Tables 8.4/1-11.

Table 8.4/1 Selected combinations of main flood hydrograph parameters of the Danube River at Berg for different exceedance probabilities P

	Constellation of variables	Exceedance probability – P $\{(Q_{max} \geq q_{max,P}) \cap (W_{max} \geq w_{max,P})\}$=P							
		0.1 %		1.0 %		2.0 %		5.0 %	
		Q_{max} (m³/s)	W_{max} (10⁶m³)	Q_{max} (m³/s)	W_{max} (10⁶m³)	Q_{max} (m³/s)	W_{max} (10⁶m³)	Q_{max} (m³/s)	W_{max} (10⁶m³)
1	$Q_{max,P}$- $W_{max,P}$	613	642	476	509	432	466	372	406
2	$Q_{max,P}$. $W_{cor,P}$	613	510	476	400	432	340	372	290
3	$Q_{cor,P}$- $W_{max,P}$	500	642	370	509	290	466	220	406
4	$Q_{Mod,P}$-$W_{Mod,P}$	550	580	430	450	370	400	320	350

Table 8.4/2 Selected combinations of main flood hydrograph parameters of the Danube River at Inglostadt for different exceedance probabilities P

	Constellation of variables	Exceedance probability – P $\{(Q_{max} \geq q_{max,P}) \cap (W_{max} \geq w_{max,P})\}$=P							
		0.1 %		1.0 %		2.0 %		5.0 %	
		Q_{max} (m³/s)	W_{max} (10⁶m³)	Q_{max} (m³/s)	W_{max} (10⁶m³)	Q_{max} (m³/s)	W_{max} (10⁶m³)	Q_{max} (m³/s)	W_{max} (10⁶m³)
1	$Q_{max,P}$- $W_{max,P}$	2483	3270	1996	2492	1850	2263	1652	1959
2	$Q_{max,P}$. $W_{cor,P}$	2483	1900	1996	1300	1850	1200	1652	1100
3	$Q_{cor,P}$- $W_{max,P}$	1600	3270	1300	2492	1100	2263	950	1959
4	$Q_{Mod,P}$-$W_{Mod,P}$	2100	2600	1700	2100	1600	1900	1500	1600

Table 8.4/3 Selected combinations of main flood hydrograph parameters of the Danube River at Regensburg for different exceedance probabilities P

	Constellation of variables	Exceedance probability – P $\{(Q_{max} \geq q_{max,P}) \cap (W_{max} \geq w_{max,P})\}$=P							
		0.1 %		1.0 %		2.0 %		5.0 %	
		Q_{max} (m³/s)	W_{max} (10⁶m³)	Q_{max} (m³/s)	W_{max} (10⁶m³)	Q_{max} (m³/s)	W_{max} (10⁶m³)	Q_{max} (m³/s)	W_{max} (10⁶m³)
1	$Q_{max,P}$- $W_{max,P}$	3081	6191	2675	4594	2530	4131	2314	3524
2	$Q_{max,P}$. $W_{cor,P}$	3081	4900	2675	3800	2530	3000	2314	2600
3	$Q_{cor,P}$- $W_{max,P}$	2600	6191	2050	4594	1900	4131	1700	3524
4	$Q_{Mod,P}$-$W_{Mod,P}$	2900	5300	2500	4000	2350	3500	2100	3000

Table 8.4/4 Selected combinations of main flood hydrograph parameters of the Danube River at Hofkirchen for different exceedance probabilities P

	Constellation of variables	Exceedance probability – P $\{(Q_{max} \geq q_{max,P}) \cap (W_{max} \geq w_{max,P})\} = P$							
		0.1 %		1.0 %		2.0 %		5.0 %	
		Q_{max} (m³/s)	W_{max} (10⁶m³)	Q_{max} (m³/s)	W_{max} (10⁶m³)	Q_{max} (m³/s)	W_{max} (10⁶m³)	Q_{max} (m³/s)	W_{max} (10⁶m³)
1	$Q_{max,P}$- $W_{max,P}$	4222	8487	3469	6576	3231	5986	2900	5184
2	$Q_{max,P}$. $W_{cor,P}$	4222	7800	3469	4900	3231	4100	2900	3800
3	$Q_{cor,P}$- $W_{max,P}$	3600	8487	2700	6576	2500	5986	2100	5184
4	$Q_{Mod,P}$-$W_{Mod,P}$	4000	7900	3250	5800	2900	5100	2700	4200

Table 8.4/5 Selected combinations of main flood hydrograph parameters of the Danube River at Achleiten for different exceedance probabilities P

	Constellation of variables	Exceedance probability – P $\{(Q_{max} \geq q_{max,P}) \cap (W_{max} \geq w_{max,P})\} = P$							
		0.1 %		1.0 %		2.0 %		5.0 %	
		Q_{max} (m³/s)	W_{max} (10⁶m³)	Q_{max} (m³/s)	W_{max} (10⁶m³)	Q_{max} (m³/s)	W_{max} (10⁶m³)	Q_{max} (m³/s)	W_{max} (10⁶m³)
1	$Q_{max,P}$- $W_{max,P}$	10810	13786	8022	11651	7271	10923	6325	9869
2	$Q_{max,P}$. $W_{cor,P}$	10810	8000	8022	6200	7271	5900	6325	5100
3	$Q_{cor,P}$- $W_{max,P}$	7300	13786	5700	11651	5100	10923	4500	9869
4	$Q_{Mod,P}$-$W_{Mod,P}$	8900	11200	6400	10100	6000	9800	5100	9000

Table 8.4/6 Selected combinations of main flood hydrograph parameters of the Danube River at Vienna for different exceedance probabilities P

	Combination of variables	Exceedance probability – P $\{(Q_{max} \geq q_{max,P}) \cap (W_{max} \geq w_{max,P})\} = P$							
		0.1 %		1.0 %		2.0 %		5.0 %	
		Q_{max} (m³/s)	W_{max} (10⁶m³)	Q_{max} (m³/s)	W_{max} (10⁶m³)	Q_{max} (m³/s)	W_{max} (10⁶m³)	Q_{max} (m³/s)	W_{max} (10⁶m³)
1	$Q_{max,P}$ - $W_{max,P}$	12610	18528	9846	15149	9046	14089	7994	12566
2	$Q_{max,P}$ - $W_{cor,P}$	12610	11000	9846	9900	9046	9600	7964	9000
3	$Q_{cor,P}$ - $W_{max,P}$	9000	18528	7010	15149	6500	14069	6000	12566
4	$Q_{Mod,P}$ -$W_{Mod,P}$	11000	16000	8500	13500	8000	12500	7150	11000

Table 8.4/7 Selected combinations of main flood hydrograph parameters of the Danube River at Bratislava for different exceedance probabilities P

	Combination of variables	Exceedance probability – $P\{(Q_{max} \geq q_{max,P}) \cap (W_{max} \geq w_{max,P})\}=P$							
		0.1 %		1.0 %		2.0 %		5.0 %	
		Q_{max} (m^3/s)	W_{max} (10^6m^3)	Q_{max} (m^3/s)	W_{max} (10^6m^3)	Q_{max} (m^3/s)	W_{max} (10^6m^3)	Q_{max} (m^3/s)	W_{max} (10^6m^3)
1	$Q_{max,P}$ - $W_{max,P}$	14190	22504	11154	18561	10260	17251	9070	15482
2	$Q_{max,P}$ - $W_{cor,P}$	14190	11600	11154	10500	10260	9800	9070	9100
3	$Q_{cor,P}$ - $W_{max,P}$	8000	22504	6000	18561	5000	17251	4000	15482
4	$Q_{Mod,P}$ - $W_{Mod,P}$	11200	19000	9200	15500	8600	14300	7900	13000

Table 8.4/8 Selected combinations of main flood hydrograph parameters of the Danube River at Bezdan for different exceedance probabilities P

	Constellation of variables	Exceedance probability – $P\{(Q_{max} \geq q_{max,P}) \cap (W_{max} \geq w_{max,P})\}=P$							
		0.1 %		1.0 %		2.0 %		5.0 %	
		Q_{max} (m^3/s)	W_{max} (10^6m^3)	Q_{max} (m^3/s)	W_{max} (10^6m^3)	Q_{max} (m^3/s)	W_{max} (10^6m^3)	Q_{max} (m^3/s)	W_{max} (10^6m^3)
1	$Q_{max,P}$- $W_{max,P}$	10490	36292	8656	30007	8072	27939	7265	25006
2	$Q_{max,P}$. $W_{cor,P}$	10490	20000	8656	15000	8072	13000	7265	11000
3	$Q_{cor,P}$- $W_{max,P}$	7000	36292	6000	30007	5400	27939	5000	25006
4	$Q_{Mod,P}$-$W_{Mod,P}$	8900	30000	7250	25000	6600	23000	6100	20500

Table 8.4/9 Selected combinations of main flood hydrograph parameters of the Danube River at Bogojevo for different exceedance probabilities P

	Constellation of variables	Exceedance probability – $P\{(Q_{max} \geq q_{max,P}) \cap (W_{max} \geq w_{max,P})\}=P$							
		0.1 %		1.0 %		2.0 %		5.0 %	
		Q_{max} (m^3/s)	W_{max} (10^6m^3)	Q_{max} (m^3/s)	W_{max} (10^6m^3)	Q_{max} (m^3/s)	W_{max} (10^6m^3)	Q_{max} (m^3/s)	W_{max} (10^6m^3)
1	$Q_{max,P}$- $W_{max,P}$	11137	39899	9358	33741	8785	31674	7985	28701
2	$Q_{max,P}$. $W_{cor,P}$	11137	25000	9358	21000	8785	19000	7985	16000
3	$Q_{cor,P}$- $W_{max,P}$	9000	39899	7600	33741	7000	31674	6100	28701
4	$Q_{Mod,P}$-$W_{Mod,P}$	10000	35000	8500	29500	7900	28000	7100	24000

Table 8.4/10 Selected combinations of main flood hydrograph parameters of the Danube River at Pančevo for different exceedance probabilities P

	Constellation of variables	Exceedance probability – P $\{(Q_{max} \geq q_{max,P}) \cap (W_{max} \geq w_{max,P})\}=P$							
		0.1 %		1.0 %		2.0 %		5.0 %	
		Q_{max} (m^3/s)	W_{max} (10^{6}m^3)	Q_{max} (m^3/s)	W_{max} (10^{6}m^3)	Q_{max} (m^3/s)	W_{max} (10^{6}m^3)	Q_{max} (m^3/s)	W_{max} (10^{6}m^3)
1	$Q_{max,P}$- $W_{max,P}$	17353	95000	15035	79500	14289	74500	13244	67500
2	$Q_{max,P}$. $W_{cor,P}$	17353	70000	15035	58000	14289	51000	13244	46000
3	$Q_{cor,P}$- $W_{max,P}$	16300	95000	14300	79500	13300	74500	12004	67500
4	$Q_{Mod,P}$-$W_{Mod,P}$	16500	90000	14500	75000	13600	70000	12500	62000

Table 8.4/11 Selected combinations of main flood hydrograph parameters of the Danube River at Orsova for different exceedance probabilities P

	Constellation of variables	Exceedance probability – P $\{(Q_{max} \geq q_{max,P}) \cap (W_{max} \geq w_{max,P})\}=P$							
		0.1 %						0.1 %	
		Q_{max} (m^3/s)	W_{max} (10^{6}m^3)	Q_{max} (m^3/s)	W_{max} (10^{6}m^3)	Q_{max} (m^3/s)	W_{max} (10^{6}m^3)	Q_{max} (m^3/s)	W_{max} (10^{6}m^3)
1	$Q_{max,P}$- $W_{max,P}$	17550	99506	15463	89004	14759	85100	13742	79086
2	$Q_{max,P}$. $W_{cor,P}$	17550	78000	15463	65000	14759	62000	13742	58000
3	$Q_{cor,P}$- $W_{max,P}$	16500	99506	15000	89004	13900	85100	12000	79086
4	$Q_{Mod,P}$-$W_{Mod,P}$	17000	95000	15200	85000	14100	80000	12700	72000

Selected constellations of variables (main flood hydrograph parameters – peak and flood wave volume) for the accepted exceedance probability $P\{(Q_{max} \geq q_{max,P}) \cap (W_{max} \geq w_{max,P})\}=1.0\%$ are shown in Appendix 8.2 in Figures 8.2.1-8.2.11 together with defined bivariate coincidence functions. All selected combinations of variables are shown in Tables 8.4/1-11 and in Appendix 8.4 in Figures 8.4.1-8.4.11.

The theoretical flood hydrographs are calculated by the LRIM method for all selected combinations of variables with exceedance probability P=1.0%. The results of the calculation are shown graphically in Appendix 8.5 in Figures 8.5.1-8.5.11.

As can be seen in Appendix 8.5 (Figures 8.5.1-8.5.11), four different hydrographs were obtained, of which hydrographs 2, 3, and 4, each from a different point of view, represent a **100-year flood hydrograph**. Theoretical hydrograph composed of marginal probabilities – $P(Q_{max,P}, W_{max,P})$, which represents the "maximum possible" hydrograph, is the "quasi-100-year" hydrograph, by both parameters (peak and maximum volume), and it basically exceeds probability p, i.e. $p>P$. This is corroborated by the position of characteristic point 1 in Appendix 8.4 (Figures 8.4.1-8.4.11), which cannot represent a 100-year theoretical hydrograph (p=1.0%), because its actual position evidently corresponds to the line of exceedance probability.

$$P\{(Q_{max} \geq q_{max,\,P}) \cap (W_{max} \geq w_{max,\,P})\} = P < p = 1.0\%.$$

Values of the exceedance probability $P\{(Q_{max} \geq q_{max,\,P}) \cap (W_{max} \geq w_{max,\,P})\} = P < p = 1.0\%$, of “maximum possible” hydrographs, i.e. “quasi-100-year” hydrograph (point 1), estimated on the basis of the coincidence shown in Figures 8.4.1-8.4.11 in Appendix 8.4, are shown in Table 8.5.

As can be seen in Table 8.5, the return periods of the combinations of 100-year flood hydrograph parameters (peak and maximum volume), point 1 in Figures 8.5.1-8.5.11 in Appendix 8.5, correspond to the return periods from 125 (Bogojevo, Pančevo and Oršava) to 670 (Achleiten) years.

It is also interesting to analyze the return periods of registered historical floods, which were used to calculate the coincidences of the main flood hydrograph paramaters at all the profiles of hydrological stations. Only historical floods with return periods greater than or equal to 100 years have been analyzed. The results of these analyzes are shown in Table 8.6. Data shown in Table 8.6 indicate that statistically the most significant historical floods, with a return period of more than 100 years, are registered at the hydrological station of Bratislava, with a total of four for the period 1876-2015.

The following are hydrological stations Achleiten and Vienna with a total of three floods between 1900 and 2006 and Ingolstadt and Regensburg with registered two statistically significant historical floods, both in the period from 1924 to 2013. At all the other hydrological stations, there was one statistically significant historical flood.

The most frequent statistically significant historical flood occurred in 1965 at six hydrological stations. Then, there is a 2013 flood which appeared at four hydrological stations, and floods in 1954, 1988 and 2006 appeared at two hydrological stations. All other historical floods are registered only at one hydrological station. From the viewpoint of statistical significance, the return periods of these registered historic floods range from 100 to 1000 years (2013 at Achleiten).

Table 8.5 Exceedance probability of point 1 at selected hydrological stations along the Danube River

No.	H. S.	$P\{(Q_{max} \geq q_{max,P}) \cap (W_{max} \geq w_{max,\,P})\} = P < p = 1.0\%$	Return period in years
1.	Berg	0.33	300
2.	Ingolstadt	0.20	500
3.	Regensburg	0.40	250
4.	Hofkirchen	0.50	200
5.	Achleiten	0.15	670
6.	Wien	0.25	400
7.	Bratislava	0.20	500
8.	Bezdan	0.20	500
9.	Bogojevo	0.80	125
10.	Pančevo	0.80	125
11.	Oršava	0.80	125

Table 8.6 Actual probability of historical flood occurrence at selected hydrological stations along the Danube River

No.	H. S.	Number of Flood Wave at H.S.	$P\{(Q_{max} \geq q_{max,P}) \cap (W_{max} \geq w_{max,P})\}$ = P <p=1.0%.		Return period in years
			Historical flood wave		
			year	p	
1.	Berg	1	1988	0.33	300
2.	Ingolstadt	1	1965	0.20	500
		2	1999	0.20	500
3.	Regensburg	1	1988	0.25	400
		2	2013	1.00	100
4.	Hofkirchen	1	2013	0.65	150
5.	Achleiten	1	2013	0.10	1000
		2	1965	0.20	500
		3	1954	0.20	500
6.	Wien	1	1965	0.20	500
		2	1975	0.25	400
		3	1954	0.33	300
7.	Bratislava	1	1965	0.20	500
		2	1899	0.33	300
		3	2013	0.40	250
		4	1876	0.90	110
8.	Bezdan	1	1965	0.25	400
9.	Bogojevo	1	1965	0.80	125
10.	Pančevo	1	2006	1.00	100
11.	Oršava		2006	1.00	100

8.5 Conclusion

The main idea of authors of Chapter 8 is to propose an entirely **new approach to defining theoretical flood hydrographs at river gauging stations**, such as official stations with long time-series of river stages and flows. This is certainly a very actual topic, which lasts permanently and will last until hydrologists around the world finally determine the appropriate standards for this type of hydrological processing and analysis.

Theoretical flood hydrographs of different probability of occurrence are one of the most important hydrological elements when of the following water management activities:

- Defense and flood protection,
- Dimensioning of accumulations and retensions in the function of flood protection,
- Dimensioning of embankments, bridges and dams,
- Risk assessment and flood risk management.

From the aspect of the mentioned activities, not all the flood hydrograph parameters are of the same significance. The most frequent practical use has the maximum ordinate of hydrograph (peak) and it plays a dominant role in almost all of these water management activities. The flood wave volume is very important for the optimal dimensioning of dams and retentions, as well as for the successful implementation of flood defense, the analysis of the flood spread in the area and the assessment of the floods risk and its management. The flood wave duration is significant for optimal dimensioning of embankments and successful flood protection, etc.

In the elaboration of this procedure, the authors started from the assumption that the main flood hydrograph parameters are random variables that follow a one-dimensional (univariate), two-dimensional (bivariate) or multidimensional (multivariate) distribution law. The bivariate probability analysis in this Chapter only confirm the wide range of different combinations of hydrograph parameters in defining the theoretical hydrograph of a certain probability of occurrence. The authors of this Chapter point out that for a certain exceedance probability $P\{(Q_{max} \geq q_{max,P})\cap(W_{max} \geq w_{max,P})\}= P$ are characteristic four points, whose coordinates (which essentially represent the hydrograph peak and the flood wave volume) define a theoretical hydrograph of the same probability of the occurrence $P \cong p$.

The practical value of theoretical flood hydrographs, determined by the coordinates of the four characteristic points, for the same exceedance probability $P\{(Q_{max} \geq q_{max,P})\cap(W_{max} \geq w_{max,P})\} = P \cong p$ is following:

1. Theoretical hydrograph, composed of marginal probabilities – $P(Q_{max,P}, W_{max,P})$, represents the “maximum possible” hydrograph by both parameters (hydrograph peak and maximum volume), and essentially exceeds the probability p, p> P. This is also confirmed by the positions of the characteristic point 1 in Figures 9.4.1-9.4.11 in Appendix 9.4, which may represent a 100-year theoretical hydrograph (p=m1.0%), but it is evident that its actual position corresponds to the exceedance probability line

$P\{(Q_{max} \geq q_{max,\,P})\cap(W_{max} \geq w_{max,\,P})\} = P < p = 1.0\%$.

i.e. its actual exceedance probability (Figures 8.5.1-8.5.11 in Appendix 8.5) corresponds to the 300-year return period.

2. 100-year theoretical hydrograph composed of the corresponding marginal probabilities – $P(Q_{max,P}, W_{cor,P})$ is 100-year (p= 1.0%) only according to the hydrograph peak, so it can practically be used only for the dimensioning of overflow constructions, embankment crowns, bridge openings, sluices, etc. It cannot be used for the dimensioning of accumulation and retention spaces, since the probability of occurrence of the flood wave volume is less than hundred years, i.e. p <1.0%.
3. On the other side, the 100-year theoretical hydrograph composed of marginal probabilities $P(Q_{cor,P}, W_{max,P})$ is 100-year (p=1.0%) only according to the hydrograph maximum volume and can be used for the dimensioning of accumulation and retention spaces, but cannot be used for the dimensioning of overflow constructions, embankment crowns, bridge openings, sluices, since the probability of occurrence of the hydrograph peak is less than 100 years, i.e. p <1.0%.
4. A theoretical hydrograph of marginal probabilities – $P(Q_{Mod,P}, W_{Mod,P})$ is the “most probable” hydrograph whose exceedance probability P and the probability of occurrence p coincide (they are identical):

$P\{(Q_{max} \geq q_{max,\,P})\cap(W_{max} \geq w_{max,\,P})\} = P = p$.

The authors of this paper suggest that this “most probable” hydrograph for any probability ($P = p$) should be used as a control in all the above mentioned cases of hydrotechnical objects dimensioning.

References

Abramowitz M., Stegun A. I., 1972: *Handbook of Mathematical Functions with Formulas*, Graphs and Mathematical Tables, Dover Publications, INC., New York.

Adamson P. T., Metcalfe A. V., Parmentier B., 1999: Bivariate extreme value distributions: An application of Gibbs sampler to analysis of floods, *Water Resources Research*, Vol. 35, No. 29, pp 2825-2832

Chebana F., Ouarda T. B. M. J., 2011: Multivariate quantiles in hydrological frequency analyzis, *Envirometrics*, Vol. 22, No. 1, pp 63-78

Chebana F., 2013: *Multivariate Analysis of Hydrological Variables*, doi:10.1002/9780470057339.vnn044

Haimes Y. Y., Lambert J. H., Li D., 1992: Risk of extreme events in multiobjective framework, *Water Resources Bulletin*, American Water Resources Association, Vol. 28, No. 1, pp 201-209

Prohaska S., Marjanović N., Čabrić M., 1978: *Dvoparametarsko definiranje velikih voda*, Vode Vojvodine, Novi Sad.

Prohaska S., Petković T., 1989: *Metode za proračun velikih voda, Deo I, Proračun velikih voda na hidrološki izučenim profilima*, Građevinski kalendar 89, Beograd.

Prohaska S. et al., 1999: *Concidence of Flood Flow of the Danube River and its Tributary*, The Danube and its Basin – A Hydrological Monograph, Follow-up volime IV, Regional Cooperation of the Danube Countries in the Frame of the International Hydrological Programme of UNESCO, Bratislava.

Prohaska S., Ristić V., 2002: *Hidrologija kroz teoriju i praksu*, Drugo prošireno izdanje, Rudarsko-geološki fakultet, Institut „Jaroslav Černi", Beograd.

Prohaska S., 2003: *Hidrologija I Deo, Hidro-meteorologija, hidrometrija i vodni režim*, Rudarsko-geološki fakultet, Institut „Jaroslav Černi", Republički hidrometeorološki zavod Srbije, Beograd.

Prohaska S., 2006: *Hidrologija II Deo, Hidrološko prognoziranje, modelovanje i praktična primena*, Institut „Jaroslav Černi", Rudarsko-geološki fakultet, Republički hidrometeorološki zavod Srbije, Beograd.

Singh V. P., Strupczewski W. G., 2002: On the status of flood frequency analysis, Hydrological Processes, Vol. 16, pp 3737-3740

Singh V. P., Strupczewski W. G., 2007: Editorial: *Journal of Hydrologic Engineering*, doi: 10.1061/(ASCE)1084-0699(2007)12:4

Yevjevich, V., 1972: *Probability and Statistics in Hydrology*, Water Resources Publications, Fort Collins, Colo. U.S.A.

9 Regionalization of flood regimes according to flood magnitudes and other hydrological characteristics through application of the multivariate copula functions

Martin Morlot, Mojca Šraj, Nejc Bezak, and Mitja Brilly

9.1 Introduction

Floods are one of the natural disasters that can cause large economic damage and have consequently significant influence on society. The Danube River and its basin is an important region of Europe in terms of flood risk and floods have occurred in the Danube River basin through the whole history. Floods are a multivariate process that is defined with several depended parameters (e.g., Šraj et al., 2015). Thus, in order to investigate flood characteristics a multivariate methods should be used. Copula functions that have been in the last years used for different application are an example of such methods (e.g., Šraj et al., 2015 and cited references). Furthermore, in order to regionalize information about floods the complete hydrological process should be taken into consideration. Thus, a multivariate analysis can present a good basis for the regionalization. However, also other parameters such as seasonality analysis should be included (e.g., Bezak et al., 2016; Burn, 1997). This kind of information will be of paramount importance in the future due to climate change impact (e.g., Bezak et al., 2016; Bormann et al., 2011; Bormann and Pinter, 2017; Blöschl et al., 2017; Hall et al., 2014; Stagl and Hattermann, 2015; Šraj et al., 2016; Villarini et al., 2012). Some European countries have even suggested use the so-called adjustment factors for the design discharge estimation (e.g., Defra, 2006; Madsen et al., 2014). The design discharge estimation is one of the most important and frequently used hydrological procedures.
The main aim of this paper is to perform the regionalization of floods in the Danube River basin taking into account the multivariate nature of the hydrological phenomena. In order to determine the homogenous regions different input information is used such as univariate flood frequency analysis results, multivariate flood frequency analysis results, seasonality analysis and station characteristics.

9.2 Data and methods

9.2.1 Danube River basin

Danube River basin is, after the Volga River, the second largest river in Europe (Morlot, 2018). The Danube River flows through ten European countries and the Danube River basin additionally covers nine more countries (Morlot, 2018). Figure 9.1 shows the Danube River basin with country boundaries. The entire Danube River basin can be further divided into upped, middle and lower Danube as proposed by Stagl and Hattermann (2015) and shown in Figure 9.2. For detailed description of the Danube River basin one should refer to Morlot (2018) and reference cited therein. Daily discharge collected at multiple locations in the Danube River basin was used in this paragraph. Figure 9.3 shows location of investigated stations. In total 87 stations were analysed. Detailed information about selected stations and time period can be found in Morlot (2018).

9.2.2 Univariate methods

In the first step of the chapter, we carried out univariate flood frequency analysis. Annual maximum method was selected to define samples (e.g., Bezak et al., 2014; Karmakar and Simonovic, 2008; Lang et al., 1999; Maidment, 1993; Salinas et al., 2014). The distribution parameters were estimated using the method of L-moments. Detailed description of L-moments method can be found in Hosking and Wallis (2005).

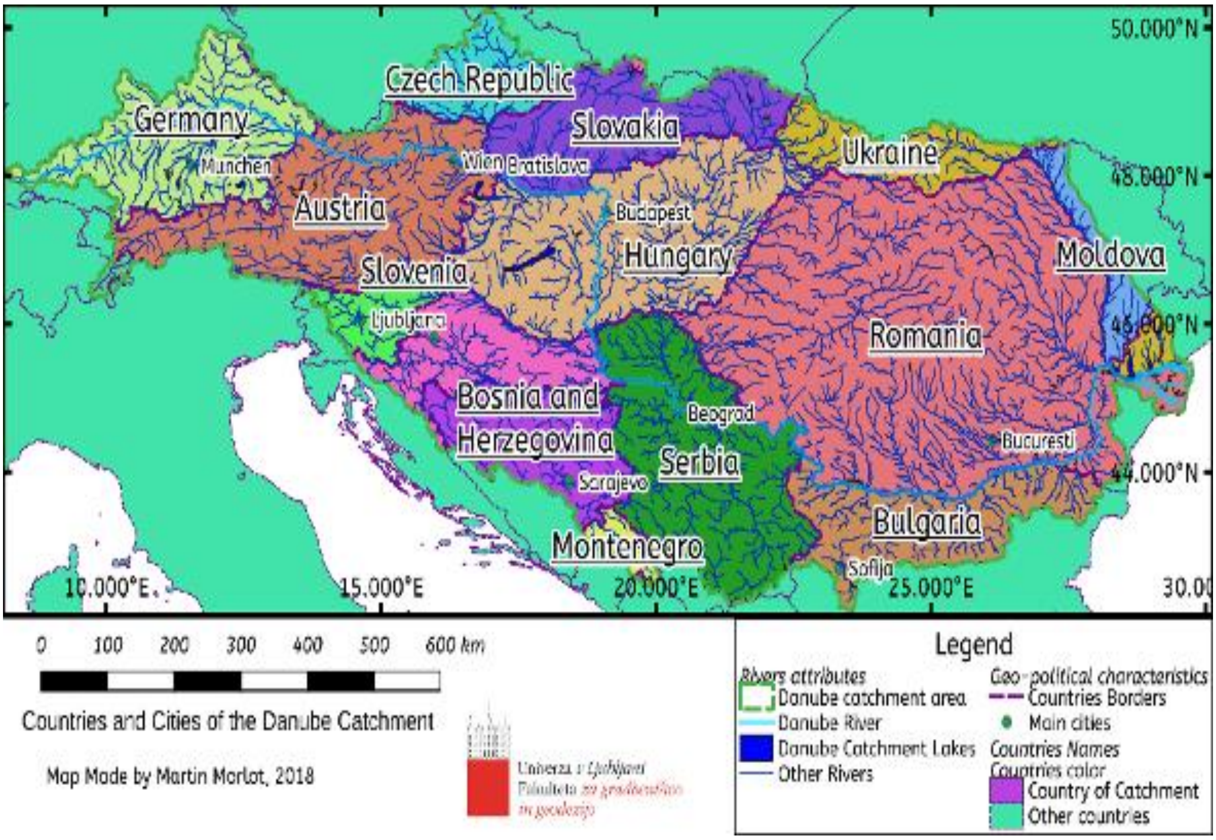

Fig.9.1 Danube River catchment (adopted from Morlot, 2018).

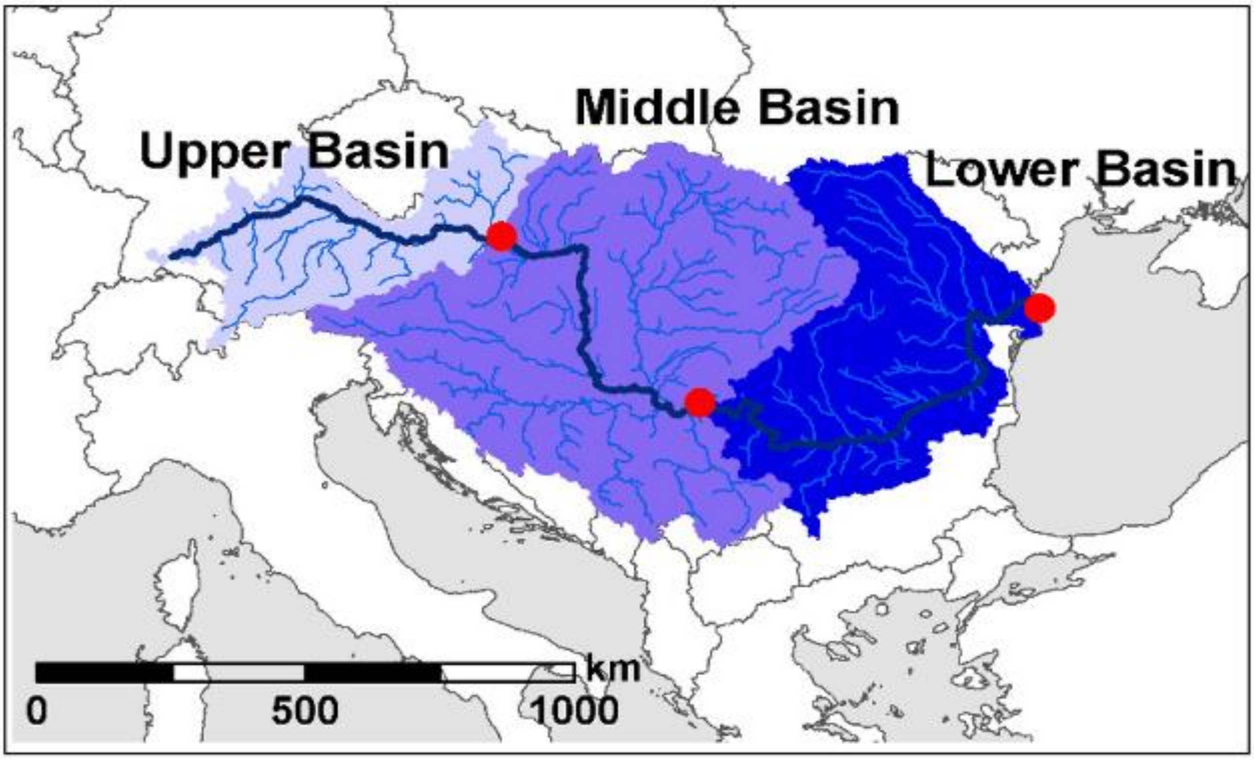

Fig. 9.2 Separation of the Danube River basin into upper, middle and lower basin (adopted from Stagl and Hattermann, 2015).

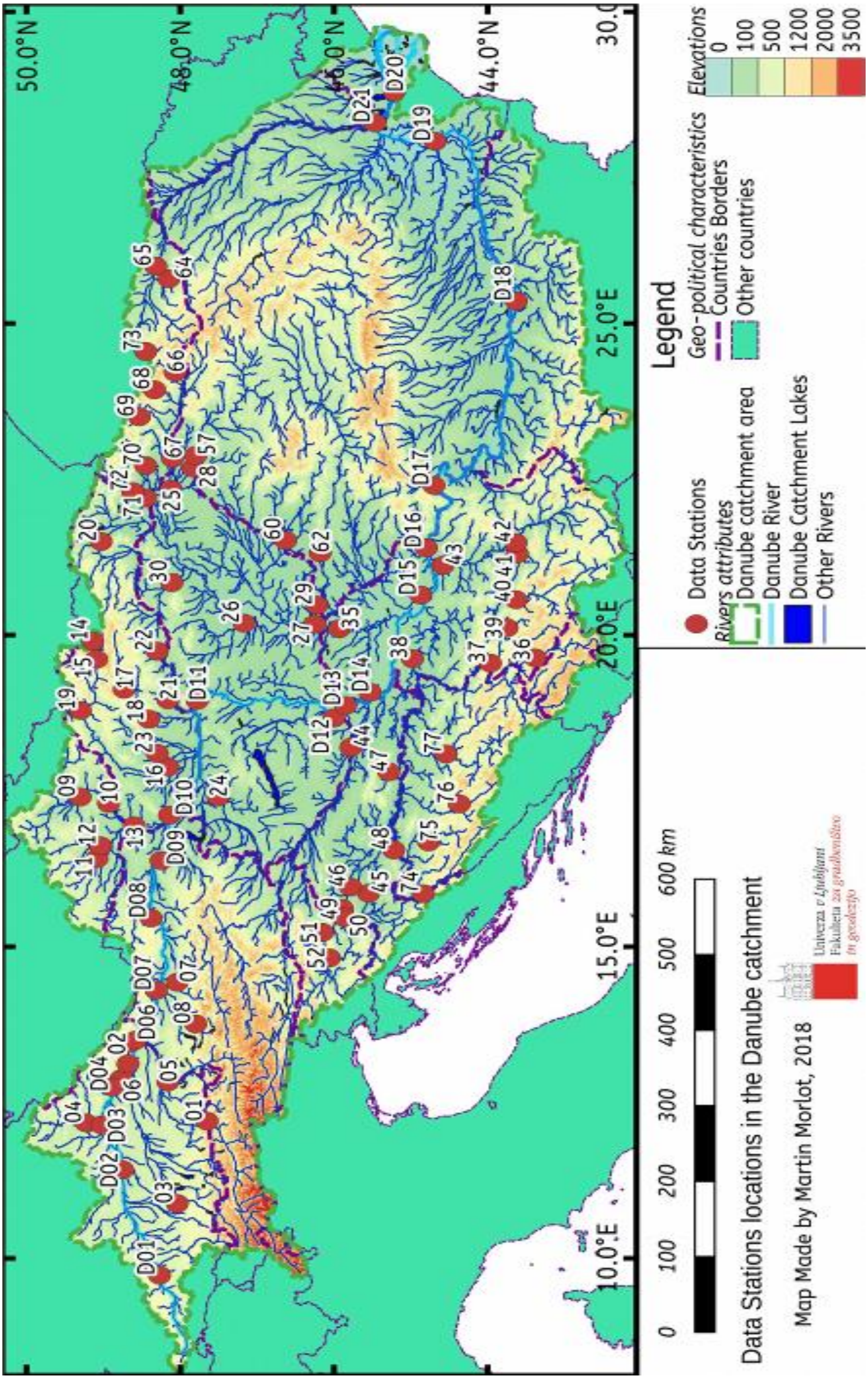

Fig. 9.3 Location of stations that were investigated in this chapter (adopted from Morlot, 2018).

Several distributions that are shown in Table 9.1 were selected, namely Gumbel, generalized extreme value (GEV), generalized logistics (GL), Pearson type 3 (P3), log-Pearson type 3 (LP3) and log-normal (LN) (Table 9.1).
For all stations shown in Figure 9.3 several distribution functions were tested. Using different statistical tests (e.g., Kolmogorov-Smirnov, Anderson-Darling) and model selection criteria (e.g., mean absolute error (MAE), root mean square error (RMSE)) we selected the most suitable distribution function for all investigated gauging stations. The description of the methodology can be found in Morlot (2018).

Table 9.1: Cumulative distribution functions (CDF) and parameters equation for different distributions (adopted after Bezak et al., 2014)

Distribution type	CDF function and parameters using L-moments
Gumbel	$F_X(x) = e^{-e^{\frac{-(x-u)}{\alpha}}}$ $\alpha = \frac{l_2}{ln(2)}$ and $u = l1 - 0.5772\alpha$
GEV	$F_X(x) = exp\left(-\left[1 - k\left(\frac{x-\xi}{\alpha}\right)\right]^{1/k}\right)$ $c = \frac{2}{3+\tau_3} - \frac{ln2}{ln3}$; $k = 7.8950c + 2.9554c^2$; $\alpha = \frac{kl_2}{\Gamma(1+k)(1-2^{-k})}$; $\xi = l_1 + \frac{\alpha(\Gamma(1+k)-1)}{k}$
GL	$F_X(x) = \left(1 + \left[1 - \frac{k}{\alpha}(x-\xi)^{1/k}\right]\right)^{-1}$ $k = -\tau_3$; $\alpha = \frac{l_2}{\Gamma(1+k)\Gamma(1-k)}$;$\xi = l_1 + \frac{l_2-\alpha}{k}$
P3	$F_X(x) = \int_c^x \frac{1}{\beta\Gamma(\alpha)}\left(\frac{x-c}{\beta}\right)^{\alpha-1} e^{-(x-c)/\beta}dx$ For:$0 < \tau_3 < 1/3 : z = 3\pi\tau_3^2$; $\alpha = \frac{1+0.2906z}{z+0.1882z^2+0.0442z^3}$ For:$0 < \tau_3 < 1/3 : z = 1 - \tau_3$; $\alpha =$ $\frac{0.36067z-0.59567z^2+0.25361z^3}{1-2.78861z+2.56096z^2-0.77045z^3}$ For all τ_3 values: $\beta = sign(\tau_3)\frac{\Gamma(\alpha)}{\Gamma(\alpha+0.5)}$; $c = l_1 - \alpha\beta$
LP3	$F_Y(y) = \int_0^y \frac{1}{\Gamma(\alpha)}\left(\frac{y-c}{\beta}\right)^{\alpha-1} e^{-(y-c)/\beta}dy$;$y = log(x)$ Same parameters equations as for the P3 distribution
LN	$F_X(x) = \int_0^x \frac{1}{x\sigma_Y\sqrt{2\pi}} e^{-(ln(x)-\mu_Y)^2/2\sigma_Y^2}dx$; $\mu_Y = l_1$ and $\sigma_Y = \sqrt{\pi}l_2$

9.2.3 Multivariate methods

We carried out multivariate flood frequency analysis using copula functions. In order to determine hydrograph volume and duration baseflow was separated from measured discharge. Based on station characteristics we selected either recursive digital filter method or base-flow method. Additional description about the selected methodology and relevant references can be found in Morlot (2018). In next step we carried out bivariate flood frequency analysis for pairs of variables: peak discharge (Q)-hydrograph volume (V); peak discharge (Q)-hydrograph duration (D) and hydrograph volume (V)-hydrograph duration (D). Distribution functions shown in Table 9.2 were used. Several statistical tests were calculated (e.g., Genest et al., 2006; Genest et al., 2009) and selection criterion proposed by Grønneberg and Hjort (2014). All copula based analyses were carried out using "copula" program R package (Kojadinovič and Yan, 2010). After selecting the most suitable copula function we calculated multivariate return periods. Detailed description can be found in Morlot (2018).

9.2.4 Seasonality investigation

We investigated the seasonal characteristics of the flows in the Danube River basin. Methodology proposed by Bayliss and Jones (1993) and Burn (1997) was used. Detailed description can be found in Morlot (2018).

9.2.5 Regionalisation

For the regionalisation we used Orange software and methods that are implemented in this software (Demšar et al., 2013). An example of Orange flowchart is shown in Figure 9.4. Several regionalisation methods such as K-means or H-clustering were tested. The homogeneity of regions was tested using methodology proposed by Hosking and Wallis (2005). As input to the regionalisation we used several indices such as basin area, station elevation, seasonality, best fitting univariate distribution, best fitting copula for the Q-V relationship, best fitting copula for the Q-D relationship and best fitting copula for the V-D relationship.

Table 9.2: Copula functions used in this chapter (adopted from Šraj et al., 2015).

Copula	$C_\theta(u,v)$	$\theta \in$
Gumbel-Hougaard	$exp\left(-\left((-lnu)^\theta + (-lnv)^\theta\right)^{1/\theta}\right)$	$[1,\infty)$
Clayton	$\left[u^{-\theta} + v^{-\theta} - 1\right]^{1/\theta}$	$[-1,\infty) \setminus \{0\}$
Frank	$-\frac{1}{\theta} ln\{1 + \frac{(e^{-\theta u} - 1)(e^{-\theta v} - 1)}{e^{-\theta} - 1}\}$	$(-\infty,\infty) \setminus \{0\}$
Joe	$1 - \left[(1-u)^\theta + (1-v)^\theta - (1-u)^\theta(1-v)^\theta\right]^{1/\theta}$	$[1,\infty)$
Galambos	$uv * exp\left(-\left((-lnu)^\theta + (-lnv)^\theta\right)^{1/\theta}\right)$	$[0,\infty)$
Husler-Reiss	$exp\left[-\tilde{u}\Phi\{\frac{1}{\theta} + \frac{\theta}{2} ln\left(\frac{\tilde{u}}{\tilde{v}}\right)\} - \tilde{v}\Phi\{\frac{1}{\theta} + \frac{\theta}{2} ln\left(\frac{\tilde{u}}{\tilde{v}}\right)\}\right]$ where $\tilde{u} = -lnu$; $\tilde{v} = -lnv$	$[0,\infty)$
Tawn	$uv * exp\left(-\left((-lnu)^\theta + (-lnv)^\theta\right)^{1/\theta}\right)$	$[0;1]$
Normal	$\int_{-\infty}^{\Phi^{-1}(u)} \int_{-\infty}^{\Phi^{-1}(v)} \frac{1}{2\pi * \sqrt{(1-\theta^2)}} exp\{-\frac{s^2 - 2\theta st + t^2}{2(1-\theta^2)}\}d.$	$[-1;1]$

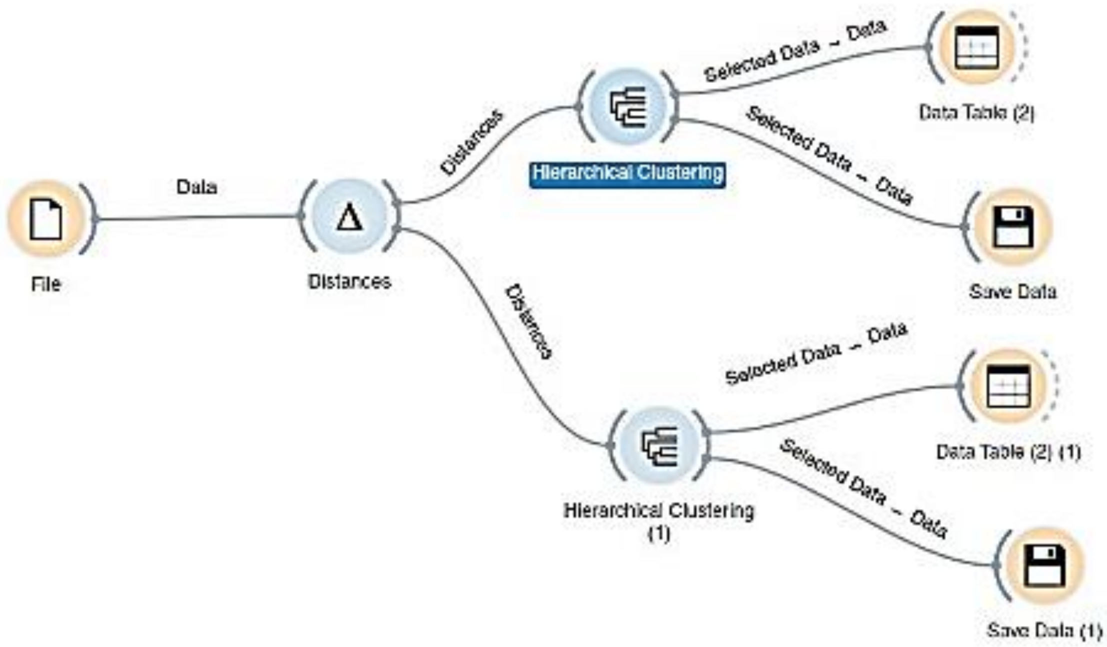

Fig.9.4. *Example of regionalization flow chart using Orange software (adopted from Morlot, 2018).*

9.3 Results and discussion

9.3.1 Univariate methods

In the first step of this chapter we carried out univariate flood frequency analysis using approach described in section 9.2.2. Table 9.3 shows number of cases that tested distributions were classified on 1st and 2nd place using several statistical tests and model selection criteria. One can notice that generally GEV, GL, LP3 and P3 performed better compared to the LN and Gumbel distributions. In most cases GEV distribution was selected as the most suitable followed by P3 and LP3 distributions (Table 9.3). Figure 9.5 shows geographical distribution of the best fitting univariate distributions on the Danube River basin map. For investigated gauging stations we also calculated design discharge values with *10* and *100*-years return period. Design discharge values with 100-years return period are shown in Figure 9.6.

Table 9.3: Summary of the univariate distributions that yielded the best performance according several criteria for the Danube River basin (adopted from Morlot, 2018).

Best Distribution Fit	1st place (# of occurrences)	2nd place (# of occurrences)
General Logistics	18	8
GEV	22	20
Gumbel	3	3
Log Normal	5	9
Log Pearson Type III	19	37
Pearson Type 3	20	10

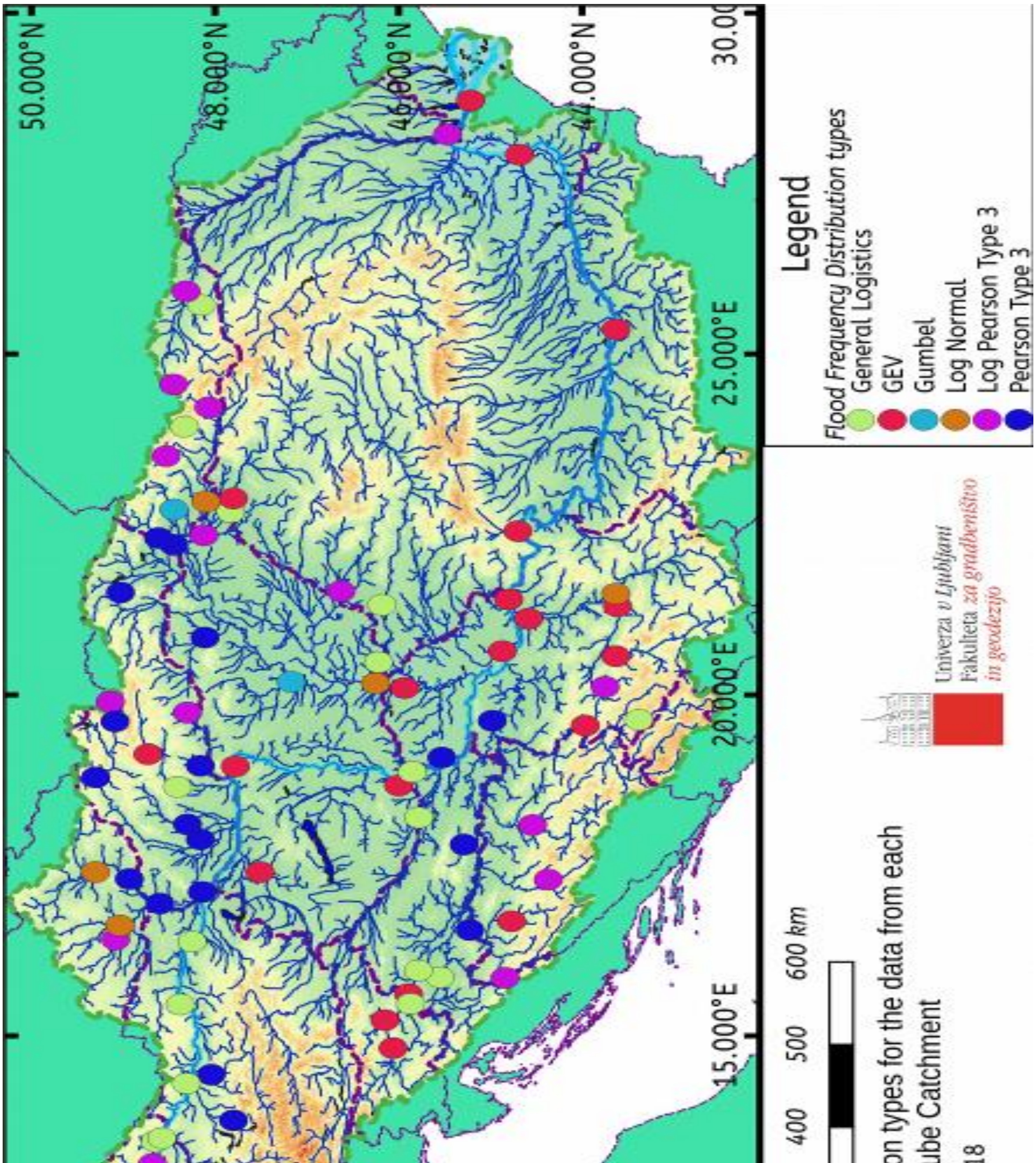

Fig. 9.5 *Best fitting univariate distribution functions according to several statistical tests (adopted from Morlot, 2018).*

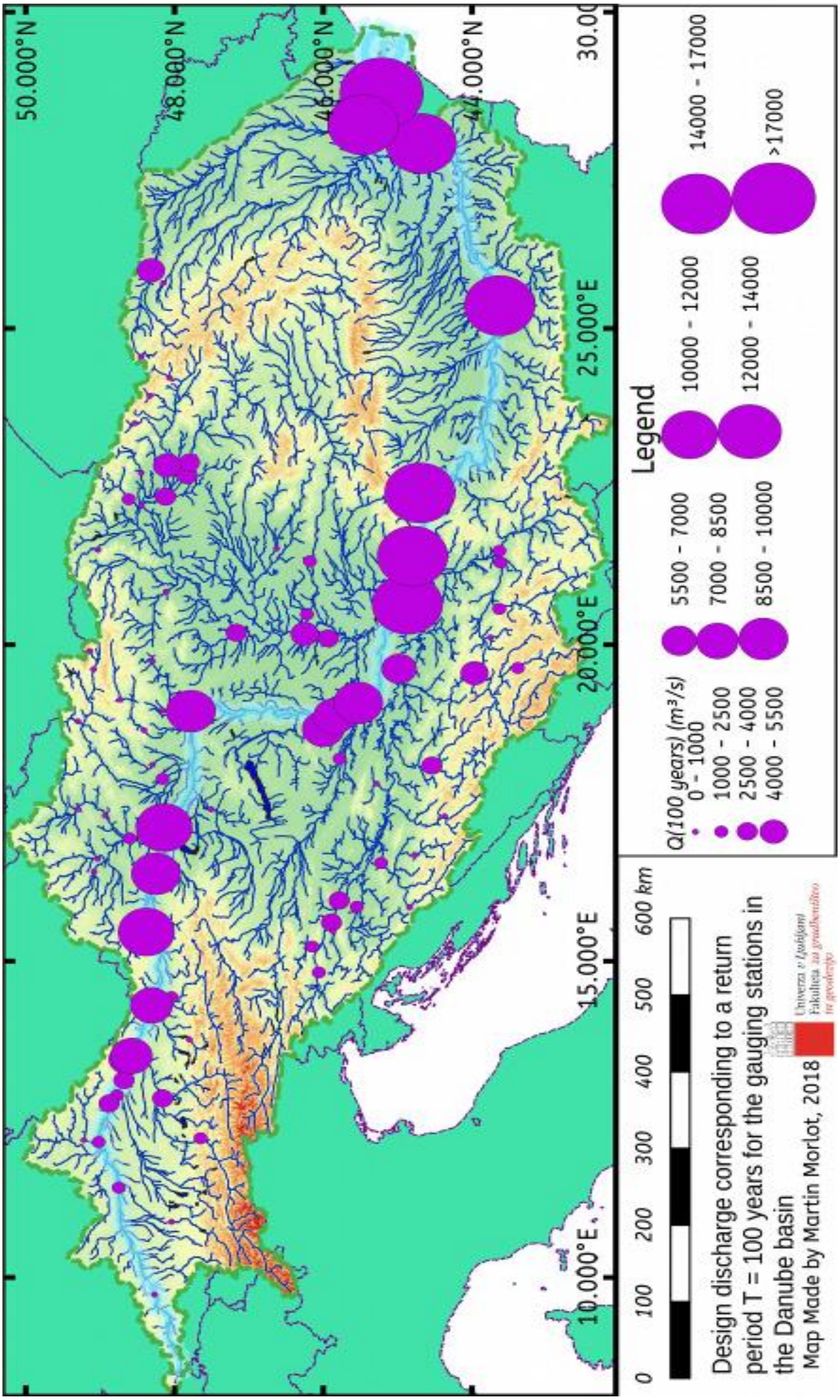

Fig.9.6 *Design discharge values with 100-years return period for the selected stations in the Danube River basin (adopted from Morlot, 2018).*

9.3.2 Multivariate methods

The methodology described in section 2.3 was used to select the most suitable copula functions for the pairs of variables Q-V, V-D and V-D. Table 9.4 shows a summary of these results. One can notice that normal copula yielded the best results for the Q-V and V-D cases and Clayton copula for the Q-D (Table 9.4). Figure 9.7 shows geographical presentation of the best fitting copula functions for different pairs of variables.

Table 9.4 Summary of the univariate distributions that yielded the best performance according several criteria for the Danube River basin (adopted from Morlot, 2018)

Copula function type	Bivariate analysis QV	Bivariate analysis QD	Bivariate analysis VD
Clayton	6	39	4
Frank	18	15	8
Galambos	2	3	0
Gumbel	1	2	2
HuslerReiss	9	8	12
Joe	1	0	2
Normal	36	14	45
Tawn	14	6	14

9.3.3 Seasonality investigation

In order to use information on seasonality in the regionalisation procedure we used the methodology described in section 2.4. Table 9.5 provides basic characteristics of the seasonality investigation. One can notice that floods most often occur in winter and spring in the Danube River basin. Figure 9.8 shows an example of the seasonality presentation for the Bratislava station on the Danube River basin. Moreover, Figure 9.9 shows geographical distribution of the seasonality of floods in the Danube River basin. Furthermore, Figure 9.10 shows variability of annual maximum events and the strength of seasonality.

Table 9.5 Summary of the seasonality characteristics of the investigated gauging stations in the Danube River basin (adopted from Morlot, 2018)

Seasons	Most common flood season (# of occurrences)	Average flood season (# of occurrences)	Largest flood on record season (# of occurrences)
Winter	29	32	11
Spring	34	36	34
Spring & Summer	1	0	0
Summer	14	14	25
Fall	9	5	17

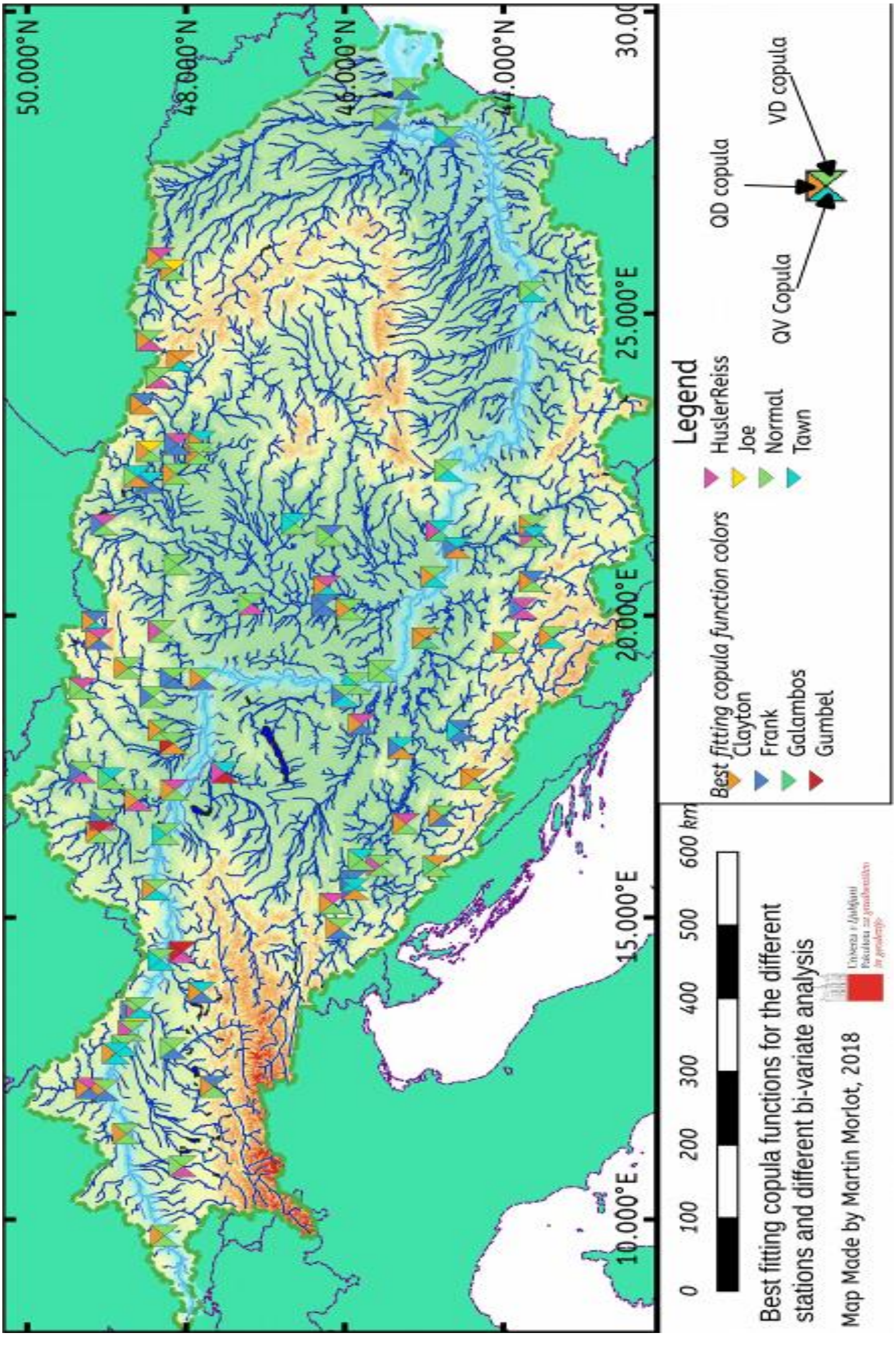

Fig.9.7 *Best fitting copula functions for investigated stations in the Danube River basin (adopted from Morlot, 2018).*

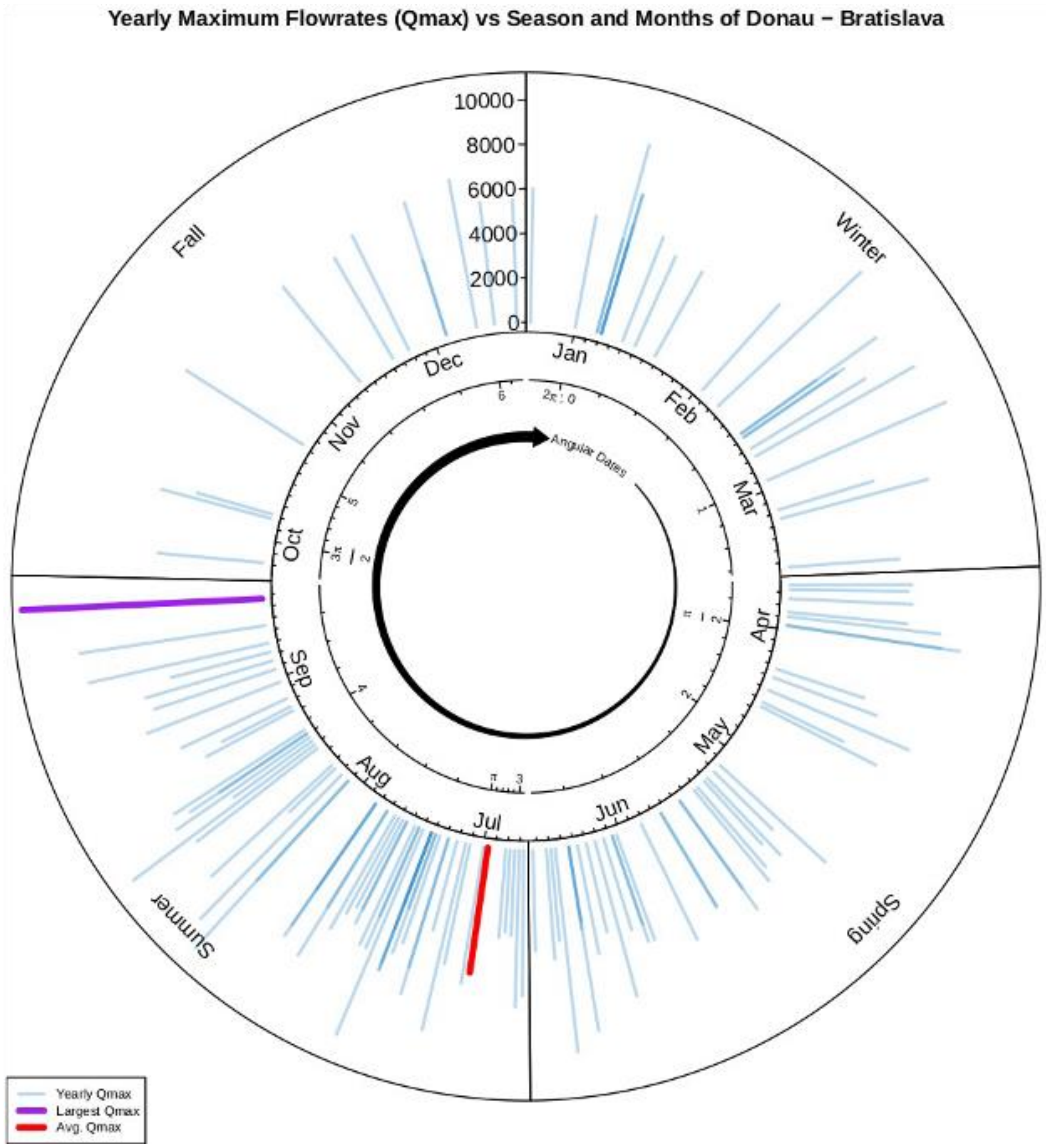

Fig.9.8 Example of the seasonality investigation for the Danube River in Bratislava, Slovakia (adopted from Morlot, 2018).

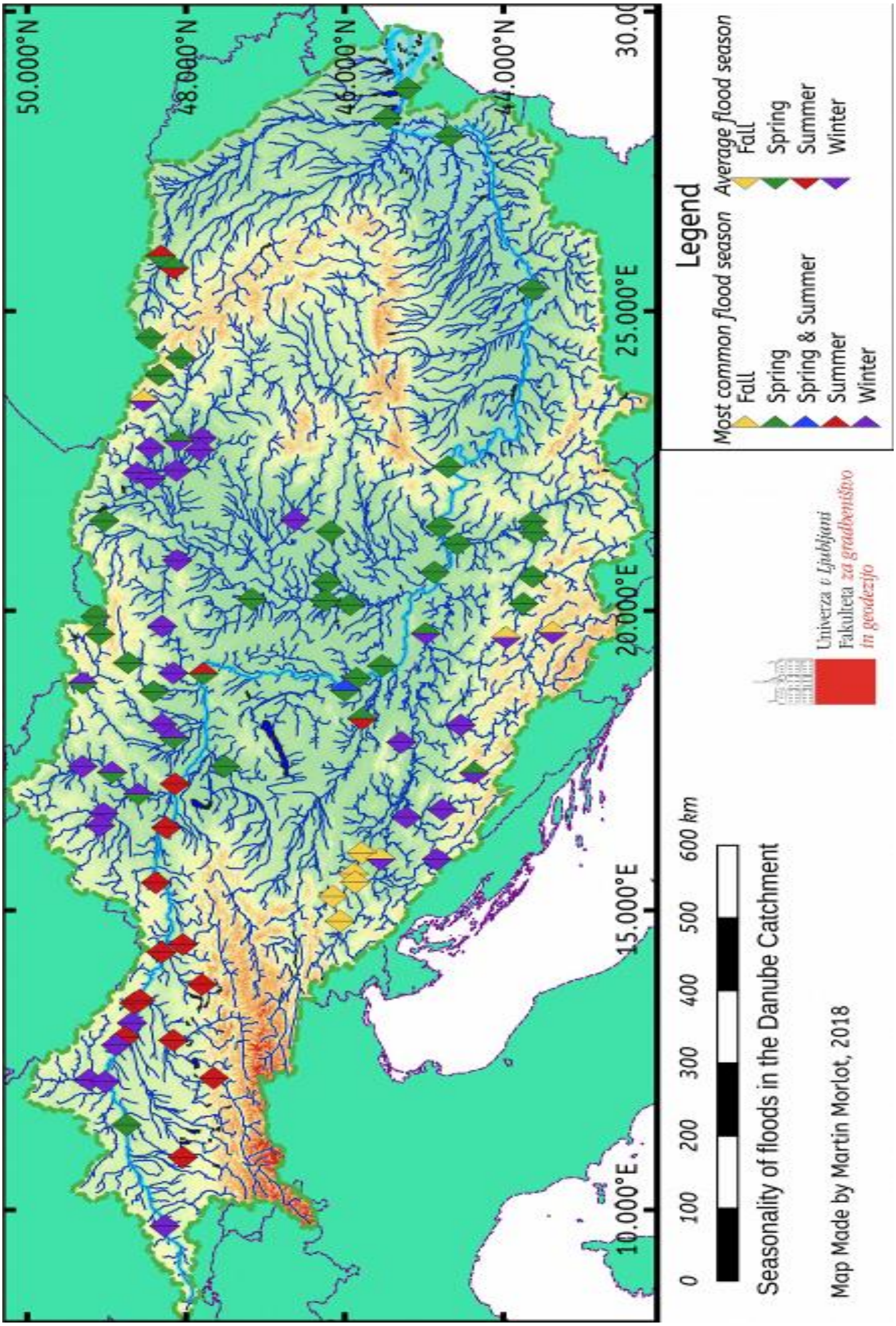

Fig,9.9 Seasonality of floods according to the most common flood season and average flood season in the investigated Danube River basin (adopted from Morlot, 2018).

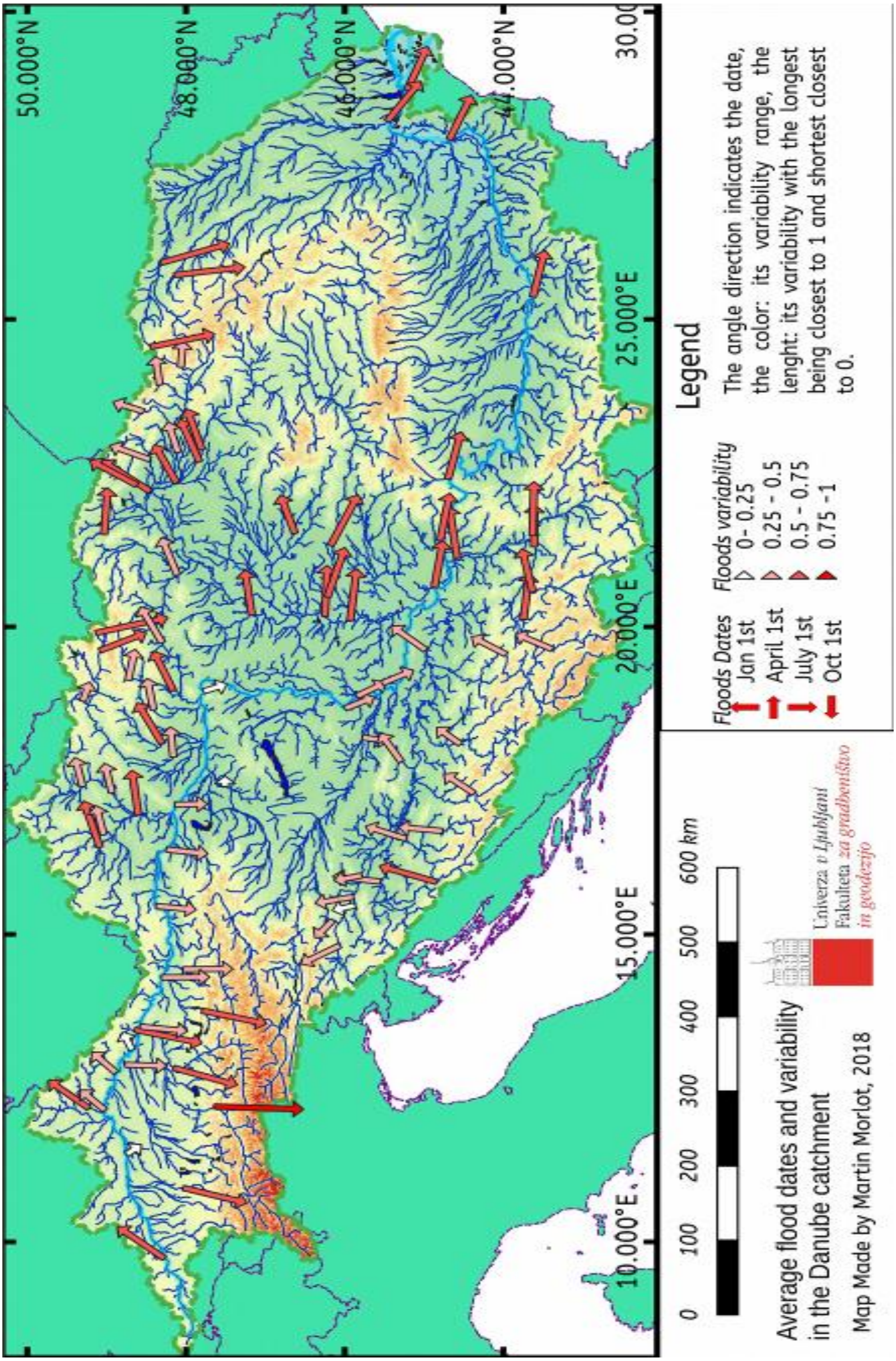

Fig.9.10 Seasonality and variability of annual flood dates in the Danube basin (adopted from Morlot, 2018).

9.3.4 Regionalisation

In the final step of the chapter we investigated the regionalisation of floods in the Danube River basin. Using input information from chapters 9.3.1, 9.3.2 and 9.3.3 we defined several regions in the Danube River basin. Table 9.6 shows input data that was used to the regionalisation in this chapter and Figure 9.11 shows geographical distribution of determined regions. Before finalizing regions several validation steps were carried out and are described by Morlot (2018).

Table 9.6 Regions and their characteristics that were used in the regionalisation process (adopted from Morlot, 2018).

Region	Mean Lat	Mean Lon	Mean Basin Area (m^2)	Mean height (m)	Most common season	Most common univariate distribution	Most common among only LP3 or GEV dist.	Most common QV copula	Most common QD copula	Most common VD copula
C10	45.99	18.9	163258	83	Spring (4/6)	General Logistics (2/6) *	GEV (2/6) *	Frank (2/6) *	Clayton (3/6)	Normal (4/6)
C12	48.58	18.25	7331	215	Winter (4/6)	Pearson Type 3 (4/6)	Log Pearson Type 3 (5/6)	Normal (4/6)	Clayton (3/6)	Normal (5/6)
C13	45.91	15.46	9153	160	Fall (3/3)	GEV (2/3)	GEV (2/3)	Frank (1/3) *	Clayton (1/3) *	Frank (1/3) *
C14	44.57	17.47	5235	246	Fall (3/7) *	GEV (3/7) *	GEV (4/7)	Normal (4/7)	Clayton (5/7)	Normal (3/7)
C15	45.55	15.96	6003	117	Fall (2/3)	General Logistics (2/3)	Other (2/3)	Normal (2/3)	Clayton (1/3) *	Husler Reiss (1/3) *
C16	48.83	12.36	35146	323	Winter (3/4)	GEV (2/4)	GEV (2/4)	Normal (2/4)	Clayton (3/4)	Normal (3/4)
C17	48.27	20.05	2663	143	Winter (5/7)	Pearson Type 3 (4/7)	Log Pearson Type 3 (5/7)	Normal (4/7)	Frank (3/7) *	Normal (4/7)
C170	48.16	22.68	8628	117	Winter (4/5)	General Logistics (1/5) *	GEV (3/5)	Normal (3/5)	Clayton (3/5)	Tawn (2/5)
C171	49.09	17.11	6700	175	Winter (3/3)	Log Normal (2/3)	Log Pearson Type 3 (2/3)	Husler Reiss (2/3)	Frank (2/3)	Normal (2/3)
C2	44.69	24.32	640803	33	Spring (6/6)	GEV (5/6)	GEV (5/6)	Tawn (3/6)	Normal (3/6)	Normal (5/6)
C3	48.33	15.35	97042	203	Summer (5/5)	General Logistics (4/5)	Log Pearson Type 3 (4/5)	Tawn (3/5)	Clayton (2/5) *	Normal (4/5)
C4	48.37	12.52	7218	384	Summer (6/8)	Log Pearson Type 3 (3/8) *	Log Pearson Type 3 (6/8)	Frank (3/8)	Clayton (3/8)	Normal (5/8)
C6	48.23	25.82	3781	260	Spring (1/2) *	General Logistics (1/2) *	Log Pearson Type 3 (1/2) *	Normal (2/2)	Clayton (2/2)	Husler Reiss (1/2) *
C8	48.6	22.62	665	563	Spring (5/6)	Log Pearson Type 3 (4/6)	Log Pearson Type 3 (6/6)	Husler Reiss (2/6) *	Clayton (5/6)	Frank (2/6) *
C9	43.66	20.87	9690	206	Spring (4/4)	GEV (2/4)	GEV (2/4) *	Normal (2/4)	Clayton (2/4)	Frank (1/4) *
C90	46.35	21.35	24710	92	Spring (3/5)	General Logistics (2/5) *	GEV (3/5)	Normal (3/5)	Clayton (2/5)	Tawn (2/5)
C91	46.45	20.15	117745	74	Spring (3/3)	GEV (1/3) *	GEV (3/3)	Frank (1/3) *	Clayton (1/3) *	Normal (2/3)

*Note: * indicate characteristics, distributions or functions of regions where ties occur and more than one attribute could be preferred*

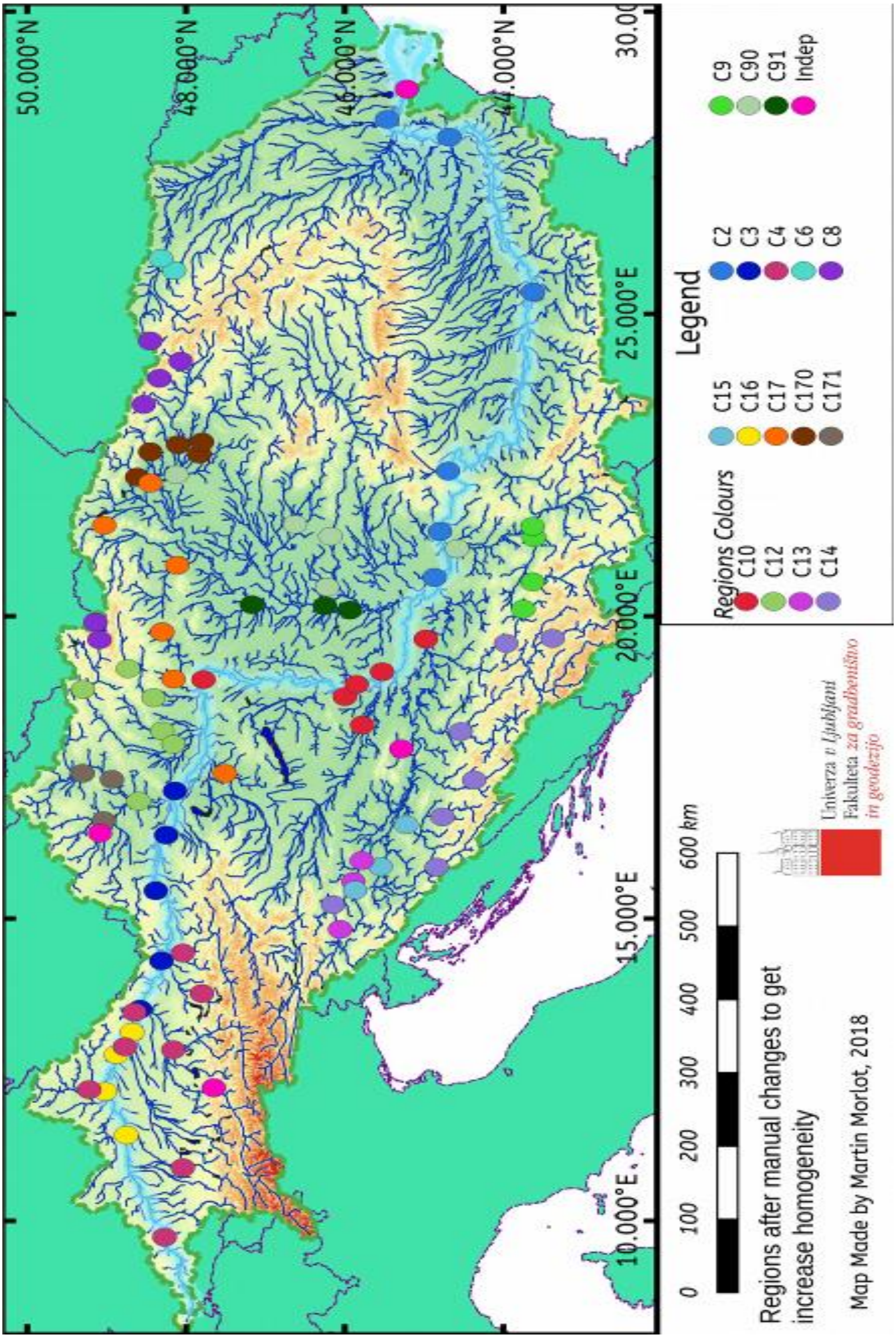

Fig. 9.11 *Danube River basin regions after several steps that increased homogeneity of regions (adopted from Morlot, 2018).*

9.4 Conclusions

This chapter presents results of the hydrological regionalisation of floods in the Danube River basin. Univariate and multivariate flood frequency analysis results, seasonality characteristics and station properties were used as an input. Based on the presented results next conclusions can be made (Morlot, 2018):

- Overall, two distribution functions, namely GEV and LP3 are found to fit well to the Danube River catchment. The univariate flood frequency analysis could be enhanced by including additional distribution functions or maybe also by using additional goodness of fit tests and selection criteria.
- For most stations baseflow index method is the most suitable for the baseflow separation. However, for stations in the downstream section of the Danube basin the recursive digital filter method is preferred. For the three bivariate analysis and among the eight different copula functions fitted and tested, the normal copula was found to be best fitting one for the Danube River catchment for both the Q-V and V-D pairs of variables while the Clayton copula was found to be the best fitting function for the Q-D pair of variables.
- Seasonality characteristics are found to be clustered and the Danuber River catchent could be divided into regions based on the seasonality characteristics.
- After several steps a total of 17 homogeneous (or possibly homogeneous) and four independent stations were detected. For each region an average region characteristics were determined (e.g., seasonality, best fitting univariate distribution, best fitting multivariate distribution, etc.). This information could be useful for the ungauged catchments in the regions. Additional characteristics such as rainfall amount, evapotranspiration, soil properties could be used to enhance the regionalisation process.

References

Bayliss, A. C., Jones, R. C. 1993. Peaks-over-threshold flood database: summary statistics and seasonality. Wallingford: Institute of Hydrology.

Bezak, N., Brilly, M., Šraj, M. (2014). Comparison between the peaks-over-threshold method and the annual maximum method for flood frequency analysis. Hydrological Sciences Journal, 59(5), 959–977. https://doi.org/10.1080/02626667.2013.831174

Bezak, N., Brilly, M., Šraj, M. 2016. Flood frequency analyses, statistical trends and seasonality analyses of discharge data: a case study of the Litija station on the Sava River. Journal of Flood Risk Management, 9, 154-168.

Bormann H., Pinter N., Elfert S. 2011. Hydrological signatures of flood trends on German rivers: flood frequencies, flood heights and specific stages. Journal of Hydrology, 404, (1–2), 50–66.

Bormann, H., Pinter, N. 2017. Trends in low flows of German rivers since 1950: Comparability of different low-flow indicators and their spatial patterns, River Research and Applications, 33(7): 1191–1204. DOI: 10.1002/rra.3152.Boukhris, O., Willems, P. 2008. Climate change impact on hydrological extremes along rivers in Belgium. In: Samuels et al. (Eds.), FloodRisk 2008 Conference, 30 Sept.–2 Oct. 2008, Oxford, UK. Flood Risk Management: Research and Practice. Taylor & Francis Group, London, pp. 1083–1091. ISBN: 978-0-415-48507-4.

Blöschl, G., et al., 2017. Changing climate shifts timing of European floods. Science, 357(6351), 588-590. doi: 10.1126/science.aan2506.

Burn, D.H. 1997. Catchment similarity for regional flood frequency analysis using seasonality measures. Journal of Hydrology, 202, 212-230.

Defra, 2006. Flood and Coastal Defence Appraisal Guidance (FCDPAG3), Economic Appraisal Supplementary Note to Operating Authorities – Climate Change Impacts. Department for Environment, Food and Rural Affairs, London, 9 pp.

Demšar, J., Curk, T., Erjavec, A., Gorup, Č., Hočevar, T., Milutinovič, M., … Zupan, B. 2013. Orange: Data Mining Toolbox in Python. Journal of Machine Learning Research, 14, 2349–2353. Retrieved from http://jmlr.org/papers/v14/demsar13a.html.

Genest, C., Quessy, J.-F., Remillard, B. 2006. Goodness-of-fit Procedures for Copula Models Based on the Probability Integral Transformation. Scandinavian Journal of Statistics, 33(2), 337–366. https://doi.org/10.1111/j.1467-9469.2006.00470.x

Genest, C., Rémillard, B., Beaudoin, D. 2009. Goodness-of-fit tests for copulas: A review and a power study. Insurance: Mathematics and Economics, 44(2), 199–213. https://doi.org/10.1016/j.insmatheco.2007.10.005

Grønneberg, S., Hjort, N. L. 2014. The Copula Information Criteria: The copula information criteria. Scandinavian Journal of Statistics, 41(2), 436–459. https://doi.org/10.1111/sjos.12042

Hall, J., et al. 2014. Understanding flood regime changes in Europe: A state-of-the-art assessment. Hydrology and Earth System Sciences, 18, 2735-2722. doi: 10.5194/hess-18-2735-2014.

Hosking, J.R.M., Wallis, J.R. 2005. Regional frequency analysis: an approach based on L-moments. Cambridge University Press.

Karmakar, S., Simonovic, S.P. 2008. Bivariate flood frequency analysis: part 1. Determination of marginals by parametric and nonparametric techniques. Journal of Flood Risk Management, 1(4), 190–200. doi:10.1111/j.1753-318X.2008.00022.x.

Kojadinovic, I., Yan, J. 2010. Modelling Multivariate Distributions with Continuous Margins Using the copula R Package. J. Stat. Softw. 2010, 34.

Lang, M., Ouarda, T.B.M.J., Bobee, B. 1999. Towards operational guidelines for over-threshold modelling. Journal of Hydrology, 225(3-4), 103-117. doi: https://doi.org/10.1016/S0022-1694(99)00167-5.

Madsen, H., Lawrence, D., Lang, M., Martinkova, M., Kjeldsen T.R. 2014. Review of trend analysis and climate change projections of extreme precipitation and floods in Europe. Journal of Hydrology, 519(D), 3635-3650. doi: https://doi.org/10.1016/j.jhydrol.2014.11.003.

Maidment, D. 1993. Handbook of hydrology. McGrow-Hill, New York, 1424 p.

Morlot, M. 2018. Characterisation of the floods in the Danube River basin through univariate and multivariate (copula functions) flood frequency analysis, seasonality and regionalisation. MCs Thesis, IHE Delft, 75 p.

Salinas, J. L., Castellarin, A., Viglione, A., Kohnová, S., Kjeldsen, T. R. 2014. Regional parent flood frequency distributions in Europe – Part 1: Is the GEV model suitable as a pan-European parent?, Hydrol. Earth Syst. Sci., 18, 4381-4389, https://doi.org/10.5194/hess-18-4381-2014.

Stagl, J. C., Hattermann, F. F. 2015. Impacts of Climate Change on the Hydrological Regime of the Danube River and Its Tributaries Using an Ensemble of Climate Scenarios. Water, 7(11), 6139–6172. https://doi.org/10.3390/w7116139

Šraj, M., Bezak, N., Brilly, M. 2015. Bivariate flood frequency analysis using the copula function: a case study of the Litija station on the Sava River. Hydrological Processes, 29(2), 225–238. https://doi.org/10.1002/hyp.10145

Šraj, M., Menih, M., Bezak, N. 2016. Climate variability impact assessment on the flood risk in Slovenia. Physical Geography, 37(1), 73-87. doi: http://dx.doi.org/10.1080/02723646.2016.1155389.

Villarini G., Smith J.A., Serinaldi F., Ntelekos A.A., Schwarz U. 2012. Analyses of extreme flooding in Austria over the period 1951–2006. International Journal of Climatology, 32, (8), 1178–1192.

Summary

There is a perception that extreme climatic and hydrological events have become more frequent in recent years, and suggestions that this phenomenon may be due to man-induced global warming. That perception is (sometimes arguably) supported by some scientific evidence, but is still not widely recognised. Trends in fluvial flooding are more difficult to detect, as changes in factors such as land use, reservoirs, drainage or flood alleviation schemes will impact on the flood regime in addition to changes due to the climate. This study is looking for evidence of changes in flood regimes of rivers in the Danube river basin, an increase in the frequency and magnitude of high flow in the observation period. The flow regime of a river is the quantity, duration and seasonal pattern of flows. The flow regime of a river system influences the flora and fauna present in a river ecosystem, it also influences the lifecycle activities of fauna such as spawning and the survival of larvae and juveniles.

Human activities such as abstraction of water, disposal of excess water, irrigation and clearing of vegetation can change the natural flow regime. These activities can lead to either an increase or a decrease in quantity of flow as well as changing the timing, duration and seasonal pattern of ecologically important flow events. Climate change is also contributing to changed flow regimes. The flow regime of a waterway is an important indicator of its health and forms part of the assessment of waterways.

In particular, the last decade has seen a significant focus on understanding the response mechanism of runoff to climate change and human activity (e.g., the construction of reservoirs to store and/or control the flow of water). A significant number of the major rivers have been dammed, including the Danube. Depending on the size and purpose of the dam, their construction can lead to different impacts on the downstream river flow regime. For example, different impacts result from changes in the variability, magnitude, timing, and frequency of flow.

In the presented follow-up volume 9 of the Danube Hydrological Monograph the authors have assessed the changes in flood regimes in the Danube River Basin from the long-term point of view using hydrological information from gauging stations in the whole river basin. Therefore, the database was created of the as long as available time series of the mean daily discharge and maximum annual discharge. The mean monthly and annual discharges were processed from the daily data. Twenty stations were selected lying on the Danube banks with time series of high quality. Experts of participating countries have selected other 65 stations lying on the tributaries of the Danube, preferably from the profiles which are not disturbed by human activities and where the long time series exist. It was not possible to fulfil this condition in all stations. The data collection, their processing and database creation are described in chapter 1.

In the second chapter the authors focused on collection of information about major historical floods on the Danube which are not included in the measured time series. One way how to obtain such information is gathering information on historical flood marks preserved in the settlements along the Danube channel. In this respect, there exist very big differences between the Upper Danube, Middle Danube and Lower Danube. There exist many flood marks even of the August 1501 flood in the cities of the Upper Danube in Germany and Austria. The historical flood marks are evidence that at least 3 higher floods than those of the last 100 years did occur between 1501 and 1900.

The homogeneity of the data time series was tested in Chapter 3. The fourth chapter deals with the identification of long-term trends and of the multi-annual variability of the mean annual discharges, as well as of the maximum annual discharges. It is necessary to take into account the natural multiannual variability of runoff in the Danube Basin. Results, which seem to show trends in short time series up to 60 years, can be only manifestation of natural long-term cycles, in fact.

The fifth chapter summarizes the results of the statistical analyses of selected characteristics of maximum monthly and daily discharge.

The sixth chapter is focused on proposition of unified methodology of *T*-year design discharge assessment in the whole Danube River Basin.

The seventh chapter presents the results of statistical analyses concerning the coincidence of flood waves on the Danube and its tributaries. The eights chapter is focused on assessment of the design flood waves on the Danube.

The final Chapter 9 presents the results of the regionalization of selected flow characteristics in the Danube Basin.

The significance of the presented work is in unified processing of all the collected data from the whole Danube River Basin. The presented Follow-up volume of the Danube Hydrological Monograph is result of 10-years collaboration of wide team of hydrologists from 11 countries of the Danube collaboration in the framework of the International Hydrological Programme of UNESCO (IHP UNESCO).

Publication of the monograph was partially supported by Slovak MVTS project “Flood regime of rivers in the Danube River basin”, the Slovak Science Granting Agency under the contract No. VEGA 2/0004/19 and by the Slovak National Commission for UNESCO.

We earnestly wish that our results will interest the hydrological community.

Pavla Pekárová and Pavol Miklánek

Appendices

The following eight attachments are recorded on the CD:

- APPENDIX I.1 – Daily discharge analysis
- APPENDIX I.2 – Yearly discharge analysis
- APPENDIX I.3 – Extreme discharge analysis
- APPENDIX III – Analysis of homogeneity
- APPENDIX V – Monthly discharge analysis
- APPENDIX VI – LP3 distribution functions – Design values
- APPENDIX VII – Coincidence of maximum annual discharges
- APPENDIX VIII – Theoretical flood hydrographs